BioMed Research International

Anticancer Properties of Natural Products

Guest Editors: István Zupkó, Walter Jaeger, Zeki Topcu, and Chin-Chung Wu

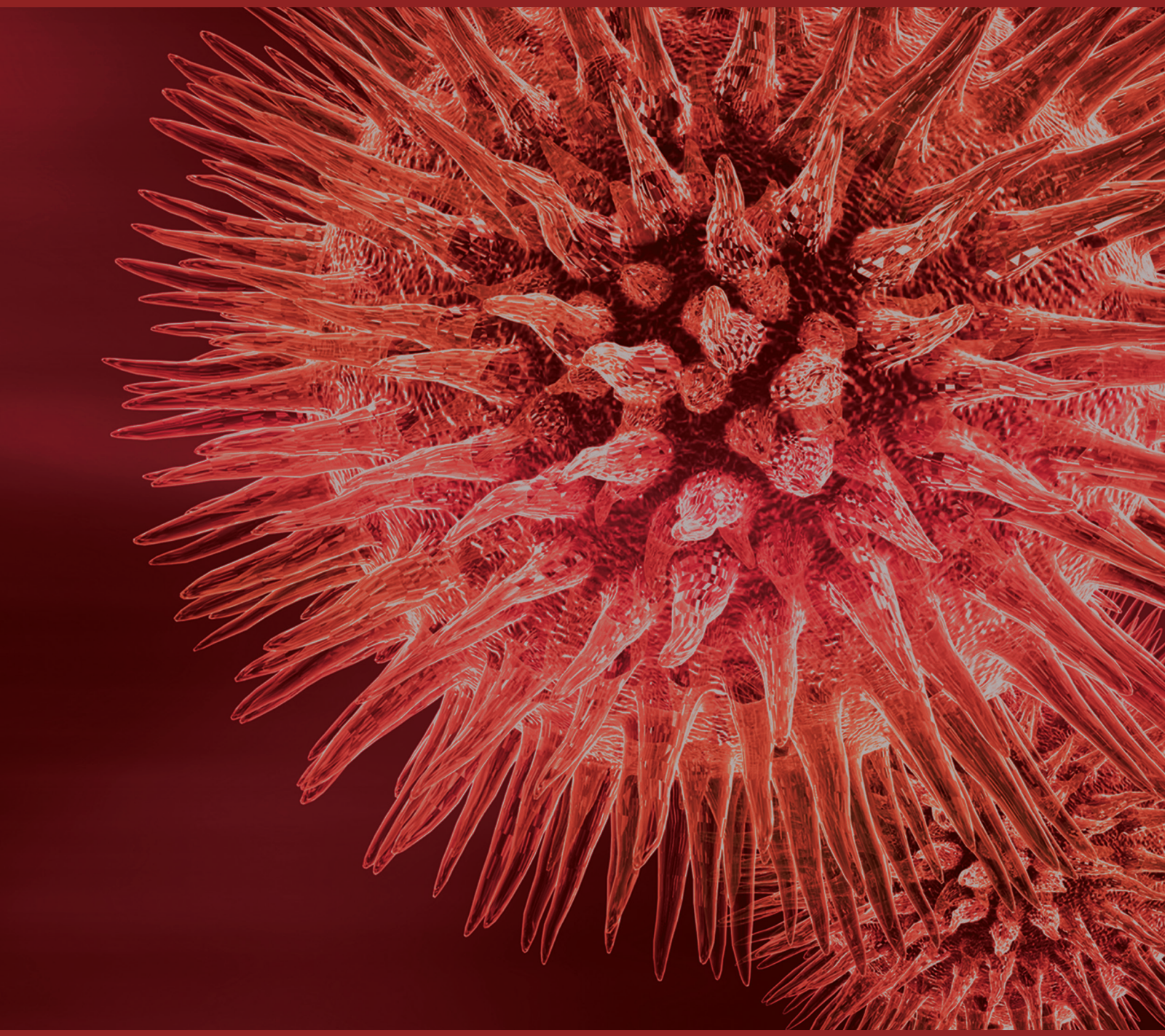

Anticancer Properties of Natural Products

BioMed Research International

Anticancer Properties of Natural Products

Guest Editors: István Zupkó, Walter Jaeger, Zeki Topcu, and Chin-Chung Wu

Contents

Hindawi Publishing Corporation
BioMed Research International
Volume 2015, Article ID 242070, 2 pages
http://dx.doi.org/10.1155/2015/242070

Editorial

Anticancer Properties of Natural Products

István Zupkó,[1] Walter Jaeger,[2] Zeki Topcu,[3] and Chin-Chung Wu[4]

[1]*Department of Pharmacodynamics and Biopharmacy, Faculty of Pharmacy, University of Szeged, Szeged 6720, Hungary*
[2]*Department of Clinical Pharmacy and Diagnostics and Faculty Center of Pharmaceutical Sciences, University of Vienna, 1090 Vienna, Austria*
[3]*Department of Pharmaceutical Biotechnology, Faculty of Pharmacy, Ege University, 35100 Izmir, Turkey*
[4]*Graduate Institute of Natural Products, College of Pharmacy, Kaohsiung Medical University, Kaohsiung 80708, Taiwan*

Correspondence should be addressed to István Zupkó; zupko@pharm.u-szeged.hu

Received 8 April 2015; Accepted 8 April 2015

Although natural products have been used by man since ancient times, it was only in the past century that active components of medicinal plants became available in chemically pure form. An impressive number of natural products have been introduced into medical practice and also used as lead or model molecules for structure optimization and for the development of more potent or better-tolerated drugs. A recent comprehensive review found that only 20.2% of the anticancer agents approved in the period 1981–2010 were purely synthetic, whereas the remaining 79.8% were natural products or inspired by natural products (D. J. Newman and G. M. Cragg, "Natural products as sources of new drugs over the 30 years from 1981 to 2010" Journal of Natural Products, vol. 75, no. 3, pp. 311–335, 2012), indicating that structures from nature are indispensable in anticancer lead-finding research.

In this special issue, we present a set of original research papers concerning various aspects of the antiproliferative properties of plant extracts or isolated natural products. Three of them describe investigations with promising extracts. The methanolic root extract of *Sclerocarya birrea* gave rise to oxidative stress and apoptosis in HepG2 cells (M. F. Armentano et al.). Fractions of the methanolic extract of *Croton sphaerogynus* exhibited antiproliferative activity against adherent cancer cell lines (K. P. dos Santos et al.). The mechanism of the anticancer action of the ethyl acetate extract of the traditional Chinese medicinal plant *Euphorbia helioscopia* was explored through the use of a hepatocellular carcinoma xenograft model in nude mice. The treatment with the extract resulted in apoptosis induction, decreased tumor growth, and invasion (J. Cheng et al.). Two papers in this issue concentrate on the isolation and subsequent investigation of natural products. Various antiproliferative xanthones were isolated from *Garcinia* species and two of them directly inhibited JAK kinase (L. Xu et al.). The natural products hamigerone and radicinol, isolated from fungi by means of a bioassay-guided procedure, exhibited antiproliferative and proapoptotic properties in adherent cancer cell lines without affecting the viability of normal cells (P. Giridharan et al.). Two further publications deal with previously identified compounds that were earlier not investigated in detail oncopharmacologically. Vitamin K1 displays antiproliferative activity, causes cell cycle arrest, and induces apoptosis in human colon cancer cell lines (A. Orlando et al.). The sesterterpene heteronemin exerted considerable growth-inhibiting activity against human cancer cell lines, including A498 renal carcinoma cells, resulting in apoptosis through the mitochondrial pathway and also autophagy in A498 cells (S.-Y. Wu et al.). Two papers describe potentially relevant interactions between natural products and therapeutically utilized anticancer agents. Curcumin and one of its analogues exhibited additive properties with the proteasome inhibitor bortezomib against HL60 cells (L. I. Nagy et al.). Three ecdysteroids sensitized both multidrug-resistant and non-resistant adherent cell lines towards traditional anticancer agents, including doxorubicin (A. Martins et al.). One of the presented papers reports on the validation of an *in vitro* method for the screening of potential anticancer extracts or compounds. Instead of the use of cultured cancer cell lines, slices of breast cancer tissues obtained from surgery were

incubated with antiproliferative agents and the viabilities of the slices were determined (I. E. Carranza-Torres et al.).

We strongly trust that these publications in this special issue will contribute to the development of natural product-based and innovative drug candidates.

Acknowledgments

Finally, we wish to thank the authors for their contributions to this special issue and the reviewers for their valuable work.

István Zupkó
Walter Jaeger
Zeki Topcu
Chin-Chung Wu

Hindawi Publishing Corporation
BioMed Research International
Volume 2015, Article ID 910453, 10 pages
http://dx.doi.org/10.1155/2015/910453

Research Article

Screening Active Compounds from *Garcinia* Species Native to China Reveals Novel Compounds Targeting the STAT/JAK Signaling Pathway

Linfeng Xu,[1,2,3] Yuanzhi Lao,[1,2] Yanhui Zhao,[3] Jian Qin,[3] Wenwei Fu,[1,2] Yingjia Zhang,[3] and Hongxi Xu[1,2]

[1]*School of Pharmacy, Shanghai University of Traditional Chinese Medicine, Shanghai 201203, China*
[2]*Engineering Research Center of Shanghai Colleges for TCM New Drug Discovery, Shanghai 201203, China*
[3]*Cell Biology Group of Shanghai Chempartner Ltd, Shanghai 201203, China*

Correspondence should be addressed to Hongxi Xu; xuhongxi88@gmail.com

Received 26 August 2014; Accepted 9 October 2014

Academic Editor: Zeki Topcu

Natural compounds from medicinal plants are important resources for drug development. In a panel of human tumor cells, we screened a library of the natural products from *Garcinia* species which have anticancer potential to identify new potential therapeutic leads and discovered that caged xanthones were highly effective at suppressing multiple cancer cell lines. Their anticancer activities mainly depended on apoptosis pathways. For compounds in sensitive cancer line, their mechanisms of mode of action were evaluated. 33-Hydroxyepigambogic acid and 35-hydroxyepigambogic acid exhibited about 1 μM IC50 values against JAK2/JAK3 kinases and less than 1 μM IC50 values against NCI-H1650 cell which autocrined IL-6. Thus these two compounds provided a new antitumor molecular scaffold. Our report describes 33-hydroxyepigambogic acid and 35-hydroxyepigambogic acid that inhibited NCI-H1650 cell growth by suppressing constitutive STAT3 activation via direct inhibition of JAK kinase activity.

1. Introduction

Compounds from natural herbs are important sources of drugs against a wide variety of diseases, including cancer [1]. For the last several decades, natural products have played a very important role as chemotherapeutic agents, either in their natural forms or in synthetically modified forms [2]. For instance, many agents with plant origins (paclitaxel, vinblastine, vincristine, camptothecin, and others) have already been applied as anticancer therapies. Natural compounds are considered to have a large degree of "drug likeness" because it has been suggested that most of them have some receptor-binding capability [3]. In addition, traditional Chinese medicine (TCM) provides an enormous variety of medicinal plants based on thousands of years of experience. With the understanding of the molecular mechanisms of cancer therapies and carcinogenesis, the development of chemotherapeutic agents from natural products is currently being accelerated by collaborations between medicinal chemists and biologists [4, 5].

In recent years, researchers obtained more than 120 caged xanthones from plantsof the *Garcinia* species, and most of them exhibited various potentially useful biological activities, such as anticancer, anti-HIV-1, antibacterial, anti-inflammatory, and neurotrophic activities [6]. Our group has focused on identifying bioactive compounds from *Garcinia* plants for a decade. We have collected all of the *Garcinia* plants in mainland China and used bioactivity-guided fractionation to obtain many active compounds [7]. We found that *Garcinia* species contained many special compounds, including xanthones, benzophenones, bioflavonoids, and biphenyls. By using different bioassay platforms, we were able to screen novel compounds targeting various signaling pathways. For example, a cell proliferation assay (such as SYBR green assay) identified some cytotoxic polyprenylated xanthones from the resin of *Garcinia hanburyi* [8].

By expressing a biosensor for caspase-3 cleavage in HeLa cells, we screened for compounds targeting apoptosis [9–11]. Recently, we found that oblongifolin C was an autophagic flux inhibitor using a GFP-LC3 expression screening platform [12]. In addition, we also found that the *Garcinia* species contained active compounds with antienteroviral activity [13]. Our previous studies suggested that the compound "libraries" from *Garcinia* plants comprised many active components with a variety of effects on cellular function. To better understand the antiproliferation activities of these compounds, it is necessary to perform a cell viability assay using multiple cell lines to establish their cytotoxicity. A screen using multiple cancer cell lines will provide essential information to elucidate the possible mechanisms of action of the active compounds.

In this study, we comprehensively analyzed the cytotoxicity of *Garcinia* compounds that we have obtained in previous studies. Among these compounds, five caged *Garcinia* xanthones were found to exhibit the strongest antiproliferation activity against NCI-H1650 cell. In addition, NCI-H1650 cell contained high endogenous JAKs activity. We then investigated their mechanisms of action on NCI-H1650 cell cycle arrest and apoptosis. Our results provided evidence that two of them (33-hydroxyepigambogic acid and 35-hydroxyepigambogic acid) were perhaps specific JAK2 and JAK3 inhibitors. Our data provide profound information on the anticancer activity of the main components from *Garcinia* plants.

2. Materials and Methods

2.1. Cell Panel Screen. All cells were obtained from the cell bank of the American Type Culture Collection (ATCC) and cultured in the supplier's recommended media supplemented with 10% FBS. The cell panel screen was measured using the CellTiter-Glo assay (Promega, Madison, WI) following a standard protocol. Briefly, cancer cells were seeded in 96-well plates and cultured overnight at 37°C with or without 5% CO_2 in an incubator. Each compound was dissolved with limited DMSO and diluted to a certain concentration with culture medium and then added to the corresponding well of the cell plate. The final concentration of compound was 20 μM. The control cells (without treatment) received the same amount of DMSO and were incubated under the same conditions. After 72 h cultivation, 100 μL of the CellTiter-Glo reagent was added directly to each well for 10-minute incubation. The plate was then read on a FlexStation 3 microplate luminometer (Molecular Devices, USA) to monitor the luminescence signal generated by the luciferase-catalyzed reaction of luciferin and ATP. The percent of growth inhibition was calculated using the following formula: (untreated cells − treated cells)/(untreated cells − background without cells) $*$ 100.

2.2. Cell Proliferation and Cell Viability Assay. For proliferation assays, the CellTiter-Glo assay (Promega, Madison, WI) was used to evaluate the proliferation of cancer cells treated with test compounds as described above. Each compound was dissolved in limited DMSO and diluted to various concentrations with culture medium and then added to the corresponding wells. A dose-response curve was plotted, and the IC50 was calculated using XLfit software.

For the cell viability assay, the cells were examined by counting (in duplicate) cells that excluded trypan blue dye. The cells were seeded in 6-well plates and cultured overnight at 37°C with 5% CO_2 in an incubator and treated with different concentrations of the compounds. At 0, 24, 48, and 72 hours, the live cells were counted using a Vi-Cell counter (Beckman).

2.3. Soft-Agar Colony Formation Assay. NCI-H1650 cells were plated in soft agar (Takara, Japan) at a density of 4000 cells/well in a 96-well plate. For the base layer, 1.2% agar stock solution was melted in an autoclave, cooled to 40°C in a water bath, and then mixed with RPMI1640 medium to obtain a solution of 0.6% agar in RPMI1640 containing 10% FBS. A cell suspension placed on the top layer was composed of RPMI1640 with 10% FBS and 0.4% agarose in each well. Then, the cells were incubated overnight. Compounds were added into the wells, and the NCI-H1650 cells were incubated for one week. After 7 days, alamar blue was added to the agar plate wells containing NCI-H1650 cell, and the plates were returned to the incubator. The fluorescence intensity (excitation 560 nm, emission 590 nm) was measured after 24 h.

2.4. Caspase-3/7 Activity Measurement. Caspase-3 and caspase-7 activities were examined using the Caspase-Glo 3/7 kits according to the manufacturer's protocol (Promega, Madison, WI). Briefly, cells were plated and grown overnight in 96-well plates (8×10^3 cells/well) and untreated or treated with compound for 8 or 24 h. The cells were then incubated with 100 μL of Caspase-Glo 3/7 reagent per well at room temperature for two hours. The caspase activity was determined by caspase substrate luminescence and recorded using a FlexStation 3 microplate luminometer (Molecular Devices, USA).

2.5. Cell Cycle Distribution Analysis. The cell cycle distribution was analyzed by flow cytometry (BD FACSCalibur, USA) with DNA staining. After treatment for 24 hours, cells were washed with phosphate buffered saline (PBS), trypsinized, and washed twice with ice-cold PBS and centrifugation at 800 g for 5 min. After overnight incubation with 70% ethanol at −20°C, the cells were washed twice with PBS. The cell pellets were resuspended gently in PBS containing 50 μg/mL of propidium iodide (PI) and 10 μg/mL of RNase A. The cells were incubated for 30 min in the dark and then the stained cells were analyzed using ModFit software.

2.6. Western Blot Analysis. Floating and adherent cells were harvested and treated with ice-cold RIPA lysis buffer (50 mM Tris-HCl, pH 7.5, 0.5% cholic acid, 2 mM EDTA, 10% glycerol, 150 mM NaCl, 0.1% SDS, and 1% Triton X-100) containing complete Mini Protease Inhibitor Cocktail (Roche Applied Science, Indianapolis, IN). Proteins were separated by sodium dodecyl sulfate polyacrylamide gel electrophoresis and transferred to nitrocellulose membranes. Membranes

were blocked with 5% BSA in washing buffer (100 mM NaCl, 10 mM Tris-HCl, pH 7.5, and 0.1% Tween-20) for 1 hr at room temperature and incubated with the respective primary antibodies in 5% BSA in washing buffer overnight at 4°C with shaking. The membranes were probed with the following antibodies: p44/42 (Cat#9107, CST), phospho-p44/42 (Cat#4370, CST), AKT (Cat#9272, CST), phospho-AKT (ser473) (Cat#9271, CST), STAT3 (Cat#9139, CST), and phospho-STAT3 (Tyr705) (Cat#9131, CST). Membranes were then washed and incubated with anti-mouse or anti-rabbit fluorescent secondary antibodies (LICOR, US) diluted in washing buffer for 1 h at room temperature with shaking. Protein bands were detected using an Odyssey Imaging system (LICOR, US).

2.7. RNA Isolation and Quantitative Real-Time PCR. The primers for PUMA (Cat. Hs00248075_m1), CDIP1 (Cat. Hs00924663_g1), and NOXA (Cat. Hs00560402_m1) for quantitative PCR were all purchased from Invitrogen. Dissociation curves and no-cDNA controls were generated for each primer pair to detect nonspecific amplification. A standard curve was generated for each primer pair as well as for glyceraldehyde-3-phosphate dehydrogenase (GAPDH; using in this case a predeveloped TaqMan assay), to which gene expression levels were normalized by a comparative threshold cycle method. Finally, a ratio was calculated comparing normalized gene expression values in treated versus untreated controls for each sample.

Total RNA was extracted from the NCI-H1650 cell line using the RNeasy kit (Qiagen). cDNA synthesis was performed using Superscript II RNase H– reverse transcriptase (Life Technologies, Bethesda, MD, USA) to transcribe 2 μg of total RNA primed with 1 μL of 500 μg/mL random hexamers. For quantitative real-time PCR analysis, an ABI TaqMan assay (HS00378697) was used in an ABI 7300 system with the following profile: 95°C for 10 min, followed by 40 cycles of 15 s at 95°C and 60 s at 60°C. PUMA, NOXA, and CDIP1 mRNA levels were normalized by comparison to GAPDH RNA levels in the same samples. Each measurement was performed at least in duplicate.

2.8. Apoptosis Induction Assay. Apoptosis induction assays were performed after 8 or 24 h incubation with compounds using the Cell Death Detection ELISA assay (Roche). Apoptosis induction is represented relative to DMSO-treated controls (set at 1.0). Error bars denote the SEM.

2.9. JAK Family Kinases Activity Measurement by Microfluidic Mobility Shift Enzyme Assay. The microfluidic mobility shift enzyme assay was performed in an on-chip incubation mode on a Caliper LabChip 2000 Drug Discovery System (Caliper Life Sciences, Hopkinton, MA). The extent of inhibition by the compounds is measured directly by quantifying the level of both unphosphorylated peptide substrate and phosphorylated product after electrophoretic separation using Caliper's LabChip assay technology. To evaluate the compounds for their target and the mechanism by which the compound affects JAK enzyme activity, the compounds were tested against JAK family kinases (JAK1, JAK2, JAK3, and Tyk2) with the Caliper microfluidic mobility-shift platform. The JAK family kinase enzymes and the FAM-labeled substrates were purchased from Carna Bioscience, Inc. (Japan) and Caliper Bioscience (US), respectively.

For JAK kinase activity measurement, the test compounds were diluted freshly with assay buffer (100 mM HEP ES, 10 mM $MgCl_2$, 1.5 mM betaine, 0.015% Brij, and 25 mM β-glycerophosphate) and added to 384-well plates. FAM-labeled peptide substrate and ATP in assay buffer were added to the wells. After that, JAK enzymes prepared in assay buffer were also added to the wells and mixed to start the reaction. After a period of incubation at room temperature, the reaction was stopped by stop solution (500 mM EDTA). Finally, the plate was put on a Caliper LabChip 2000 system and a droplet of the reaction mixture was applied for electrophoretic separation in the chips of the machine. The enzyme conversion data then was read out for analysis.

2.10. Compounds Library and Materials. All of the compounds were obtained from our laboratory and originated and isolated from the different plant parts of 8 species of the genus *Garcinia* (Guttiferae) collected from the south of China (see Table S1 in Supplementary Material available online at http://dx.doi.org/10.1155/2015/910453). All chemicals and consumables for experiments were purchased from Sigma-Aldrich. All of the media for cell culture were purchased from Invitrogen Life Sciences. The antibodies were ordered from Cell Signaling Technology. The enzymes and the FAM-labeled substrates were obtained from Carna Bioscience, Inc. (Japan).

3. Results and Discussion

3.1. Antiproliferation Properties of Natural Compounds Library from Garcinia Species. In current drug market, more than 50% of the drugs discovered within the past 25 years were directly or indirectly from natural products [14]. Thus, there is growing interest in the possible therapeutic potential of natural products against a variety of ailments. Because natural compounds are considered to be affordable and safe, many potential compounds are now in different phases of clinical trials. In the past decade, we focused on applying different screening platforms to search for novel anticancer compounds from *Garcinia* plants. The natural compound library mainly includes polycyclic polyprenylated acylphloroglucinols (PPAPs), benzophenones, xanthones, and caged xanthones [15]. In this study, we profiled all of the natural compounds that we isolated from *Garcinia* plants and placed in our compound library using cell viability-based screening.

The cytotoxicity of 64 *Garcinia* compounds (Table S1) from our previous studies was evaluated in panel of 35 cancer cell lines, which included lung, breast, urinary bladder, uterus, brain, liver, pancreas, stomach, colon, kidney, leukemia, and adrenal gland cancer cells. As shown in Table S2, many compounds showed strong antiproliferation activity against most of the cell lines. More than 20 compounds showed more than 90% inhibition of all of the tested cell lines at 20 μM. Notably, five caged xanthones exhibited strong cytotoxicity on all of the cell lines, which are highlighted

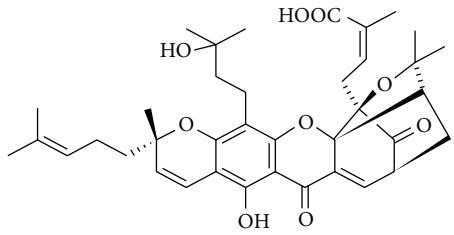

GB39 (33-hydroxyepigambogic acid)

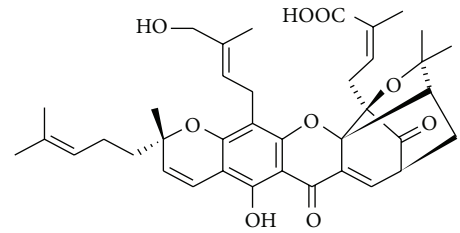

GB40 (35-hydroxyepigambogic acid)

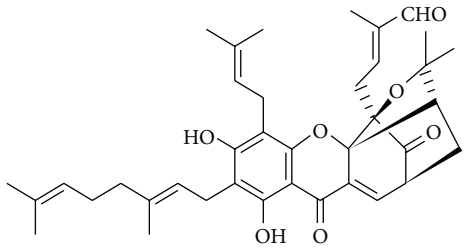

GB49 (isogambogenin)

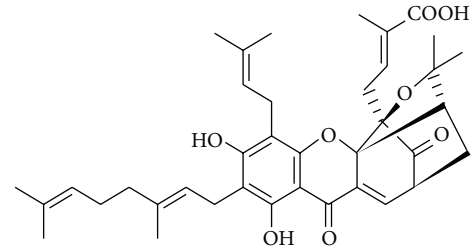

GB63 (isogambogenic acid)

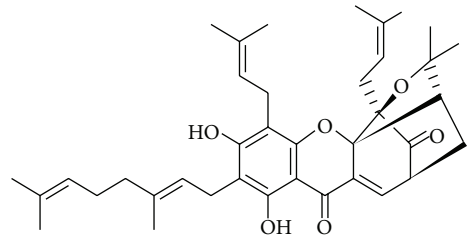

GB32 (desoxygambogenin)

Figure 1: The chemical structure of the five chosen compounds (GB32, GB39, GB40, GB49, and GB63).

in gray in Table S2. The structures of these compounds were elucidated in Figure 1. We then examined the IC50 values of these xanthones against thirteen cancer cell lines, including lung, brain, colon, vulva, skin, and bone cancer cells. From the data shown in Table 1, we found that all of the xanthone compounds exhibited high potency on all of the cancer lines, with IC50s less than 5 μM (except on H1573 cells). We noticed that the caged xanthones had the lowest IC50s against NCI-H1650 cells. It is notable that NCI-H1650 cells contained high STAT3 activity. In addition, gambogic acid, another caged xanthone, was able to inhibit STAT3 activation upon IL-6 treatment in multiple cancer cell lines [16]. We then intended to investigate if these caged xanthones were specific essential inhibitors for STAT signaling pathway. Therefore, NCI-H1650 cells were chosen for further studies of the effects of these compounds on viability and colony formation. For effects on viability, Figure 2(a) showed that 5 caged xanthone compounds inhibited the growth of NCI-H1650 cells in a time-dependent manner, which was assessed by a trypan blue exclusion assay. To measure the IC50s of these compounds, cell proliferation curves were generated using the CellTiter-Glo kit. NCI-H1650 cells were treated for 72 hr with compounds at concentrations ranging from 20 μM to 0.009 μM in serial 3-fold dilutions. The IC50s were less than 2 μM for all five compounds. In addition, these caged xanthones significantly suppressed the clonogenic activity of the cells (Figure 2(b)). Particularly, GB39 and GB40 were more potent than other three compounds in both cell growth and colony formation assays.

3.2. The Five Caged Xanthones Induce Caspase-Dependent Apoptosis and Cell Cycle Arrest in NCI-H1650 Cells. To determine whether the cell growth inhibition in response to the caged xanthones was mediated by apoptosis and was caspase dependent, NCI-H1650 cells were treated with 20, 6.66, 2.22, 0.74, and 0.24 μM of the five caged xanthones for 8 and 24 h. As shown in Figures 3(a) and 3(b), caspase-3/7 activity was activated in a dose-dependent manner. Caged xanthones significantly increased caspase-3/7 activity more than 10-fold at a certain concentration and time point. Because GB32,

Table 1: The IC50s for the chosen 5 compounds and reference compound (staurosporine) against the 13 cancer cell lines and the control HuVec cell line.

Cell	GB32	GB39	GB40	GB49	GB63	Staurosporine
NCI-H838	3.15 ± 0.04	1.5 ± 0.07	1.68 ± 0.19	2.72 ± 0.15	2.65 ± 0.2	0.011 ± 0.004
A549	2.88 ± 0.06	3.04 ± 0.1	2.45 ± 0.06	3.46 ± 0.2	3.77 ± 0.06	0.008 ± 0.002
NCI-H1573	4.36 ± 0.15	6.08 ± 0.21	5.99 ± 0.19	7.89 ± 0.14	7.92 ± 0.29	0.039 ± 0.01
NCI-H1975	1.58 ± 0.12	1.25 ± 0.14	0.96 ± 0.05	1.69 ± 0.15	1.71 ± 0.22	0.002 ± 0.001
NCI-H1993	2.47 ± 0.11	1.03 ± 0.13	1.29 ± 0.05	2.55 ± 0.14	2.15 ± 0.1	0.021 ± 0.007
NCI-H1650	**1.09 ± 0.15**	**0.95 ± 0.03**	**0.62 ± 0.03**	**0.97 ± 0.04**	**1.43 ± 0.09**	**0.022 ± 0.004**
CHP212	1.45 ± 0.08	1.2 ± 0.08	1.18 ± 0.05	1.43 ± 0.03	3.51 ± 0.08	0.004 ± 0.001
U118MG	1.19 ± 0.07	1.15 ± 0.09	1.03 ± 0.15	1.22 ± 0.05	3.05 ± 0.1	0.003 ± 0.001
SW48	3.84 ± 0.09	1.44 ± 0.06	1.47 ± 0.1	2.97 ± 0.06	4.02 ± 0.15	0.025 ± 0.003
LnCap	1.8 ± 0.14	0.84 ± 0.08	0.79 ± 0.12	1.91 ± 0.06	2.17 ± 0.21	0.061 ± 0.009
SW954	2.43 ± 0.17	0.94 ± 0.04	1.02 ± 0.1	1.88 ± 0.1	2.58 ± 0.16	0.006 ± 0.001
SK-MEL-28	1.51 ± 0.07	0.82 ± 0.11	0.73 ± 0.21	1.51 ± 0.12	1.75 ± 0.16	0.37 ± 0.058
SW1353	1.41 ± 0.05	0.76 ± 0.03	0.83 ± 0.05	1.29 ± 0.05	2.48 ± 0.11	0.004 ± 0.001
HuVec	1.63 ± 0.06	0.89 ± 0.09	0.68 ± 0.01	1.47 ± 0.07	1.9 ± 0.03	0.004 ± 0.002

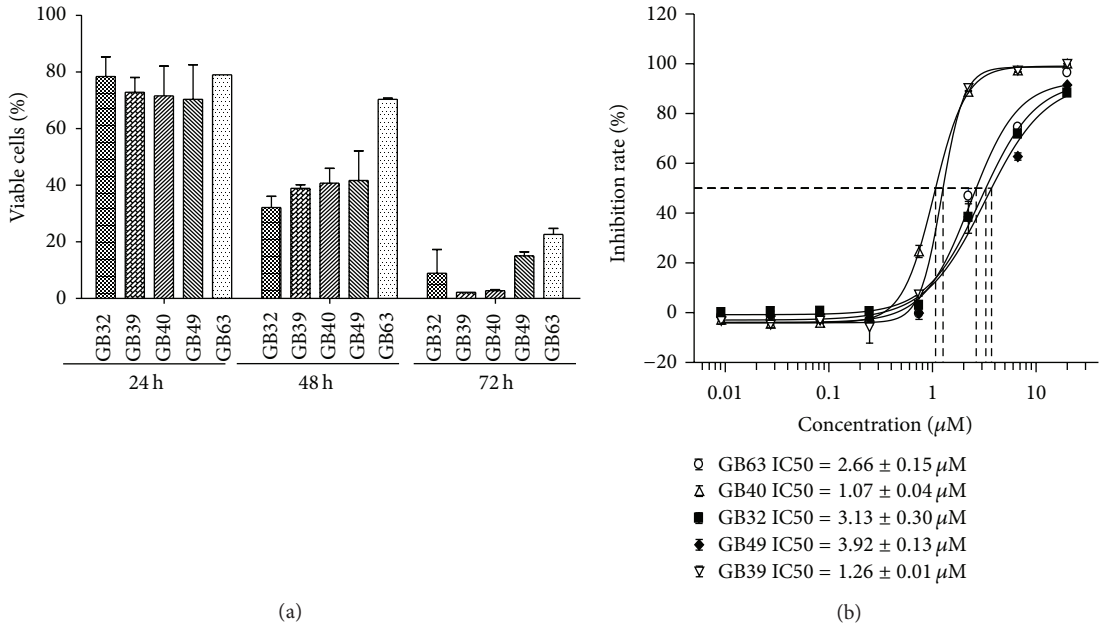

Figure 2: The inhibition effect of the five chosen compounds (GB32, GB39, GB40, GB49, and GB63) on NCI-H1650 cells. (a) Inhibitory effects of compounds on the viability of NCI-H1650 cells assayed by trypan blue exclusion. Cells were treated for 24, 48, and 72 hr, and the viable cells were identified by trypan blue exclusion and counted. The IC50 values were calculated using XLfit software and a four-parameter model. NCI-H1650 cells were treated for 72 hr with compounds at concentrations ranging from 20 μM to 0.009 μM in serial 3-fold dilutions. (b) Cell colony formation curve after compound treatment measured using the Alamar Blue reagent from Invitrogen. The IC50 values were calculated using XLfit software and a four-parameter model.

GB39, and GB40 showed more potency after 8-hour treatment, we chose these three compounds for confirmation of their apoptotic effect using an ELISA-based assay (Cell Death Analysis kit, Roche). This photometric assay measured the histone-associated DNA fragments that are released during apoptotic cell death. We found that the majority (>90%) of NCI-H1650 cells treated with GB39 or GB40 underwent rapid apoptosis after 8 h, but GB32 showed significant apoptosis after 24 h (Figures 3(c) and 3(d)). To further confirm the apoptosis induction by these compounds, we applied a pan-caspase inhibitor (Z-VAD) to investigate whether Z-VAD could rescue the cells from death. As shown in Figure 3(e), Z-VAD cotreatment completely suppressed GB32-, GB39-, and GB40-induced oligonucleosomal fragmentation, suggesting that these caged xanthones caused caspase-dependent cell death. In addition, cell necrosis was not detected at any of the tested concentrations (data not shown), indicating that apoptosis is the predominant mechanism of cell death. In

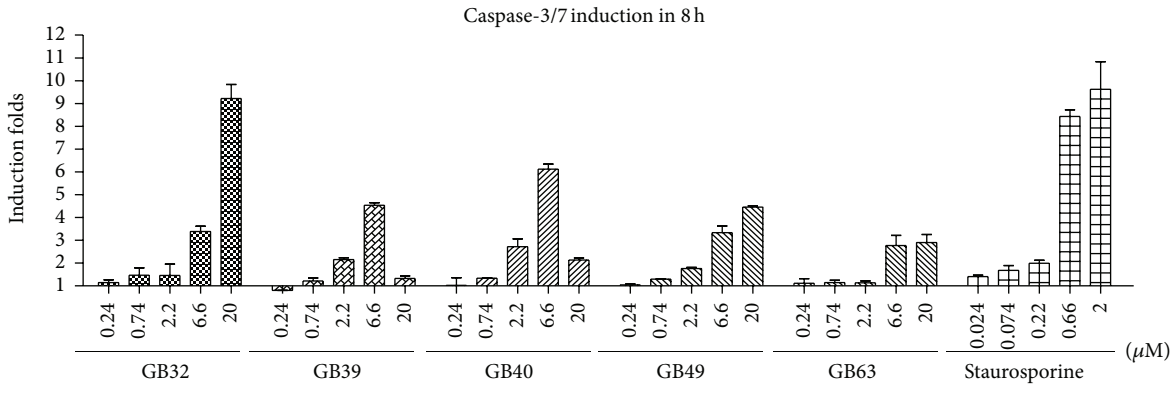

(a)

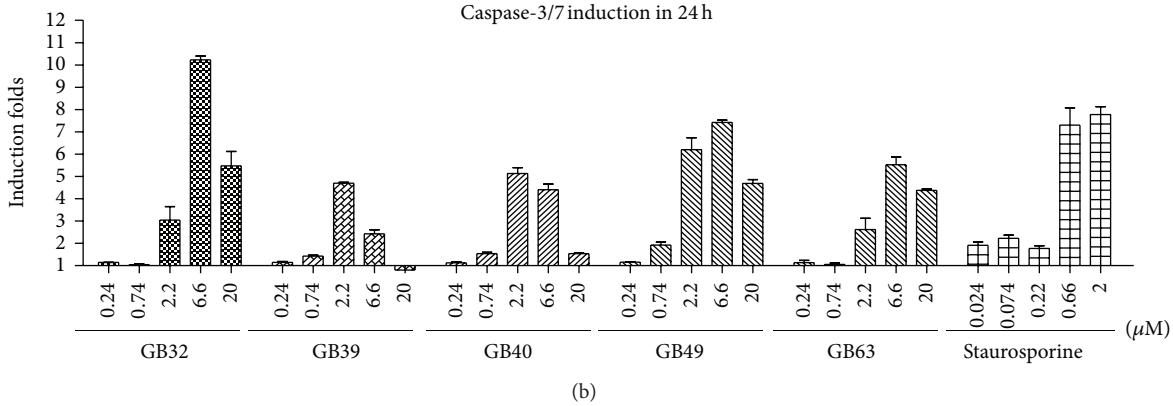

(b)

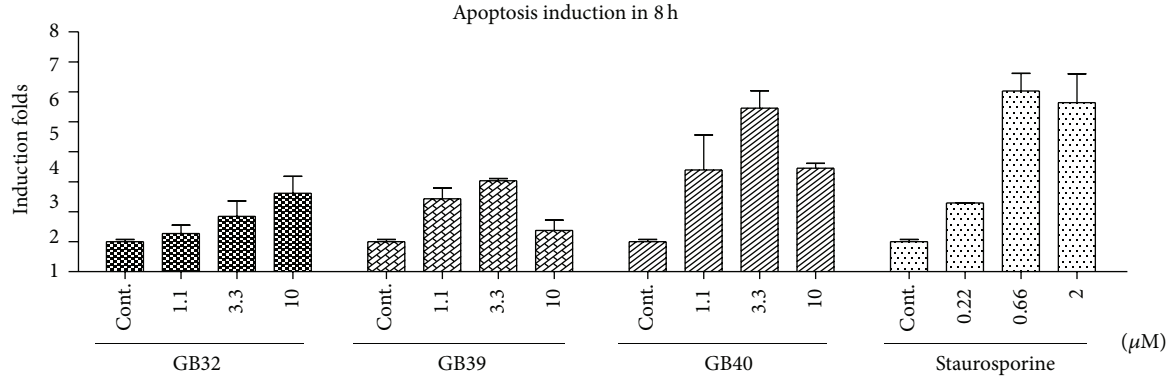

(c)

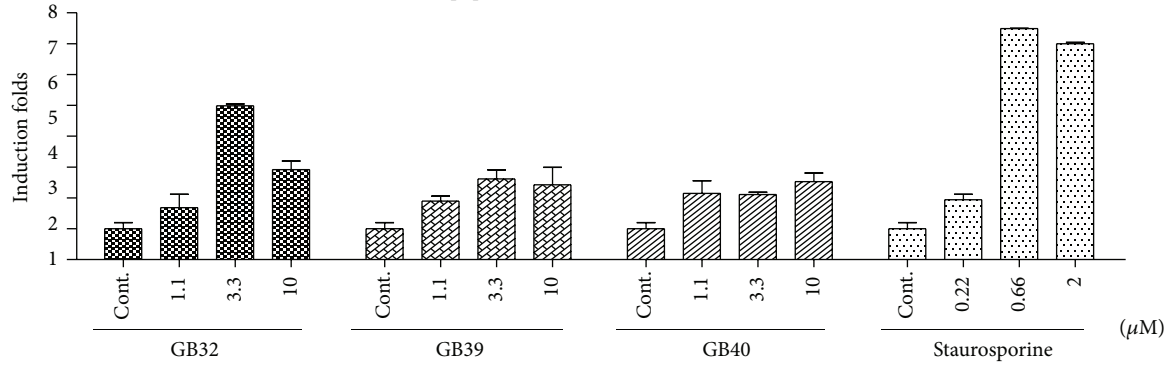

(d)

Figure 3: Continued.

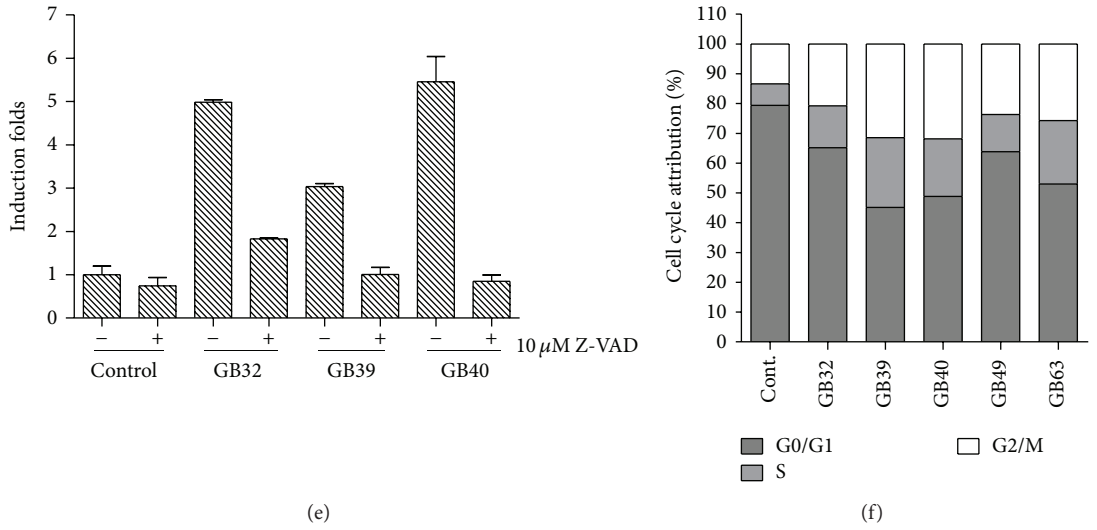

Figure 3: Caspase-3/7 induction and apoptosis induction by cell death detection in NCI-H1650 cells after compound treatment. (a) and (b) Caspase-3/7 activity induction was evaluated after 8 and 24 hr of treatment with the five compounds (GB32, GB39, GB40, GB49, and GB63) using Caspase-Glo 3/7 kit from Promega. Bars on the graph represent the mean fold induction relative to the DMSO control. (c) and (d) Apoptosis induction of cell lysate was assessed by oligonucleosomal fragmentation after 8-hour and 24-hour incubation with treatment compounds (GB32, GB39, and GB40). Data are shown relative to DMSO controls set at 1.0 ± SEM. (e) Apoptosis induction in NCI-H1650 cells by GB32, GB39, and GB40 was assessed ± the caspase inhibitor Z-VAD (10 μmol/L). The maximal apoptosis induction for each compound was chosen for the assessment of apoptosis reversal by Z-VAD. Data are shown relative to DMSO controls set at 1.0 ± SEM. (f) Compounds induced accumulation of G2 phase cells. NCI-H1650 cells were treated with 2.5 μM of each compound for 16 h. The cells were harvested, fixed in 70% EtOH, and stained with PI. The cell cycle was detected by FACS.

the above experiments, the treatment for 24 h sometimes caused the decreased induction of caspase-3/7 and apoptosis (Figures 3(b) and 3(d)). It might due to the apoptosis occurring in the early time point so that there was less amount of cells in the 24 h.

To examine whether the inhibitory effect on proliferation is caused by cell cycle arrest, we used propidium iodide (PI) staining and flow cytometry to analyze the cell cycle. NCI-H1650 cells were treated with the five compounds for 24 hours at 2 μM. A persistent accumulation of S or G2/M phase cells was observed, as shown in Figure 3(f). Taken together, our results suggested that these caged xanthones inhibited cell growth by inducing caspase-dependent apoptosis and cell cycle arrest.

3.3. The Caged Xanthones Activate Proapoptotic BH3-Only Genes. Global analysis of gene expression has yielded numerous novel transcriptional target genes, including some with clear proapoptotic properties, such as the BH3-only proteins BBC3/PUMA [17, 18], PMAIP1/NOXA [19], and CDIP [20].

Quantitative real-time reverse transcription-PCR confirmed that these proapoptotic genes (PUMA, NOXA, and CDIP) were upregulated preferentially in GB39- and GB40-treated NCI-H1650 cells. As shown in Figure 4(a), there was greater than 5-fold induction of NOXA for GB39 and GB40 treatment, 3-fold induction of PUMA and CIDP for GB39, and 2-fold induction of PUMA and CIDP following 24-hour treatment of NCI-H1650 cells with GB40. On the contrary, treatment with GB32, GB49, or GB63 had no effect on these three proapoptotic genes in NCI-H1650 cells.

3.4. Caged Xanthones Inhibit the JAK-STAT3 Signaling Pathway in Cancer Cells. Several studies have demonstrated that STAT3 is required for efficient cellular transformation by oncogenes including Ras, v-Src, SV40 T antigen, and EGFR, further validating the importance of STAT3 in cancer biology [21–25]. STAT3 is both a cytoplasmic signaling molecule and a nuclear transcription factor that is activated by the phosphorylation of specific tyrosine residue in its carboxyl-terminus by JAK kinases in response to cytokines, including IL-6, IFN, epidermal growth factor, and FGF [26, 27]. In the nucleus, STAT3 regulates the expression of the proteins that regulate mitochondria-mediated apoptosis, such as Bcl-2, Mcl-1, and cIAP [28]. The STAT3 tyrosine phosphorylation in malignancies is activated via increased/sustained IL-6 (family)/gp130 signaling [29, 30]. The other "oncogenic" pathways, such as those mediated by EGFR, HER2, Ras, and Rho, can also result in increased IL-6 production and subsequent STAT3 activation [31–33]. STAT3 is activated in lung adenocarcinomas through a mutant EGFR regulating the expression of the IL-6 cytokine, which, in turn, activates the gp130/JAK pathway. NCI-H1650 is a lung adenocarcinoma cell, in which a mutant EGFR regulates the expression of the IL-6 cytokine and leads to the activation of JAK/STAT3 pathway.

NCI-H1650 cancer cells contain an EGFR mutant and a constitutively high level of STAT3 phosphorylation. We then investigated whether the caged xanthones induced apoptosis via modulation of the JAK-STAT3 signaling pathway [34]. We evaluated the protein level of STAT3 and the phosphorylation level of STAT3 at Tyr705. Figure 4(b) shows that GB39 and

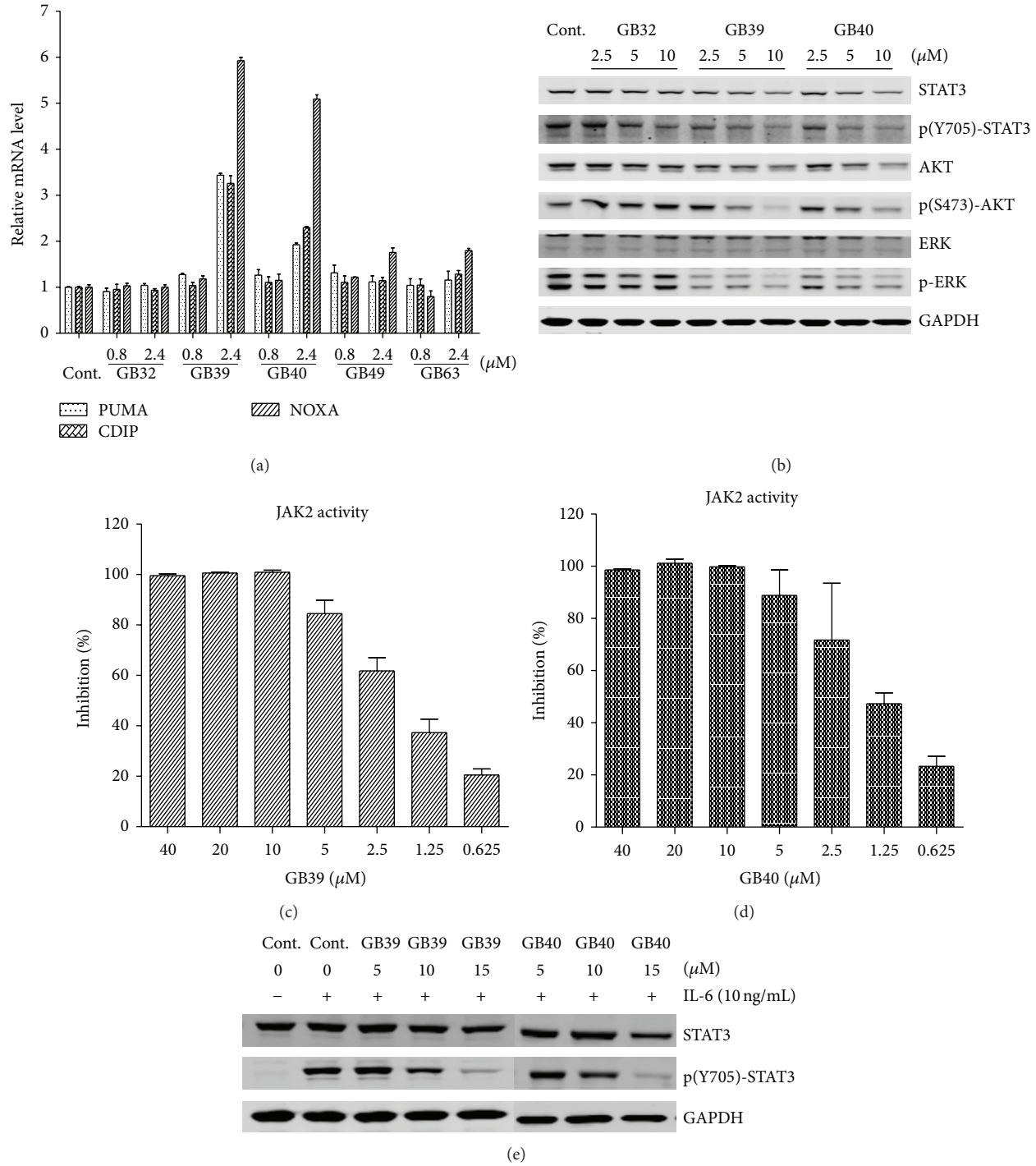

Figure 4: Assessing the mechanism of apoptosis induction for the compounds. (a) mRNA expression level of proapoptotic genes after treatment. NCI-H1650 cells were treated with different concentrations of each compound for 24 hr. Cells were harvested for RNA extraction. Q-PCR was performed by the TaqMan method on total RNA using primers specific for the PUMA, NOXA, and CDIP genes. (b) Immunoblot demonstrating the effect of GB32, GB39, and GB40 treatment on ERK, AKT, and STAT3 in NCI-H1650 cells. Treatment compounds were incubated for 8 h, and then whole cell lysates were processed for western blot analysis. Immunoblots were probed with the indicated antibodies. GAPDH served as a loading control. (c) GB39 significantly inhibits JAK2 of JAK family in a dose-dependent manner. After compound and substrates were added, the enzyme reaction was initiated by adding JAK2 enzyme and incubated for 2 hours. The reaction was then stopped, and the signal was detected using a Caliper LabChip 2000 plate reader. (d) GB40 significantly inhibits JAK2 of JAK family in a dose-dependent manner. After compound and substrates were added, the enzyme reaction was initiated by adding JAK2 enzyme and incubating for 2 hours. The reaction was then stopped, and the signal was detected using a Caliper LabChip 2000 plate reader. (e) HepG2 cells were pretreated with GB39 and GB40 for 2 h before stimulation by IL-6 (10 ng/mL) for 15 min. Whole cell lysates were processed for western blot analysis, and immunoblots were probed with the indicated antibodies. GAPDH served as a loading control.

Table 2: The IC50s for GB32, GB39, and GB40 against the JAK1, JAK2, JAK3, and Tyk2 enzymes.

IC50 [μM]	GB32	GB39	GB40
JAK1	>40	12.2 ± 0.3	14.2 ± 0.4
JAK2	37.3 ± 6.9	1.7 ± 0.1	1.4 ± 0.1
JAK3	17.5 ± 1.5	3.8 ± 0.3	3.2 ± 0.2
Tyk2	>40	13 ± 1.6	12.9 ± 0.9

GB40 inhibited STAT3 expression and its phosphorylation in a dose-dependent manner. We further examined the other components involved in the STAT3 signaling pathway. Phosphorylation of ERK and AKT was also inhibited by GB39 and GB40, which confirmed that these two caged xanthones could regulate the STAT3 pathway.

STAT3 has been reported to be activated by soluble tyrosine kinases of the JAK family, and the phosphorylation of STAT3 at residue Tyr705 is mediated by receptor-associated tyrosine kinases, such as JAKs. We therefore examined the activity of these compounds against commercial, recombinant JAK enzymes (TYK2, JAK1, JAK2, and JAK3) using an enzymatic test. As shown in Table 2, GB32, GB39, and GB40 exhibited different inhibitory activities on the JAK family enzymes. GB39 and GB40 showed stronger inhibition and lower IC50 against JAK2/JAK3. Particularly, these two compounds are the more potent against JAK2 (IC50 value of approximately 1 μM) than against the other three Jak kinases. A 10-fold difference in IC50s was observed between JAK2 and Tyk2 for GB39 and GB40. Figures 4(c) and 4(d) show the dose-dependent inhibition of JAK2 activity by GB39 and GB40, respectively. These data suggested that GB39 and GB40 directly inhibited the catalytic activity, especially that of JAK2, and the inhibition of JAK family enzymes leads to the blockade of phosphorylation of STAT3. Meanwhile, GB32 only showed minor inhibition of JAK2/JAK3 and had no effect on TYK2/JAK1. In addition, we examined the effects of GB39 and GB40 on IL-6-stimulated STAT3 activation. As shown in Figure 4(e), these two compounds efficiently suppressed the phosphorylation of STAT3 upon IL-6 stimulation in HepG2 cells. Our study indicated that GB39 and GB40 were identified as potent inhibitors of the JAK/STAT3 signaling pathway. In addition, the direct targets of GB39 and GB40 were discovered to be JAK2 and JAK3. GB39 and GB40 significantly inhibited JAK2/ JAK3 kinase activities, and the Y705 site in STAT3 was not phosphorylated after GB39 and GB40 treatment. Furthermore, the inhibitory effects of GB39 and GB40 on JAK kinase activities were JAK2/3-specific. GB39 and GB40 had minor inhibitory effects on JAK1/Tyk2 (Table 2), which indicated that GB39 and GB40 have the potential to be JAK/STAT3 signaling pathway-specific inhibitors. Interestingly, we also detected the similar inhibitory effects on STAT3 phosphorylation of gambogic acid, a caged xanthone, on both NCI-H1650 and HepG2 cells (Supplement Figures S1(A) and S1(B)). Taken together, our results indicated that the caged xanthones family could inhibit STAT3 activation through suppressing JAKs activities. Therefore, it will be promising to develop specific JAKs inhibitors from the large amount of natural caged xanthones. Alternatively, the caged xanthones might also be used to combine treatment with other anticancer agents to show synergetic antitumor effects.

4. Conclusions

Overall, our study suggested that caged xanthones exhibited strong anticancer activity on a panel of cancer cell lines, especially those whose survival and growth are dependent on constitutively active STAT3 signaling. We discovered that GB39 and GB40, two natural caged xanthones, were potent inhibitors of the JAK/STAT3 signaling pathway. GB39 and GB40 suppressed constitutive STAT3 activation by direct inhibition of JAK kinase activity. Finally, our results suggested that two caged xanthones were JAK2 kinase inhibitors and were potentially worth developing as novel anticancer drugs. Future studies will focus on evaluating the antitumor activities of GB39 and GB40 in animal models.

Abbreviations

GA: Gambogic acid
IL-6: Interleukin 6
PI: Propidium iodide
STAT: Signal transducer of activator of transcription
PPAPs: Polycyclic polyprenylated acylphloroglucinols.

Conflict of Interests

The authors declare that there is no conflict of interests regarding the publication of this paper.

Authors' Contribution

Linfeng Xu and Yuanzhi Lao contributed equally to this work.

Acknowledgments

This work was supported by the National Natural Science Foundation of China (no. 81273403 and no. 81173485) and Engineering Research Center of Shanghai Colleges for Drug Discovery from TCM (no. GCZX14012). The authors are grateful to Ying Kong, Jianan Qian, and Zhen Wang for their technical assistance.

References

[1] D. J. Newman and G. M. Cragg, "Natural products as sources of new drugs over the 30 years from 1981 to 2010," *Journal of Natural Products*, vol. 75, no. 3, pp. 311–335, 2012.

[2] A. D. Kinghorn, Y. W. Chin, and S. M. Swanson, "Discovery of natural product anticancer agents from biodiverse organisms," *Current Opinion in Drug Discovery and Development*, vol. 12, no. 2, pp. 189–196, 2009.

[3] M. Feher and J. M. Schmidt, "Property distributions: Differences between drugs, natural products, and molecules from combinatorial chemistry," *Journal of Chemical Information and Computer Sciences*, vol. 43, no. 1, pp. 218–227, 2003.

[4] D. Hanahan and R. A. Weinberg, "Hallmarks of cancer: the next generation," *Cell*, vol. 144, no. 5, pp. 646–674, 2011.

[5] K.-H. Lee, "Discovery and development of natural product-derived chemotherapeutic agents based on a medicinal chemistry approach," *Journal of Natural Products*, vol. 73, no. 3, pp. 500–516, 2010.

[6] N. Anantachoke, P. Tuchinda, C. Kuhakarn, M. Pohmakotr, and V. Reutrakul, "Prenylated caged xanthones: chemistry and biology," *Pharmaceutical Biology*, vol. 50, no. 1, pp. 78–91, 2012.

[7] W.-W. Fu, H.-S. Tan, and H.-X. Xu, "Research progress of chemistry and anti-cancer activities of natural products from Chinese garcinia plants," *Yao Xue Xue Bao*, vol. 49, no. 2, pp. 166–174, 2014.

[8] Q.-B. Han, Y.-L. Wang, L. Yang et al., "Cytotoxic polyprenylated xanthones from the resin of *Garcinia hanburyi*," *Chemical and Pharmaceutical Bulletin*, vol. 54, no. 2, pp. 265–267, 2006.

[9] S. X. Huang, C. Feng, Y. Zhou et al., "Bioassay-guided isolation of xanthones and polycyclic prenylated acylphloroglucinols from Garcinia oblongifolia," *Journal of Natural Products*, vol. 72, no. 1, pp. 130–135, 2009.

[10] X.-M. Gao, T. Yu, F. S. F. Lai et al., "Identification and evaluation of apoptotic compounds from *Garcinia paucinervis*," *Bioorganic & Medicinal Chemistry*, vol. 18, no. 14, pp. 4957–4964, 2010.

[11] X. Liu, T. Yu, X. M. Gao et al., "Apoptotic effects of polyprenylated benzoylphloroglucinol derivatives from the twigs of garcinia multiflora," *Journal of Natural Products*, vol. 73, no. 8, pp. 1355–1359, 2010.

[12] Y. Lao, G. Wan, Z. Liu et al., "The natural compound oblongifolin C inhibits autophagic flux and enhances antitumor efficacy of nutrient deprivation," *Autophagy*, vol. 10, no. 5, pp. 736–749, 2014.

[13] H. Zhang, L. Tao, W.-W. Fu et al., "Prenylated benzoylphloroglucinols and xanthones from the leaves of *Garcinia oblongifolia* with antienteroviral activity," *Journal of Natural Products*, vol. 77, no. 4, pp. 1037–1046, 2014.

[14] D. J. Newman, "Natural products as leads to potential drugs: an old process or the new hope for drug discovery?" *Journal of Medicinal Chemistry*, vol. 51, no. 9, pp. 2589–2599, 2008.

[15] Q. B. Han and H. X. Xu, "Caged Garcinia xanthones: development since 1937," *Current Medicinal Chemistry*, vol. 16, no. 28, pp. 3775–3796, 2009.

[16] S. Prasad, M. K. Pandey, V. R. Yadav, and B. B. Aggarwal, "Gambogic acid inhibits STAT3 phosphorylation through activation of protein tyrosine phosphatase SHP-1: potential role in proliferation and apoptosis," *Cancer Prevention Research*, vol. 4, no. 7, pp. 1084–1094, 2011.

[17] K. Nakano and K. H. Vousden, "PUMA, a novel proapoptotic gene, is induced by p53," *Molecular Cell*, vol. 7, no. 3, pp. 683–694, 2001.

[18] J. Yu, L. Zhang, P. M. Hwang, K. W. Kinzler, and B. Vogelstein, "PUMA induces the rapid apoptosis of colorectal cancer cells," *Molecular Cell*, vol. 7, no. 3, pp. 673–682, 2001.

[19] E. Oda, R. Ohki, H. Murasawa et al., "Noxa, a BH3-only member of the Bcl-2 family and candidate mediator of p53-induced apoptosis," *Science*, vol. 288, no. 5468, pp. 1053–1058, 2000.

[20] L. Brown, P. P. Ongusaha, H. G. Kim et al., "CDIP, a novel pro-apoptotic gene, regulates TNFα-mediated apoptosis in a p53-dependent manner," *The EMBO Journal*, vol. 26, no. 14, pp. 3410–3422, 2007.

[21] K. Leslie, S. P. Gao, M. Berishaj et al., "Differential interleukin-6/Stat3 signaling as a function of cellular context mediates Ras-induced transformation," *Breast Cancer Research*, vol. 12, no. 5, p. R80, 2010.

[22] J. F. Bromberg, C. M. Horvath, D. Besser, W. W. Lathem, and J. E. Darnell Jr., "Stat3 activation is required for cellular transformation by v-src," *Molecular & Cellular Biology*, vol. 18, no. 5, pp. 2553–2558, 1998.

[23] A. Vultur, R. Arulanandam, J. Turkson, G. Niu, R. Jove, and L. Raptis, "Stat3 is required for full neoplastic transformation by the Simian Virus 40 large tumor antigen," *Molecular Biology of the Cell*, vol. 16, no. 8, pp. 3832–3846, 2005.

[24] J. V. Alvarez, H. Greulich, W. R. Sellers, M. Meyerson, and D. A. Frank, "Signal transducer and activator of transcription 3 is required for the oncogenic effects of non-small-cell lung cancer-associated mutations of the epidermal growth factor receptor," *Cancer Research*, vol. 66, no. 6, pp. 3162–3168, 2006.

[25] R. Chiarle, W. J. Simmons, H. Cai et al., "Stat3 is required for ALK-mediated lymphomagenesis and provides a possible therapeutic target," *Nature Medicine*, vol. 11, no. 6, pp. 623–629, 2005.

[26] D. E. Levy and J. E. Darnell Jr., "STATs: transcriptional control and biological impact," *Nature Reviews Molecular Cell Biology*, vol. 3, no. 9, pp. 651–662, 2002.

[27] J. Bromberg and T. C. Wang, "Inflammation and cancer: IL-6 and STAT3 complete the link," *Cancer Cell*, vol. 15, no. 2, pp. 79–80, 2009.

[28] S. Bhattacharya, R. M. Ray, and L. R. Johnson, "STAT3-mediated transcription of Bcl-2, Mcl-1 and C-IAP2 prevents apoptosis in polyamine-depleted cells," *Biochemical Journal*, vol. 392, part 2, pp. 335–344, 2005.

[29] M. Berishaj, S. P. Gao, S. Ahmed et al., "Stat3 is tyrosine-phosphorylated through the interleukin-6/glycoprotein 130/Janus kinase pathway in breast cancer," *Breast Cancer Research*, vol. 9, no. 3, article R32, 2007.

[30] Z. T. Schafer and J. S. Brugge, "IL-6 involvement in epithelial cancers," *Journal of Clinical Investigation*, vol. 117, no. 12, pp. 3660–3663, 2007.

[31] B. Ancrile, K.-H. Lim, and C. M. Counter, "Oncogenic Ras-induced secretion of IL6 is required for tumorigenesis," *Genes & Development*, vol. 21, no. 14, pp. 1714–1719, 2007.

[32] S. P. Gao, K. G. Mark, K. Leslie et al., "Mutations in the EGFR kinase domain mediate STAT3 activation via IL-6 production in human lung adenocarcinomas," *The Journal of Clinical Investigation*, vol. 117, no. 12, pp. 3846–3856, 2007.

[33] V. Sriuranpong, J. I. Park, P. Amornphimoltham, V. Patel, B. D. Nelkin, and J. S. Gutkind, "Epidermal growth factor receptor-independent constitutive activation of STAT3 in head and neck squamous cell carcinoma is mediated by the autocrine/paracrine stimulation of the interleukin 6/gp130 cytokine system," *Cancer Research*, vol. 63, no. 11, pp. 2948–2956, 2003.

[34] L. Song, B. Rawal, J. A. Nemeth, and E. B. Haura, "JAK1 activates STAT3 activity in non-small-cell lung cancer cells and IL-6 neutralizing antibodies can suppress JAK1-STAT3 signaling," *Molecular Cancer Therapeutics*, vol. 10, no. 3, pp. 481–494, 2011.

Hindawi Publishing Corporation
BioMed Research International
Volume 2015, Article ID 601015, 9 pages
http://dx.doi.org/10.1155/2015/601015

Research Article

Hepatocellular Carcinoma Growth Is Inhibited by *Euphorbia helioscopia* L. Extract in Nude Mice Xenografts

Junsheng Cheng,[1,2,3,4] Wei Han,[1,2,3] Zheyuan Wang,[1,2,3] Yuan Shao,[1,2,3] Yingzhen Wang,[1,2] Yawu Zhang,[1,2,3] Zhongxin Li,[4] Xiaodong Xu,[1,2,3] and Youcheng Zhang[1,2,3]

[1]*Department of General Surgery, Lanzhou University Second Hospital, Cuiyingmen 82, Chengguan District, Lanzhou 730030, China*
[2]*Hepato-Biliary-Pancreatic Institute, Lanzhou University Second Hospital, Lanzhou 730030, China*
[3]*Gansu Provincial-Level Key Laboratory of Digestive System Tumors, Lanzhou 730030, China*
[4]*Department of General Surgery, Gansu Provincial Second Hospital, Lanzhou 730030, China*

Correspondence should be addressed to Youcheng Zhang; zhangychmd@126.com

Received 21 July 2014; Revised 20 September 2014; Accepted 5 October 2014

Academic Editor: Zeki Topcu

Euphorbia helioscopia L. is a traditional Chinese medicine; recently research found that its ethyl acetate extract (EAE) plays an important role on tumor cell proliferation, apoptosis, invasion, and metastasis *in vitro*. But the effect of EAE for tumor cells *in vivo* has not been reported. To explore the inhibitory effect of EAE and molecular mechanism on hepatocellular carcinoma (HCC) SMMC-7721 cells *in vivo*, we utilized the nude mouse xenograft model of HCC. Treated with EAE (50, 100, and 200 μg/mL), the volume of xenograft was measured during the entire process of EAE treatment. In EAE treatment group, the volume of xenograft was significantly reduced compared with the control group ($P < 0.05$) and the protein expressions of CyclinD1, bcl-2, and MMP-9 were reduced, while those of bax, caspase-3, and nm23-H1 were increased. A significant change trend with increasing EAE concentrations has presented, compared with controls. Moreover, the ultrastructural morphology of xenografts showed significant changes, including nuclear pyknosis and chromatin condensation, We found that EAE could effectively inhibit tumor growth, induce apoptosis, and inhibit tumor invasion and metastasis *in vivo*; it is suggested that EAE is a potential candidate for as a new anticancer agent.

1. Introduction

Hepatocellular carcinoma (HCC), the fifth most common neoplasm worldwide [1], is one of the primary causes of cancer-related death in the world [2]. Since the 1990s, HCC has become the second leading cause of cancer death in China. Importantly, diagnosis in the advanced stages, paucity of effective therapeutic options, and high rate of tumor recurrence give rise to its high lethality [3]. Although the methods of diagnosis and treatment in liver cancer made a greatly progress, as an aggressive solid tumor, its prognosis was poor [4]. The 5-year survival is 35–45% after surgical resection [5, 6] and 47–61% after transplantation [7].

In China, surgical resection has been accepted as one of the best approaches of treating HCC. However, recurrence and metastasis were major obstacles for further prolonging of survival after resection. Therefore, many studies aimed to explore new effective drugs to decrease cancer metastasis and relapse, as well as to relieve symptoms. Accordingly, some drugs which have a high specificity and efficiency and low toxicity to patients were produced by chemical synthesis in a current. However, the high cost and time consumption have restricted the development of chemical drugs. In recent years, lots of studies on plants and their derivatives which aim at tumor therapy were prevailing.

Euphorbia helioscopia L. is herbaceous plant that is widely distributed in most parts of China. It belongs to the plant family Euphorbiaceae and genus *Euphorbia* [8]. The stem of *E. helioscopia* L. contains a milky liquid that can produce a toxic reaction in the skin and mucous membranes [9]. As a traditional Chinese medicine, *E. helioscopia* L. has been widely used to treat different disease conditions, such as

ascites, tuberculosis, dysentery, scabies, lung cancer, cervical carcinoma, and esophageal cancer, for centuries [10–12]. In a word, *E. helioscopia* L. has features of slightly toxic and widely pharmacological effects, no obvious toxic effect when patient takes orally its water decoction 150 g/day clinically, and also no death to mice to fill the stomach with 125 g/kg. To date, numerous studies revealed that the secondary metabolites of *E. helioscopia* L. included diterpenoids [13–20], flavonoids [21, 22], triterpenoids [23], polyphenols [24], steroids, and lipids [17]. In addition, a high content of Quercetin, a plant-derived flavonoid, has been detected in the leaves of *E. helioscopia* L. [25], which have been confirmed to have anticancer properties [26, 27].

More recently, our study found that the extracts of *E. helioscopia* L. had effectively inhibited the growth of human HCC lines SMMC-7721, BEL-7402, HepG2, gastric carcinoma cell line SGC-7901, and colorectal cancer cell line SW-480. After extracts of *E. helioscopia* L., we found EAE had markedly inhibited the proliferation of SMMC-7721 cells in a time and dose dependent manner. EAE treatment arrested cell cycle in G-1 phase and EAE used at the concentration range of 100–200 μg/mL induced a marked increase of subdiploid peak. After EAE treatment at the concentrations of 150 and 200 μg/mL, the percentage of apoptotic cells was increased. At the EAE concentration of 200 μg/mL, the typical morphology of early apoptotic change was observed in SMMC-7721 cells. Inhibited the proliferation of SMMC-7721 cells rely on time and dose shown that the EAE was an active fraction of antitumor [28].

In the present study, we utilized the EAE to treat nude mice xenografts of human HCC and investigated its effect on tumor progression with regard to growth, apoptosis, invasion, and metastasis.

2. Materials and Methods

2.1. Herbs and Extraction. An entire plant of *E. helioscopia* L. was collected in June 2012 from Dingxi, Gansu, China. The field of collection was approved by the Agriculture Committee of Dingxi, where it did not involve endangered and protected species, and was identified in the Institute of Botany, School of Life Sciences, Lanzhou University and Gansu Institute for Drug Control. The extraction of *E. helioscopia* L. was performed in the Pharmacy of Xuan Wu Hospital Capital Medical University, Beijing, China. The dried *E. helioscopia* L. was ground and extracted with 70% ethanol for 5 hr and then filtered. The filtrate was concentrated by rotary evaporator (BUCHI, Switzerland). Fractionating the extract of concentration was done by petroleum ether, chloroform, ethyl acetate, and n-butanol, individually. The residue from each fractionation step was used to obtain the subsequent fraction. The extracts from each fractionation step were evaporated to dryness under vacuum.

2.2. Cell Culture. The human HCC cell line SMMC-772 was purchased from the Cell Bank of Shanghai Institute of Cell Biology, Chinese Academy of Sciences (Shanghai, China). Cells were cultured in RPMI-1640 medium (Gibco, Grand Island, NY, USA). Culture media were supplemented with 10% fetal bovine serum (FBS; Gibco, Melbourne, Australia) and antibiotics (50 U/mL penicillin and 50 μg/mL streptomycin) and maintained at 37°C in a humidified atmosphere of 5% CO_2.

2.3. In Vivo Experiments. Four-week-old nude mice were purchased from Vital River Laboratory Animal Technology Co. Ltd. (Beijing, China). These mice were fed a standard rodent diet and water *ad libitum* in an aseptic laminar flow room with 60%–70% humidity at 25°C. This study was approved by the Ethics Committee of the Second Hospital of Lanzhou University (lzuec 20130011). All animals received humane care and all efforts were made to minimize suffering. One week following the arrival of the nude mice, 100 μL cell solutions (containing 2×10^6 logarithmic growth phase tumor cells) were injected subcutaneously into the animals' necks. The mice were observed daily for diet consumption, bowel function, and mental state, and tumor size was measured every 5 days. The length and width of the tumor were measured with Vernier calipers and calculated using the following formula for tumor volume: length $\times$ width^2 $\times$ 0.5. On the 5th day after inoculation, EAE was administered daily, for 30 days. The EAE was mixed with sterile water, at a concentration of 1 mg/mL. The mice were randomly distributed into 5 experimental groups ($n = 6$ per group). The 5 experimental groups were as follows: untreated control group, 5-fluorouracil (Fu) treatment group (10 mg/kg/day), and 3 EAE treatment groups (50 μg/mL, 100 μg/mL, 200 μg/mL, resp.). All mice were sacrificed the day after the last treatment; tumor masses were surgically excised and preserved in liquid nitrogen and fixed in 10% formalin and 2.5% glutaraldehyde, respectively.

2.4. Immunohistochemical Analysis. For immunohistochemical staining, 4 μm sections were cut from formalin-fixed paraffin-embedded xenografts using a microtome, placed on a flotation water bath at 45°C, placed onto glass slides, deparaffinized in xylene, rehydrated in decreasing concentration washes of ethanol, and rinsed in phosphate buffered saline. Antigen retrieval was performed by incubating the tissue sections in a microwave oven at medium power for 10 minutes with 10 mM citrate buffer (pH = 6.0). The activity of endogenous peroxidase was blocking with 3% hydrogen peroxide in deionized water for 10 minutes and blocking nonspecific binding site of the primary antibody with normal serum for 15 minutes, target protein localization with the first antibody and visualization and color reaction with secondary antibody as described above.

Primary antibodies included caspase-3, bcl-2, bax, CyclinD1, MMP-9, and nm23-H1 rabbit anti-human polyclonal antibody (Santa Cruz Biotechnology Inc., Santa Cruz, CA, USA). The secondary antibody was goat anti-rabbit antibody.

Immunostaining results were reviewed and scored using a light microscope by two pathologists blinded to the treatment group. Positivity of the stained paraffin sections was defined by staining intensity and percentage of tumor cells; the staining intensity of caspase-3, bcl-2, bax, CyclinD1,

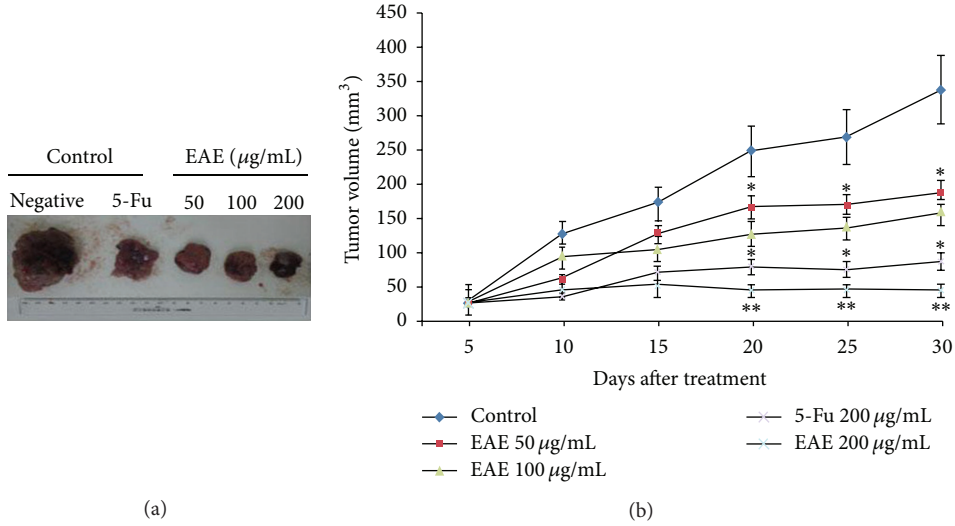

Figure 1: EAE suppresses tumor growth *in vivo*. SMMC-7721 cells (2×10^6) were inoculated subcutaneously into the neck region of nude mice (the volume of xenografts was measured once every 5 days) and treated with EAE. (a) The specimen of xenografts from nude mouse. (b) The growth curve of xenografts. The data represent mean ± S.D of xenografts volume and presented a statistical difference ($^{**}P < 0.01$, $^{*}P < 0.05$). In EAE treatment groups, 200 μg/mL significantly inhibited tumor growth compared to the control group ($^{**}P < 0.01$) and better than 5-Fu 200 μg/mL ($^{*}P < 0.05$), EAE 50 μg/mL ($^{**}P < 0.01$), and 100 μg/mL ($^{*}P < 0.05$), respectively.

MMP-9, and nm23-H1 expression was classified semiquantitatively into negative, weak, moderate, and strongly positive (0, +, ++, and +++), respectively.

2.5. Scanning Electron Microscopy. Tissue blocks were fixed in 2.5% glutaraldehyde in 0.1 M phosphate buffered saline (PBS, pH 7.2). Tissue blocks were dehydrated using a graded series of acetone and propylene oxide and embedded in epoxy resin Epon-812. Embedded tissues were sliced into ultrathin sections and stained with uranyl acetate and lead citrate. The sections were examined by scanning electron microscope (JEM-1230, Japan).

2.6. Western Blotting. For Western blotting analysis, frozen tissue specimens were homogenized in ice-cold lysis buffer containing inhibitors of proteases (Roche Applied Science, Mannheim, Germany). Protein concentration was determined using the BCA protein assay reagent (Pierce, Rockford, IL, USA). Total protein extracts (20 μg/lane) were separated in 10% SDS-PAGE and transferred onto PVDF membranes (Immobilon-P, Millipore, Billerica, MA, USA). The membranes were blocked in 5% skimmed milk powder for 2 hours. To detect target protein, the membrane was incubated with primary antibody and diluted to 1 : 1000 in blocking buffer for 2 hours and then incubated at 4°C for 12 hours. The primary rabbit anti-human polyclonal antibodies were as follows: caspase-3, bcl-2, bax, CyclinD1, MMP-9, and nm23-H (Santa Cruz Biotechnology Inc., Santa Cruz, CA, USA). The secondary antibody, goat anti-rabbit horseradish peroxidase (HRP) (Sigma), was diluted to 1 : 8000 in blocking buffer for 2 hours. As a loading control, the membrane was probed with anti-actin antibody (Sigma). Following treatment, the membrane was washed and developed by enhanced chemiluminescence using an ECL kit (Amersham Pharmacia Biotech).

2.7. Statistical Analysis. Statistical analysis was performed with Graphpad Prism software. Statistical differences between groups were determined using Student's *t*-test. A *P* value of ≤0.05 was considered to be statistically significant.

3. Result

3.1. EAE Inhibits Xenografts Growth In Vivo. The volume of xenografts was measured in the 5th day after tumor cells inoculation and treatment with EAE by intraperitoneal administration. The tumor growth was inhibited compared to the control group ($^{**}P < 0.01$); with EAE concentration increasing, the tumor volume presented a significant decrease. Compared to control group, the tumor volume was significantly decreased in EAE treatment groups and showed an obvious concentration tendency. The most obvious effect of EAE was 200 μg/mL compared to 50 μg/mL ($^{**}P < 0.01$), 100 μg/mL ($^{*}P < 0.05$), and 5-Fu 200 μg/mL ($^{*}P < 0.05$), respectively (Figure 1).

3.2. EAE Modulates the Cell Cycle In Vivo. To confirm the effect of EAE on the cell cycle *in vivo*, we had detected CyclinD1 protein expression in xenografts and found that it was significantly reduced in the cytoplasm after EAE treatment, compared with the control groups, as measured by immunohistochemical staining (red arrow; Figure 3(a)). After EAE treatment, the protein expression of CyclinD1 was significantly decreased in the EAE treatment groups compared to controls ($^{*}P < 0.05$, $^{**}P < 0.01$)

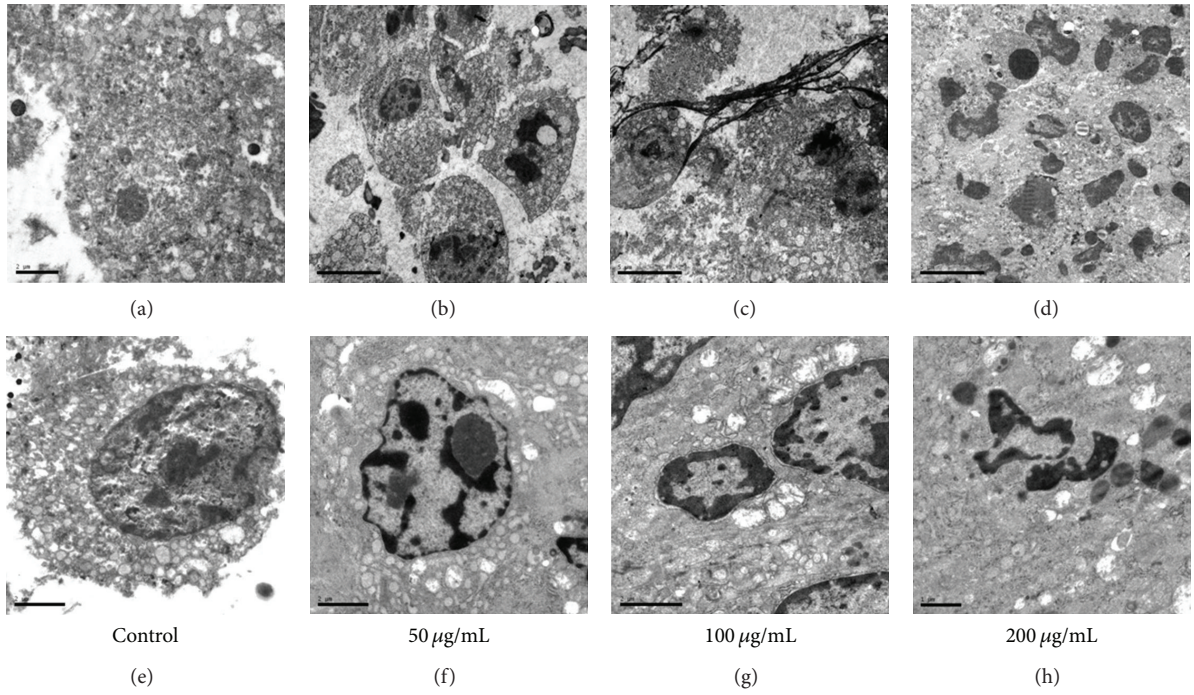

Figure 2: Scanning electron microscope. The ultrastructural morphology of xenografts. ((a) and (e)) Control group. ((b)–(d) and (f)–(h)) 50, 100, and 200 μg/mL EAE treatment groups. The change of ultrastructure in xenografts by treatment with EAE is shown as observed by scanning electron microscopy ((a)–(d), ×6000; (e)–(h), ×12000).

detected by Western blot and varied with rising concentration (Figure 3(b)).

3.3. EAE Induces Tumor Apoptosis In Vivo. To evaluate EAE induced apoptosis *in vivo*, we observed the ultrastructural morphology of xenografts by scanning electron microscopy and found that the changes of nuclear pyknosis (Figure 2(b)), chromatin condensation, chromatin marginalization (Figures 2(g) and 2(h)), organelle swelling, cytoplasm vacuolization, apoptotic bodies (Figure 2(f)), and fibroplasia surrounded the tumor cells (Figure 2(c)) in EAE treatment groups. Compared with control groups, the expression of bcl-2 (Figures 4(a) and 4(d)) was reduced and that of bax (Figures 4(b) and 4(e)) and caspase-3 (Figures 4(c) and 4(f)) was increased (red arrow) in the cytoplasm after treatment with EAE, showed by immunohistochemical staining.

The result of Western blotting showed that bcl-2 protein expression decreased after EAE treatment; in 200 μg/mL treatment group a significant decrease had appeared compared with control group ($^{**}P < 0.01$) and 5-Fu 200 μg/mL treatment group ($^{*}P < 0.05$). The protein expressions of bax and caspase-3 were increased after treatment by EAE compared with control group ($^{**}P < 0.01$) and 5-Fu 200 μg/mL treatment group ($^{*}P < 0.05$; Figures 4(g) and 4(h)).

3.4. EAE Suppresses Tumor Invasion and Metastasis In Vivo. To determine EAE suppression of tumor invasion and metastasis *in vivo*, MMP-9 and nm23-H1 expressions were examined. Immunohistochemical staining showed that in EAE treatment groups nm23-H1 (Figures 5(b) and 5(d)) expression was increased and MMP-9 (Figures 5(a) and 5(c)) expression was decreased compared to controls (red arrow). By Western blotting, we found that nm23-H1 and MMP-9 protein expression have presented an obvious concentration tendency, compared to controls; nm23-H1 was increased and MMP-9 was reduced, especially in 200 μg/mL group ($^{**}P < 0.01$; Figures 5(e) and 5(f)).

4. Discussion

In this study, we assessed the anticancer effect of EAE *in vivo* by the nude mice xenograft model of HCC. The growth was inhibited and the volume significantly decreased after being subjected to EAE treatment for xenografts and shown in dose dependent manner among 50–200 μg/mL EAE compared to control groups (Figure 1). With EAE concentration increasing, the inhibition effect on tumor growth was enhanced. Cell cycle regulation protein CyclinD1 plays a very important role in the G1 phase; the changes of expression were observed in EAE treatment groups (Figure 3). We observed a significant downregulation of cyclinD1 protein expression after treatment with EAE (Figure 3(b)), and the staining in the cytoplasm was reduced compared with controls (Figure 3(a)). Cell cycle data showed that EAE primarily arrested cells in the G-1 phase in a dose and time dependent manner and reduced the percentage of cells in the S phase [28] and that cyclinD1 expression was markedly downregulated. The effect of growth inhibition is mainly mediated by inhibition of cell proliferation, which is associated with a profound

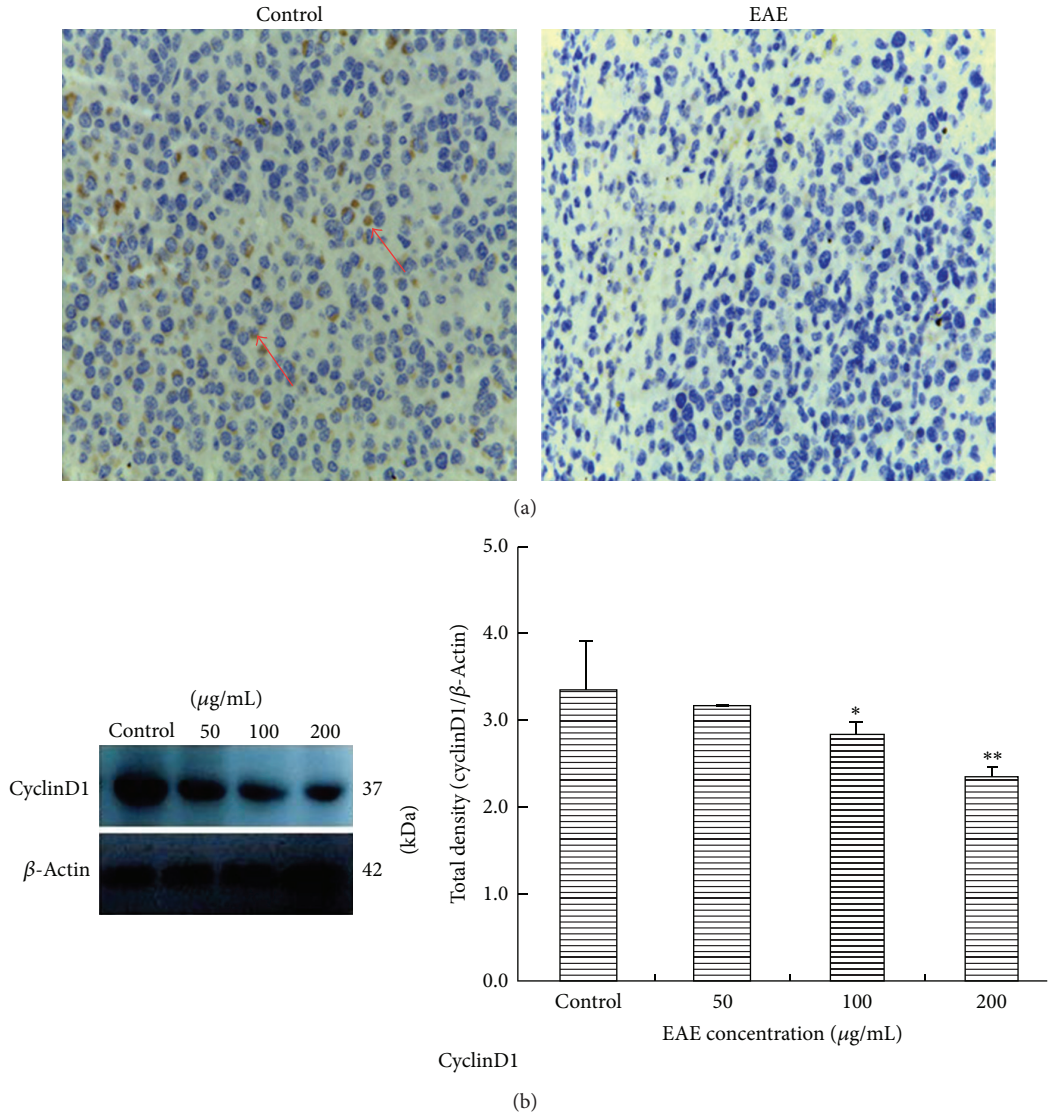

FIGURE 3: CyclinD1 protein expression in nude mouse xenografts. (a) Immunohistochemical staining detected CyclinD1 in xenografts. EAE treatment group hardly expressed CyclinD1 protein compared to control groups (red arrow). ×400 magnification. (b) Analysis of CyclinD1 protein expression in xenografts by Western blot. Total protein was extracted from xenografts and subjected to Western blot analyses. CyclinD1 protein expression was obviously reduced in EAE treatment groups compared with the control group ($^{*}P < 0.05$), especially in 200 μg/mL group ($^{**}P < 0.01$), different significantly. β-Actin was used as the loading control.

modulation of the expression of cell cycle mediators, and the cell cycle machinery disruption; the expression of cyclinD1 was almost completely abrogated with EAE treatment. EAE treatment arrested the cell cycle in the G-1 phase and induced a marked increase of subdiploid peaking. After EAE treatment the percentage of apoptotic cells was increased. The typical morphology of early apoptotic change was observed in SMMC-7721 cells. In addition, EAE treatment displayed a dose dependent inhibitory effect on tumor cell invasion *in vitro* [28].

To induce apoptosis is contributed to EAE inhibiting tumor growth. The Bcl-2 family played a critical role in apoptosis and the members are classified antiapoptosis factors, which mainly include Bcl-2, Bcl-XL, Bcl-W, and proapoptotic factors, which mainly include Bax, Bak, Bik, and Bid. A very important mediating role in apoptosis was caspase family, and caspase-3 is a key effector and functions in many apoptosis signaling transduction pathways [29]. We found that the expression protein of bcl-2 exhibited an obvious declining tendency after EAE treatment, and the bax and caspase-3 exhibited an obvious increasing tendency (Figure 4). This result suggests that EAE, mediating the protein expression of bcl-2 downregulation and bax and caspase-3 upregulation in tumor cells, led to antiapoptosis factor being reduced and proapoptosis factor being increased, to induce cells apoptosis in xenografts. In the EAE treatment groups, the protein expression of bcl-2 was significantly lower than in the control group ($P < 0.05$), and those of bax and caspase-3 were significantly higher than in the control group ($P < 0.05$; Figures 4(g) and 4(h)). Compared with

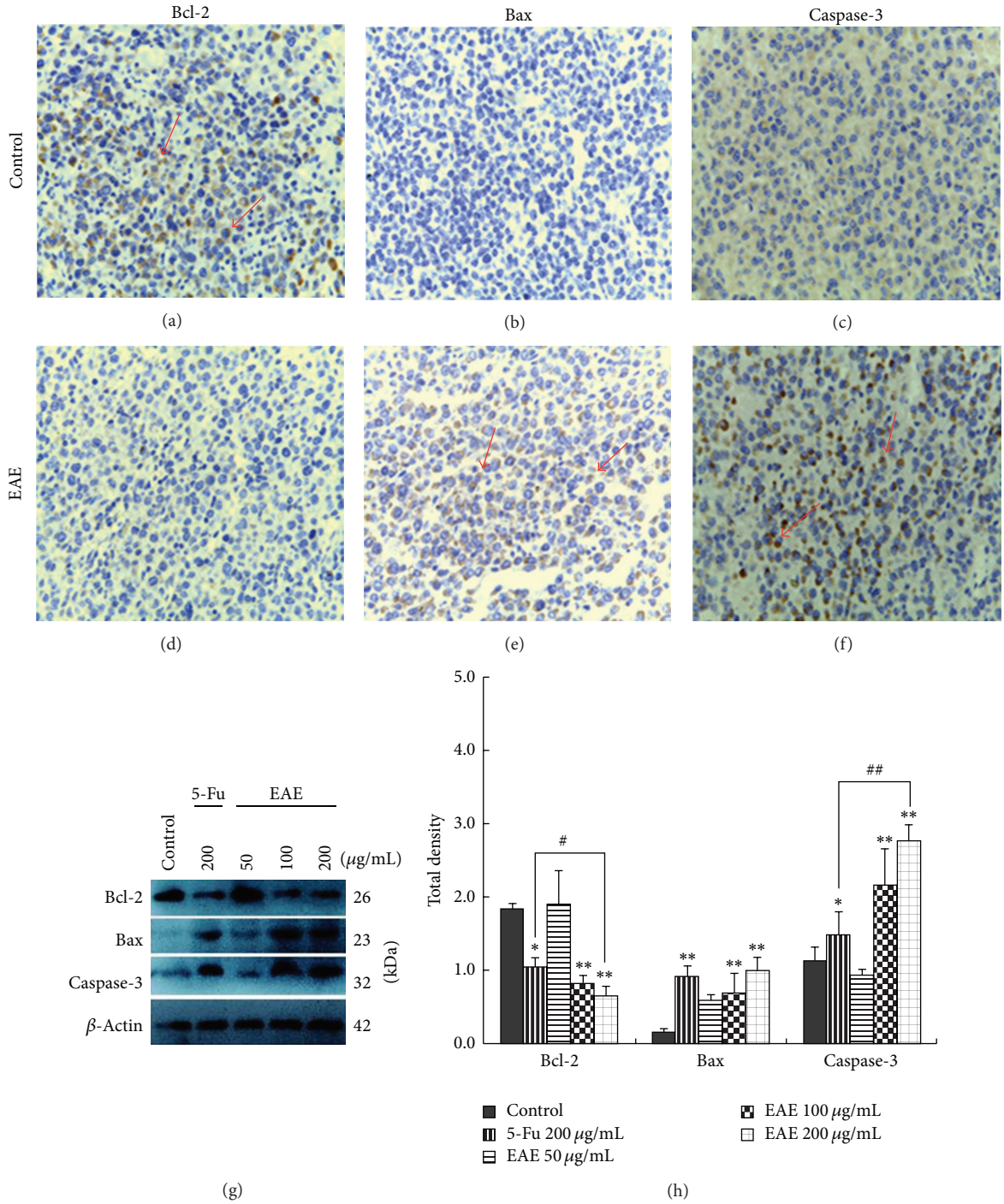

FIGURE 4: Bcl-2, bax, and caspase-3 protein expressions in nude mouse xenografts. ((a)–(f)) Immunohistochemical staining detected bcl-2, bax, and caspase-3 protein expressions in xenografts. The significant changes of bcl-2, bax, and caspase-3 protein expressions in EAE treatment groups compared to controls; after EAE treatment bcl-2 protein expression was decreased as shown in (a) and (d), but bax and caspase-3 expressions were increased as shown from (b) to (f) (red arrow), ×400 magnification. ((g), (h)) The protein expressions of bcl-2, bax, and caspase-3 in xenografts were analyzed by Western blot. Total protein was extracted from xenografts and subjected to Western blot analyses. As shown compared with the control group ($^{**}P < 0.01$), bcl-2 protein expression was obviously reduced, but bax and caspase-3 expressions were increased. As EAE concentration increasing the quantity of protein expressions have presented a significantly change trend, and the effect of EAE 200 μg/mL better than 5-Fu 200 μg/mL ($^{*}P < 0.05$).

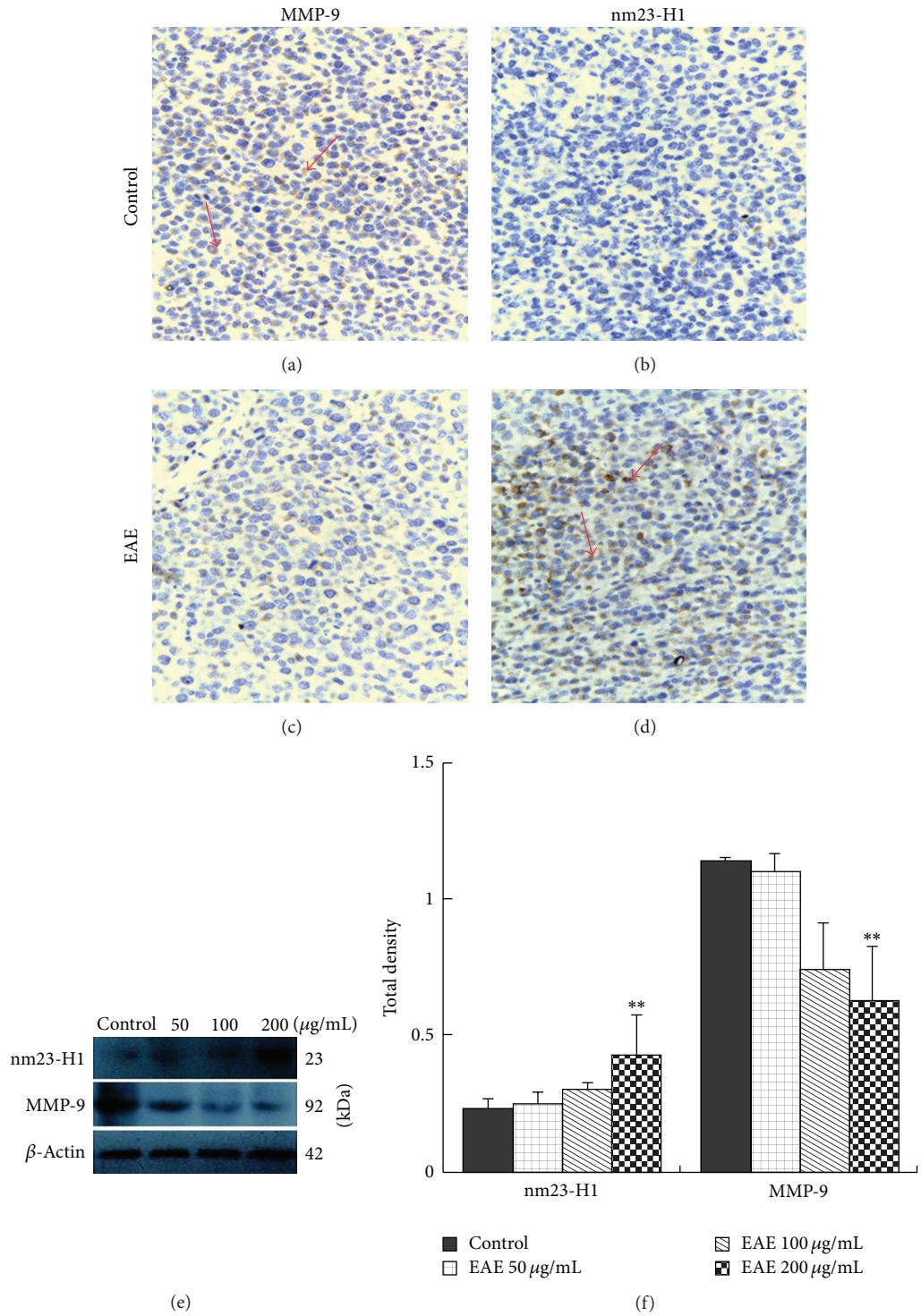

Figure 5: MMP-9 and nm23-H1 protein expressions in nude mouse xenografts. ((a)–(d)) Immunohistochemical staining detected nm23-H1 and MMP-9 protein expressions in xenografts. Compared to control groups, nm23-H1 expression was increased and MMP-9 expression was decreased in EAE treatment groups, as shown ((a) and (c), (b) and (d)) (red arrow). ×400 magnification. ((e), (f)) Western blot analyzed nm23-H1 and MMP-9 protein expressions in xenografts. Total protein was extracted from HCC xenografts and subjected to Western blot analyses for nm23-H1 and MMP-9. Compared with control groups, in EAE treatment groups nm23-H1 protein expression was obviously increased and MMP-9 expression was reduced, especially in 200 μg/mL group ($^{**}P < 0.01$).

5-Fu 200 μg/mL group, 200 μg/mL EAE induces apoptosis better than 200 μg/mL 5-Fu, but 50 μg/mL and 200 μg/mL EAE less than 5-Fu 200 μg/mL. As can be seen from these results, EAE can induce apoptosis of HCC *in vivo*, the effect is to enhance with dose increase and better than 200 μg/mL 5-Fu. This demonstrates that EAE exhibits antitumor activity in a dose dependent manner.

Degradation of extracellular matrix by matrix metalloproteinases (MMPs) was a first step for cancer cell migration and invasion, so MMP-9 plays an important role in tumor invasion [30, 31]. The first metastasis suppressor gene, nm23, was identified in 1988 by differential colony hybridization [32]. Nm23-H1 has a variety of validated molecular activities, with at least some playing important roles in regulating its ability to inhibit metastasis [33]. Nm23-H1 and abnormal wing discs, the Drosophila ortholog of Nm23-H1 and Nm23-H2, have also been proposed to be activators of the GTPase dynamin that facilitate endocytosis of growth factor receptors, thereby attenuating their signaling [34–36]. Nm23-H1 and nm23-H2 also interact with proteins involved in cell movement and adhesion [37, 38]. In this study, we found that the protein expression of MMP-9 significantly decreased in EAE treatment groups, and nm23-H1 was significantly increased, compared with the control groups (Figure 5). The change tendency of nm23-H1 and MMP-9 presented in dose dependent manner (Figures 5(e) and 5(f)). Thus, we think that the EAE may have downregulated MMP-9 protein expression and upregulated nm-23H1 in HCC *in vivo*; the more reduced the MMP-9 protein expression the less degraded the extracellular matrix; cancer cell migration and invasion were suppressed, the same effect as nm23-H1 increased in HCC. Although, the development of agents with potential antimetastatic properties is difficult issue, on the basis of these data, we believe that EAE as a new drugs target to play an important role in suppressing tumor metastasis.

5. Conclusions

In conclusion, HCC xenografts presented growth inhibition and CyclinD1 protein expression significantly decreased in the G1-phase when subjected to treatment by EAE. To induce cell apoptosis by changing Bcl-2, Bax, and caspase-3 protein expressions in xenografts, the changes of MMP-9 and nm23-H1 protein expressions have shown that the invasion and metastasis of tumor cells may be suppressed by EAE. In sum, EAE can effectively inhibit tumor cells growth both *in vitro* and *in vivo*, making it as an attractive drug candidate. The mechanism of the anticancer effect of EAE remains to be determined. Further research may demonstrate a clinical target for this drug.

Conflict of Interests

The authors confirm that they have no conflict of interests.

Acknowledgment

This research was supported by the Fundamental Research Funds for the Central Universities (lzujbky-2013-145).

References

[1] J. Bruix, L. Boix, M. Sala, and J. M. Llovet, "Focus on hepatocellular carcinoma," *Cancer Cell*, vol. 5, no. 3, pp. 215–219, 2004.

[2] American Cancer Society, *Cancer Facts and Figures*, American Cancre Society, Atlanta, Ga, USA, 2010.

[3] P. A. Farazi and R. A. DePinho, "The genetic and environmental basis of hepatocellular carcinoma," *Discovery Medicine*, vol. 6, no. 35, pp. 182–186, 2006.

[4] D. M. Parkin, "Global cancer statistics in the year 2000," *The Lancet Oncology*, vol. 2, no. 9, pp. 533–543, 2001.

[5] E. C. S. Lai, S.-T. Fan, C.-M. Lo, K.-M. Chu, C.-L. Liu, and J. Wong, "Hepatic resection for hepatocellular carcinoma: an audit of 343 patients," *Annals of Surgery*, vol. 221, no. 3, pp. 291–298, 1995.

[6] J.-N. Vauthey, D. Klimstra, D. Franceschi et al., "Factors affecting long-term outcome after hepatic resection for hepatocellular carcinoma," *The American Journal of Surgery*, vol. 169, no. 1, pp. 28–35, 1995.

[7] H. Y. Yoo, C. H. Patt, J.-F. Geschwind, and P. J. Thuluvath, "The outcome of liver transplantation in patients with hepatocellular carcinoma in the United States between 1987 and 2001: 5-Year survival has improved significantly with time," *Journal of Clinical Oncology*, vol. 21, no. 23, pp. 4329–4335, 2003.

[8] "Editorial Committee of the Administration Bureau of Traditional Chinese Medicine," *Chinese Materia Medica*, vol. 4, pp. 782–785, 1998, Shanghai: Shanghai Science & Technology Press.

[9] K. Wilken and C. M. Schempp, "Toxic phytodermatitis caused by *Euphorbia helioscopia* L. (sun spurge)," *Hautarzt*, vol. 56, no. 10, pp. 955–958, 2005.

[10] Editorial Committee of the Administration Bureau of Traditional Chinese Medicine, *Chinese Materia Medica (Zhonghua Bencao)*, Shanghai Science & Technology Press, Shanghai, China, 1998 (Chinese).

[11] L. Yang, H.-X. Chen, and W.-Y. Gao, "Advances in studies on chemical constituents in *Euphorbia helioscopia* and their biological activities," *Chinese Traditional and Herbal Drugs*, vol. 38, no. 10, pp. 1585–1589, 2007.

[12] D. X. Pang and J. W. Lian, "Investigation on therapy of Ze Qi Decoction syndrome in Diseases, Synopsis of Golden Chamber. [Abstract]," *China Journal of Traditional Chinese Medicine and Pharmacy*, vol. 22, pp. 829–831, 2007.

[13] S. Yamamura, Y. Shizuri, S. Kosemura et al., "Diterpenes from *Euphorbia helioscopia*," *Phytochemistry*, vol. 28, no. 12, pp. 3421–3436, 1989.

[14] Y. Shizuri, S. Kosemura, J. Ohtsuka, Y. Terada, and S. Yamamura, "Structural and conformational studies on *Euphohelioscopins* A and B and related diterpenes," *Tetrahedron Letters*, vol. 24, no. 25, pp. 2577–2580, 1983.

[15] Y. Shizuri, S. Kosemura, J. Ohtsuka et al., "Structural and conformational studies on euphornin and related diterpenes," *Tetrahedron Letters*, vol. 25, no. 11, pp. 1155–1158, 1984.

[16] Y. Shizuri, J. Ohtsuka, S. Kosemura, Y. Terada, and S. Yamamura, "Biomimetic reactions of some macrocyclic diterpenes," *Tetrahedron Letters*, vol. 25, no. 48, pp. 5547–5550, 1984.

[17] S. Kosemura, Y. Shizuri, and S. Yamamura, "Isolation and structures of *euphohelins*, new toxic diterpenes from *Euphorbia helioscopia* L," *Bulletin of The Chemical Society of Japan*, vol. 58, no. 11, pp. 3112–3117, 1985.

[18] W. Zhang and Y.-W. Guo, "Chemical studies on the constituents of the Chinese medicinal herb *Euphorbia helioscopia* L," *Chemical and Pharmaceutical Bulletin*, vol. 54, no. 7, pp. 1037–1039, 2006.

[19] E. Barile, M. Borriello, A. Di Pietro et al., "Discovery of a new series of jatrophane and lathyrane diterpenes as potent and specific P-glycoprotein modulators," *Organic & Biomolecular Chemistry*, vol. 6, no. 10, pp. 1756–1762, 2008.

[20] H.-W. Tao, X.-J. Hao, P.-P. Liu, and W.-M. Zhu, "Cytotoxic macrocyclic diterpenoids from *Euphorbia helioscopia*," *Archives of Pharmacal Research*, vol. 31, no. 12, pp. 1547–1551, 2008.

[21] A. Kawase and N. Kutani, "Some properties of a new flavonoid, tithymalin, isolated from the herbs of *Euphorbia Helioscopia* L innaeous," *Agricultural and Biological Chemistry*, vol. 32, pp. 121–122, 1968.

[22] Y. Ghen, Z. J. Tang, F. X. Jiang, X. X. Zhang, and A. N. Lao, "Studies on the active principles of Ze-Qi (*Euphorbia helioscopia* L.), a drug used for chronic bronchitis (I)," *Acta Pharmaceutica Sinica*, vol. 14, no. 2, pp. 91–95, 1979 (Chinese).

[23] M. Nazir, W. Ahmad, and W. Kreiser, "Isolation and NMR-assignments of 19αH-lupeol from *E. helioscopia* Linn (N.O. *Euphorbiaceae)*," *Pakistan Journal of Scientific and Industrial Research*, vol. 41, no. 1, pp. 6–10, 1998.

[24] W.-S. Feng, L. Gao, X.-K. Zheng, and Y.-Z. Wang, "Polyphenols of *Euphorbia helioscopia*," *Chinese Journal of Natural Medicines*, vol. 7, no. 1, pp. 37–39, 2009.

[25] H. P. Liu, X. F. Shi, Y. C. Zhang, Z. X. Li, L. Zhang, and Z. Y. Wang, "Quantitative analysis of quercetin in *Euphorbia helioscopia* L by RP-HPLC," *Cell Biochemistry and Biophysics*, vol. 61, no. 1, pp. 59–64, 2011.

[26] T.-B. Kang and N.-C. Liang, "Studies on the inhibitory effects of quercetin on the HL-60 leukemia cells," *Biochemical Pharmacology*, vol. 54, no. 9, pp. 1013–1018, 1997.

[27] S. Caltagirone, C. Rossi, A. Poggi et al., "Flavonoids apigenin and quercetin inhibit melanoma growth and metastatic potential," *International Journal of Cancer*, vol. 87, no. 4, pp. 595–600, 2000.

[28] Z. Y. Wang, H. P. Liu, Y. C. Zhang, L. Q. Guo, Z. X. Li, and X. F. Shi, "Anticancer potential of *Euphorbia helioscopia* L extracts against human cancer cells," *The Anatomical Record*, vol. 295, no. 2, pp. 223–233, 2012.

[29] A. Galmiche, Z. Ezzoukhry, C. François et al., "BAD, a proapoptotic member of the BCL2 family, is a potential therapeutic target in hepatocellular carcinoma," *Molecular Cancer Research*, vol. 8, no. 8, pp. 1116–1125, 2010.

[30] C. M. Overall and O. Kleifeld, "Validating matrix metalloproteinases as drug targets and anti-targets for cancer therapy," *Nature Reviews Cancer*, vol. 6, no. 3, pp. 227–239, 2006.

[31] M. J. Duffy, P. M. McGowan, and W. M. Gallagher, "Cancer invasion and metastasis: changing views," *Journal of Pathology*, vol. 214, no. 3, pp. 283–293, 2008.

[32] P. S. Steeg, G. Bevilacqua, R. Pozzatti, L. A. Liotta, and M. E. Sobel, "Altered expression of NM23, a gene associated with low tumor metastatic potential, during Adenovirus 2 Ela inhibition of experimental metastasis," *Cancer Research*, vol. 48, no. 22, pp. 6550–6554, 1988.

[33] P. S. Steeg, C. E. Horak, and K. D. Miller, "Clinical-translational approaches to the Nm23-H1 metastasis suppressor," *Clinical Cancer Research*, vol. 14, no. 16, pp. 5006–5012, 2008.

[34] F. Palacios, J. K. Schweitzer, R. L. Boshans, and C. D'Souza-Schorey, "ARF6-GTP recruits Nm23-H1 to facilitate dynamin-mediated endocytosis during adherens junctions disassembly," *Nature Cell Biology*, vol. 4, no. 12, pp. 929–936, 2002.

[35] K. S. Krishnan, R. Rikhy, S. Rao et al., "Nucleoside diphosphate kinase, a source of GTP, is required for dynamin-dependent synaptic vesicle recycling," *Neuron*, vol. 30, no. 1, pp. 197–210, 2001.

[36] V. Dammai, B. Adryan, K. R. Lavenburg, and T. Hsu, "*Drosophila awd*, the homolog of human *nm23*, regulates FGF receptor levels and functions synergistically with *shi/dynamin* during tracheal development," *Genes & Development*, vol. 17, no. 22, pp. 2812–2824, 2003.

[37] B. C. Gallagher, K. A. Parrott, G. Szabo, and A. de S. Otero, "Receptor activation regulates cortical, but not vesicular localization of NDP kinase," *Journal of Cell Science*, vol. 116, no. 15, pp. 3239–3250, 2003.

[38] H.-N. Fournier, S. Dupé-Manet, D. Bouvard et al., "Integrin cytoplasmic domain-associated protein 1α (ICAP-1α) interacts directly with the metastasis suppressor nm23-H2, and both proteins are targeted to newly formed cell adhesion sites upon integrin engagement," *Journal of Biological Chemistry*, vol. 277, no. 23, pp. 20895–20902, 2002.

Hindawi Publishing Corporation
BioMed Research International
Volume 2015, Article ID 738241, 13 pages
http://dx.doi.org/10.1155/2015/738241

Research Article

Heteronemin, a Spongean Sesterterpene, Induces Cell Apoptosis and Autophagy in Human Renal Carcinoma Cells

Szu-Ying Wu,[1] Ping-Jyun Sung,[2,3] Ya-Ling Chang,[1] Shiow-Lin Pan,[4,5] and Che-Ming Teng[1]

[1] *Pharmacological Institute, College of Medicine, National Taiwan University, No. 1 Jen-Ai Road, Section 1, Taipei 10051, Taiwan*
[2] *Graduate Institute of Marine Biology, National Dong Hwa University, Pingtung 944, Taiwan*
[3] *National Museum of Marine Biology and Aquarium, Pingtung 944, Taiwan*
[4] *The Ph.D. Program for Cancer Biology and Drug Discovery, College of Medical Science and Technology, Taipei Medical University, No. 250 Wu-Hsing Street, Taipei 11031, Taiwan*
[5] *Department of Pharmacology, College of Medicine, Taipei Medical University, No. 250 Wu-Hsing Street, Taipei 110311, Taiwan*

Correspondence should be addressed to Shiow-Lin Pan; slpan@tmu.edu.tw and Che-Ming Teng; cmteng@ntu.edu.tw

Received 23 July 2014; Accepted 26 August 2014

Academic Editor: Chin-Chung Wu

Heteronemin is a bioactive marine sesterterpene isolated from the sponge *Hyrtios* sp. Previous reports have shown that heteronemin possesses anticancer activity. Here, heteronemin displayed cytotoxic effects against three human cancer cell lines (A549, ACHN, and A498) and exhibited potent activity in A498 human renal carcinoma cells, with an IC_{50} value of 1.57 μM by MTT assay and a GI_{50} value of 0.77 μM by SRB assay. Heteronemin initiates apoptotic cell death by downregulating Bcl-2 and Bcl-xL and upregulating Bax, leading to the disruption of the mitochondrial membrane potential and the release of cytochrome *c* from the mitochondria. These effects were associated with the activation of caspase-3/caspase-8/caspase-9, followed by PARP cleavage. Furthermore, heteronemin inhibited the phosphorylation of AKT signaling pathway and ERK and activated p38 and JNK. The specific inhibition of the p38 pathway by SB203580 or p38 siRNA treatment reversed the heteronemin-induced cytotoxicity and apoptotic signaling. Heteronemin also induced autophagy in A498 cells, and treatment with chloroquine (autophagy inhibitor) or SP600125 (JNK inhibitor) inhibited autophagy and increased heteronemin-induced cytotoxicity and apoptotic signaling. Taken together, this study proposes a novel treatment paradigm in which the combination of heteronemin and autophagy inhibitors leads to enhanced RCC cell apoptosis.

1. Introduction

Natural products are a source of compounds that sometimes have pharmacological activity that can be of therapeutic benefit in treating human diseases. Many compounds have potential anticancer effects involving multiple signaling pathways by mediating the complex signal transduction [1]. Recently, intense attention has been focused on marine natural products, such as pachymatismin, bryostatins, didemnin B, and bromovulone III [2–6]. Heteronemin, a marine sesterterpene isolated from the sponge *Hyrtios* sp., is endowed with an attractive pharmacological profile for drug development. Originally studied for its antimicrobial effects [7, 8], heteronemin has been reported recently as an apoptosis inducer, an inhibitor of tumor intravasation *in vitro* [9], and a potent modulator of the TNFα-induced NF-κB pathway through the inhibition of the proteasome system [10].

Autophagy is an intracellular self-degradation process whereby double-membrane organelles termed autophagosomes deliver cytoplasmic materials to lysosomes [11]. The autophagosomes fuse with the lysosomes to become autolysosomes and the sequestered cargo is degraded [12]. Cells utilize the autophagy recycling system for removing both damaged cytosolic proteins and aged organelles to maintain quality and generate nutrient supply under adverse conditions. Besides these fundamental roles, autophagy is considered to be involved in the degradation of intracellular bacteria, antigen presentation, tumor suppression, cell survival, and cell death [12–15]. Whereas low autophagy levels promote cell survival, high autophagy levels cause catastrophic damage to a cell

resulting in autophagic cell death [16]. Anticancer drugs induce autophagic and apoptotic cell death in various cancer cells [17, 18]. However, the interplay between autophagy and apoptosis is intricate. Autophagy can inhibit apoptosis by promoting cell survival, or autophagy and apoptosis may cooperate to induce cell death [19].

The members of the mitogen-activated protein kinase (MAPK) family are activated by cellular stress, UV light radiation, growth factor withdrawal, and proinflammatory cytokines, resulting in the regulation of cell proliferation, differentiation, survival, death, transformation, and adaptation [20–22]. The mammalian MAPK family comprises extracellular signal-regulated kinase (ERK), p38, and c-Jun NH2-terminal kinase (JNK, also known as stress-activated protein kinase or SAPK). In general, ERKs are associated with growth and proliferation, whereas JNKs and p38 are involved in cell death, including apoptosis [23]. p38 has four isoforms, p38α, p38β, p38γ, and p38δ. MKK3 and MKK6 phosphorylate p38 at Thr 180 and Tyr 182 and activate its kinase activity. In mammalian genomes, three genes encode the JNK family: JNK1, JNK2, and JNK3. The upstream MKK4 and MKK7 kinases mediate JNK activation via dual phosphorylation at Thr 183 and Tyr 185. The role of p38 and JNK in cell death is cell type- and stimuli-dependent. p38 can induce apoptosis through two different mechanisms: indirectly by promoting the transcription of proapoptotic genes or directly by activating Bax, Bim and belonging to the apoptosis-related Bcl-2 family proteins [24]. Furthermore, the phosphorylation of p38 acts as a mediator for caspase-8 in manganese-induced mitochondria-dependent cell death suggesting a strong link between p38 and the mitochondrial apoptotic pathway [25]. Conversely, the role of JNK in apoptosis is complex and it has been reported to have proapoptotic or antiapoptotic role or no role in the process. The role of JNK in autophagy is clearer: JNK signaling is required to upregulate LC3 in ceramide-induced autophagy in human nasopharyngeal carcinoma cells [26]. In addition, ROS is a strong activator of the JNK-AP-1 signaling pathway and plays an important role in JNK-dependent autophagy regulation [27, 28]. Analyzing the role of JNK in the crosstalk between apoptosis and autophagy remains an important challenge.

In this study, we report that heteronemin induces apoptosis and autophagy in the human renal cell carcinoma (RCC) A498 cell line. We demonstrate the role of p38 in heteronemin-induced cell apoptosis and the role of JNK in heteronemin-induced autophagy. We show in this system that inhibiting autophagy leads to a significantly enhanced cell death and apoptosis response. Heteronemin also inhibits the AKT signaling pathway and the phosphorylation of ERK. Our study is the first report that provides evidence that, besides apoptosis, heteronemin also induces autophagy in A498 cells. We propose that the combination of heteronemin with autophagy inhibitors leads to enhanced apoptosis in A498 cells.

2. Materials and Methods

2.1. Reagents and Chemicals. Heteronemin was extracted from marine sponge *Hyrtios erecta* and purified in Professor Ping-Jyun Sung's Lab. Minimum Essential Medium (MEM), RPMI 1640 medium, fetal bovine serum (FBS), penicillin, and streptomycin were obtained from Gibco BRL Life Technologies (Grand Island, NY). EGTA, EDTA, leupeptin, dithiothreitol, phenylmethylsulfonyl fluoride (PMSF), propidium iodide (PI), dimethyl sulfoxide (DMSO), MTT (3-[4,5]-2,5-diphenyltetrazolium bromide), 4′-6-diamidino-2-phenylindole (DAPI), SB203580, SP600125, and chloroquine were obtained from Sigma (St. Louis, MO). Antibodies to various proteins were obtained from the following sources: anti-mouse and anti-rabbit IgGs, poly-ADP-ribose polymerase (PARP), Bcl-2, Bcl-xL, Bax, and p62 antibodies were purchased from Santa Cruz Biotechnology (Santa Cruz, CA); p-AKT (Ser 473), AKT, p-ERK (Thr 202/Tyr 204), ERK, p-p70S6K (Thr 421/Ser 424), p70S6K, p-4EBP1 (Thr 37/46), 4EBP1, p-JNK (Thr 183/Tyr 185), JNK, p-p38 (Thr 180/Tyr 182), p38, p-HSP27 (Ser 78), Atg5, cleaved caspase-3, caspase-9, and caspase-8 were purchased from Cell Signaling Technology (Boston, MA); cytochrome *c* was purchased from BD Biosciences (San Diego, CA); caspase-3 was purchased from Imgenex (San Diego, CA); LC3 was purchased from Novus (Littleton, CO); actin and GAPDH were purchased from Millipore (Billerica, MA).

2.2. Cell Culture. Human cancer cell lines A549, ACHN, and A498 were purchased from the American Type Culture Collection (Manassas, VA). Cell lines were maintained in either RPMI 1640 medium (A549 and ACHN) or Minimum Essential Medium (A498) containing 10% heat-inactivated fetal bovine serum and 1% penicillin/streptomycin at 37°C under a humidified atmosphere with 5% CO_2.

2.3. Cytotoxicity Assay. Cells were plated in 96-well plates for 24 h. The medium was removed, and the cells were treated with various concentrations of heteronemin. After treatment, 100 μL MTT solution (0.5 mg/mL in phosphate-buffered saline (PBS)) was added to each well. After 1 h incubation at 37°C, MTT solution was removed and DMSO was added to dissolve dye. Absorbance at 550 nm was measured using a microplate reader (Thermo Multiskan GO, Waltham, MA), using RPMI or MEN medium as a blank.

2.4. Sulforhodamine B (SRB) Assay. Cells were seeded in 96-well plates in complete media. After overnight culture, cells were treated with various concentrations of heteronemin for 48 h and then cells were fixed with 10% trichloroacetic acid (TCA) and SRB at 0.4% (wt/vol) in 1% acetic acid. SRB bound cells were solubilized with 10 mM Trizma base and absorbance was read at a wavelength of 515 nm by using a microplate reader. Growth inhibition of 50% (GI_{50}) is calculated as described previously [29].

2.5. In Situ Labeling of Apoptotic Cells. Heteronemin-induced A498 cell apoptosis was detected using the terminal deoxynucleotidyl transferase-mediated nick-end labeling (TUNEL) staining assay. Briefly, cells were seeded in 4-well chamber slides. After overnight culture, cells were exposed to 3 μM

heteronemin for 24 h and then fixed for 10 min by using ice-cold 1% paraformaldehyde. Staining was performed according to the TUNEL staining protocol provided by Promega Corporation (Madison, WI). Finally, photomicrographs of the TUNEL-stained cells were observed and photographed using Axioplan 2 fluorescence microscope (Carl Zeiss, Jena, Germany) equipped with a CCD camera (Nikon, Japan) at 20x magnification. Data were analysed by AxioVision software.

2.6. Cell Death Detection Assay. Cell death detection ELISA (Roche Applied Science, Indianapolis, IN) was used to quantify histone-complexed DNA fragments (nucleosomes) in cytoplasm of the apoptotic cells after induction of apoptosis. The manufacturer's protocol was applied from Roche and data were measured by microplate reader. Data were calculated and compared with those of a control group.

2.7. Western Blot Analysis. Whole cell lysates were prepared by extracting proteins using a lysis buffer. Proteins were size-fractionated by 10–12% SDS-PAGE and transferred electrophoretically onto polyvinylidene difluoride membranes. The membranes were sequentially hybridized with primary antibody and followed with a horseradish peroxidase-conjugated secondary antibody. Finally, the membranes were visualized using an enhanced chemiluminescence kit (VISUAL PROTEIN, Taiwan).

2.8. Measurement of the Change of Mitochondrial Membrane Potential ($\Delta\Psi_m$). Mitochondrial membrane potential was monitored by FACScan flow cytometric analysis. Cells were treated with heteronemin for the indicated time periods. Thirty minutes before the termination of incubation, the rhodamine 123 solution (final concentration of 5 mM) was added to the cells and incubated for the last 30 min at 37°C. The media were removed and cells were washed once with phosphate-buffered saline (PBS). After detachment by trypsinization, cells were resuspended in PBS and subjected to FACScan analysis.

2.9. Preparation of Cytosolic and Mitochondrial Fractions. Cytosolic fraction was isolated by using Cytochrome *c* Releasing Apoptosis Assay kit from BioVision Research Products (Mountain View, CA, USA). Briefly, after treatment, cells were harvested by trypsinization, washed once in ice-cold PBS, and resuspended in Cytosol Extraction Buffer. After incubation on ice for 10 min, cells were homogenized by gentle douncing (100 strokes) in a glass microgrinder and centrifuged at 700 g for 10 min at 4°C to pellet nuclei and unbroken cells. Supernatants from the centrifugation were further centrifuged at 10 000 g for 30 min at 4°C to get cytosolic fraction (supernatant) and mitochondrial fraction (pellet). The levels of cytochrome *c* in the cytosolic fractions were detected by western blot analysis.

2.10. Small Interfering RNA Transfection. Small interfering RNA (siRNA) against p38, Atg5, and the negative control was purchased from Ambion (Austin, TX), and the assay was performed as described previously [30]. Briefly, A498 cells were seeded in 6 cm dishes overnight and then transfected with 10 μL negative control and siRNA (200 pmol) by using 10 μL Lipofectamine 2000 (Invitrogen, Carlsbad, CA). After 24 h, the medium was replaced with growth medium and cells were treated with heteronemin for the indicated time.

2.11. GFP-LC3 Localization by Fluorescence Microscopy. Autophagy was confirmed by the presence of fluorescent puncta in cells transfected with a GFP-LC3. Briefly, A498 cells were seeded in 4-well chamber slides and transiently transfected with 2 μg/mL GFP-LC3 plasmid (purchased from Addgene, Cambridge, MA) using Lipofectamine 2000. After 24 h, cells were treated with 3 μM heteronemin for 6 h and then fixed with 4% paraformaldehyde and stained with DAPI for nuclei observation. The staining was examined and photographed using Axioplan 2 fluorescence microscope equipped with a CCD camera at 20x magnification. Data were analysed by AxioVision software.

2.12. Statistical Analysis. All experiments were performed at least three times. Data are expressed as mean ± SE for the indicated number of separate experiments. Statistical analysis of data was done with Student's *t*-test. *P* values less than 0.05 were considered significant.

3. Results

3.1. Heteronemin-Induced Cell Apoptosis in A498 Cells. We assessed the impact of heteronemin treatment on three human cancer cell lines: A549, ACHN, and A498. Using the MTT assay, we first measured cell viability. Heteronemin induces cytotoxicity in a concentration-dependent manner in the ACHN and A498 human renal carcinoma cell lines but not in the lung adenocarcinoma epithelial cell line A549. The cytotoxic activity against ACHN and A498 cell lines showed IC_{50} values of 3.54 μM and 1.57 μM, respectively (Figure 1(a)). With the IC_{50} values being in the same range, we chose to continue our investigation using only the A498 cell line.

We used the SRB assay to determine the antiproliferative activity of heteronemin in A498 cells. We treated the cells with different concentrations of heteronemin and found that heteronemin shows a potent antiproliferative effect with a GI_{50} value of 0.77 μM (Figure 1(b)).

We next investigated whether the reduced cell viability was due to apoptosis or necrosis using *in situ* labeling. Using TUNEL staining, heteronemin induced DNA fragmentation in A498 cells (Figure 1(c)). In light-field pictures, A498 cells appeared to be spindle-shaped, adhered to the surface of the culture plate, and were confluent after 24-hour incubation. After treatment with 3 μM heteronemin, typical apoptotic features were observed such as cell rounding, cell shrinkage, and plasma membrane blebbing (Figure 1(c), upper panel). We also demonstrated that heteronemin increases the sub-G1 phase population in a concentration- and time-dependent manner (Figure S1 in the Supplementary Material available online at http://dx.doi.org/10.1155/2014/738241), which is consistent with a role in apoptotic cell death induction.

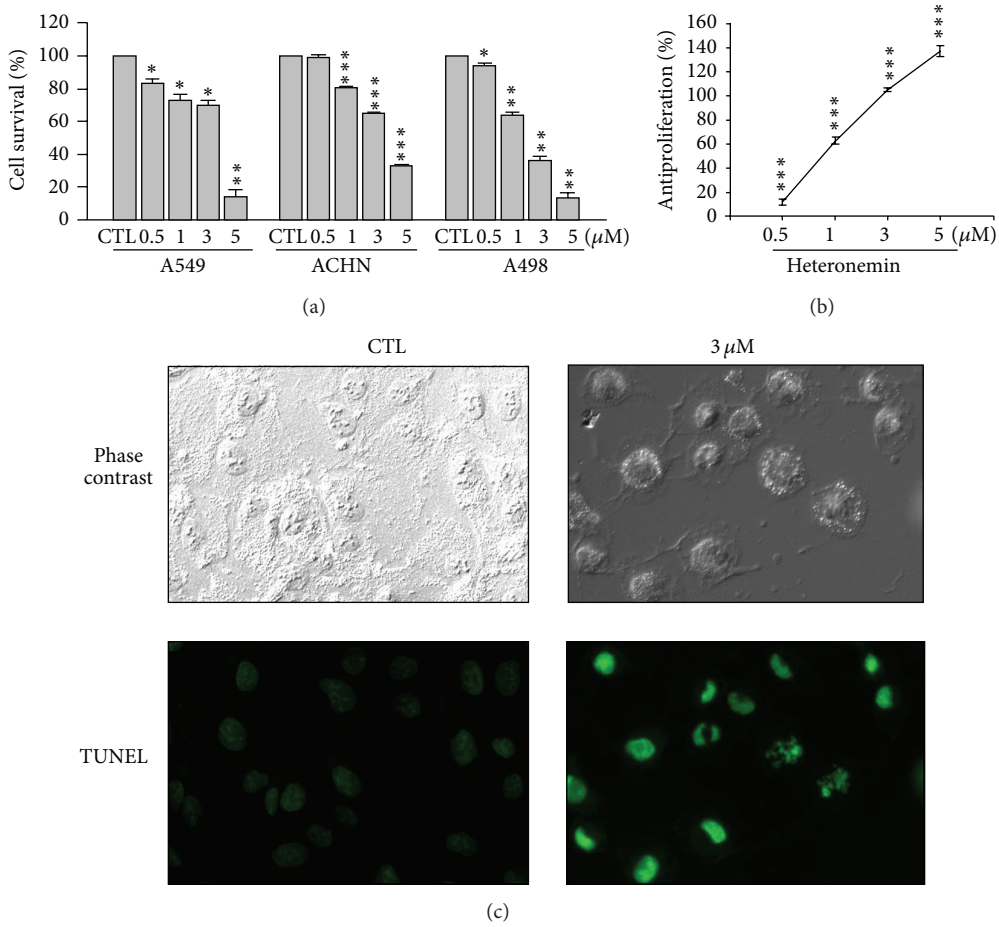

Figure 1: Effects of heteronemin on cell viability in human cancer cell lines. A549, ACHN, and A498 were treated with DMSO or heteronemin at various concentrations for 24 h for MTT assay (a) and for 48 h for SRB assay in A498 cells (b). Fluorescence microscopy of untreated or heteronemin-treated A498 cells for 24 h followed by TUNEL staining (at 20x magnification) (c). Data are expressed as the mean percentage of control ± S.D. of three independent experiments. $^{*}P < 0.05$, $^{**}P < 0.01$, and $^{***}P < 0.001$ compared with the control group. DMSO was used as the vehicle control (CTL).

Heteronemin triggered concentration-dependent apoptosis was independently confirmed using the cell death Detection ELISA kit (Figure 2(a)). In addition, heteronemin treatment resulted in the cleavage of PARP, caspase-3, and caspase-8 and the decrease of procaspase-9 in a concentration- and time-dependent manner (Figures 2(b) and 2(c)). Taken together, these results demonstrated that heteronemin induced cell death via the apoptotic pathway.

3.2. Heteronemin-Induced Apoptosis via a Mitochondrial-Mediated Pathway. The pivotal role of mitochondria in apoptosis induction is well established in mammals [31, 32]. In many types, cytochrome *c* is released from the mitochondrial intermembrane space in response to apoptotic stimuli. Cytochrome *c* is required for the assembly and the activity of the apoptosome, which is composed of the apoptosis-protease activating factor 1 (Apaf-1) and the initiator caspase, caspase-9 [33]. Heteronemin treatment caused loss of the mitochondrial membrane potential in a time-dependent manner and induced the release of cytochrome *c* into the cytosol (Figures 3(a) and 3(b)). In addition, the Bcl-2 protein family regulated mitochondrial permeability and the release of cytochrome *c* to control cell apoptosis. Heteronemin downregulated the expression of Bcl-2 and Bcl-xL and upregulated the expression of Bax (Figure 3(c)). These results suggested that heteronemin induced cell death in A498 cells through the mitochondrial apoptosis pathway.

3.3. Heteronemin Inhibited PI3K/AKT Pathway and ERK in A498 Cells. The PI3K/AKT and MAPK signaling pathways are major pathways regulating the apoptotic process. Thus, we determined whether heteronemin affects these pathways via the expression levels of their downstream signaling proteins. Heteronemin treatment significantly decreased the phosphorylation of AKT, p70S6K, 4EBP-1, and ERK in 3–24 h (Figure 4(a)). Our results also show that heteronemin treatment fast decreased the phosphorylation of ERK and AKT within 0.5–1 h (Figure 4(b)). In addition, we examined the phosphorylation of other MAPKs, JNK, and p38, previously linked to apoptosis as a response to

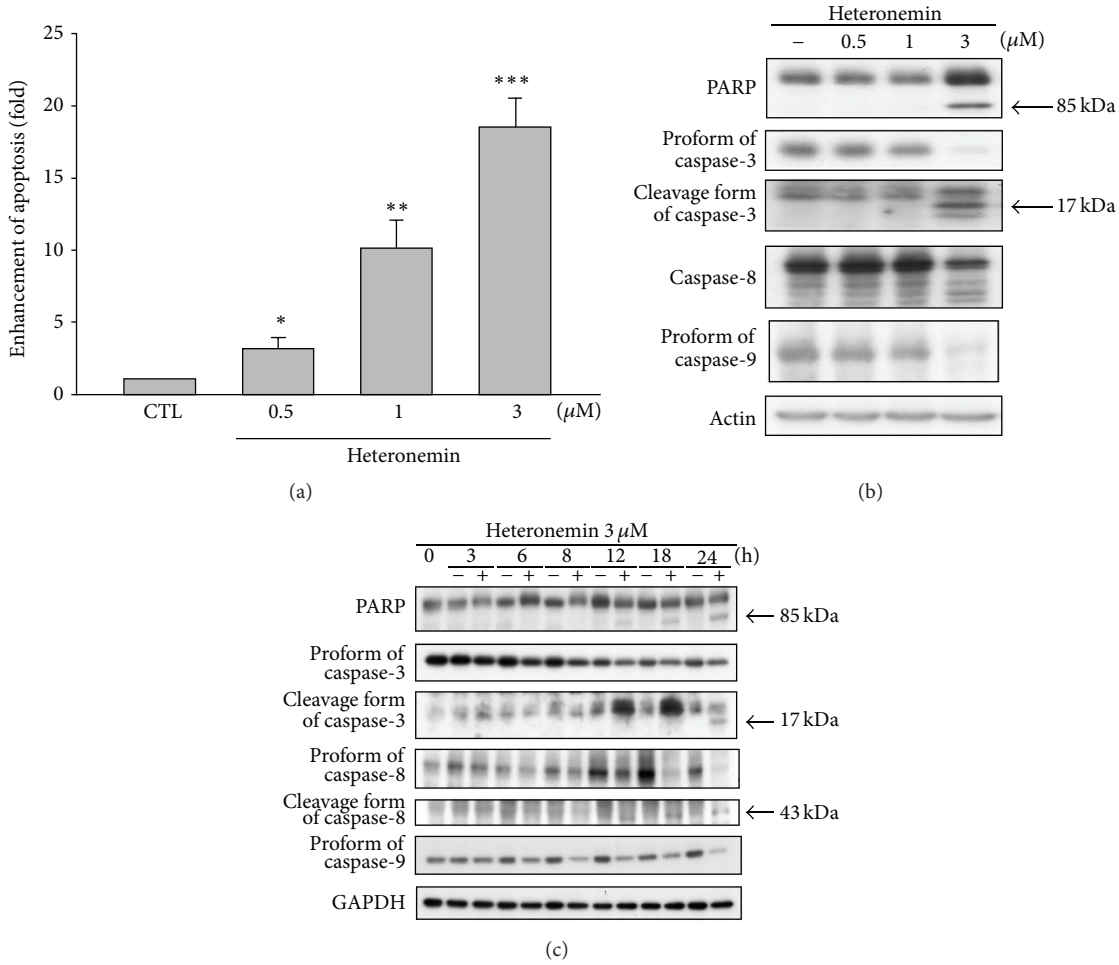

Figure 2: Effects of heteronemin treatment on cell apoptosis induction and expression of apoptosis-related proteins in A498 cells. (a) Cells were treated with DMSO or heteronemin at various concentrations (0.5, 1, and 3 μM) for 24 h. Formation of cytoplasmic DNA was quantitatively measured by cell death ELISA^{PLUS} kit. Data are expressed as the mean percentage of control ± S.D. of three independent experiments. $^{*}P < 0.05$, $^{**}P < 0.01$, and $^{***}P < 0.001$ compared with the control group. A498 cells were incubated in the absence or presence of heteronemin at various concentrations (0.5, 1, and 3 μM) for 24 h (b) or treated for indicated times (c), and cells were harvested and prepared for detection by western blotting. DMSO was used as the vehicle control (CTL).

stress [23, 34]. Western blotting revealed that heteronemin increased the phosphorylation of p38, p38 downstream effector HSP27, and JNK. In summary, our results demonstrated that AKT/p70S6K/4EBP1 signaling pathway and ERK are blocked by heteronemin, whereas p38 and JNK are activated by heteronemin in A498 cells.

3.4. p38 Played an Essential Role in Apoptosis Induction by Heteronemin. To further delineate the role of p38 in heteronemin-induced cytotoxicity, we used the p38 inhibitor SB203580. The results showed that SB203580 reversed the effect of heteronemin-mediated suppression of cell viability (Figure 5(a)). Moreover, transient transfection with p38 siRNA leads to the downregulation of p38 and significantly prevented heteronemin-induced cell death (Figure 5(b)), inhibiting the cleavage of PARP and the downregulation of procaspase-3 (Figure 5(c)). These results demonstrated that heteronemin-induced cell apoptosis is mediated through p38 regulation.

3.5. Heteronemin Induced Autophagy in A498 Cells. The conversion of soluble LC3-I to lipid bound LC3-II via proteolytic cleavage and lipidation can be used as a marker for autophagy induction [35]. Western blotting revealed that heteronemin treatment markedly induced the expression of LC3-II in A498 cells, suggestive of autophagy induction (Figure 6(a)). During autophagy, p62 is wrapped into autophagosome and degraded in autolysosome. In heteronemin-treated cells, the expression of p62 was reduced as revealed by western blotting analysis, and this decrease correlates with the induction of autophagy. Furthermore, we assessed the ability of heteronemin to facilitate the conversion of LC3-I to LC3-II in GFP-LC3-expressing A498 cells. After heteronemin treatment, the GFP-LC3-transfected A498 cells showed a significant increase

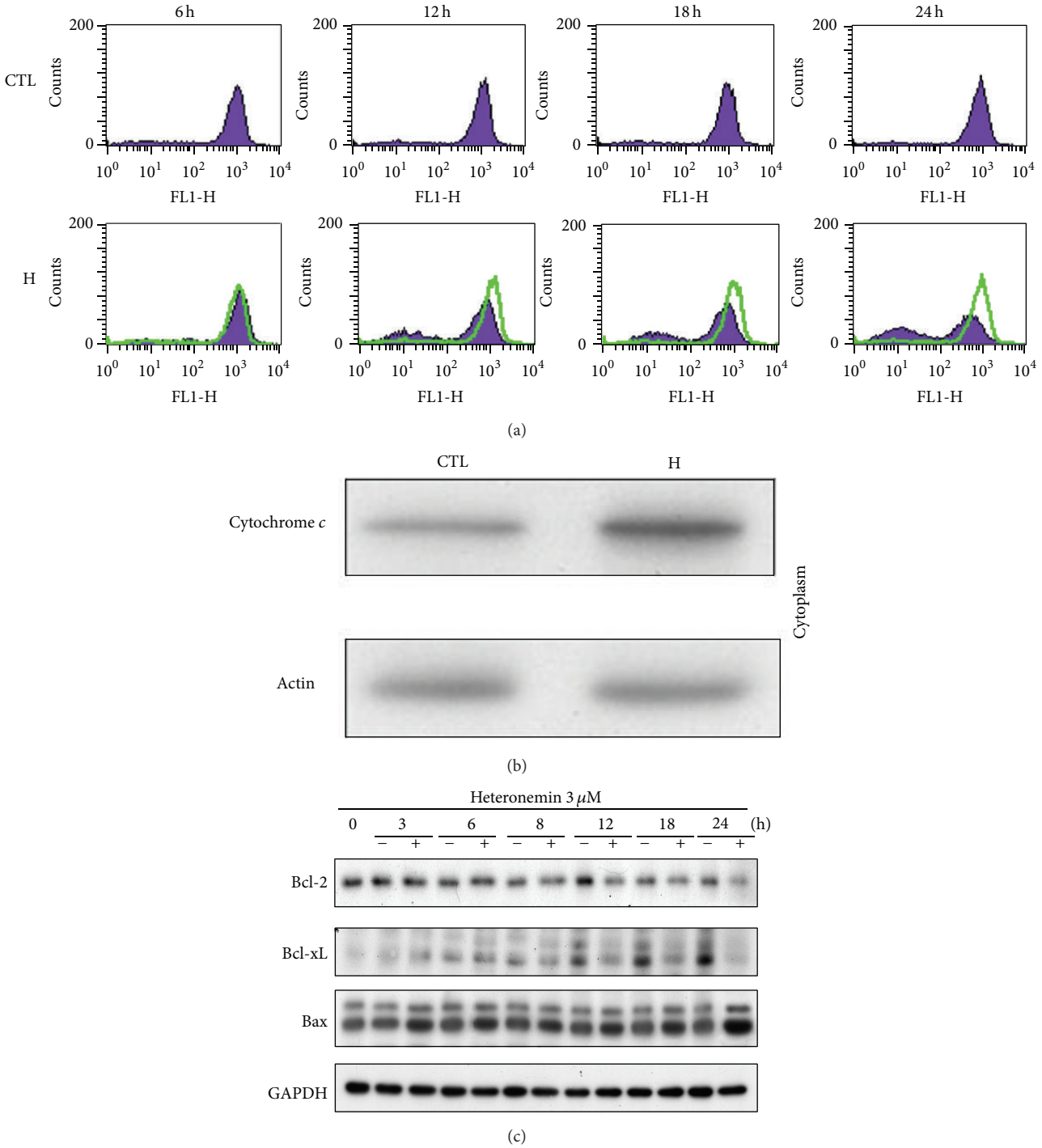

Figure 3: Effect of heteronemin on reduction of $\Delta\psi_m$ and release of cytochrome *c*. A498 cells were incubated in the DMSO or 3 μM heteronemin for indicated time, and cells were harvested and prepared for detection, (a) mitochondria membrane potential by using FACScan analysis, (b) release of cytochrome *c* in cytosol for 24 h, and (c) Bcl-2, Bcl-xL, and Bax expression by using western blotting analysis. DMSO was used as the vehicle control (CTL).

of punctate cytoplasmic dots, indicating autophagosome formation [36] (Figure 6(b)). Taken together, these data demonstrated for the first time that heteronemin induced autophagy in A498 cells.

3.6. Inhibition of Heteronemin-Induced Autophagy Enhanced Apoptosis in A498 Cells. The role of autophagy in cancer remains controversial. Autophagy can induce autophagic cell death through an overdegradation of the cytoplasm, or it

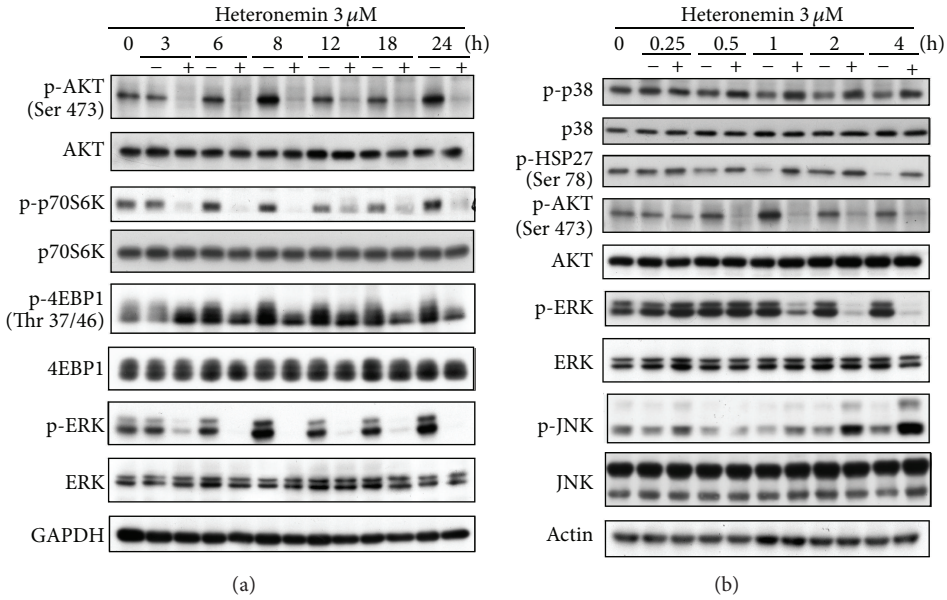

Figure 4: Effects of heteronemin on PI3K/AKT and MAPK signaling pathway in A498 cells. A498 cells were incubated with DMSO or 3 μM heteronemin for the indicated time periods. After treatment, cells were harvested and lysed for detection of the expression of indicated protein via western blotting. DMSO was used as the vehicle control (CTL).

can protect cancer cells from apoptosis by reducing the cellular stress [37]. To clarify the function of autophagy in heteronemin-induced cell death, chloroquine, an inhibitor of autophagy, was used. When cells were cotreated with chloroquine and heteronemin, heteronemin-induced cell death increased (Figure 7(a)). Because of Atg5 involved in the elongation of isolation membrane in autophagosome formation, we confirmed this effect by transfection A498 cells with Atg5-targeting siRNA (Figure 7(b)) and found that heteronemin promoted the cleavage of PARP and caspase-3 after Atg5 knockdown (Figure 7(c)).

Heteronemin induced the phosphorylation of JNK (Figure 4(b)). Using the JNK inhibitor SP600125 together with heteronemin, we showed (Figures 7(d) and 7(e)) that cytotoxicity and the cleavage of PARP and caspase-3 were intensified in the same way compared to when cells are cotreated with chloroquine or with Atg5-targeting siRNA. Taken together, these data suggested that when heteronemin-induced autophagy is inhibited, cytotoxicity and the apoptotic effects of the drug are potentiated.

4. Discussion

The ocean has a rich ecosystem and has recently attracted a lot of interest as a source of natural products for drug discovery. To date, approximately 16,000 marine natural products have been isolated from marine organisms and several of them exhibit a biological activity [38]. The ocean is now considered a source of potential drugs.

Many bioactive marine compounds are terpenes. Sesterterpenes and triterpenes are common terpenes extracted from sponges. Most bioactive compounds from sponges can be classified as anti-inflammatory, antitumor, immunosuppressive or neurosuppressive, antiviral, antimalarial, antibiotic, or antifouling [39]. Here, we investigated the anticancer activity of heteronemin, a natural compound derived from the marine sponge *Hyrtios* sp. Heteronemin triggers A498 cell cytotoxicity, growth inhibition, and apoptosis in a concentration- and time-dependent manner. Heteronemin-induced cell apoptosis is mediated by the release of cytochrome *c* into the cytosol upon the disruption of the mitochondria membrane potential. Cytosolic cytochrome *c* mediates the allosteric activation of Apaf-1, and together they form the apoptosome. The apoptosome recruits caspase-9 leading to the amplification of the apoptotic signal through the proteolytic cleavage and the activation of capase-9 and caspase-3 [40].

Bcl-2 family proteins are involved in the regulation of the outer mitochondrial membrane permeabilization and are divided into two groups: pro- and antiapoptotic proteins. Proapoptotic proteins, such as Bax and Bak, homooligomerize and participate in the formation of pores in the outer mitochondrial membrane through which proapoptotic molecules escape, including second mitochondria-derived activator of caspase (Smac) (also known as Diablo) and cytochrome *c*. Antiapoptotic proteins, such as Bcl-2 and Bcl-xL, block cell death by preventing the activation and homooligomerization of Bax and Bak [41]. We found that heteronemin downregulates the expression of Bcl-2 and Bcl-xL, upregulates the expression of Bax, and induces the loss of mitochondria membrane potential. These results suggest that the mitochondrial apoptotic pathway is important in heteronemin-induced cell death in A498 cells.

The PI3K/AKT signaling pathway regulates many normal cellular functions that are also critical for tumorigenesis,

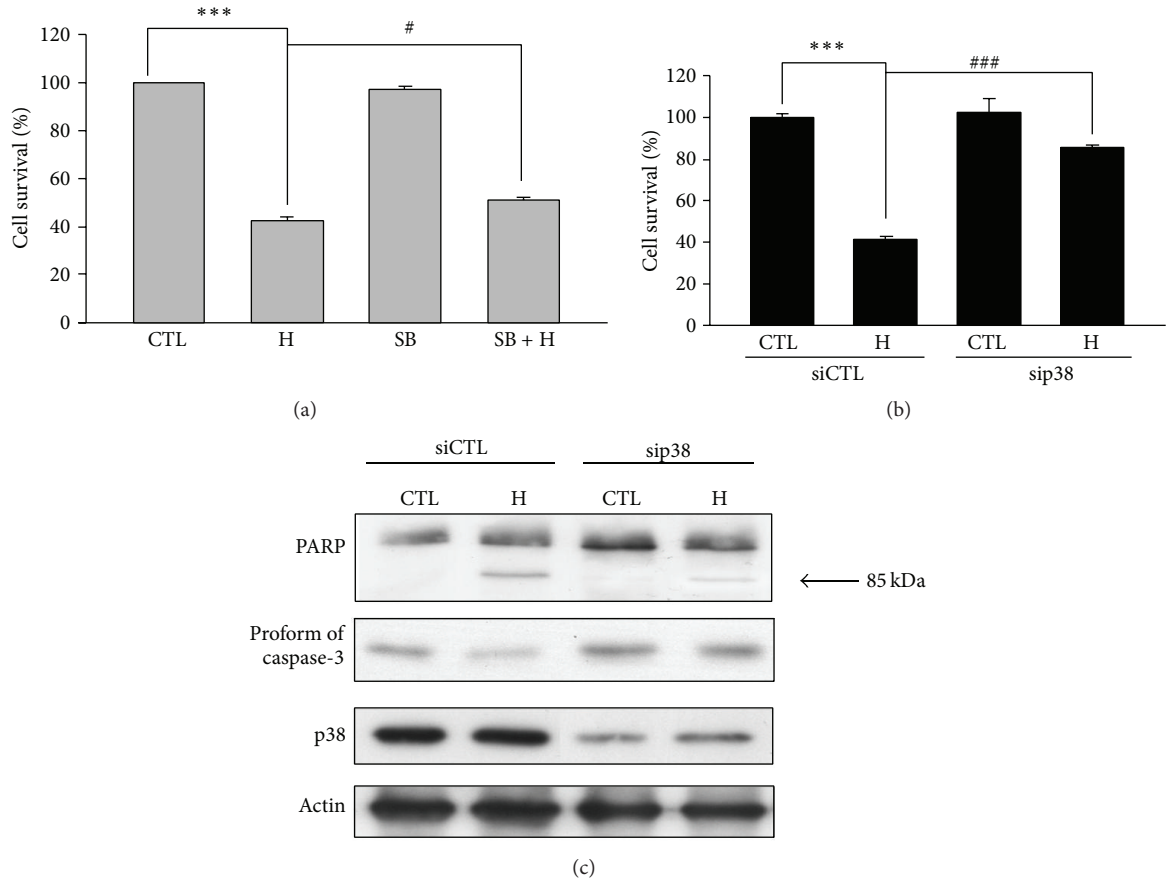

Figure 5: p38 involved in heteronemin-induced cell apoptosis in A498 cells. (a) p38 inhibitor, SB203580, was preincubated for 30 min and cell viability was determined by MTT assay. $^{***}P < 0.001$ compared with the control group. $^{\#}P < 0.05$ and $^{\#\#\#}P < 0.001$ compared with the heteronemin-treated group. p38 siRNA was transfected to evaluate the role in heteronemin-induced A498 cell death by using the MTT assay (b), expression of apoptosis-related proteins (PARP and procaspase-3) (c) for 24 h. H and SB are indicated as heteronemin 3 μM and SB203580 25 μM, respectively. CTL is indicated as control.

including cell proliferation, growth, survival, and motility. Several studies show that PI3K/AKT pathway is abnormally overexpressed in RCC [42–45], making it an attractive target for anticancer therapy [46–48]. For cell survival, AKT activates the NF-κB pathway via the regulation of IκB kinase (IKK), resulting in transcription of prosurvival genes. The transcription factor NF-κB transactivates various antiapoptotic NF-κB target genes, including inhibitor of apoptosis proteins (IAPs), Bcl-xL, and Bcl-2 [49]. A previous study had reported that heteronemin completely prevents TNFα-induced degradation of IκBα and the subsequent translocation of p50 and p65 to the nucleus and that heteronemin is able to inhibit the activation of the NF-κB pathway [10]. Our study shows that heteronemin treatment markedly suppresses the activation of AKT and its related downstream proteins. The ability of heteronemin to inhibit the AKT and NF-κB pathways demonstrates that heteronemin is an effective bioactive marine natural compound.

The p38 signaling pathway is closely associated with the initiation of apoptosis in various types of cells, and this pathway is the target of many antitumor compounds [24]. AD-1, a novel ginsenoside derivative, increased the phosphorylation level of p38 which contributed to the antiproliferative effect, and *in vivo* data showed that treatment of AD-1 led to p38 activation, which correlated with decreased angiogenesis and the inhibition of tumor growth [50]. Arctigenin, a dietary phytoestrogen, increased superoxide anion and hydrogen peroxide levels by nicotinamide adenine dinucleotide phosphate (NADPH) oxidase 1 (NOX1) and activated p38 pathway to induce apoptosis in human breast cancer MDA-MB-231 cells by triggering the mitochondrial caspase-independent apoptotic pathway [51]. In addition to apoptosis, p38 can also mediate autophagy in response to chemotherapeutic agents. However, the treatment with p38 inhibitor had no influence on the expression of LC3 in our model (Figure S2). Here, we found that heteronemin rapidly activates p38 and the inhibition of p38 reverses heteronemin-induced cell apoptosis, demonstrating that p38 is involved in the cell apoptotic pathway but not in the autophagic pathway.

At low levels, autophagy is a process that allows cells to adapt to stress and avoid cell death; however, at high levels and under some cellular circumstances, autophagy offers

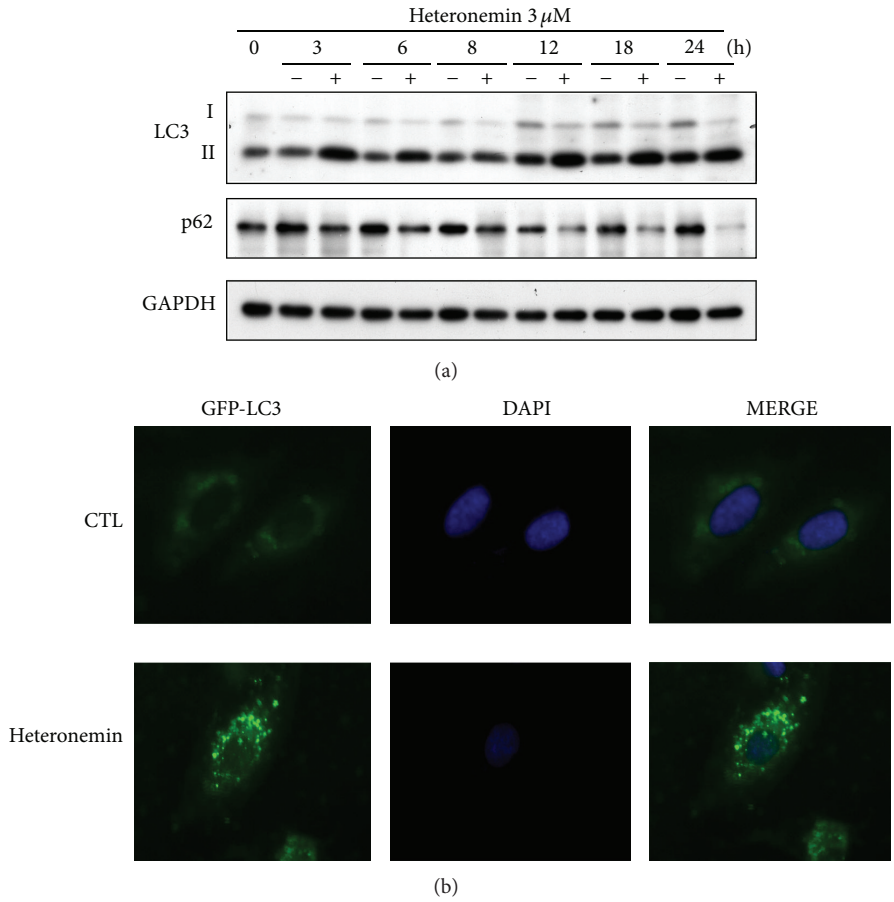

Figure 6: Effects of heteronemin on autophagy in A498 cells. (a) Cells were treated with 3 μM heteronemin for indicated times, and cell lysates were subjected to western blot analysis of the expression of LC3 and p62. DMSO was used as the vehicle control (CTL). (b) Microscopic analysis of the effect of DMSO or heteronemin on the pattern of GFP-LC3 fluorescence. A498 cells were transfected with vectors encoding GFP-LC3, cultured in complete medium for 24 h, and treated for 18 h with DMSO or 3 μM heteronemin. Representative images of GFP-LC3 puncta are shown, as photographed under microscopy.

an alternative pathway to kill abnormal cells. We observed autophagy induction in A498 cells after heteronemin treatment, as evidenced by the upregulation of LC3-II protein. However, the addition of the autophagy inhibitor chloroquine increased heteronemin cytotoxicity in A498 cells, suggesting a potential avenue for an enhanced therapeutic activity. It has been reported that autophagy inhibitors given in combination with chemotherapy suppressed tumor growth and triggered cell death to a greater extent than did chemotherapy alone, both *in vitro* and *in vivo* [52]. These data indicate that the prosurvival autophagy is a novel therapeutic target. Moreover, several studies have shown that the JNK pathway also induces autophagy. JNK signaling was a key requirement for upregulation of LC3 during ceramide-induced autophagy in human nasopharyngeal carcinoma cells [26]. Bortezomib induced autophagy in head and neck squamous cell carcinoma cells via JNK activation [53]. We found that heteronemin induces the phosphorylation of JNK and the cotreatment with a JNK inhibitor increases heteronemin-induced cytotoxicity and apoptotic signaling in A498 cells at a level similar to that with chloroquine. The activation of JNK modulates autophagy through two distinct mechanisms. (i) It promotes the phosphorylation of Bcl-2/Bcl-xL resulting in the dissociation of the Beclin 1-Bcl-2/Bcl-xL complex, thereby stimulating autophagy [54]. (ii) JNK leads to the upregulation of damage-regulated autophagy modulator (DRAM). DRAM can stimulate the accumulation of autophagosomes by regulating the autophagosome-lysosome fusion to generate autolysosomes [55]. Therefore, the crosstalk between JNK activation and heteronemin-induced autophagy needs to be further investigated.

Taken together, this study shows that heteronemin induces apoptosis and autophagy in human renal carcinoma A498 cells. Heteronemin inhibits the phosphorylation of ERK and AKT signaling pathway and increases the phosphorylation of p38 and JNK. The inhibition of p38, but not JNK, can reverse heteronemin-induced cytotoxicity and apoptotic signaling. Heteronemin also induces autophagy in A498 cells, and cotreatment with chloroquine or SP600125 inhibits autophagy and increases heteronemin-induced cytotoxicity and apoptotic signaling (Figure 8). Therefore, this investigation provides new insight into the role of heteronemin as

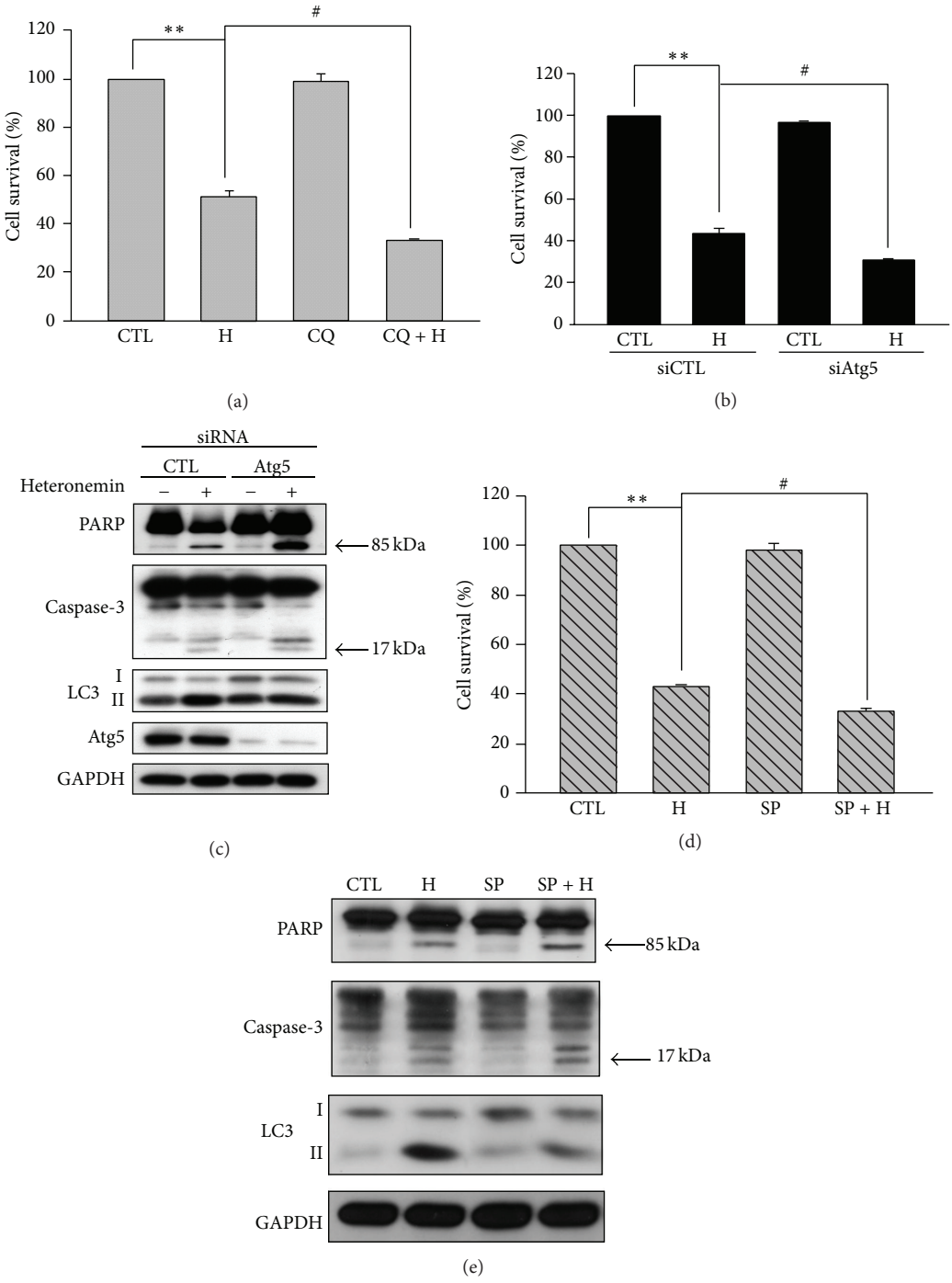

FIGURE 7: Inhibition of autophagy enhanced the anticancer effect of heteronemin in A498 cells. A498 cells were pretreated with autophagy inhibitor, chloroquine, for 30 min, then 3 μM heteronemin was added for 24 h, and (a) the cell viability was determined using MTT assay. A498 cells were transfected with Atg5 siRNA or negative control and (b) the cell viability was determined using MTT assay and (c) the expression of apoptosis-related proteins (PARP and procaspase-3) and autophagy-related proteins (LC3 and Atg5) was evaluated for 24 h by western blotting. A498 cells were pretreated with JNK inhibitor, SP600125, for 30 min, then 3 μM heteronemin was added for 24 h, and (d) the cell viability was determined using MTT assay and (e) the expression of apoptosis-related proteins (PARP and procaspase-3) and LC3 was evaluated for 24 h by western blotting. H, CQ, and SP are indicated as heteronemin 3 μM, chloroquine 50 μM, and SP600125 20 μM, respectively. $^{**}P < 0.01$ compared with the control group. $^{\#}P < 0.05$ compared with the heteronemin-treated group. CTL is indicated as control. DMSO was used as the vehicle control (CTL).

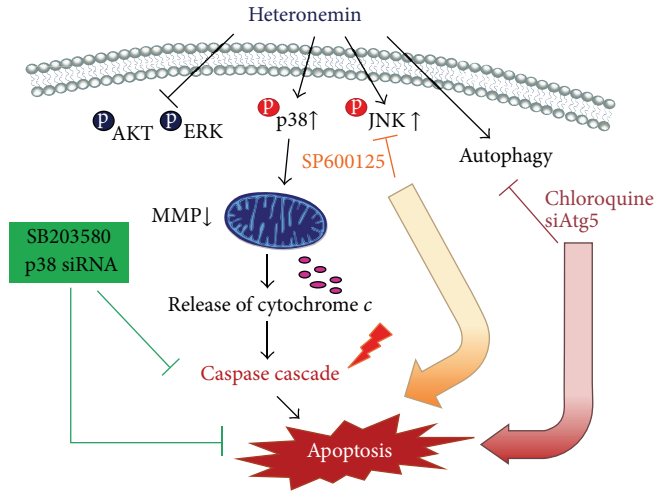

Figure 8: Schematic representation of the different pathways shown in this report to be activated by heteronemin leading to apoptosis in A498 cells.

a potential anticancer agent and suggests that the combination of heteronemin with autophagy inhibitors further enhances its therapeutic effects.

Conflict of Interests

The authors have declared that no conflict of interests exists.

Acknowledgment

This work was supported by a Research Grant from the National Science Council of Taiwan (NSC 99-2628-B-002-024-MY2).

References

[1] F. H. Sarkar, Y. Li, Z. Wang, and D. Kong, "Cellular signaling perturbation by natural products," *Cellular Signalling*, vol. 21, no. 11, pp. 1541–1547, 2009.

[2] M. Zidane, P. Pondaven, C. Roussakis, and M.-T. More, "Effects in vitro of pachymatismin, a glycoprotein from the marine sponge Pachymatisma johnstonii, on a non-small-cell bronchopulmonary carcinoma line (NSCLC-N6)," *Anticancer Research*, vol. 16, no. 5, pp. 2805–2812, 1996.

[3] R. Mutter and M. Wills, "Chemistry and clinical biology of the bryostatins," *Bioorganic and Medicinal Chemistry*, vol. 8, no. 8, pp. 1841–1860, 2000.

[4] G. R. Pettit, C. L. Herald, and Y. Kamano, "Structure of the Bugula neritina (marine bryozoa) antineoplastic component bryostatin 3," *Journal of Organic Chemistry*, vol. 48, no. 26, pp. 5354–5356, 1983.

[5] G. R. Pettit, C. L. Herald, Y. Kamano, D. Gust, and R. Aoyagi, "The structure of bryostatin 2 from the marine Bryozoan Bugula neritina," *Journal of Natural Products*, vol. 46, no. 4, pp. 528–531, 1983.

[6] P.-C. Chiang, C.-L. Chien, S.-L. Pan et al., "Induction of endoplasmic reticulum stress and apoptosis by a marine prostanoid in human hepatocellular carcinoma," *Journal of Hepatology*, vol. 43, no. 4, pp. 679–686, 2005.

[7] S.-N. Wonganuchitmeta, S. Yuenyongsawad, N. Keawpradub, and A. Plubrukarn, "Antitubercular sesterterpenes from the Thai sponge *Brachiaster* sp," *Journal of Natural Products*, vol. 67, no. 10, pp. 1767–1770, 2004.

[8] H. N. Kamel, Y. B. Kim, J. M. Rimoldi, F. R. Fronczek, D. Ferreira, and M. Slattery, "Scalarane sesterterpenoids: semisynthesis and biological activity," *Journal of Natural Products*, vol. 72, no. 8, pp. 1492–1496, 2009.

[9] S. Kopf, K. Viola, A. G. Atanasov et al., "In vitro characterisation of the anti-intravasative properties of the marine product heteronemin," *Archives of Toxicology*, vol. 87, no. 10, pp. 1851–1861, 2013.

[10] M. Schumacher, C. Cerella, S. Eifes et al., "Heteronemin, a spongean sesterterpene, inhibits TNFα-induced NF-κB activation through proteasome inhibition and induces apoptotic cell death," *Biochemical Pharmacology*, vol. 79, no. 4, pp. 610–622, 2010.

[11] N. Mizushima, Y. Ohsumi, and T. Yoshimori, "Autophagosome formation in mammalian cells," *Cell Structure and Function*, vol. 27, no. 6, pp. 421–429, 2002.

[12] B. Levine and G. Kroemer, "Autophagy in the pathogenesis of disease," *Cell*, vol. 132, no. 1, pp. 27–42, 2008.

[13] K. Kirkegaard, M. P. Taylor, and W. T. Jackson, "Cellular autophagy: surrender, avoidance and subversion by microorganisms," *Nature Reviews Microbiology*, vol. 2, no. 4, pp. 301–314, 2004.

[14] C. Münz, "Autophagy and antigen presentation," *Cellular Microbiology*, vol. 8, no. 6, pp. 891–898, 2006.

[15] B. Levine and D. J. Klionsky, "Development by self-digestion: molecular mechanisms and biological functions of autophagy," *Developmental Cell*, vol. 6, no. 4, pp. 463–477, 2004.

[16] B. Levine and J. Yuan, "Autophagy in cell death: an innocent convict?" *Journal of Clinical Investigation*, vol. 115, no. 10, pp. 2679–2688, 2005.

[17] E. H. Baehrecke, "Autophagy: dual roles in life and death?" *Nature Reviews Molecular Cell Biology*, vol. 6, no. 6, pp. 505–510, 2005.

[18] R. A. Lockshin and Z. Zakeri, "Caspase-independent cell deaths," *Current Opinion in Cell Biology*, vol. 14, no. 6, pp. 727–733, 2002.

[19] A. Eisenberg-Lerner, S. Bialik, H. U. Simon, and A. Kimchi, "Life and death partners: apoptosis, autophagy and the cross-talk between them," *Cell Death and Differentiation*, vol. 16, no. 7, pp. 966–975, 2009.

[20] J. A. McCubrey, M. M. LaHair, and R. A. Franklin, "Reactive oxygen species-induced activation of the MAP kinase signaling pathways," *Antioxidants and Redox Signaling*, vol. 8, no. 9-10, pp. 1775–1789, 2006.

[21] S. Torii, T. Yamamoto, Y. Tsuchiya, and E. Nishida, "ERK MAP kinase in G_1 cell cycle progression and cancer," *Cancer Science*, vol. 97, no. 8, pp. 697–702, 2006.

[22] A. S. Dhillon, S. Hagan, O. Rath, and W. Kolch, "MAP kinase signalling pathways in cancer," *Oncogene*, vol. 26, no. 22, pp. 3279–3290, 2007.

[23] Z. Xia, M. Dickens, J. Raingeaud, R. J. Davis, and M. E. Greenberg, "Opposing effects of ERK and JNK-p38 MAP kinases on apoptosis," *Science*, vol. 270, no. 5240, pp. 1326–1331, 1995.

[24] A. Cuadrado and A. R. Nebreda, "Mechanisms and functions of p38 MAPK signalling," *Biochemical Journal*, vol. 429, no. 3, pp. 403–417, 2010.

[25] K. Azijli, S. Yuvaraj, I. Van Roosmalen et al., "MAPK p38 and JNK have opposing activities on TRAIL-induced apoptosis activation in NSCLC H460 cells that involves RIP1 and caspase-8 and is mediated by Mcl-1," *Apoptosis*, vol. 18, no. 7, pp. 851–860, 2013.

[26] T. Sun, D. Li, L. Wang et al., "C-Jun NH2-terminal kinase activation is essential for up-regulation of LC3 during ceramide-induced autophagy in human nasopharyngeal carcinoma cells," *Journal of Translational Medicine*, vol. 9, no. 1, article 161, 2011.

[27] R. J. H. West and S. T. Sweeney, "Oxidative stress and autophagy: mediators of synapse growth?" *Autophagy*, vol. 8, no. 2, pp. 284–285, 2012.

[28] P. Haberzettl and B. G. Hill, "Oxidized lipids activate autophagy in a JNK-dependent manner by stimulating the endoplasmic reticulum stress response," *Redox Biology*, vol. 1, no. 1, pp. 56–64, 2013.

[29] C. C. Yu, P. C. Chiang, P. H. Lu et al., "Antroquinonol, a natural ubiquinone derivative, induces a cross talk between apoptosis, autophagy and senescence in human pancreatic carcinoma cells," *Journal of Nutritional Biochemistry*, vol. 23, no. 8, pp. 900–907, 2012.

[30] S. Y. Wu, S. L. Pan, T. H. Chen et al., "YC-1 induces apoptosis of human renal carcinoma A498 cells in vitro and in vivo through activation of the JNK pathway," *The British Journal of Pharmacology*, vol. 155, no. 4, pp. 505–513, 2008.

[31] N. N. Danial and S. J. Korsmeyer, "Cell death: critical control points," *Cell*, vol. 116, no. 2, pp. 205–219, 2004.

[32] D. D. Newmeyer and S. Ferguson-Miller, "Mitochondria: releasing power for life and unleashing the machineries of death," *Cell*, vol. 112, no. 4, pp. 481–490, 2003.

[33] X. Jiang and X. Wang, "Cytochrome C-mediated apoptosis," *Annual Review of Biochemistry*, vol. 73, no. 1, pp. 87–106, 2004.

[34] E. F. Wagner and Á. R. Nebreda, "Signal integration by JNK and p38 MAPK pathways in cancer development," *Nature Reviews Cancer*, vol. 9, no. 8, pp. 537–549, 2009.

[35] F. Hu, J. Han, B. Zhai et al., "Blocking autophagy enhances the apoptosis effect of bufalin on human hepatocellular carcinoma cells through endoplasmic reticulum stress and JNK activation," *Apoptosis*, vol. 19, no. 1, pp. 210–223, 2014.

[36] D. J. Klionsky, H. Abeliovich, P. Agostinis et al., "Guidelines for the use and interpretation of assays for monitoring autophagy in higher eukaryotes," *Autophagy*, vol. 4, no. 2, pp. 151–175, 2008.

[37] I. Dikic, T. Johansen, and V. Kirkin, "Selective autophagy in cancer development and therapy," *Cancer Research*, vol. 70, no. 9, pp. 3431–3434, 2010.

[38] D. S. R. D. S. Bhakuni, *Bioactive Marine Natural Products*, Springer, Amsterdam, The Netherlands, 2005.

[39] D. Sipkema, M. C. R. Franssen, R. Osinga, J. Tramper, and R. H. Wijffels, "Marine sponges as pharmacy," *Marine Biotechnology*, vol. 7, no. 3, pp. 142–162, 2005.

[40] C. Garrido, L. Galluzzi, M. Brunet, P. E. Puig, C. Didelot, and G. Kroemer, "Mechanisms of cytochrome c release from mitochondria," *Cell Death and Differentiation*, vol. 13, no. 9, pp. 1423–1433, 2006.

[41] J. K. Brunelle and A. Letai, "Control of mitochondrial apoptosis by the Bcl-2 family," *Journal of Cell Science*, vol. 122, no. 4, pp. 437–441, 2009.

[42] N. Rasmussen and W. K. Rathmell, "Looking beyond inhibition of VEGF/mTOR: emerging targets for renal cell carcinoma drug development," *Current Clinical Pharmacology*, vol. 6, no. 3, pp. 199–206, 2011.

[43] I. R. Konings, J. Verweij, E. A. Wiemer, and S. Sleijfer, "The applicability of mTOR inhibition in solid tumors," *Current Cancer Drug Targets*, vol. 9, no. 3, pp. 439–450, 2009.

[44] G. R. Hudes, "Targeting mTOR in renal cell carcinoma," *Cancer*, vol. 115, no. 10, pp. 2313–2320, 2009.

[45] P. J. Wysocki, "MTOR in renal cell cancer: modulator of tumor biology and therapeutic target," *Expert Review of Molecular Diagnostics*, vol. 9, no. 3, pp. 231–241, 2009.

[46] D. Morgensztern and H. L. McLeod, "PI3K/Akt/mTOR pathway as a target for cancer therapy," *Anti-Cancer Drugs*, vol. 16, no. 8, pp. 797–803, 2005.

[47] R. J. Shaw and L. C. Cantley, "Ras, PI(3)K and mTOR signalling controls tumour cell growth," *Nature*, vol. 441, no. 7092, pp. 424–430, 2006.

[48] B. T. Hennessy, D. L. Smith, P. T. Ram, Y. Lu, and G. B. Mills, "Exploiting the PI3K/AKT pathway for cancer drug discovery," *Nature Reviews Drug Discovery*, vol. 4, no. 12, pp. 988–1004, 2005.

[49] O. N. Ozes, L. D. Mayo, J. A. Gustin, S. R. Pfeffer, L. M. Pfeffer, and D. B. Donner, "NF-κB activation by tumour necrosis factor requires tie Akt serine- threonine kinase," *Nature*, vol. 401, no. 6748, pp. 82–85, 1999.

[50] L.-H. Zhang, Y.-L. Jia, X.-X. Lin et al., "AD-1, a novel ginsenoside derivative, shows anti-lung cancer activity via activation of p38 MAPK pathway and generation of reactive oxygen species," *Biochimica et Biophysica Acta—General Subjects*, vol. 1830, no. 8, pp. 4148–4159, 2013.

[51] C. J. Hsieh, P. L. Kuo, Y. C. Hsu, Y. F. Huang, E. M. Tsai, and Y. L. Hsu, "Arctigenin, a dietary phytoestrogen, induces apoptosis of estrogen receptor-negative breast cancer cells through the ROS/p38 MAPK pathway and epigenetic regulation," *Free Radical Biology and Medicine*, vol. 67, pp. 159–170, 2014.

[52] Z. J. Yang, C. E. Chee, S. Huang, and F. A. Sinicrope, "The role of autophagy in cancer: therapeutic implications," *Molecular Cancer Therapeutics*, vol. 10, no. 9, pp. 1533–1541, 2011.

[53] C. Li and D. E. Johnson, "Bortezomib induces autophagy in head and neck squamous cell carcinoma cells via JNK activation," *Cancer Letters*, vol. 314, no. 1, pp. 102–107, 2012.

[54] F. Zhou, Y. Yang, and D. Xing, "Bcl-2 and Bcl-xL play important roles in the crosstalk between autophagy and apoptosis," *FEBS Journal*, vol. 278, no. 3, pp. 403–413, 2011.

[55] S. Lorin, G. Pierron, K. M. Ryan, P. Codogno, and M. Djavaheri-Mergny, "Evidence for the interplay between JNK and p53-DRAM signalling pathways in the regulation of autophagy," *Autophagy*, vol. 6, no. 1, pp. 153–154, 2010.

Hindawi Publishing Corporation
BioMed Research International
Volume 2015, Article ID 296721, 15 pages
http://dx.doi.org/10.1155/2015/296721

Research Article

Vitamin K1 Exerts Antiproliferative Effects and Induces Apoptosis in Three Differently Graded Human Colon Cancer Cell Lines

Antonella Orlando,[1] Michele Linsalata,[1] Valeria Tutino,[2] Benedetta D'Attoma,[1] Maria Notarnicola,[2] and Francesco Russo[1]

[1]*Laboratory of Nutritional Pathophysiology, National Institute for Digestive Diseases IRCCS "Saverio de Bellis", Castellana Grotte, 70013 Bari, Italy*
[2]*Laboratory of Nutritional Biochemistry, National Institute for Digestive Diseases IRCCS "Saverio de Bellis", Castellana Grotte, 70013 Bari, Italy*

Correspondence should be addressed to Francesco Russo; francesco.russo@irccsdebellis.it

Received 25 September 2014; Accepted 29 November 2014

Academic Editor: István Zupkó

Vitamin K1 has been demonstrated as having anticancer potentiality mainly in liver cancer cells. Beyond the reported mechanisms of cancer inhibition (cell cycle arrest and induction of apoptosis), a possible control by vitamin K1 on molecules affecting cell growth could be hypothesized. In the literature, few (if any) data are available on its antitumor effects on colon cancer cells. Therefore, the aims of the study were to investigate in three differently graded human colon cancer cell lines (Caco-2, HT-29, and SW480) the effects of increasing concentrations of vitamin K1 (from 10 μM to 200 μM) administered up to 72 h on (1) cell proliferation, (2) apoptosis with the possible involvement of the MAPK pathway, and (3) polyamine biosynthesis. Vitamin K1 treatment caused a significant antiproliferative effect and induced apoptosis in all the cell lines, with the involvement of the MAPK pathway. A concomitant and significant decrease in the polyamine biosynthesis occurred. This is the first study demonstrating a significant polyamine decrease in addition to the antiproliferative and proapoptotic effects following vitamin K1 administration to colon cancer cell lines. Therapeutically, combinations of vitamin K1 with polyamine inhibitors and/or analogues may represent a suitable option for chemoprevention and/or treatment in future strategies for colorectal cancer management.

1. Introduction

Colorectal cancer (CRC) is a major health problem in industrialized countries [1], but the treatment is still far from being satisfying since approximately 90% of patients do not respond to chemotherapy protocols [2].

Thus, the development of new treatment modalities is necessary to improve the overall survival rate of patients with CRC.

In the last years, an emerging role has been attributed to micronutrients, such as vitamin K (VK). VK is an essential vitamin that was discovered as a fat-soluble antihemorrhagic agent. Physiologically, VK acts as cofactor for the γ-carboxylation of selected glutamates at the N-terminus of prothrombin and other VK-dependent coagulation factors. VK is a family of structurally similar 2-methyl-1,4-naphthoquinones, including phylloquinone (VK1), menaquinone (VK2), and menadione (VK3). All members of the VK family possess an identical naphthoquinone skeleton with various side chains that distinguish them. VK1 is found in many higher plants as well as algae, with the highest concentrations found in green leafy vegetables. VK2 also occurs naturally but is not made by plants being produced by a wide array of bacteria in the intestine. VK3 is not considered a natural VK, but rather a synthetic analogue acting as a provitamin with a much simpler structure and no aliphatic chain prosthetic group at position 3 [3].

Although VK is usually identified as a critical factor in blood coagulation, recent research has demonstrated its ability to inhibit cancer cell growth in both *in vitro* and *in*

vivo studies [4]. The naturally occurring VK and its analogs are able to inhibit the survival of various cancer cell lines [5, 6]. Among the various mechanisms suggested as explaining these effects, the altered expression of some growth related genes (e.g., cyclin D1, cdk4, p21, and p27) that causes cell cycle arrest at G1/S [5] and the induction of apoptosis by the phosphorylation of extracellular signal-regulated kinase (ERK) [7] have been reported.

Although most of the anticancer research on VK has focused on VK2 and VK3, there have also been studies demonstrating the VK1 anticancer effects [4]. The majority of the published data on VK1 are related to hepatocellular carcinoma (HCC) [6] and there are reports supporting the notion that also glioma and pancreatic cancer cell lines are sensitive to phylloquinone [7, 8]. In contrast, to our knowledge, no data are available on its antitumor effects on colon cancer cells.

Beyond the above cited mechanisms of cancer inhibition, a possible control by VK1 on different molecules involved in cell growth mechanisms could be hypothesized. In this context, the cellular polyamines spermidine (Spd) and spermine (Spm), as well as their precursor putrescine (Put), might be considered. These polycations are essential for growth and DNA synthesis and their intracellular content homeostasis is lost during dysregulation of cell proliferation, leading to cancer development [9]. Besides, the mucosal polyamine levels are known to be elevated in cancer cells compared to normal ones and they have also been suggested as specific markers for neoplastic proliferation [10]. Ornithine decarboxylase (ODC) is the key enzyme involved in polyamine biosynthesis. Increased ODC activity and the associated elevation in intracellular polyamines have been implicated in carcinogenesis of many human tissues, including large intestine [11]. Therefore, the polyamine biosynthesis can be regarded as an attractive target for cancer chemotherapy.

Different substances that affect polyamine metabolism, including ODC inhibitors and agents that stimulate polyamine catabolism, have been studied *in vitro* and *in vivo* as new potential therapeutic tools for cancer treatment and prevention [12]. But no data are available about the use of nutritional components such as VK1 for targeting the polyamine pathway in the treatment of CRC.

Starting from these bases, the aims of the present study were to investigate in three human colon cancer cells the effects of increasing concentrations of VK1 on (1) the cell proliferation, (2) the apoptotic processes with the possible involvement of the mitogen-activated protein kinase (MAPK) pathway, and finally (3) the polyamine biosynthesis. In order to evaluate if these effects could vary depending on the peculiarities of cancer cell lines, differently graded human colon cancer cell lines (Caco-2, HT-29, and SW480) were used.

2. Materials and Methods

2.1. Cell Culture Conditions. Human colon adenocarcinoma-derived Caco-2 cell line (well differentiated) (G1-2) (from adenocarcinoma), HT-29 cell line (moderately well differentiated) (G2) (from adenocarcinoma grade II), and SW480 cell line (low differentiated) (G3-4) (from adenocarcinoma grades III-IV) were obtained from the Interlab Cell Line Collection (Genoa, Italy). These colonic adenocarcinoma cells were used since they may represent the spectrum of cellular changes seen in precancerous lesions and manifest tumors [13]. Cells were routinely cultured in RPMI-1640, McCoy's 5A, and Leibovitz L-15 medium, respectively, supplemented with 10% fetal bovine serum (FBS), 2 mM glutamine, 100 U/mL penicillin, and 100 μg/mL streptomycin, in a monolayer culture, and incubated at 37°C in a humidified atmosphere containing 5% CO_2 in air. At confluence, the grown cells were harvested by means of trypsinization and serially subcultured with a 1 : 4 split ratio. All cell culture components were purchased from Sigma-Aldrich (Milan, Italy).

2.2. VK1 Treatment. Caco-2, HT-29, and SW480 cells (25th–30th passage) were seeded at a density of 2×10^5 cells/5 mL of supplemented RPMI-1640, McCoy's 5A, and Leibovitz L-15 medium, respectively, in 60 mm tissue culture dishes (Corning Costar Co., Milan, Italy). After 24 h, to allow attachment the medium was removed and supplemented with culture medium containing increasing concentrations of VK1 (10 μM, 50 μM, 100 μM, and 200 μM) for 24 h, 48 h, and 72 h. Triplicate cultures were set up for each treatment and for the control, and each experiment was repeated 3 times. In the set of experiments investigating the role of ERK 1/2 in the VK1-induced apoptosis, the three cell lines were treated with 20 μM MEK inhibitor (UO126) 2 h prior to 100 μM and 200 μM VK1 treatment for 48 h.

2.3. Assessment of Cell Proliferation. After Caco-2, HT-29, and SW480 cells had been cultured for 24 h, 48 h, and 72 h with increasing concentrations of VK1, the proliferative response was measured by colorimetric 3-(4,5 di-methylthiazol-2-yl)-2,5-diphenyltetrazolium bromide (MTT) test. To determine cell growth by colorimetric test, MTT stock solution (5 mg/mL in medium) was added to each dish at a volume of one-tenth the original culture volume and incubated for 2 h at 37°C in humidified CO_2. At the end of the incubation period, the medium was removed, and the blue formazan crystals were solubilized with acidic isopropanol (0.1 N HCl absolute isopropanol). MTT conversion to formazan by metabolically viable cells was monitored by spectrophotometer at an optical density of 570 nm.

2.4. Apoptosis. The apoptosis was measured by evaluation of Bax and Bcl-2 mRNA expression (using quantitative PCR (qPCR) method with SYBR1 green dye) and protein expression of Bax, Bcl-2, caspase-3, and caspase-9 (using western blot analysis). Cells were washed twice in phosphate buffer saline (PBS) and then trypsinized and centrifuged at 280 ×g. The cell pellets were resuspended in 0.3 mL of pure distilled water and used for RNA extraction. Total cell RNA was extracted using Tri-Reagent (Mol. Res. Center Inc., Cincinnati, Ohio, USA), following the manufacturer's instructions. About 2 μg total cell RNA, extracted from both

the control and treated cells, was used for cDNA synthesis. Reverse transcription (RT) was carried out in 20 μL of the final volume at 41°C for 60 min, using 30 pmol antisense primers for analyses of Bax, Bcl-2, and β-actin gene [14]. The β-actin gene was utilized as an internal control and was chosen as a reference gene because it is a housekeeping gene. Real-time PCRs were performed in 25 μL of final volume containing 2 μL of cDNA, master mix with SYBR Green (iQ SYBR Green Supermix Bio-Rad, Milan, Italy), and sense and antisense primers for Bax, Bcl-2, and β-actin gene. Real-time PCRs were carried out in a CFX96 Real-Time PCR Detection System (Bio-Rad Laboratories, Inc.) using the following protocol: 45 cycles at 95°C for 3 min, 95°C for 10 s, and 55°C for 30 s followed by a melting curve step at 65–95°C with a heating rate of 0.5°C per cycle for 80 cycles. The PCR products were quantified by external calibration curves, one for each tested gene, obtained with serial dilutions of known copy number of molecules (10^2–10^7 molecules). All expression data were normalized by dividing the target amount by the amount of β-actin used as internal control for each sample. The specificity of the PCR product was confirmed by gel electrophoresis.

As concerns western blot, Caco-2, HT-29, and SW480 cells were collected and lysed on ice in RIPA buffer (Pierce RIPA buffer, Thermo Scientific, Rockford, IL, USA). After homogenization and centrifugation at 18000 ×g for 15 min at 4°C, protein concentration was measured by a standard Bradford assay (Bio-Rad Laboratories, Milan, Italy). Aliquots of 50 μg of total proteins were separated in 4–12% precast polyacrylamide gels (Invitrogen, Life Technologies, OR, USA) and transferred onto a PVDF membrane (Bio-Rad Laboratories, Milan, Italy) with the Transblot Turbo (Bio-Rad Laboratories). Bax, Bcl-2, caspase-3, caspase-9, P-ERK 1/2, and β-actin protein expressions were evaluated by 1 : 500 diluted Bax, Bcl-2 (D55G8), cleaved caspase-3 (Asp175), caspase-3 (3G2), cleaved caspase-9, caspase-9, phospho-p44/42 MAPK (ERK 1/2) (197G2), p44/42 MAPK (L34F12), and β-actin antibody, respectively (Cell Signaling Technology, Danvers, MA, USA). After overnight incubation, the membranes were further incubated with a horseradish peroxidase-conjugated goat secondary antibody (Bio-Rad Laboratories). The proteins were detected by chemiluminescence (ECL, Thermo Scientific, Rockford, IL, USA) and the densitometric analysis of each protein-related signal was obtained using the Molecular Imager Chemidoc (Bio-Rad Laboratories) and normalized against β-actin expression.

2.5. Polyamine Biosynthesis. For the evaluation of polyamine levels after VK1 treatment, each cell culture pellet was homogenized in 700 μL of 0.9% sodium chloride mixed with 10 μL (200 nmol/mL) of the internal standard 1,10-diaminodecane (1,10-DAD). An aliquot of the homogenate was used to measure the total protein content. Then, to precipitate proteins, 50 μL of 3 M perchloride acid was added to the homogenate. After 30 min of incubation in ice, the homogenate was centrifuged for 15 min at 7000 ×g. The supernatant was filtered (Millex-HV13 pore size 0.45 μm, Millipore, Bedford, MA, USA) and lyophilized. The residue was dissolved in 300 μL of 0.1 N HCl. Dansylation and the extraction of dansyl-polyamine derivatives were performed as previously described [15]. After extraction, aliquots of 200 μL were injected into a high-performance liquid chromatography system (UltiMate 3000, Dionex Corp., Sunnyvale, CA, USA) equipped with a reverse-phase column (Sunfire C18, 4.6 × 100 mm, 3.5 μm particle size, Waters, Milford, MA, USA). Polyamines were eluted with a linear gradient ranging from acetonitrile-water (50 : 50, v : v) to acetonitrile (100%) for 30 min. The flow was 0.5–1.0 mL/min from 0 to 12 min and was then set at a constant rate (1.0 mL/min) until the 30th min. The fluorescent intensity was monitored by a fluorescence detector (UltiMate 3000 RS, Dionex Corp., Sunnyvale, CA, USA) with excitation at 320 nm and emission at 512 nm. Polyamine levels were expressed as concentration values in nmol/mg of protein.

As concerns ODC activity, it was measured with a radiometric technique that estimated the amount of $^{14}CO_2$ liberated from DL-[1-^{14}C]-ornithine (specific activity, 56.0 mCi/mmol; New England Nuclear) [16]. The cell culture pellet (2–4 × 10^6 cells) was homogenized in 0.6 mL ice-cold 15 mM Tris-HCl (pH 7.5) containing 2.5 mM dithiothreitol, 40 μM pyridoxal-5-phosphate, and 100 μM ethylenediaminetetraacetate and then centrifuged at 30000 ×g for 30 min at 4°C. An aliquot of supernatant (200 μL) was added to a glass test tube containing 0.05 μCi DL-[1-^{14}C]-ornithine and 39 nmol DL-ornithine. After incubation for 60 min at 37°C, the reaction was stopped by adding trichloroacetic acid to a final concentration of 50%. $^{14}CO_2$ liberated from DL-[1-^{14}C]-ornithine was trapped on filter paper pretreated with 40 μL of 2 N NaOH, which was suspended in a center well above the reaction mixture. Radioactivity on the filter papers was determined by a liquid scintillation counter (model 1219 Rackbeta; LKB-Pharmacia, Uppsala, Sweden). ODC activity was expressed as pmolCO_2/h/mg of protein. Enzymatic activity was found to be linear within the range of 50–600 μg of protein (r^2 = 0.99). The intra-assay and interassay variation coefficients (CV%) were 6% and 8%, respectively. The effects of VK1 treatment on ODC mRNA levels were evaluated using the above described qPCR method with SYBR1 green dye and the appropriate primers.

2.6. Statistical Analysis. Due to the nonnormal distribution of the data, nonparametric tests were performed. Data were analyzed by Kruskal-Wallis analysis of variance and Dunn's multiple comparison test. All data are expressed as mean and SEM. Differences were considered significant at $P < 0.05$. A specific software package (SigmaStat for Windows version 3.00 SPSS Inc., San Jose, CA, USA) was used.

3. Results

3.1. Effects of VK1 on Cell Proliferation. Exposure of Caco-2, HT-29, and SW480 cell lines to increasing concentrations of VK1 up to 72 h caused an evident antiproliferative effect (Figure 1). After 24 h and 48 h, concentrations equal to or higher than 100 μM caused a significant reduction ($P < 0.05$) in the conversion of the MTT tetrazolium salt in all

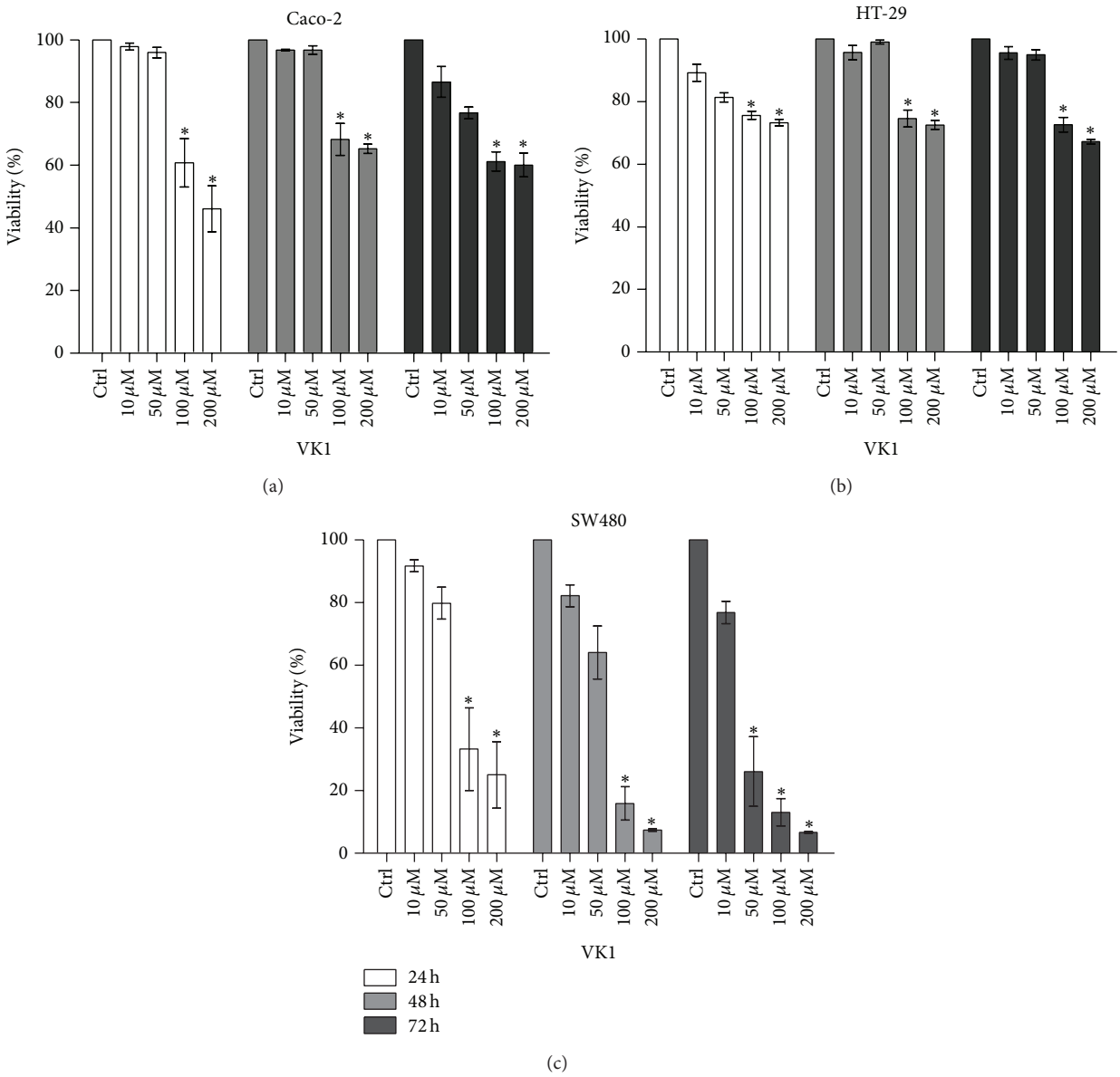

Figure 1: Proliferative response of Caco-2, HT-29, and SW480 cell lines to vitamin K1 (VK1) treatment. Effects of increasing concentrations of VK1 (10 μM, 50 μM, 100 μM, and 200 μM) on the conversion of MTT tetrazolium salt in Caco-2 (a), HT-29 (b), and SW480 (c) cell lines after 24 h, 48 h, and 72 h of treatment. All data represent the result of three different experiments (mean ± SEM). For each time of treatment, data were analyzed by Kruskal-Wallis analysis of variance and Dunn's multiple comparison test. $^*P < 0.05$ compared to control cells.

the tested cells compared to untreated ones. After 72 h, the same concentrations remained effective for Caco-2 and HT-29 cells, while for SW480 a significant reduction ($P < 0.05$) was also caused by lower VK1 concentrations (starting from 50 μM) compared to control cells. In addition, this cell line experienced a dramatic reduction in the percentage of viability at all the tested times with a decrease by approximately 90% at 200 μM after 48 h and 72 h, thus demonstrating a more marked susceptibility to the antiproliferative action by VK1.

3.2. Effects of VK1 on Apoptosis. Figure 2 shows the effects of increasing VK1 concentrations administered up to 72 h on apoptosis evaluated by Bax and Bcl-2 mRNA levels and expressed as Bax/Bcl-2 ratio. As concerns Caco-2 cells, a significant increase ($P < 0.05$) in the Bax/Bcl-2 ratio was observed only at 48 h and at the highest VK1 concentration (200 μM) compared to control cells. At the same time, HT-29 cells exhibited a significant proapoptotic effect ($P < 0.05$) at VK1 concentrations equal to or higher than 100 μM compared to untreated cells. As concerns SW480 cells, after 48 h of exposure the resulting Bax/Bcl-2 ratio significantly increased ($P < 0.05$) at VK1 concentrations equal to or higher than 100 μM compared to control cells. Interestingly, after 72 h of treatment VK1 continued to significantly induce apoptosis only when administered at 100 μM, while the Bax/Bcl-2 ratio

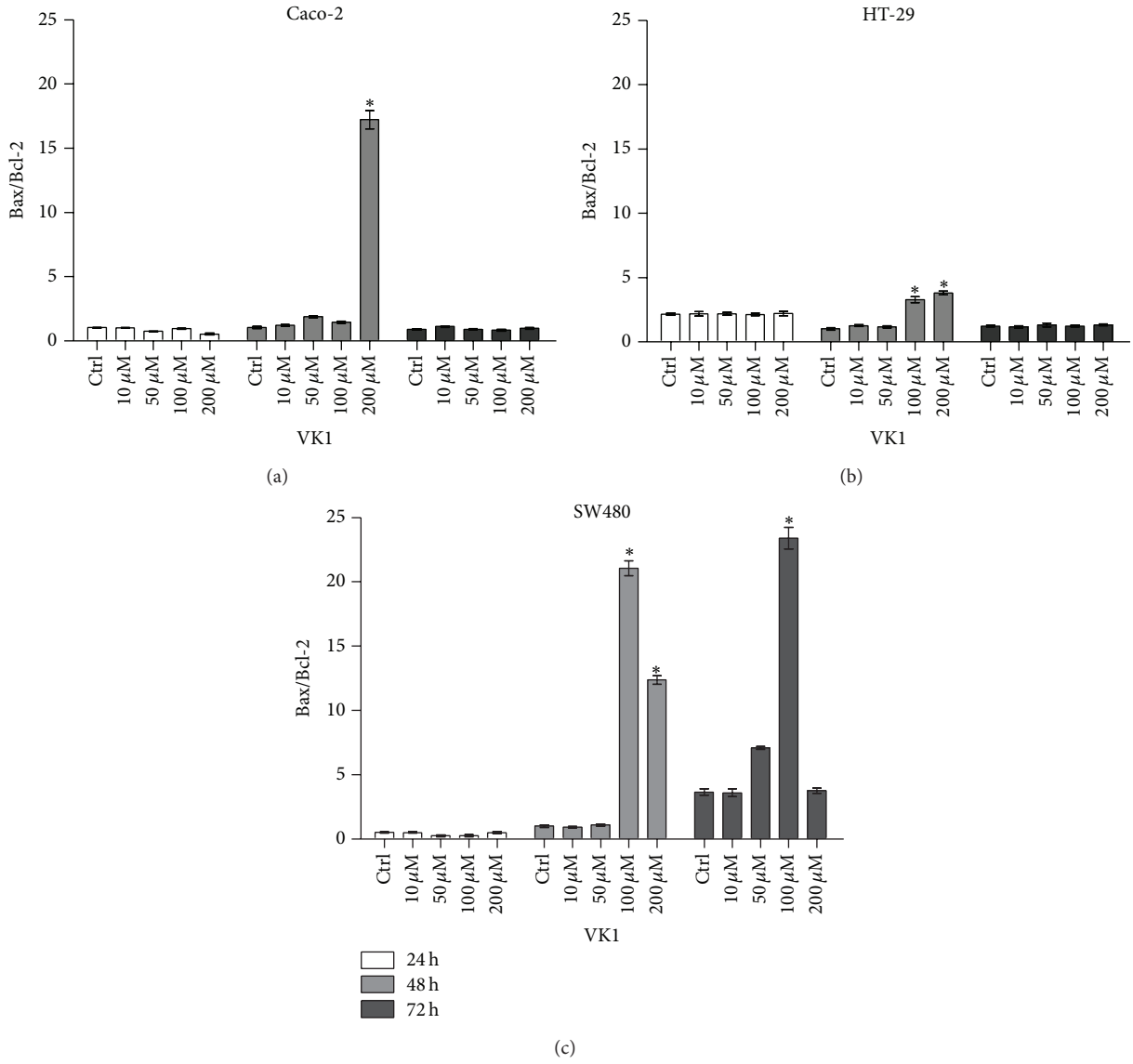

Figure 2: Apoptotic response of Caco-2, HT-29, and SW480 cell lines to vitamin K1 (VK1) treatment. Effects of increasing concentrations of VK1 (10 μM, 50 μM, 100 μM, and 200 μM) on the Bax/Bcl-2 mRNA level in Caco-2 (a), HT-29 (b), and SW480 (c) cell lines after 24 h, 48 h, and 72 h of treatment. All data represent the result of three different experiments (mean ± SEM). For each time of treatment, data were analyzed by Kruskal-Wallis analysis of variance and Dunn's multiple comparison test. $^*P < 0.05$ compared to control cells.

dramatically decreased at the highest 200 μM concentration, probably as a consequence of VK1 toxic effect causing an increase in the dead cell number.

The effects of increasing VK1 concentrations were also investigated by western blot analysis. The protein levels of Bax, Bcl-2, caspase-3, and caspase-9 were evaluated. A significant proapoptotic effect was observed only at 48 h. More specifically, Bax/Bcl-2 ratio in Caco-2 cells increased significantly ($P < 0.05$) at VK1 concentrations equal to or higher than 100 μM, compared to control cells (Figure 3). This effect was caused only by a significant decrease ($P < 0.05$) of Bcl-2 protein compared to untreated cells. Besides, Bax/Bcl-2 ratio in HT-29 cells increased significantly ($P < 0.05$) at all the VK1 concentrations compared to control cells (Figure 4). In this cell line, Bax protein levels significantly increased ($P < 0.05$) at the highest VK1 concentration (200 μM) while Bcl-2 decreased ($P < 0.05$) at all the VK1 concentrations compared to control cells. Finally, Bax/Bcl-2 ratio in SW480 cells increased significantly ($P < 0.05$) at VK1 concentrations starting from 50 μM compared to untreated cells (Figure 5). Bax protein significantly increased ($P < 0.05$) at VK1 concentrations equal to or higher than 100 μM, while Bcl-2 decreased ($P < 0.05$) at all the VK1 concentrations compared to control cells. The participation of caspases in VK1-induced apoptosis in the three cell lines was also evaluated. No significant cleavage of caspase-3, an executioner caspase, or caspase-9, an initiator caspase, after treatment with VK1 was observed (Figure 6). These findings

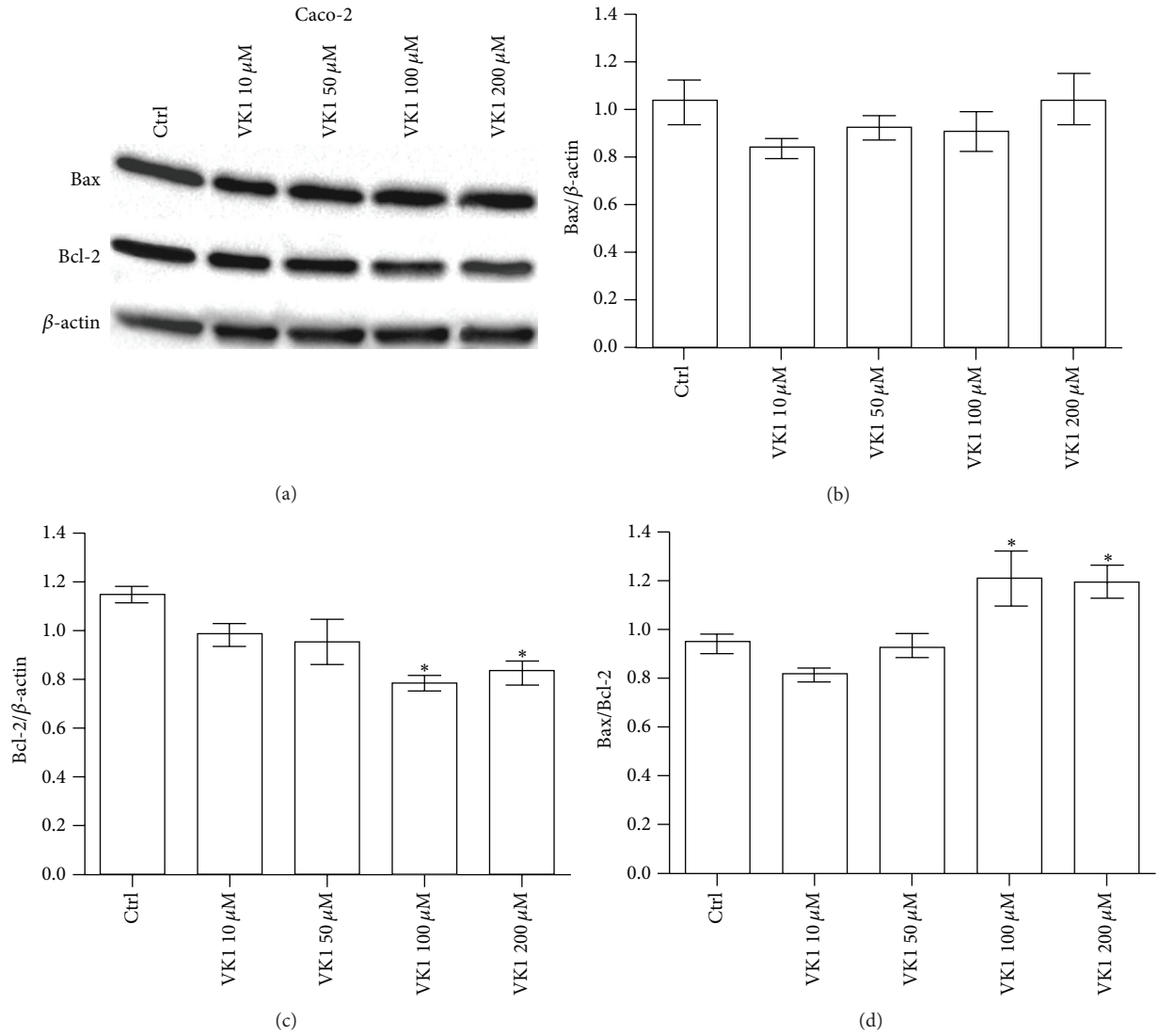

Figure 3: Western blot analysis of Bax and Bcl-2 in Caco-2 cells after 48 h of vitamin K1 (VK1) treatment. The cells were exposed to increasing concentrations of VK1 (10 μM, 50 μM, 100 μM, and 200 μM). Immunoreactive bands were quantified using Quantity One program. The diagrams show quantification of the intensity of bands, calibrated to the intensity of β-actin bands. All data represent the result of three different experiments (mean ± SEM). Data were analyzed by Kruskal-Wallis analysis of variance and Dunn's multiple comparison test. $^{*}P < 0.05$ compared to control cells.

suggest that VK1 is able to induce apoptosis in these colon cancer cells without involving the caspase activation.

3.3. Role of ERK 1/2 on the VK1-Induced Apoptosis. Since ERK 1/2 has been linked to the regulation of cellular growth, apoptosis, and chemoresistance [17], the regulation of this signaling molecule by VK1 in colon cancer cells was investigated. The phosphorylation of ERK 1/2 was evaluated by treating cells with increasing concentrations of VK1 (from 10 μM to 200 μM) for 24 h, 48 h, and 72 h (data not shown). A dose-dependent increase in phospho-ERK 1/2 (P-ERK 1/2) was observed only after 48 h, in HT-29 and SW480 cells. The effect was significant ($P < 0.05$) at VK1 concentrations equal to or higher than 100 μM in HT-29, while SW480 cells were susceptible to all the used VK1 concentrations (Figure 7). When the cells were pretreated with 20 μM UO126 for 2 h, followed by VK1 treatment (100 μM and 200 μM) for 48 h, there was no induction of P-ERK 1/2 (Figure 7). Interestingly, the addition of the MEK inhibitor UO126 blocked sensitive colon cancer cells from VK1 mediated induction of apoptosis, thus indicating an involvement of the MAPK pathway in this process.

3.4. Effects of VK1 on Polyamine Biosynthesis. As concerns the polyamine profile, Table 1 shows the results obtained in Caco-2, HT-29, and SW480 cell lines following exposure to VK1 increasing concentrations up to 72 h. VK1 treatment led to a significant decrease of the single and total polyamine contents in all the tested cells. In detail, after 24 h the decrease in Caco-2 cells was significant ($P < 0.05$) compared to control

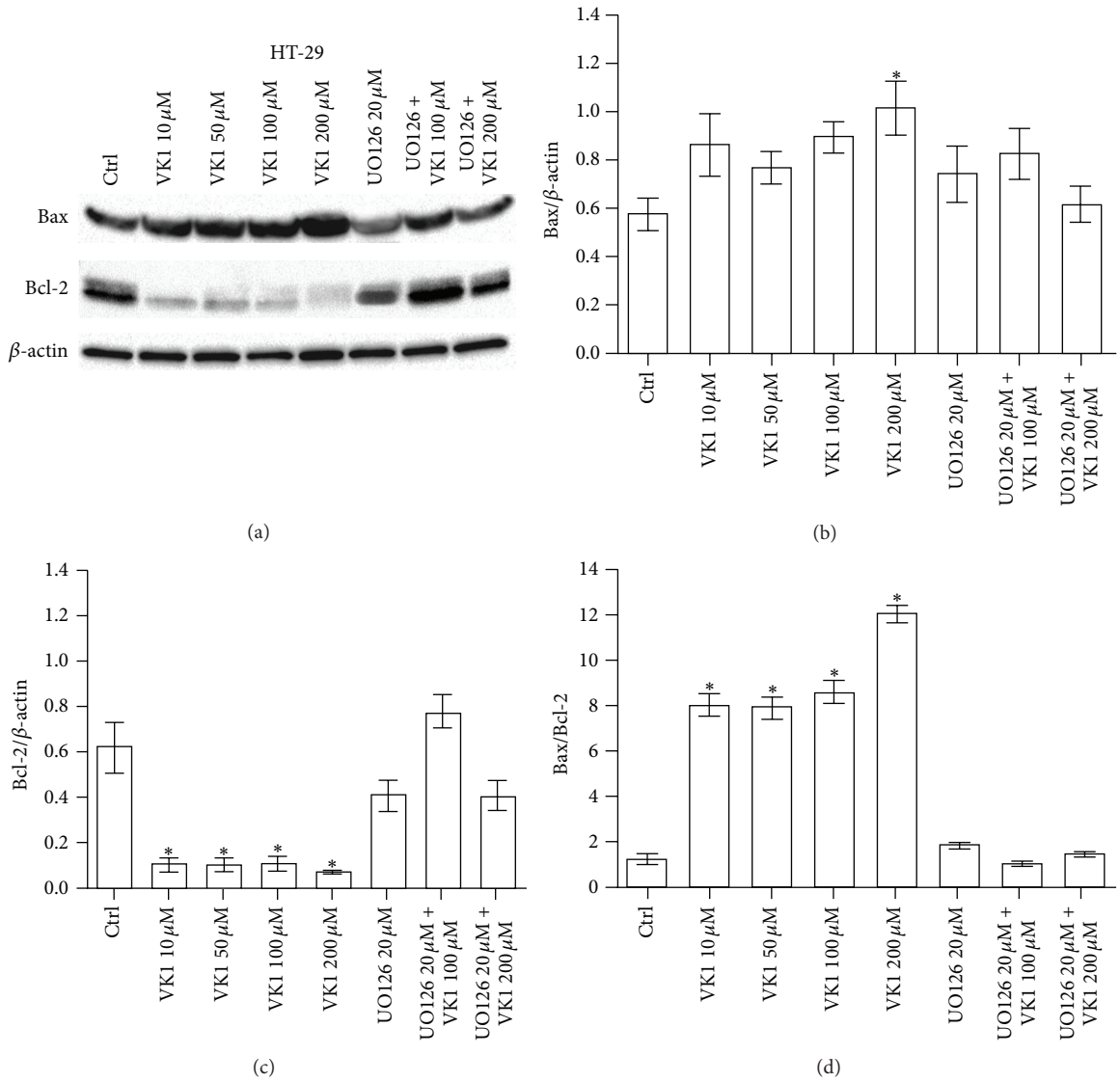

FIGURE 4: Western blot analysis of Bax and Bcl-2 in HT-29 cells after 48 h of vitamin K1 (VK1) treatment. The cells were exposed to increasing concentrations of VK1 (10 μM, 50 μM, 100 μM, and 200 μM), 20 μM UO126 alone, or in combination with 100 μM and 200 μM VK1. Immunoreactive bands were quantified using Quantity One program. The diagrams show quantification of the intensity of bands, calibrated to the intensity of β-actin bands. All data represent the result of three different experiments (mean ± SEM). Data were analyzed by Kruskal-Wallis analysis of variance and Dunn's multiple comparison test. $^{*}P < 0.05$ compared to control cells.

cells as concerns Put, Spd, and the total polyamine content following exposure to VK1 concentrations equal to or higher than 100 μM. After 48 h, lower VK1 concentrations (starting from 50 μM) caused a significant reduction ($P < 0.05$) in Put and the total polyamine levels compared to untreated cells. After 72 h, the decrease was significant ($P < 0.05$) starting from the same VK1 concentration (50 μM) for all the single and total polyamines. In contrast, in HT-29 cells the significant reduction ($P < 0.05$) in the single and total polyamine content was observed only after 48 h and 72 h of VK1 exposure. The decrease was significant ($P < 0.05$) at VK1 concentrations equal to or higher than 100 μM, for all the single and total polyamines, compared to control cells. Finally, SW480 cells administered with VK1 concentrations equal to or higher than 100 μM showed a significant reduction ($P < 0.05$) of the single and total polyamine contents compared to control cells at all the tested times.

ODC activity of Caco-2, HT-29, and SW480 cell lines following VK1 treatment was studied at increasing concentrations up to 72 h (Figure 8). As shown, ODC activity in Caco-2 cells was significantly reduced ($P < 0.05$) only after 24 h of exposure to VK1 concentrations equal to or higher than 50 μM compared to untreated cells. In contrast, VK1 administered for 24 h at concentrations equal to or higher than 100 μM to HT-29 cells significantly reduced ($P < 0.05$) ODC activity compared to control cells. In these cells,

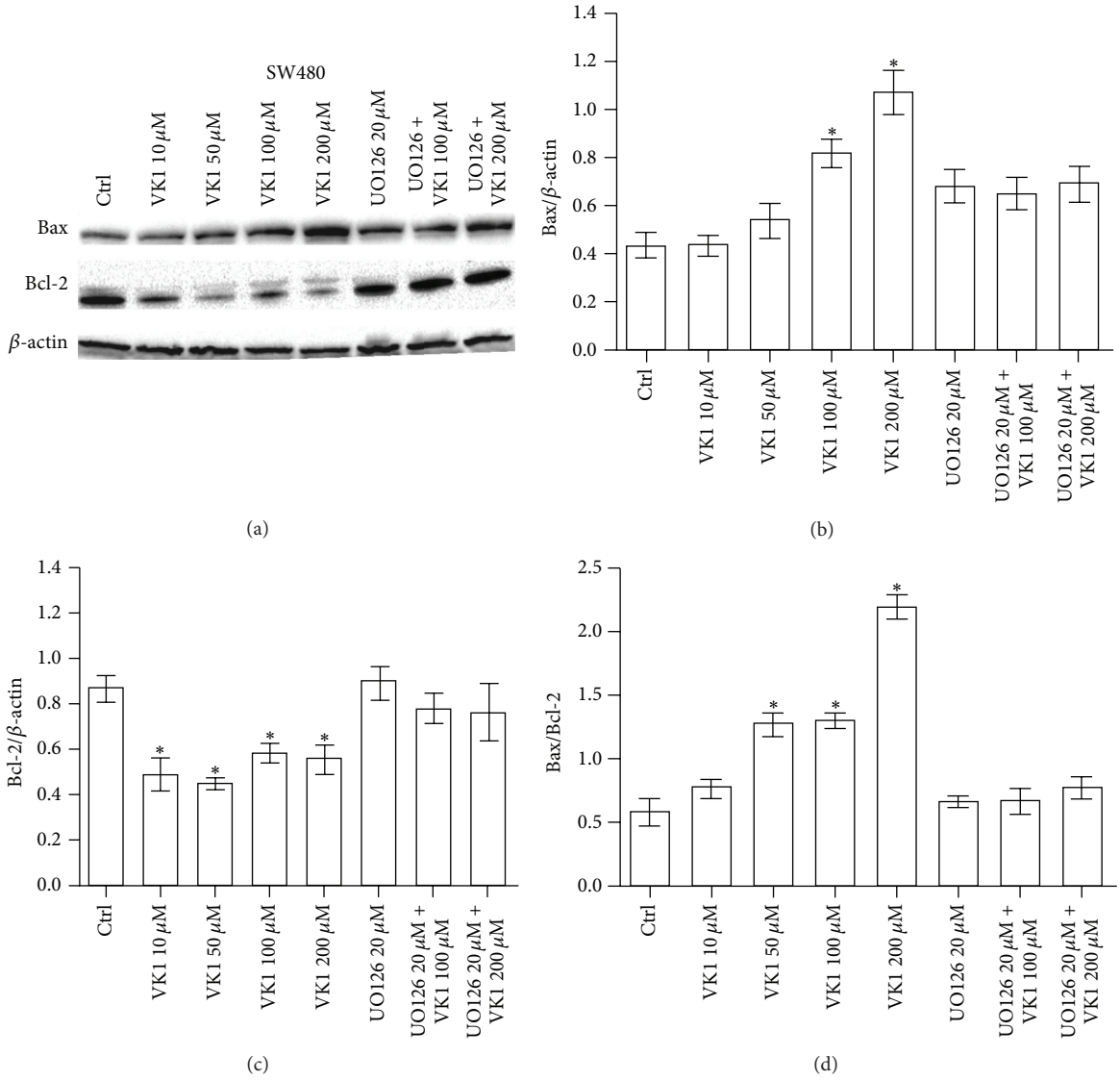

Figure 5: Western blot analysis of Bax and Bcl-2 in SW480 cells after 48 h of vitamin K1 (VK1) treatment. The cells were exposed to increasing concentrations of VK1 (10 μM, 50 μM, 100 μM, and 200 μM), 20 μM UO126 alone, or in combination with 100 μM and 200 μM VK1. Immunoreactive bands were quantified using Quantity One program. The diagrams show quantification of the intensity of bands, calibrated to the intensity of β-actin bands. All data represent the result of three different experiments (mean ± SEM). Data were analyzed by Kruskal-Wallis analysis of variance and Dunn's multiple comparison test. $^{*}P < 0.05$ compared to control cells.

ODC activity was also significantly reduced by lower VK1 concentrations (starting from 50 μM) administered for 48 h and 72 h. Finally, in the less differentiated SW480 cells, VK1 concentrations equal to or higher than 50 μM significantly reduced ($P < 0.05$) ODC activity compared to untreated cells at all the tested times. As concerns ODC expression, no significant effect was observed in Caco-2 cells following VK1 treatment. In contrast, in HT-29 and SW480 cell lines, 24 h administration of VK1 concentrations equal to or higher than 100 μM caused a significant reduction ($P < 0.05$) of ODC mRNA levels compared to untreated cells. Longer period of administration (48 h and 72 h) caused no significant effect on ODC mRNA levels (data not shown).

4. Discussion

VK, an essential nutrient often associated with the clotting cascade, has also been demonstrated to have an anticancer potential. Much of the available data focused on VK3, but also VK2 and VK1 have been shown to possess antineoplastic properties as reported in a variety of cancer cells including HCC, glioma, and pancreatic cell lines [6–8]. A number of hypotheses have been proposed suggesting for these compounds a possible role as inhibitors of the growth in different cancer cells by actively inducing cell cycle arrest, differentiation, and apoptosis [5, 6].

In the present study, the administration of increasing VK1 concentrations up to 72 h influenced the growth as

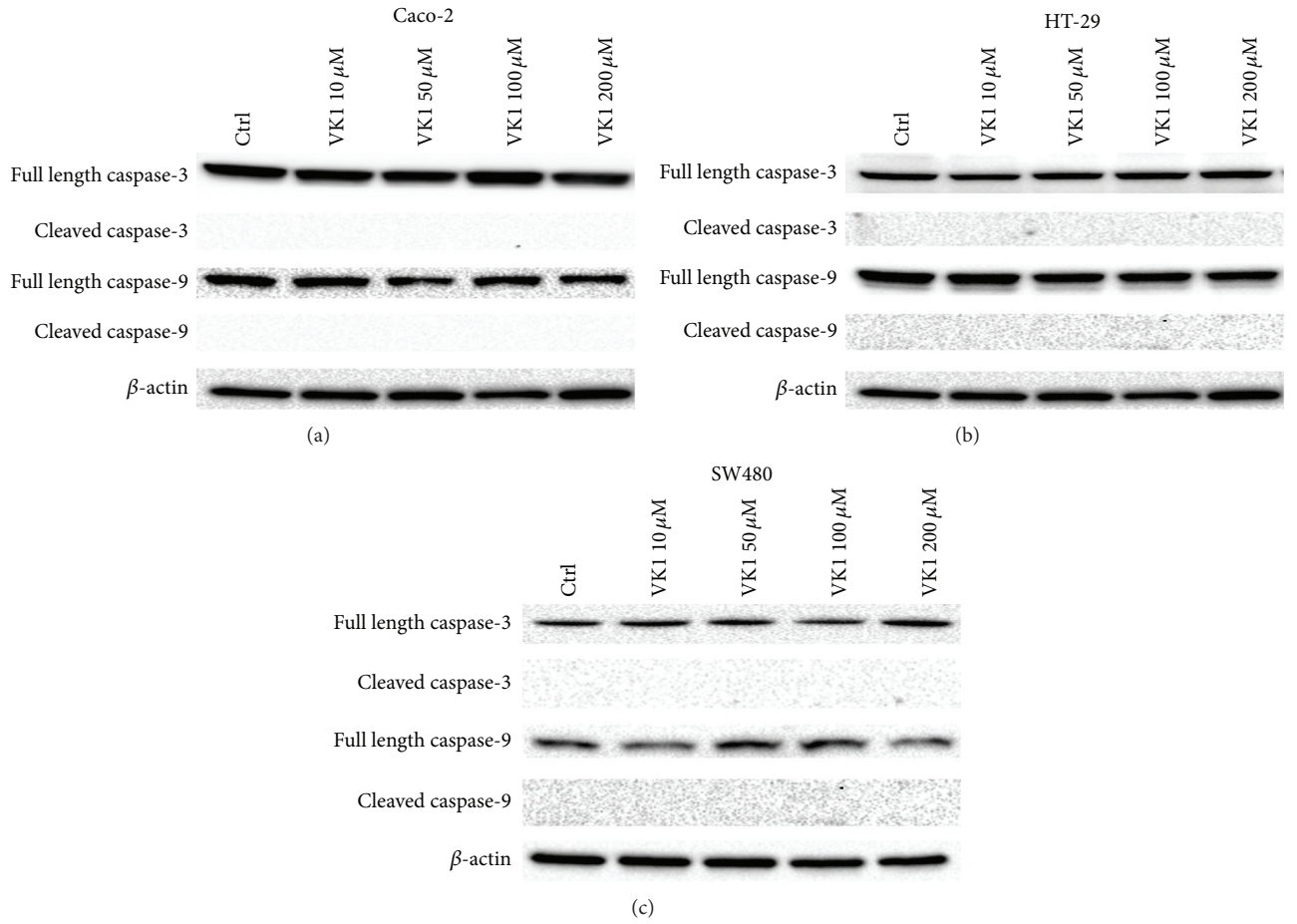

Figure 6: Western blot analysis of caspase-3 and caspase-9 in Caco-2, HT-29, and SW480 cells after 48 h of vitamin K1 (VK1) treatment. The cells were exposed to increasing concentrations of VK1 (10 μM, 50 μM, 100 μM, and 200 μM). Immunoreactive bands were quantified using Quantity One program.

well as the polyamine metabolism of three differently graded human colon cancer cell lines (namely, Caco-2, HT-29, and SW480). In particular, as demonstrated by the reduction in MTT conversion, all the tested cells showed a significant antiproliferative effect when exposed to the highest VK1 concentrations (100 μM and 200 μM). Interestingly, after 72 h a significant reduction in MTT conversion in SW480 was also caused by VK1 at 50 μM, thus indicating a more pronounced susceptibility of this cell line to VK1 antiproliferative effect.

As concerns apoptosis, in our study the three cell lines exhibited a significant induction of apoptosis after 48 h of VK1 treatment, as indicated by the significant increase in the Bax/Bcl-2 ratio. In Caco-2 cells, the ratio increase was exclusively due to the significant downregulation of the antiapoptotic Bcl-2 levels. In contrast, a significant increase in the proapoptotic Bax protein levels was observed in the other two cell lines, although with different susceptibility to VK1 concentrations (200 μM and 100 μM for HT-29 and SW480, resp.). Other differences in Bax/Bcl-2 ratio were also present between HT-29 and SW480. As a matter of fact, SW480 cells showed a tenfold lower ratio compared to HT-29 ones. In the latter cell line, a more pronounced decrease of Bcl-2 protein occurred starting from the significant VK1 concentration of 10 μM.

Overall, VK1 proved to be a potent stimulator of apoptosis in a manner similar to VK3 or VK2 analogs [18] and its effect was mediated mainly via Bcl-2 downregulation. The apoptotic process is determined by the balance of proapoptotic and antiapoptotic proteins and Bcl-2 represents a broad anti-apoptotic factor and opposes cell deaths following ionizing radiation, cancer drugs, and hormonal manipulations [19].

Noteworthy, VK1-induced apoptosis was not mediated by the activation of caspases since western blot analysis revealed no active products of caspase-3, an executioner caspase, and caspase-9, an initiator caspase. Even if caspases are recognized players of apoptosis in various models, increasing evidence demonstrated that apoptosis may be induced without their activation [20].

To determine whether the proven VK1-induced cell death was associated with the activation of ERK, belonging to the MAPK family, western blot was performed. VK1 treatment caused a significant dose-dependent increase in ERK phosphorylation in a cell-type specific manner; HT-29 and SW480 cells exhibited a significant induction of P-ERK, starting from

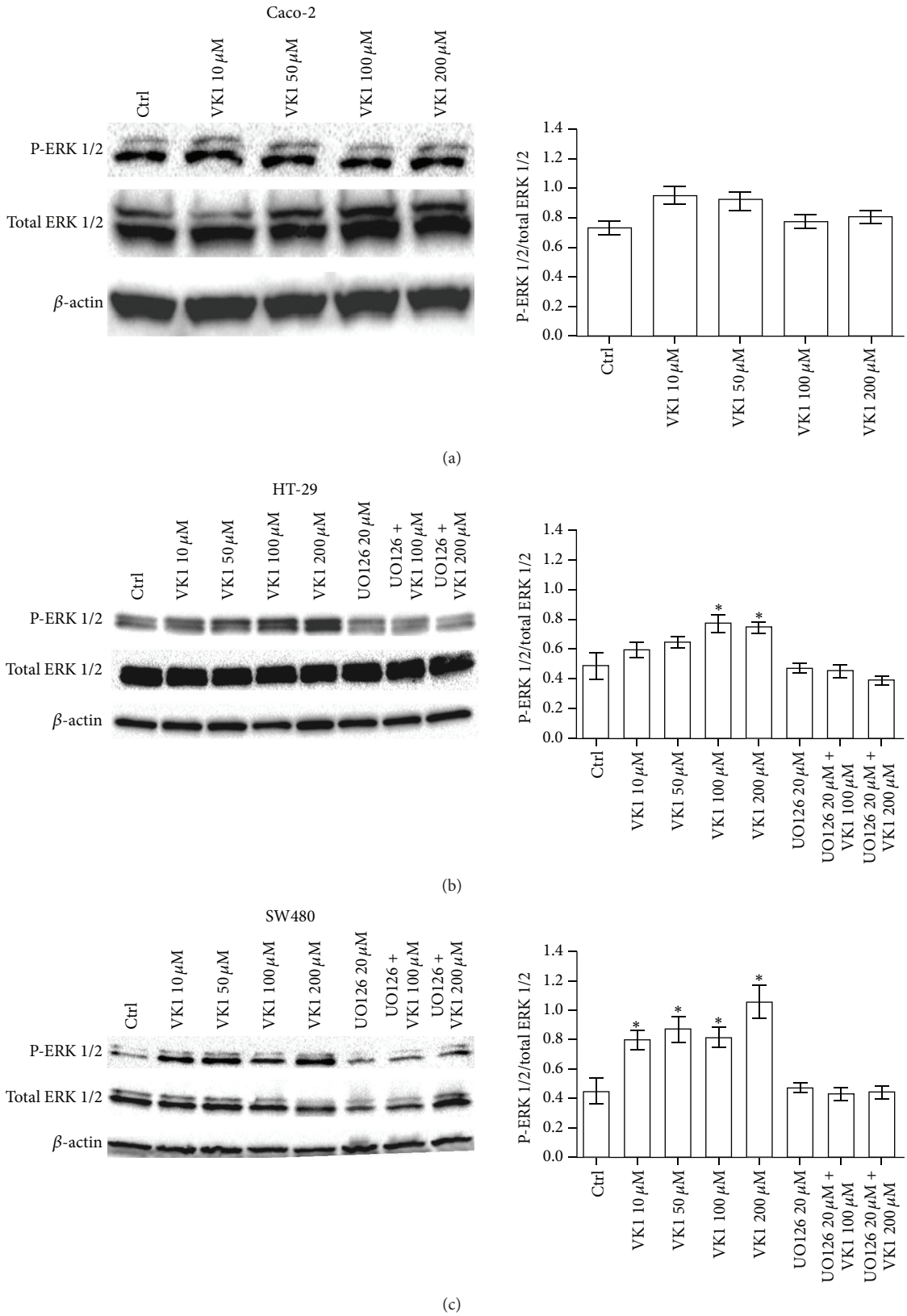

Figure 7: Western blot analysis of P-ERK 1/2 and total ERK 1/2 in Caco-2, HT-29, and SW480 cells after 48 h of vitamin K1 (VK1) treatment. The cells were exposed to increasing concentrations of VK1 (10 μM, 50 μM, 100 μM, and 200 μM) or to 20 μM UO126 alone or in combination with 100 μM and 200 μM VK1. Immunoreactive bands were quantified using Quantity One program. The diagrams show quantification of the intensity of bands, calibrated to the intensity of β-actin bands. All data represent the result of three different experiments (mean ± SEM). Data were analyzed by Kruskal-Wallis analysis of variance and Dunn's multiple comparison test. $^{*}P < 0.05$ compared to control cells.

Table 1: The polyamine profile: putrescine (Put), spermidine (Spd), spermine (Spm), and total polyamine (Total) in Caco-2, HT-29, and SW480 cell lines following administration of vitamin K1 (VK1) increasing concentrations (from 10 μM to 200 μM) after 24 h, 48 h, and 72 h.

Caco-2		Control	VK1 10 μM	VK1 50 μM	VK1 100 μM	VK1 200 μM
24 h	Put	0.70 ± 0.06	0.34 ± 0.03	0.30 ± 0.05	0.15 ± 0.03*	0.13 ± 0.03*
	Spd	12.17 ± 0.44	12.30 ± 0.95	9.43 ± 0.35	8.13 ± 1.07*	7.93 ± 0.71*
	Spm	11.63 ± 0.33	12.07 ± 0.52	10.87 ± 0.29	11.53 ± 0.26	11.33 ± 0.67
	Total	**24.50 ± 0.72**	**24.71 ± 0.39**	**20.60 ± 0.62**	**19.82 ± 0.86***	**19.40 ± 0.70***
48 h	Put	0.87 ± 0.07	0.57 ± 0.07	0.33 ± 0.04*	0.32 ± 0.03*	0.32 ± 0.05*
	Spd	16.47 ± 0.33	10.53 ± 0.37	9.63 ± 0.38	8.87 ± 0.29*	8.53 ± 0.29*
	Spm	13.07 ± 0.69	12.73 ± 0.48	12.13 ± 0.47	12.60 ± 0.49	11.97 ± 0.022
	Total	**30.41 ± 0.83**	**23.57 ± 0.74**	**21.96 ± 0.70***	**21.78 ± 0.39***	**21.15 ± 0.53***
72 h	Put	0.57 ± 0.04	0.48 ± 0.05	0.19 ± 0.03*	0.24 ± 0.03*	0.23 ± 0.03*
	Spd	10.53 ± 0.32	9.72 ± 0.40	6.51 ± 0.46*	5.89 ± 0.31*	5.93 ± 0.48*
	Spm	15.83 ± 0.35	14.93 ± 0.46	13.25 ± 0.52*	13.37 ± 0.43*	13.40 ± 0.38*
	Total	**26.94 ± 0.70**	**25.13 ± 0.92**	**19.95 ± 0.88***	**19.50 ± 0.67***	**19.56 ± 0.75***
HT-29		Control	VK1 10 μM	VK1 50 μM	VK1 100 μM	VK1 200 μM
24 h	Put	0.76 ± 0.05	0.65 ± 0.04	0.53 ± 0.13	0.55 ± 0.10	0.58 ± 0.08
	Spd	13.04 ± 0.05	12.67 ± 0.18	13.03 ± 0.12	12.93 ± 0.18	12.76 ± 0.23
	Spm	9.70 ± 0.32	9.93 ± 0.28	9.60 ± 0.63	10.13 ± 0.54	9.97 ± 0.24
	Total	**23.49 ± 0.39**	**23.27 ± 0.35**	**23.30 ± 0.76**	**23.71 ± 0.55**	**23.38 ± 0.47**
48 h	Put	1.41 ± 0.11	1.14 ± 0.23	1.06 ± 0.18	0.33 ± 0.12*	0.22 ± 0.04*
	Spd	10.11 ± 0.27	9.43 ± 0.24	9.45 ± 0.19	6.93 ± 0.49*	6.25 ± 0.16*
	Spm	14.40 ± 0.47	14.47 ± 0.20	13.40 ± 0.40	7.27 ± 0.39*	7.13 ± 0.42*
	Total	**25.92 ± 0.81**	**25.04 ± 0.55**	**23.91 ± 0.43**	**14.53 ± 0.91***	**13.60 ± 0.54***
72 h	Put	0.53 ± 0.18	0.52 ± 0.08	0.30 ± 0.03	0.27 ± 0.04*	0.21 ± 0.04*
	Spd	8.44 ± 0.29	8.46 ± 0.31	7.50 ± 0.43	7.23 ± 0.34*	6.60 ± 0.32*
	Spm	13.50 ± 0.32	10.50 ± 0.46	8.30 ± 0.32	6.87 ± 0.38*	6.87 ± 0.97*
	Total	**22.47 ± 0.79**	**19.48 ± 0.84**	**16.10 ± 0.66**	**14.37 ± 0.76***	**13.68 ± 1.29***
SW480		Control	VK1 10 μM	VK1 50 μM	VK1 100 μM	VK1 200 μM
24 h	Put	2.24 ± 0.20	1.45 ± 0.09	1.03 ± 0.14	0.72 ± 0.12*	0.78 ± 0.15*
	Spd	13.27 ± 0.26	11.74 ± 0.14	9.73 ± 0.32	8.53 ± 0.41*	8.24 ± 0.33*
	Spm	12.93 ± 0.29	12.03 ± 0.20	10.77 ± 0.29	9.33 ± 0.18*	9.22 ± 0.23*
	Total	**28.44 ± 0.75**	**25.22 ± 0.43**	**21.53 ± 0.75**	**18.59 ± 0.64***	**18.24 ± 0.50***
48 h	Put	1.59 ± 0.17	1.04 ± 0.18	0.79 ± 0.11	0.35 ± 0.06*	0.36 ± 0.09*
	Spd	9.93 ± 0.29	8.73 ± 0.39	7.60 ± 0.40	6.02 ± 0.36*	5.83 ± 0.45*
	Spm	13.13 ± 0.40	13.05 ± 0.62	12.16 ± 0.20	11.68 ± 0.29*	11.87 ± 0.24*
	Total	**24.65 ± 0.52**	**22.82 ± 0.45**	**20.55 ± 0.72**	**18.05 ± 0.53***	**18.06 ± 0.54***
72 h	Put	1.79 ± 0.11	1.57 ± 0.14	1.65 ± 0.09	0.93 ± 0.12*	0.93 ± 0.13*
	Spd	7.31 ± 0.21	6.58 ± 0.25	6.27 ± 0.17	4.91 ± 0.27*	4.77 ± 0.22*
	Spm	12.58 ± 0.23	12.18 ± 0.18	12.38 ± 0.38	12.03 ± 0.16*	11.83 ± 0.20*
	Total	**21.68 ± 0.55**	**20.33 ± 0.46**	**20.30 ± 0.64**	**17.87 ± 0.44***	**17.53 ± 0.47***

*$P < 0.05$ compared to control cells.

very different VK1 concentrations (100 μM and 10 μM for HT-29 and SW480, resp.). This induction was time-dependent with a peak increase after 48 h. Of note, simultaneous cotreatment of cells with a MEK inhibitor and VK1 at the highest concentrations (100 μM and 200 μM) prevented the induction of ERK phosphorylation. In addition, the MEK inhibitor blocked sensitive colon cancer cells from VK1-mediated induction of apoptosis, implicating the involvement of the MAPK pathway in this process.

The MAPK family, including ERK, the c-jun N-terminal kinase/stress-activated protein kinases (JNK/SAPK), and p38 kinases, has emerged as playing a crucial role in the cellular proliferation, differentiation, and apoptosis [21]. ERK pathway is known to prevent cell death, whereas the JNK/SAPK and p38 pathways have shown proapoptotic actions. However, reports in the literature have proposed a different interpretation of the phosphorylation of ERK. Leppä et al. [22] proved that ERK pathway stimulated c-jun synthesis

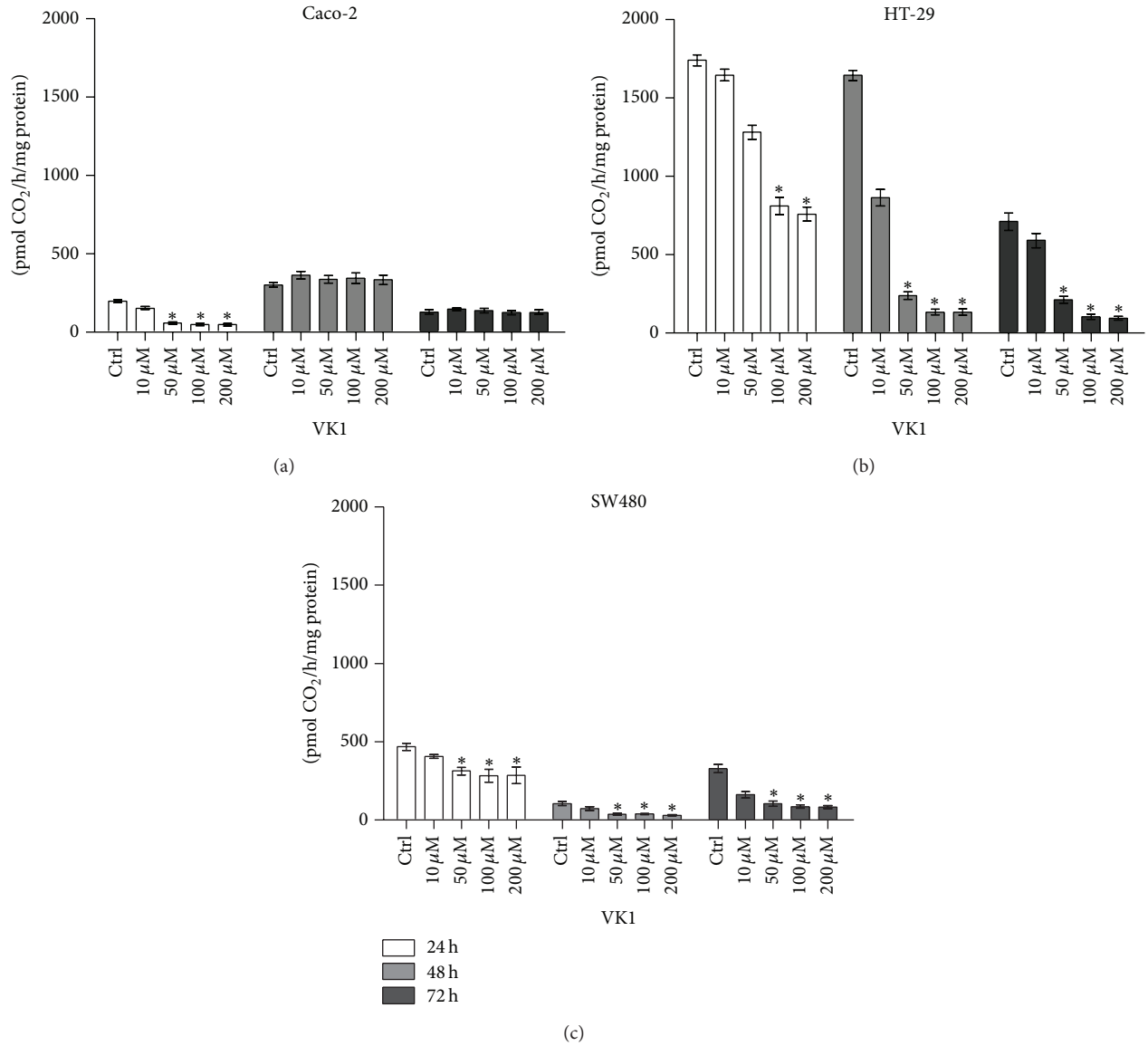

Figure 8: Ornithine decarboxylase (ODC) activity of Caco-2, HT-29, and SW480 cell lines in response to vitamin K1 (VK1) treatment. Effects of increasing concentrations of VK1 (10 μM, 50 μM, 100 μM, and 200 μM) on the ODC activity in Caco-2 (a), HT-29 (b), and SW480 (c) cell lines after 24 h, 48 h, and 72 h of treatment. All data represent the result of three different experiments (mean ± SEM). For each time of treatment, data were analyzed by Kruskal-Wallis analysis of variance and Dunn's multiple comparison test. $^{*}P < 0.05$ compared to control cells.

and phosphorylation. Since c-jun itself is implicated in the apoptotic processes, the activation of the ERK pathway also can relate to cell death. Zhu et al. [23] showed a proapoptotic role of the ERK pathway in T-cell in which the inhibition of ERK phosphorylation antagonized apoptosis. Pumiglia et al. [24] provided evidence that a sustained increase of ERK activity inhibited cell cycle dependent kinase and induced growth arrest. Similar results were obtained more recently by Showalter et al. [8] in a study performed on pancreatic cancer cell lines treated with either VK1 or VK2 at inhibitory doses. Besides, Du et al. [7] demonstrated that VK1 enhanced the cytotoxicity effect of sorafenib through inhibiting the Raf/MEK/ERK signaling pathway in glioma cells. Matsumoto et al. [25] demonstrated that VK2 induced apoptosis and activated the MEK/ERK signaling pathway in liver cancer cells in a cell-type specific manner.

In order to identify other possible mechanisms implicated in VK1 ability to affect neoplastic cell growth, polyamines and their rate-limiting enzyme, ODC, were evaluated. A significant decrease in the polyamine content was observed at different VK1 concentrations (50 μM for Caco-2 and 100 μM for HT-29 and SW480 cells). Besides, after 24 h, a concomitant and significant decrease in ODC activity occurred in the three cell lines, starting from the concentration of 50 μM. In

HT-29 and SW480 cells this effect persisted also after 48 h and 72 h.

A significant decrease in ODC gene expression occurred only in HT-29 and SW480 cells after 24 h of VK1 treatment. In Caco-2 cell line the decrease of ODC activity after 24 h of treatment was not sustained by a concomitant inhibition of gene expression, probably due to the fact that VK1 exerts its effects on the modulation of protein enzymatic activity without any consequence on ODC gene.

ODC is a key regulator in polyamine metabolism, being now considered as a true oncogene [26]. This enzyme influences mainly Put and Spd levels, which are more involved in cell proliferation than Spm; the latter is implicated essentially in cell differentiation and neoplastic transformation, with different processes involved in maintaining its critical levels. High ODC expression along with increased polyamine concentrations is associated with fast proliferating cells [27]. In CRC, polyamine levels are significantly increased compared with either normal or preneoplastic tissue and are considered as reliable markers of neoplastic cell proliferation [28]. Polyamines stabilize chromatin and nuclear enzymes due to their ability to create complexes with organic polyanions, such as groups of proteins and DNA. It has been proposed that stabilization of the chromatin structure by polyamines may represent a mechanism by which these molecules affect nuclear processes including cell division and apoptosis [29]. Moreover, it is known that polyamines influence the expression of various genes involved in cell proliferation, tumor invasion, and metastasis [30].

To our knowledge, this is the first study investigating the behavior of polyamine metabolism on colon cancer cell lines treated with VK1 and a significant decrease in the polyamine content was demonstrated. A similar response has also been observed in previous studies performed in the same as well as other cell lines treated with drugs or natural molecules that inhibit polyamine biosynthesis, such as DFMO, anandamide, or probiotics [14, 31, 32].

As concerns the apoptotic processes, interestingly, an active involvement of either the MAPK pathway or the polyamine metabolism could be hypothesized, since a link between polyamine decrease and apoptosis exists [33]. It has been demonstrated that the depletion of polyamines can lead to cell cycle arrest or apoptosis by affecting numerous cell cycle regulatory pathways [34]. Polyamines have been proven as pivotal in regulating ion transport and stabilization of different cellular components such as cell membranes and chromatin structure. Hence, a decrease in the levels of these polycations might cause a destabilization of important cell structures, leading to alterations in cell integrity and inducing cell death.

We used three human colon cancer cells with distinct degree of differentiation, according to their grade of infiltration or metastasis, in an attempt to represent the variety of cellular changes occurring in precancerous lesions as well as manifest tumors. The obtained data suggest that the antiproliferative and proapoptotic effects by VK1 were also related to the characteristics of the colon cancer cell line. In fact, the less differentiated SW480 cells (from a moderately differentiated colon adenocarcinoma, grade IV Duke B) showed a more pronounced susceptibility to VK1 action due to a more marked antiproliferative effect, an increased Bax/Bcl-2 ratio persisting up to 72 h, and a significant increase in the phosphorylation of ERK 1/2 starting from low VK1 concentrations in comparison to the more differentiated HT-29 and Caco-2 cell lines. These data are in accordance with the reported high capacity of *de novo* polyamine biosynthesis and of polyamine uptake ascribed to this cell line, representing probably a precondition for the rapid growth ability shown by SW480 [35].

Regarding the different doses of VK1 used in this study, concentrations ranging from 10 μM to 200 μM can be considered pharmacological since normal serum levels of VK1 were found to be approximately 0.61 ng/mL. Yet, VK1 appears to be without toxicity and studies performed in humans established that mega doses of VK1 (up to 1000 mg orally daily) were used without side effects in patients with HCC [36]. Additionally, other studies clearly indicated that VK1 alone did not alter P-ERK levels, except at very high concentrations starting from 100 μM, the same concentrations needed to exert the anticancer effects seen in our human colon cancer cells [37].

5. Conclusions

Undoubtedly, the significance of investigations performed *in vitro* related to the *in vivo* situations has to be taken with caution due to the presence of several differences; besides, cell sensitivity is only one factor and is not necessarily the most important in determining specificity of VK1 action. Anyway, it is possible to postulate that the colon cancer cells may be a good candidate tumor system to evaluate the antiproliferative and proapoptotic ability of VK1. Our future studies will be aimed at continuing to uncover the exact mechanisms underlying VK1 anticancer effect in colon cancer cells and whether polyamine depletion by itself is directly responsible for the observed proapoptotic action. Finally, considering that VK1 is safe and nontoxic, further research in humans is required to support these properties, also focusing better on the doses needed to obtain *in vivo* the same relevant effects produced in experimental models. From a therapeutic point of view, more probably, combinations of natural substances such as VK1 with other compounds (e.g., polyamine inhibitors and/or analogues) would enhance their properties, representing a suitable option for chemoprevention and/or treatment of colon cancer.

Conflict of Interests

The authors declare that there is no conflict of interests regarding the publication of this paper.

Acknowledgment

This research was supported by the Ministry of Health, Project no. 9/14.

References

[1] C. Lepage, S. Hamza, and J. Faivre, "Epidemiologie et recommandations pour le depistage du cancer colorectal [Epidemiology and screening of colon cancer]," *La Revue du Praticien*, vol. 60, no. 8, pp. 1062–1067, 2010.

[2] A. Russo, S. Corsale, P. Cammareri et al., "Pharmacogenomics in colorectal carcinomas: future perspectives in personalized therapy," *Journal of Cellular Physiology*, vol. 204, no. 3, pp. 742–749, 2005.

[3] M. J. Shearer and P. Newman, "Metabolism and cell biology of vitamin K," *Journal of Thrombosis and Haemostasis*, vol. 100, no. 4, pp. 530–547, 2008.

[4] D. W. Lamson and S. M. Plaza, "The anticancer effects of vitamin K," *Alternative Medicine Review*, vol. 8, no. 3, pp. 303–318, 2003.

[5] I. Ozaki, H. Zhang, T. Mizuta et al., "Menatetrenone, a vitamin K2 analogue, inhibits hepatocellular carcinoma cell growth by suppressing cyclin D1 expression through inhibition of nuclear factor κB activation," *Clinical Cancer Research*, vol. 13, no. 7, pp. 2236–2245, 2007.

[6] T. Mizuta and I. Ozaki, "Hepatocellular carcinoma and vitamin K," *Vitamins and Hormones*, vol. 78, pp. 435–442, 2008.

[7] W. Du, J.-R. Zhou, D.-L. Wang, K. Gong, and Q.-J. Zhang, "Vitamin K1 enhances sorafenib-induced growth inhibition and apoptosis of human malignant glioma cells by blocking the Raf/MEK/ERK pathway," *World Journal of Surgical Oncology*, vol. 10, article 60, 2012.

[8] S. L. Showalter, Z. Wang, C. L. Costantino et al., "Naturally occurring K vitamins inhibit pancreatic cancer cell survival through a caspase-dependent pathway," *Journal of Gastroenterology and Hepatology*, vol. 25, no. 4, pp. 738–744, 2010.

[9] C. Moinard, L. Cynober, and J.-P. de Bandt, "Polyamines: metabolism and implications in human diseases," *Clinical Nutrition*, vol. 24, no. 2, pp. 184–197, 2005.

[10] T. Thomas and T. J. Thomas, "Polyamine metabolism and cancer," *Journal of Cellular and Molecular Medicine*, vol. 7, no. 2, pp. 113–126, 2003.

[11] L. M. Shantz and V. A. Levin, "Regulation of ornithine decarboxylase during oncogenic transformation: mechanisms and therapeutic potential," *Amino Acids*, vol. 33, no. 2, pp. 213–223, 2007.

[12] R. A. Casero Jr. and L. J. Marton, "Targeting polyamine metabolism and function in cancer and other hyperproliferative diseases," *Nature Reviews Drug Discovery*, vol. 6, no. 5, pp. 373–390, 2007.

[13] H. Brunner, F. Hausmann, R. C. Krieg et al., "The effects of 5-aminolevulinic acid esters on protoporphyrin IX production in human adenocarcinoma cell lines," *Photochemistry and Photobiology*, vol. 74, no. 5, pp. 721–725, 2001.

[14] M. Linsalata, M. Notarnicola, V. Tutino et al., "Effects of anandamide on polyamine levels and cell growth in human colon cancer cells," *Anticancer Research*, vol. 30, no. 7, pp. 2583–2589, 2010.

[15] M. Linsalata, F. Russo, M. Notarnicola, P. Berloco, and A. Di Leo, "Polyamine profile in human gastric mucosa infected by *Helicobacter pylori*," *Italian Journal of Gastroenterology and Hepatology*, vol. 30, no. 5, pp. 484–489, 1998.

[16] H. S. Garewal, D. Sloan, R. E. Sampliner, and B. Fennerty, "Ornithine decarboxylase assay in human colorectal mucosa. Methodologic issues of importance to quality control," *International Journal of Cancer*, vol. 52, no. 3, pp. 355–358, 1992.

[17] J. A. McCubrey, L. S. Steelman, W. H. Chappell et al., "Roles of the Raf/MEK/ERK pathway in cell growth, malignant transformation and drug resistance," *Biochimica et Biophysica Acta: Molecular Cell Research*, vol. 1773, no. 8, pp. 1263–1284, 2007.

[18] Z. Wang, M. Wang, F. Finn, and B. I. Carr, "The growth inhibitory effects of vitamins K and their actions on gene expression," *Hepatology*, vol. 22, no. 3, pp. 876–882, 1995.

[19] C. L. Sentman, J. R. Shutter, D. Hockenbery, O. Kanagawa, and S. J. Korsmeyer, "bcl-2 inhibits multiple forms of apoptosis but not negative selection in thymocytes," *Cell*, vol. 67, no. 5, pp. 879–888, 1991.

[20] O. A. Mareninova, K.-F. Sung, P. Hong et al., "Cell death in pancreatitis: caspases protect from necrotizing pancreatitis," *The Journal of Biological Chemistry*, vol. 281, no. 6, pp. 3370–3381, 2006.

[21] X. Sui, N. Kong, L. Ye et al., "P38 and JNK MAPK pathways control the balance of apoptosis and autophagy in response to chemotherapeutic agents," *Cancer Letters*, vol. 344, no. 2, pp. 174–179, 2014.

[22] S. Leppä, R. Saffrich, W. Ansorge, and D. Bohmann, "Differential regulation of c-Jun by ERK and JNK during PC12 cell differentiation," *The EMBO Journal*, vol. 17, no. 15, pp. 4404–4413, 1998.

[23] L. Zhu, X. Yu, Y. Akatsuka, J. A. Cooper, and C. Anasetti, "Role of mitogen-activated protein kinases in activation-induced apoptosis of T cells," *Immunology*, vol. 97, no. 1, pp. 26–35, 1999.

[24] K. M. Pumiglia, K. M. Pumiglia, S. J. Decker, and S. J. Decker, "Cell cycle arrest mediated by the MEK/mitogen-activated protein kinase pathway," *Proceedings of the National Academy of Sciences of the United States of America*, vol. 94, no. 2, pp. 448–452, 1997.

[25] K. Matsumoto, J.-I. Okano, T. Nagahara, and Y. Murawaki, "Apoptosis of liver cancer cells by vitamin K2 and enhancement by MEK inhibition," *International Journal of Oncology*, vol. 29, no. 6, pp. 1501–1508, 2006.

[26] A. E. Pegg, "Regulation of ornithine decarboxylase," *Journal of Biological Chemistry*, vol. 281, no. 21, pp. 14529–14532, 2006.

[27] K. Alm and S. Oredsson, "Cells and polyamines do it cyclically," *Essays in Biochemistry*, vol. 46, no. 1, pp. 63–76, 2009.

[28] M. Linsalata, M. G. Caruso, S. Leo, V. Guerra, B. D'Attoma, and A. Di Leo, "Prognostic value of tissue polyamine levels in human colorectal carcinoma," *Anticancer Research*, vol. 22, no. 4, pp. 2465–2469, 2002.

[29] T. Thomas and T. J. Thomas, "Polyamines in cell growth and cell death: molecular mechanisms and therapeutic applications," *Cellular and Molecular Life Sciences*, vol. 58, no. 2, pp. 244–258, 2001.

[30] E. A. Paz, J. Garcia-Huidobro, and N. A. Ignatenko, "Polyamines in cancer," *Advances in Clinical Chemistry*, vol. 54, pp. 45–70, 2011.

[31] H. M. Wallace and A. V. Fraser, "Inhibitors of polyamine metabolism: review article," *Amino Acids*, vol. 26, no. 4, pp. 353–365, 2004.

[32] M. Linsalata and F. Russo, "Nutritional factors and polyamine metabolism in colorectal cancer," *Nutrition*, vol. 24, no. 4, pp. 382–389, 2008.

[33] N. Seiler and F. Raul, "Polyamines and apoptosis," *Journal of Cellular and Molecular Medicine*, vol. 9, no. 3, pp. 623–642, 2005.

[34] K. Igarashi and K. Kashiwagi, "Modulation of cellular function by polyamines," *International Journal of Biochemistry and Cell Biology*, vol. 42, no. 1, pp. 39–51, 2010.

[35] B. Duranton, V. Holl, Y. Schneider et al., "Polyamine metabolism in primary human colon adenocarcinoma cells (SW480) and their lymph node metastatic derivatives (SW620)," *Amino Acids*, vol. 24, no. 1-2, pp. 63–72, 2003.

[36] G. Wei, M. Wang, T. Hyslop, Z. Wang, and B. I. Carr, "Vitamin K enhancement of sorafenib-mediated HCC cell growth inhibition in vitro and in vivo," *International Journal of Cancer*, vol. 127, no. 12, pp. 2949–2958, 2010.

[37] G. Wei, M. Wang, and B. I. Carr, "Sorafenib combined vitamin K induces apoptosis in human pancreatic cancer cell lines through RAF/MEK/ERK and c-Jun NH2-terminal kinase pathways," *Journal of Cellular Physiology*, vol. 224, no. 1, pp. 112–119, 2010.

Hindawi Publishing Corporation
BioMed Research International
Volume 2015, Article ID 895360, 8 pages
http://dx.doi.org/10.1155/2015/895360

Research Article

Ecdysteroids Sensitize MDR and Non-MDR Cancer Cell Lines to Doxorubicin, Paclitaxel, and Vincristine but Tend to Protect Them from Cisplatin

Ana Martins,[1,2] Péter Sipos,[3] Katalin Dér,[3] József Csábi,[4] Walter Miklos,[5] Walter Berger,[5,6] Attila Zalatnai,[7] Leonard Amaral,[8] Joseph Molnár,[1] Piroska Szabó-Révész,[3] and Attila Hunyadi[4]

[1] *Department of Medical Microbiology and Immunobiology, Faculty of Medicine, University of Szeged, Dóm tér 10, Szeged 6720, Hungary*
[2] *Unidade de Parasitologia e Microbiologia Médica, Instituto de Higiene e Medicina Tropical, Universidade Nova de Lisboa, Rua da Junqueira 100, 1349-008 Lisbon, Portugal*
[3] *Department of Pharmaceutical Technology, Faculty of Pharmacy, University of Szeged, Eötvös Ucta 6, Szeged 6720, Hungary*
[4] *Institute of Pharmacognosy, Faculty of Pharmacy, University of Szeged, Eötvös Ucta 6, Szeged 6720, Hungary*
[5] *Department of Medicine I, Institute of Cancer Research and Comprehensive Cancer Center, Medical University of Vienna, Borschkegasse 8A, 1090 Vienna, Austria*
[6] *Institute of Inorganic Chemistry and Research Platform "Translational Cancer Therapy Research", University of Vienna, Waehringer Strasse 42, 1090 Vienna, Austria*
[7] *First Department of Pathology and Experimental Cancer Research, Semmelweis University, Üllői út 26, Budapest 1085, Hungary*
[8] *Centro de Malária e Outras Doenças Tropicais (CMDT), Instituto de Higiene e Medicina Tropical, Universidade Nova de Lisboa, Rua da Junqueira 100, 1349-008 Lisbon, Portugal*

Correspondence should be addressed to Attila Hunyadi; hunyadi.a@pharm.u-szeged.hu

Received 26 December 2014; Revised 25 February 2015; Accepted 10 March 2015

Academic Editor: Zeki Topcu

Ecdysteroids, analogs of the insect molting hormone, are known for their various mild, nonhormonal bioactivities in mammals. Previously, we reported that less-polar ecdysteroids can modulate the doxorubicin resistance of a multidrug resistant (MDR) mouse lymphoma cell line expressing the human ABCB1 transporter. Here, we describe the ability of 20-hydroxyecdysone (**1**) and its mono- (**2**) and diacetonide (**3**) derivatives to sensitize various MDR and non-MDR cancer cell lines towards doxorubicin, paclitaxel, vincristine, or cisplatin. Drug IC_{50} values with or without ecdysteroid were determined by MTT assay. Compound **3** significantly sensitized all cell lines to each chemotherapeutic except for cisplatin, whose activity was decreased. In order to overcome solubility and stability issues for the future *in vivo* administration of compound **3**, liposomal formulations were developed. By means of their combination index values obtained via checkerboard microplate method, a formulation showed superior activity to that of compound **3** alone. Because ecdysteroids act also on non-ABCB1 expressing (sensitive) cell lines, our results demonstrate that they do not or not exclusively exert their adjuvant anticancer activity as ABCB1 inhibitors, but other mechanisms must be involved, and they opened the way towards their *in vivo* bioactivity testing against various cancer xenografts.

1. Introduction

Ecdysteroids represent a particularly interesting group of natural compounds from several aspects, with functions in all kingdoms of nature: in insects, they play a crucial hormonal role controlling molting and development [1]; in plants, they appear to serve as part of the chemical defense against nonadapted herbivores [2]; and, although with a less-studied and unclear role, they are also present in fungi [3]. These compounds show fundamental differences to the mammalian

steroid hormones, which make them unable to interact with their hormonal system [4]. Despite this, a number of rather beneficial metabolic effects have been attributed to them in mammals including humans: a mild anabolic activity of ecdysteroids undoubtedly exists [4], and these compounds can also influence both glucose and lipid homeostasis [5], altogether resulting in a so-called adaptogenic or "antistress" effect.

The role of ecdysteroids in cancer is yet to be understood. In accordance with their "general strengthening" effect on mammals, *in vitro* antiapoptotic effect of muristerone A was observed in RKO human colon carcinoma cells [6]. As a result of a thorough study on many natural and semisynthetic ecdysteroids, we have recently reported that certain derivatives can significantly decrease the doxorubicin resistance of a multidrug resistant (MDR) mouse lymphoma cell line ($L5178_{MDR}$) that has been transfected with the pHa MDR1/A retrovirus to express the human ABCB1 or P-glycoprotein, an ATP-binding cassette (ABC) transporter [7]. Mild to strong synergism with doxorubicin was found for the less-polar derivatives, while classical, polar ecdysteroids, such as, for example, 20-hydroxyecdysone (20E; **1**), could act in a weak antagonism or indifferent way with this chemotherapeutic agent [7]. Our following structure-activity relationship studies revealed that the introduction of apolar groups at the 20,22 and particularly at the 2,3 position is of key importance in order to have a sensitizing effect on doxorubicin in the aforementioned cell line [7–9]. Interestingly, although several of the less-polar ecdysteroids could inhibit the function of ABCB1, this inhibition was moderate or negligible and only a very marginal correlation to the strength of synergism with doxorubicin could be found [7].

Two derivatives of 20E (**1**), 20-hydroxyecdysone 20,22-acetonide (**2**), and 20-hydroxyecdysone 2,3;20,22-diacetonide (**3**) are of particular interest in our studies; structures of these three compounds are shown in Figure 1.

Compounds **2** and **3** can also be found in the nature but their semisynthetic preparation from the abundant 20E (**1**) is extremely simple and economic; moreover, compound **3** was among the most active ecdysteroids in our previous studies [7–9]. In fact, compounds **1**–**3** represent good examples for the different levels of activity of ecdysteroids in $L5178_{MDR}$ cells from the weak antagonism to the strong synergism when coadministered with doxorubicin, which makes these three compounds an ideal choice to further study the effects of ecdysteroids in cancer and also the mechanism by which they exert their activity. On the other hand, the well-known acid sensitivity of acetonide groups (resulting in a quick decomposition of compound **3** to compound **2** at gastric pH [7]) and solubility problems, mainly of compound **3**, could be an impediment to further *in vivo* studies. This fact made further formulations necessary prior to performing animal studies.

Nanosized drug delivery systems, such as liposomes, are potential carriers for the encapsulation of bioactive agents, both hydrophilic and hydrophobic molecules, peptides, and so forth. Synthetic and natural phospholipids and cholesterol derivatives are important components of the biocompatible, less immunogenic, and nontoxic liposomes [10, 11]. Controlled or targeted drug release and reduction of the number and strength of side effects are the main advantages.

In the present paper, we report the investigation of compounds **1**–**3** in combination with various chemotherapeutic agents against a panel of different drug-sensitive and drug-resistant cancer cell lines, as well as the development of a liposomal formulation of compound **3** in order to allow future *in vivo* studies.

Table 1: Composition of liposome samples LIP-1, LIP-2, and LIP-3.

Components	LIP-1 (mol%)	LIP-2 (mol%)	LIP-3 (mol%)
Compound **3**	9	8	8
L-PC	44	24	25,9
Lecithin	21	15	16
C-24	7	12	12,8
b-DG	3	7	0
PEG-3000 PE	0	0	0,3
Cholesterol	16	34	37

2. Materials and Methods

2.1. Chemicals and Reagents. 20E (90% purity, originating from the roots of *Cyanotis arachnoidea*) was purchased from Shaanxi KingSci Biotechnology Co. Ltd. (Shanghai, China) and further purified by crystallization to possess 97.8% purity; this served as the starting material for the semisynthesis of compounds **2** and **3** as published before [8]. Phosphatidylcholines as L-alpha phosphatidylcholine and lecithin and 1,2-distearoyl-*sn*-glycero-3-phosphoethanolamine-N-[methoxy(polyethylene glycol)-3000] (ammonium salt) as PEG-3000 PE were purchased from Avanti Polar Lipids Inc. (US). Cholesterol, polyoxyethylene-24-cholesterly ether, beta-D-glucopyranoside, anhydrous ethanol, sodium chloride, and sodium phosphate buffer salt ($Na_2HPO_4{\cdot}2H_2O$) were purchased from VWR Int. Ltd. (Austria). PES syringes and membrane syringe filters with pore sizes of 100, 220, and 900 nm and a diameter of 25 mm were purchased from Phenomenex Inc. (Gen-Lab Ltd., Hungary).

2.2. Preparation of Liposomes. Liposomes were prepared by the hydration of thin dry lipid film method. The compositions used were selected according to a preliminary preformulation study (in preparation). Briefly, L-alpha phosphatidylcholine (L-PC), cholesterol, lecithin, polyoxyethylene-24-cholesterly ether (C-24), and beta-D-glucopyranoside or PEG-3000 PE were solubilized together with compound **3** in anhydrous ethanol at 65°C; compositions of formulae LIP-1, LIP-2, and LIP-3 are shown in Table 1. Polyoxyethylene-24-cholesterly ether, beta-D-glucopyranoside (b-DG), and cholesterol were used to stabilize the liposome bilayer. The PEG-3000 PE was used as material for PEGylation of the liposomes. The solvent was later removed by evaporation on a rotary vacuum evaporator (Büchi Rotavapor R-210 System, Büchi Labortechnik, Switzerland) at $p = 150$ mbar. The lipid film layer

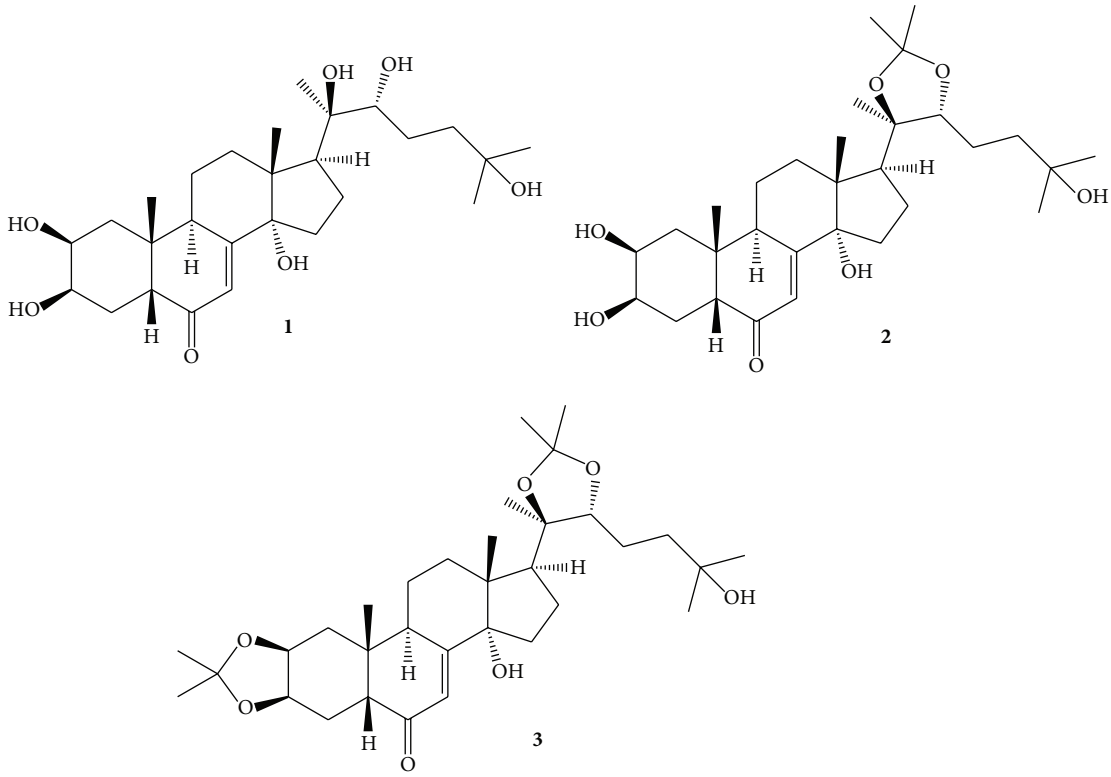

Figure 1: The structures of compounds **1**, **2**, and **3**.

was rehydrated in filtered (100 nm) phosphate buffer saline solution (pH 7.4) having the osmolality of 279 mOsm/L. The liposome dispersion was kept in a refrigerator at 4°C for 2 h prior to the droplet size reduction. The process was achieved by sonicating the liposome dispersion for 15 min at 100% amplitude (Elma TH075EL Ultrasonic bath, ELMA GmbH & Co. KG, Germany). Liposomes of uniform size were prepared by filtration (membrane filters, PES) once through 900 and 220 nm pore size filters. Sorbic acid (0.05% w/v) was added to the buffer solution in order to ensure microbiological stability.

2.3. Determination of the Average Hydrodynamic Size and Surface Electric Charge of Liposome Dispersion. The liposome dispersion was characterized for average droplet size, polydispersity index (PDI, representing size distribution), and surface electric charge by DLS (dynamic laser scattering) method with a Zetasizer Nano ZS (Malvern Instruments Ltd., UK). The optical parameters (i.e., refractive index of the dispersion and the buffer solution) and the conductivity were measured before the DLS measurement. The liposomes were stored at 25°C for 1 h prior to analysis and then diluted with ultrapure water. Liposomes were measured after 1 week storage time, which is enough to observe the possible phase separation (i.e., the conflux of liposome droplets) that could be caused by any undesirable alteration of the preparation process ($n = 3$).

*2.4. Quantitative Analysis of Compound **3** within Liposomes.* 0.5 mL of LIP-1, LIP-2, or LIP-3 was measured into a 5.0 mL volumetric flask, diluted to 1.5 mL with HPLC-gradient water and adjusted to 5.0 mL with HPLC grade methanol. HPLC analysis was performed on a system of two Jasco PU-2080 pumps connected to a Jasco MD-2010 Plus photodiode-array detector, in isocratic mode by 70% aqueous methanol on a Zorbax XDB-C8 column (5 μm, 4.6 × 150 mm) at a flow rate of 1.5 mL/min at $\lambda = 243$ nm. Each measurement was performed in triplicates, as well as the calibration that was performed by injecting 0.2, 0.5, 1.0, 3.0, and 5.0 μg of compound **3**.

2.5. Cell Lines. Six human derived cancer cell lines were used in this study: breast cancer MCF7 cells and their subcell line obtained by adaptation to doxorubicin, $MCF7_{dox}$ [12] cultured in EMEM media supplemented with nonessential amino acids, 1 mM Na-pyruvate, and 10% inactivated fetal bovine serum ($MCF7_{dox}$ was cultured in the presence of 1 μM of doxorubicin each third passage); prostate cancer cells PC3 and LNCaP cultured in RPMI 1640 media supplemented with 10% inactivated fetal bovine serum; in case of LNCaP medium also contained 1 mM Na-pyruvate, HEPES, and glucose; epidermal carcinoma cell line KB-3-1 and its subline KB-C-1 obtained by stepwise adaption to colchicine (generously donated by D. W. Shen, Bethesda, USA) cultured in RPMI 1640 media supplemented with 10% inactivated fetal bovine serum. All cells were cultured at 37°C and

5% CO_2; all media contained nystatin, 2 mM L-glutamine, 100 U penicillin, and 0.1 mg streptomycin.

Two mouse lymphoma cell lines were also used: a parental (L5178) cell line, L5178 mouse T-cell lymphoma cells (ECACC catalog number 87111908, U.S. FDA, Silver Spring, MD, U.S.), and a multidrug resistant ($L5178_{MDR}$) cell line derived from L5178 by transfection with pHa MDR1/A retrovirus [13]. Cells were cultured in McCoy's 5A media supplemented with nystatin, L-glutamine, penicillin, streptomycin, and inactivated horse serum, at 37°C and 5% CO_2. MDR cell line was selected by culturing the infected cells with 60 μg/L colchicine (Sigma).

Media, fetal bovine serum, horse serum, and antibiotics were purchased from Sigma.

2.6. Cytotoxicity Assays

Cytotoxic Activity. Cytotoxic activities were evaluated by serial-dilution method in 96-well flat-bottom microtiter plates. In case of L5178 and $L5178_{MDR}$ cell lines, 6×10^3 cells were added to each well and results were evaluated using 10% MTT after 72 h incubation at 37°C, 5% CO_2. In case of PC3 and LNCaP cell lines, 1×10^4 cells were added to each well and results were evaluated using 10% MTT after 48 h. With respect to the MCF7, $MCF7_{DOX}$, KB-3-1, and KB-C-1 cell lines, 1×10^4 cells per well were seeded overnight and serial dilutions of the compound were added the following day and incubated for 48 h or 72 h. In all cases, the precipitate formed in the MTT reaction was diluted with 10% SDS-HCl after 4 h. Plates were incubated overnight and optical density was measured at 540 and 630 nm using an ELISA reader (Multiskan EX, Lab Systems, U.S.). Fifty per cent inhibitory concentrations (IC_{50}) were calculated using nonlinear regression curve fitting of log(inhibitor) versus normalized response and variable slope with a least squares (ordinary) fit of GraphPad Prism 5 software.

2.7. Combination Studies at Fixed Ecdysteroid Concentration. As compounds **1**–**3** were found to exert very low cytotoxicity activity on each cell line (see below), the activity of 50 μM of compound on the IC_{50} of doxorubicin (Teva), paclitaxel (Mayen) cisplatine (Teva), or vincristine was tested using the same protocol as described above to the cytotoxicity testing for the respective cell lines. In each case, statistical analysis was carried out by one-way ANOVA with Bonferroni's post hoc test, and differences were considered significant at $^{*}P < 0.05$, $^{**}P < 0.01$, and $^{***}P < 0.001$. In order to prevent any possible false positive results and strengthen the relevance of our data for possible *in vivo* studies, we also set up a stricter criterion: statistically significant potentiation was considered relevant only when at least a two-time decrease in the IC_{50} of the chemotherapeutic agent was observed. Such measures were not applied in case of an antagonistic effect (see results for cisplatin).

*2.8. Combination Studies with Liposomes Containing Compound **3**.* The combined activity of doxorubicin (Teva) and formulations LIP-1, LIP-2, and LIP-3 on the $L5178_{MDR}$ mouse lymphoma cells was determined using the checkerboard microplate method in 96-well flat-bottom microtiter plates as published before [7]. Briefly, 1×10^4 cells/well were incubated with different concentrations of doxorubicin and liposomes containing compound **3** for 48 h at 37°C under 5% CO_2. Cell viability rate was determined through MTT staining, and the interaction was evaluated by using the CompuSyn software (CompuSyn, Inc., U.S.) for the constant liposome versus doxorubicin ratios. Combination index (CI) values are presented for 50%, 75%, and 90% of growth inhibition. In each case, the amounts of liposomes were applied so that they represent the same amount of compound **3** within, based on the results of the quantitative determination by HPLC (see above, Section 2.4). As such, M/M ratios of compound **3** versus doxorubicin were used to calculate the results, which was performed according to that suggested by Chou [14].

3. Results and Discussion

Our previous observations on the strong activity of compound **3**, a less-polar ecdysteroid, against the doxorubicin resistance of ABCB1 expressing MDR murine lymphoma cells [7] led to the need of a thorough study on these compounds using various human cell lines and chemotherapeutics. The chosen cell lines included drug susceptible/MDR cell line pairs, such as the previously used L5178 and the ABCB1 transfected $L5178_{MDR}$ (mouse lymphoma), MCF7 and its ABCB1 expressing subcell line $MCF7_{dox}$ adapted to doxorubicin (mammary gland), and KB-3-1 and its ABCB1 expressing subcell line KB-C-1 adapted to colchicine (cervix). Two prostate cancer cell lines were also used in our experiments, the steroid dependent LNCaP and the nonsteroid dependent PC3. When tested alone on these cell lines, compounds **1**, **2**, and **3** exerted very low cytotoxic activities with IC_{50} values of typically >100 μM, except for compound **3** on the L5178 (81.12 ± 5.5 μM) and compound **2** on the MCF7 cell line (89.67 ± 4.1 μM).

The effect of 50 μM of compounds **1**–**3** was tested on the cytotoxic activity of chemotherapeutics with distinct mechanisms of action, such as doxorubicin (topoisomerase II inhibitor, ABCB1 substrate), paclitaxel (stabilizes microtubule polymer, ABCB1 substrate), vincristine (antitubulin agent on tubulin dimers, ABCB1 substrate), and cisplatin (alkylating agent, non-ABCB1 substrate); results are shown in Figure 2.

It is important to mention that even though compounds **1**–**3** exert negligible intrinsic cytotoxic activity at the applied concentration of 50 μM, this approach is still a simplification as compared to an appropriate calculation of synergism, for example, by using the checkerboard plate method [14], and, as such, it could lead to false positive results. Considering this and also taking into account our previous observations on the IC_{50} patterns in combination studies on checkerboard plates [7], we decided to accept only those results as actual sensitizing activity, where at least a two-time decrease in the IC_{50} value of the chemotherapeutic could be observed.

Compound **3** exerted a significant sensitization effect on all cell lines when applied together with doxorubicin, vincristine, or paclitaxel. Results with doxorubicin could not be determined on the highly resistant $MCF7_{dox}$ cell line

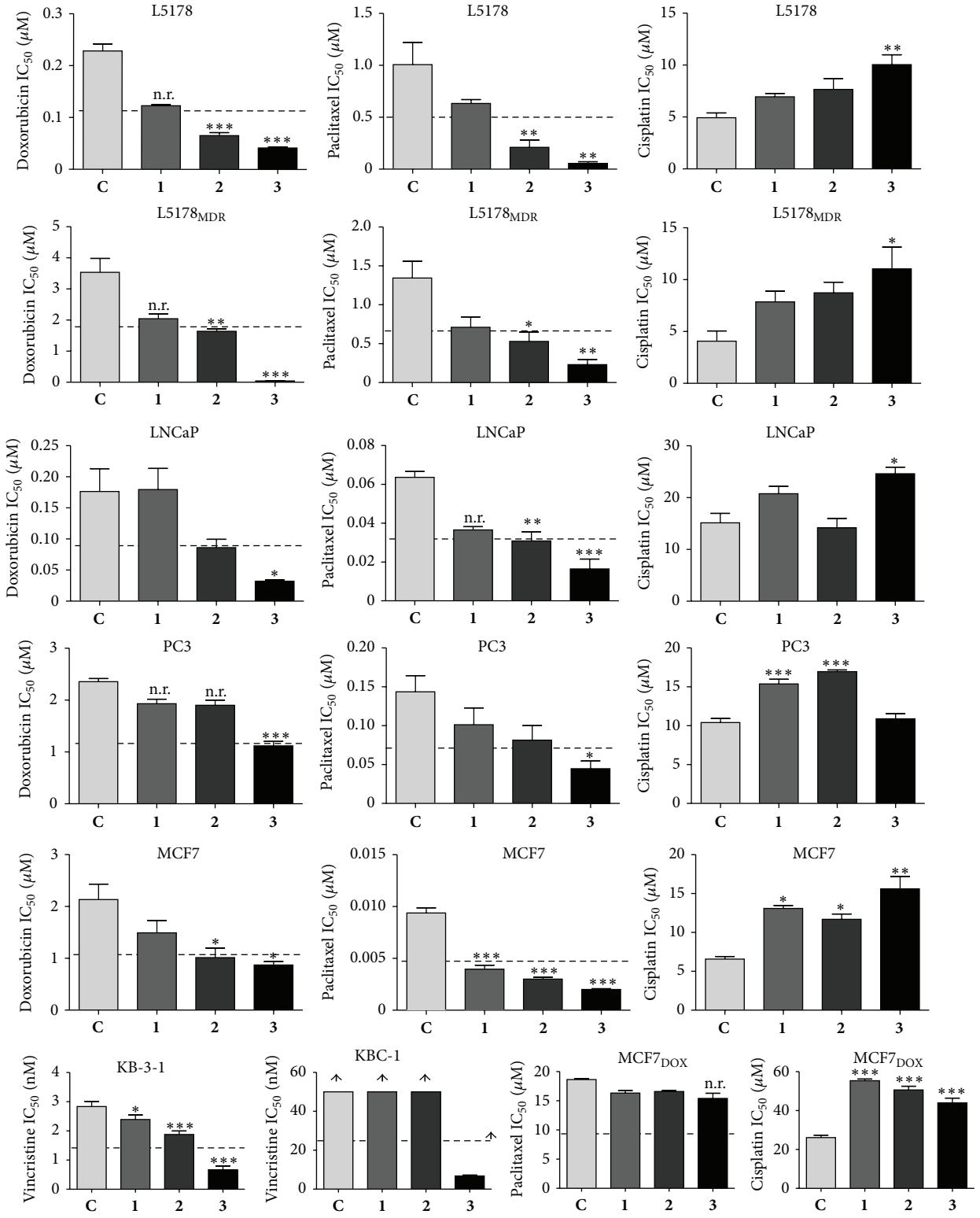

FIGURE 2: The effect of 50 μM of **1**, **2**, or **3** on the IC_{50} values of chemotherapeutics in various susceptible and MDR cell lines. $^{*}P < 0.05$, $^{**}P < 0.01$, and $^{***}P < 0.001$ by means of one-way ANOVA followed by Bonferroni post hoc test as compared to that of the chemotherapeutic agent alone (**C**); n.r.: statistically significant, but not relevant sensitization.

Table 2: Droplet size characteristics and encapsulation efficiency of compound **3** within liposome samples LIP-1, LIP-2, and LIP-3 ($n = 3$).

Liposome samples	Average hydrodynamic size [nm]	Droplet size distribution	Polydispersity index (PDI)	Surface electric charge [mV]	Entrapment efficiency (%)
LIP-1	92.1 ± 0.5	30–300 nm (100%)	0.16	−2.16 ± 0.77	43%
LIP-2	83.2 ± 0.9	20–200 nm (100%)	0.16	−2.46 ± 0.45	8%
LIP-3	84.7 ± 1.3	20–220 nm (100%)	0.19	−1.37 ± 0.56	50%

since that chemotherapeutic agent had to be applied in such high doses that the measurements were disturbed by its own color (data not shown); paclitaxel resistance of this cell line could also not be reverted. Altogether, the results that are in agreement with those observed by us previously and strongly support our previous assumption [7] that less-polar ecdysteroids do not or not exclusively act as ABCB1 inhibitors: compound **3** could effectively sensitize non-MDR human cell lines with no detectable (MCF7 [12, 15], KB-3-1 [16, 17]) or very low (LNCaP [18]) expression of the ABCB1 protein, as well as the drug-sensitive mouse lymphoma cell line (L5178). Moreover, the IC_{50} of doxorubicin in the L5178 cell line and its ABCB1 transfected counterpart $L5178_{MDR}$ was decreased to practically the same values, 41.7 and 45.6 nM, respectively (no significant difference by unpaired t-test), in the presence of 50 μM of compound **3**, while the IC_{50} values for doxorubicin alone on the L5178 and the $L5178_{MDR}$ cell lines were 228.3 and 3537 nM, respectively. Compound **3** was also able to reduce the paclitaxel resistance of PC3 cells to the same level of those of untreated LNCaP cells (IC_{50} = 44.8 and 63.5 nM, resp. and no significant difference by unpaired t-test), while the treatment of LNCaP cells with compound **3** led to an even stronger cytotoxic activity of paclitaxel (IC_{50} = 16.5 nM). Moreover, KB-3-1 cells were sensitized by compound **3** to vincristine in a way that it reached much lower IC_{50} values than observed in KB-C-1 cells treated with the combination: the IC_{50} value was 0.67 nM (without compound **3**: 2.84 nM) in case of KB-3-1, while it was ca. 10 times higher, 6.78 (without compound **3**: >50 nM) in case of the MDR subline KB-C-1. A comparison of these values also reveals that resistance of KB-C-1 cells to vincristine could not completely be reverted by compound **3**: even though a strong sensitizing activity was observed, the cytotoxicity of vincristine was still significantly weaker than in the parental KB-3-1 cell line ($P < 0.001$ by unpaired t-test).

The 20,22-acetonide compound (**2**) showed tendencies for an activity pattern similar to the diacetonide **3**, but with much weaker and in several cases irrelevant activities. Interestingly and somewhat unexpectedly, compound **1**, 20-hydroxyecdysone, was also found to show significant and relevant sensitizing activity in case of one cell line, MCF7, when coadministered with paclitaxel.

On the other hand, the tested ecdysteroids showed an obvious general tendency to decrease the activity of cisplatin in all cell lines, especially in the two breast cancer cells lines (MCF7 and $MCF7_{dox}$) where all compounds significantly elevated its IC_{50} values. In case of the two prostate carcinoma cell lines, the compounds showed different behaviors: only compound **3** could significantly protect the steroid dependent LNCaP cells from the effect of cisplatin, while compounds **1** and **2** exerted such an activity in the PC3 cells where compound **3** did not influence the efficacy of cisplatin. Although androgen hormone dependency is a major difference between these two cell lines, it should be noted that ecdysteroids do not exert androgenic activity [4]. Relevance of our results in terms of a possible interference with actual chemotherapy with cisplatin in cancer patients will have to be clarified by further studies; considering the large number of food supplements containing high amounts of ecdysteroids (mainly compound **1**) available on the market, the possibility of unwanted interactions cannot be excluded. On the other hand, Konovalova et al. have previously found that 10 mg/kg of compound **1** could potentiate the activity and decrease the toxicity of cisplatin in P388 leukemia or B16 melanoma bearing mice, and the authors suggested that beneficial metabolic and immune system modulatory effects of this compound might be the reason for this phenomenon [19]. Such mechanisms could indeed overwrite an otherwise antagonistic effect observed in our experimental *in vitro* setup. Nevertheless, the strong potentiating activity of compound **3** on the activity of doxorubicin, vincristine, and paclitaxel on various cell lines is highly promising.

As the next step towards animal experiments, the slight acid sensitivity of compound **3** (resulting in its decomposition to compound **2** with a half-life of *ca.* 7.30 min at gastric pH [7]), as well as solubility problems attributed to this compound needed to be solved; in order to fulfill these objectives, liposomal formulations were developed.

The average hydrodynamic size and surface electric charge (zeta potential) parameters of liposome samples of various lipid compositions are shown in Table 2. The droplet size and the PDI values are typical of SUV (small unilamellar vesicle) type liposomes, ranging from 83 to 92 nm and from 0.16 to 0.19, respectively. One size fraction of liposomes was observed in the range of 20–220 or 20–300 nm, irrespective of the lipid composition used for the preparation. A slight increase in the zeta potential from −2.16 (LIP-1) and −2.46 (LIP-2) mV to the value of −1.37 mV (LIP-3) was observed with the addition of PEG-PE lipid.

Encapsulation of compound **3** into LIP-1, LIP-2, and LIP-3 resulted in entrapment efficiencies of 43, 8, and 50%, respectively (Table 2). LIP-1 and LIP-2 represent different compositions, containing more L-PC and lecithin (LIP-1) or more cholesterol and C-24 (POE-cholesteryl-ether) (LIP-2). Cholesterol and C-24 were used as bilayer stabilizers, but their increased concentration was not enough to achieve complete droplet stability for LIP-2. However, the compositions of LIP-2 and LIP-3 are rather similar; the difference is the addition of the PEG-3000 PE component in the latter case. The increase of the entrapment efficiency from 8% to 50% could be due to

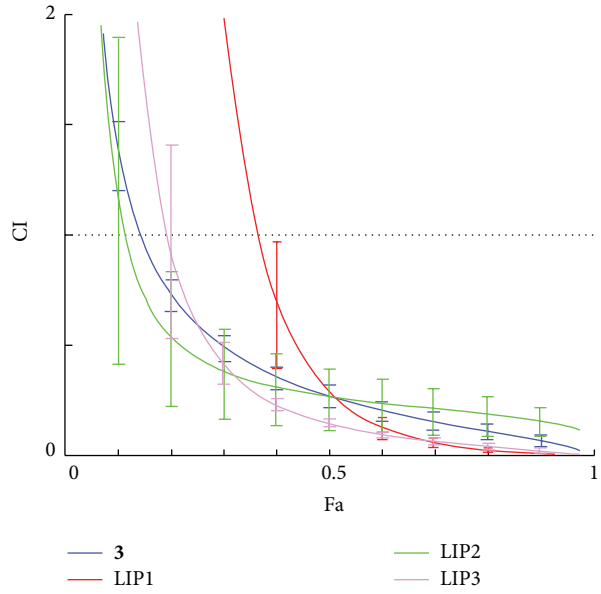

Sample	CI values at			D_m	m	r	Cl_{avg}
	ED_{50}	ED_{75}	ED_{90}				
3	0.27	0.14	0.07	11.68	3.25	0.96	0.13
LIP1	0.29	0.04*	0.01*	4.07	3.28	0.95	0.07
LIP2	0.27	0.20	0.16	4.30	2.60	0.91	0.19
LIP3	0.15*	0.06*	0.03*	4.53	2.35	1.00	0.06

FIGURE 3: Fa-CI plots of the nonformulated compound **3** and that enclosed within liposomes (LIP-1, LIP-2, and LIP-3) tested on the $L5178_{MDR}$ cell line. Concentrations correspond to compound **3**/doxorubicin ratio of 20.4 M/M in each case. Fa = fraction affected. Dashed horizontal line shows CI = 1, and CI < 1, CI = 1, and CI > 1 represent synergism, additivity, and antagonism, respectively. The error bars show 95% confidence intervals by means of serial deletion analysis. In the table, CI values are presented at 50%, 75%, and 90% of inhibition (ED_{50}, ED_{75}, and ED_{90}, resp.); $CI_{avg} = (CI_{50} + 2CI_{75} + 3CI_{90})/6$; D_m, m, and r represent antilog of the x-intercept, slope, and linear correlation coefficient of the median-effect plot, respectively. These parameters indicate the activity (IC_{50}), shape of the dose-effect curve, and conformity of the data, respectively [7]; ∗: significantly stronger synergism with doxorubicin as compared to compound **3** by means of nonoverlapping confidence intervals.

the fact that the exact average molecular weight of PEG-3000 PE material is around tenfold higher (3772.36) than those of the other components. This relatively high molecular weight could ensure better physicochemical stability and therefore a much higher entrapment of compound **3** [20].

In order to investigate the activity of the liposomes containing compound **3** in comparison with that of the nonformulated compound, interactions between LIP-1, LIP-2, and LIP-3 and doxorubicin were tested on checkerboard plates. This experimental setup was chosen because in these complex systems there were too many factors that could have influenced the results, and hence we decided not to apply the simplification presented above. Synergism/antagonism was quantified by using the CompuSyn software as in our previous work [7, 9]. Quantitative determination of compound **3** within the formulations allowed us to apply the same doses in each case, as expressed in compound **3** equivalents. Results of these experiments are shown in Figure 3.

Based on our results, the formulations not only keep the strong synergistic activity of compound **3** and doxorubicin, but also, particularly in case of LIP-3, are able to show favorable activity as compared to the free compound. The slight increase in the potentiating activity might be explained by the liposomes ability to fuse with the cell membranes and deliver the enclosed compound to the cells more efficiently even *in vitro*; however, the favorable effect on the solubility of compound **3** in the aqueous environment can also be among the reasons for this phenomenon. It is also important to note that the acidic pH of around 5 maintained within the lysosomes [21] (that compound **3** likely faces upon the phagocytosis of the liposomes) is apparently not enough to hydrolyze the acetonide groups, which could have been a serious pitfall for these formulations if compound **3** would decompose to the much less active compound **2** [7].

4. Conclusions

We demonstrated that the 20,22-acetonide (**2**) and in particularly the 2,3;20,22-diacetonide (**3**) derivatives of 20-hydroxyecdysone (**1**) are able to exert sensitizing activity to doxorubicin, paclitaxel, and vincristine in MDR cell lines, which express the ABCB1 membrane transporter, as well as in their susceptible counterparts. Even though, in this work, no conclusions can be made about the mechanism(s) of action of these compounds, these results strongly support our previous assumptions [7] that these ecdysteroids do not or not only act as ABCB1 inhibitors when exerting their adjuvant anticancer activity.

Moreover, all ecdysteroids showed significant protective effects towards cisplatin treatment on some of the cell lines tested *in vitro*, highlighting the importance of further studies in this direction.

Compound **3** enclosed in liposomes (LIP-3) showed stronger synergistic activity in combination with doxorubicin on $L5178_{MDR}$ cells as compared to the case when it was applied in solution. Based on these results, LIP-3 represents

a highly prospective formulation for *in vivo* studies. Such studies have most recently started within our research program; results are going to be presented in the near future.

Conflict of Interests

The authors declare that there is no conflict of interests regarding the publication of this paper.

Acknowledgments

The authors acknowledge the support from the European Union cofunded by the European Social Fund (TÁMOP 4.2.2.A-11/1/KONV-2012-0035), the Fundação para a Ciência e a Tecnologia (FCT), Portugal (PEsT-OE/SAU/UI0074/2011), and the Foundation for Cancer Research, Szeged, Hungary. A. Martins was supported by the Grant SFRH/BPD/81118/2011, FCT, Portugal. The work presented here was performed within the framework of COST Action CM1106, Chemical Approaches to Targeting Drug Resistance in Cancer Stem Cells.

References

[1] P. Karlson, "Mode of action of ecdysones," in *Invertebrate Endocrinology and Hormonal Heterophylly*, W. B. Burdette, Ed., pp. 43–54, Springer, Berlin, Germany, 1974.

[2] E. A. Schmelz, R. J. Grebenok, D. W. Galbraith, and W. S. Bowers, "Damage-induced accumulation of phytoecdysteroids in spinach: a rapid root response involving the octadecanoic acid pathway," *Journal of Chemical Ecology*, vol. 24, no. 2, pp. 339–360, 1998.

[3] R. Lafont, J. Harmatha, F. Marion-Poll, L. Dinan, and I. D. Wilson, *The Ecdysone Handbook*, 3rd edition, 2002, http://ecdybase.org/.

[4] M. Báthori, N. Tóth, A. Hunyadi, Á. Márki, and E. Zádor, "Phytoecdysteroids and anabolic-androgenic steroids. Structure and effects on humans," *Current Medicinal Chemistry*, vol. 15, no. 1, pp. 75–91, 2008.

[5] A.-S. Foucault, V. Mathé, R. Lafont et al., "Quinoa extract enriched in 20-hydroxyecdysone protects mice from diet-induced obesity and modulates adipokines expression," *Obesity*, vol. 20, no. 2, pp. 270–277, 2012.

[6] I. Oehme, S. Bösser, and M. Zörnig, "Agonists of an ecdysone-inducible mammalian expression system inhibit Fas Ligand- and TRAIL-induced apoptosis in the human colon carcinoma cell line RKO," *Cell Death and Differentiation*, vol. 13, no. 2, pp. 189–201, 2006.

[7] A. Martins, N. Tóth, A. Ványolós et al., "Significant activity of ecdysteroids on the resistance to doxorubicin in mammalian cancer cells expressing the human ABCB1 transporter," *Journal of Medicinal Chemistry*, vol. 55, no. 11, pp. 5034–5043, 2012.

[8] A. Balázs, A. Hunyadi, J. Csábi et al., " ^{1}H and ^{13}C NMR investigation of 20-hydroxyecdysone dioxolane derivatives, a novel group of MDR modulator agents," *Magnetic Resonance in Chemistry*, vol. 51, no. 12, pp. 830–836, 2013.

[9] A. Martins, J. Csábi, A. Balázs et al., "Synthesis and structure-activity relationships of novel ecdysteroid dioxolanes as MDR modulators in cancer," *Molecules*, vol. 18, no. 12, pp. 15255–15275, 2013.

[10] D. D. Lasic and Y. Barenholz, *Handbook of Nonmedical Applications of Liposomes, Volume 4: From Gene Delivery and Diagnosis to Ecology*, CRC Press, New York, NY, USA, 1996.

[11] S. Ichikawa, S. Sugiura, M. Nakajima, Y. Sano, M. Seki, and S. Furusaki, "Formation of biocompatible reversed micellar systems using phospholipids," *Biochemical Engineering Journal*, vol. 6, no. 3, pp. 193–199, 2000.

[12] M. D. Kars, Ö. D. Işeri, U. Gündüz, A. U. Ural, F. Arpaci, and J. Molnár, "Development of rational in vitro models for drug resistance in breast cancer and modulation of MDR by selected compounds," *Anticancer Research*, vol. 26, no. 6, pp. 4559–4568, 2006.

[13] I. Pastan, M. M. Gottesman, K. Ueda, E. Lovelace, A. V. Rutherford, and M. C. Willingham, "A retrovirus carrying an MDR1 cDNA confers multidrug resistance and polarized expression of P-glycoprotein in MDCK cells," *Proceedings of the National Academy of Sciences of the United States of America*, vol. 85, no. 12, pp. 4486–4490, 1988.

[14] T. C. Chou, "Theoretical basis, experimental design, and computerized simulation of synergism and antagonism in drug combination studies," *Pharmacological Reviews*, vol. 58, pp. 621–681, 2006.

[15] A. M. Calcagno, J. M. Fostel, K. K. W. To et al., "Single-step doxorubicin-selected cancer cells overexpress the ABCG2 drug transporter through epigenetic changes," *British Journal of Cancer*, vol. 98, no. 9, pp. 1515–1524, 2008.

[16] P. Heffeter, M. Pongratz, E. Steiner et al., "Intrinsic and acquired forms of resistance against the anticancer ruthenium compound KP1019 [indazolium trans-[tetrachlorobis(1H-indazole)ruthenate (III)] (FFC14A)," *Journal of Pharmacology and Experimental Therapeutics*, vol. 312, no. 1, pp. 281–289, 2005.

[17] P. Heffeter, M. A. Jakupec, W. Körner et al., "Multidrug-resistant cancer cells are preferential targets of the new antineoplastic lanthanum compound KP772 (FFC24)," *Biochemical Pharmacology*, vol. 73, no. 12, pp. 1873–1886, 2007.

[18] R. Rotem, Y. Tzivony, and E. Flescher, "Contrasting effects of aspirin on prostate cancer cells: suppression of proliferation and induction of drug resistance," *The Prostate*, vol. 42, no. 3, pp. 172–180, 2000.

[19] N. P. Konovalova, Y. I. Mitrokhin, L. M. Volkova, L. I. Sidorenko, and I. N. Todorov, "Ecdysterone modulates antitumor activity of cytostatics and biosynthesis of macromolecules in tumor-bearing mice," *Biology Bulletin of the Russian Academy of Sciences*, vol. 29, no. 6, pp. 530–536, 2002.

[20] V. S. Trubetskoy and V. P. Torchilin, "Polyethylene glycol based micelles as carriers of therapeutic and diagnostic agents," *STP Pharma Sciences*, vol. 6, no. 1, pp. 79–86, 1996.

[21] G. M. Cooper, "Lysosomes," in *The Cell: A Molecular Approach*, Sinauer Associates, Sunderland, Mass, USA, 2nd edition, 2000.

Hindawi Publishing Corporation
BioMed Research International
Volume 2015, Article ID 212809, 7 pages
http://dx.doi.org/10.1155/2015/212809

Research Article

Antiproliferative Activity of Flavonoids from *Croton sphaerogynus* Baill. (Euphorbiaceae)

Kátia Pereira dos Santos,[1] Lucimar B. Motta,[2] Deborah Y. A. C. Santos,[1] Maria L. F. Salatino,[1] Antonio Salatino,[1] Marcelo J. Pena Ferreira,[1] João Henrique G. Lago,[3] Ana Lúcia T. G. Ruiz,[4] João E. de Carvalho,[4] and Cláudia M. Furlan[1]

[1]*Departamento de Botânica, Instituto de Biociências, Universidade de São Paulo, Rua do Matão 277, 05508-090 São Paulo, SP, Brazil*
[2]*Universidade Paulista, Rua Apeninos 267, 01533-000 São Paulo, SP, Brazil*
[3]*Instituto de Ciências Ambientais, Químicas e Farmacêuticas, Universidade Federal de São Paulo, Rua Professor Arthur Riedel 275, 09972-270 Diadema, SP, Brazil*
[4]*Divisão de Farmacologia e Toxicologia, CPQBA, CP 6171, Universidade Estadual de Campinas, 13083-970 Campinas, SP, Brazil*

Correspondence should be addressed to Kátia Pereira dos Santos; katiapsp@gmail.com

Received 15 December 2014; Revised 11 February 2015; Accepted 12 February 2015

Academic Editor: István Zupkó

Croton sphaerogynus is a shrub from the Atlantic Rain Forest in southeastern Brazil. A lyophilized crude EtOH extract from leaves of *C. sphaerogynus*, obtained by maceration at room temperature (seven days), was suspended in methanol and partitioned with hexane. The purified MeOH phase was fractionated over Sephadex LH-20 yielding five fractions (**F1–F5**) containing flavonoids, as characterized by HPLC-DAD and HPLC-MS analyses. The antiproliferative activity of the crude EtOH extract, MeOH and hexane phases, and fractions **F1–F5** was evaluated on *in vitro* cell lines NCI-H460 (nonsmall cell lung), MCF-7 (breast cancer), and U251 (glioma). The MeOH phase showed activity (mean log GI_{50} 0.54) higher than the hexane phase and EtOH extract (mean log GI_{50} 1.13 and 1.19, resp.). **F1** exhibited activity against NCI-H460 (nonsmall cell lung) (GI_{50} 1.2 μg/mL), which could be accounted for the presence of flavonoids and/or diterpenes. **F4** showed moderate activity (mean log GI_{50} 1.05), while **F5** showed weak activity (mean log GI_{50} 1.36). It is suggested that the antiproliferative activity of the crude EtOH extract and MeOH phase is accounted for a synergistic combination of flavonoids and diterpenes.

1. Introduction

Croton L. (Euphorbiaceae) has approximately 1300 species of herbaceous, shrubs, trees, and lianas forms. The genus is widely distributed in tropical and subtropical regions around the world, including Brazil, a country with 316 species, among which 253 are endemic [1, 2].

Medicinal and toxic properties of *Croton* species have been ascribed to a wide variety of chemical compounds, such as terpenoids and steroids, alkaloids, and phenolic compounds, the latter including predominantly flavonoids, lignans, and proanthocyanidins [3–5].

According to the International Agency for Research on Cancer (IARC), the world impact of cancer has more than duplicated in the last 30 years [6]. The 2014 and 2015 annual estimative regarding Brazil foresees the emergence of approximately 576,000 new cancer cases, including nonmelanoma skin cancer. This latter cancer type is expected to become the most frequent among the Brazilian population (32% new cases), followed by prostate tumors (12%), female breast (10%), colon and rectum (6%), lung (5%), stomach (3.5%), and cervical (3%) [7].

Among drugs currently used in cancer treatment, over 60% are products directly or indirectly derived from plants [8]; most of them related to alkaloids and terpenoids [9].

Several studies dealing with *Croton* species have reported the isolation of cytotoxic derivatives. Shoots of *C. hieronymi* Griseb. showed strong activity against lung A-549 carcinoma cells, mouse lymphoma, and human colon carcinoma [10]. The CH_2Cl_2 extract of leaves of *C. macrobothrys* Baill. and

C. zambesicus Müll. Arg. showed cytotoxicity against human lung and leukemia cells [11] and cervix carcinoma cells [12], respectively. Ent-kaurane diterpenoids from *Croton tonkinensis* have activity against colorectal cancer cells [13]; *ent*-kaur-16-ene-6a,19-diol from *C. floribundus* Spreng. exhibited a moderate effect against MDA-MB-435 (melanoma), HCT-8 (colorectal adenocarcinoma), and HCT-116 (colorectal adenocarcinoma) cell lines [14]. Isopimara-7,15-dien-3b-ol from *C. zambesicus* showed weak cytotoxic activity against cancer (HeLa, human cervix carcinoma cells; HL-60, human promyelocytic leukemia) and noncancer (WI-38, human lung fibroblast) cell lines [15]. An epimer of kaurenoic acid from *C. antisyphiliticus* Mart. showed cytotoxic activity, with half maximal inhibitory concentration values of 59.41, 68.18, and 60.30 μg/mL for the B-16 (murine melanoma), HeLa (human cervix carcinoma cells), and 3T3 (normal mouse embryo fibroblasts) cell lines, respectively [16]. These compounds are considered valuable toward the development of new and highly effective anticancer chemotherapeutic agents, due to their efficacy toward the induction of apoptosis [17, 18].

Individuals of *Croton sphaerogynus* Baill. sect. *Cleodora* grow in the states of Bahia, Rio de Janeiro, Espírito Santo, and São Paulo (Brazil). Most of its populations are distributed in moist forests of seashore plains ("restinga forests"). Two other species of this section, *Croton cajucara* Benth., popularly known as "sacaca," and *Croton heterocalyx* Baill., have been traditionally exploited for their medicinal properties (e.g., [4, 5, 19]). CH_2Cl_2 and hexane extracts from leaves of *C. sphaerogynus* exhibited antiproliferative activity against NCI-H460 (nonsmall cell lung) (GI_{50} 0.26 μg/mL and 0.33 μg/mL, resp.) and K562 cell lines (GI_{50} 0.60 μg/mL and <0.25 μg/mL, resp.). These activities were related to the presence of abietane, podocarpane, and clerodane diterpenes [20].

The main goal of this study was to characterize the major polar constituents of the EtOH extract from leaves of *C. sphaerogynus* and evaluate their *in vitro* antiproliferative activities against tumor cell lines. This study differs from that of Motta et al. [20], which focused on the antiproliferative activity of diterpenes of nonpolar extracts from *C. sphaerogynus* and thus did not deal with its flavonoid constituents and their antiproliferative activity.

2. Material and Methods

2.1. Plant Material. Leaves of *Croton sphaerogynus* were collected in January 2012, in an area of Atlantic Forest in the municipality of Itanhaém, State of São Paulo (Southeastern Brazil). A voucher specimen (LBM 65) was deposited in the herbarium Maria Eneyda P. K. Fidalgo (SP), São Paulo.

2.2. Extraction Procedure. Dried and powdered leaf material (1 kg) was extracted by maceration with EtOH (5 L) for seven days at room temperature. Crude EtOH extract (**EE**) was concentrated under reduced pressure, evaporated to dryness under a stream of nitrogen, and lyophilized, affording 70.62 g of crude EtOH extract (yield: 7%). Part of the crude EtOH extract (65 g) was resuspended in MeOH and partitioned using hexane. The hexane phase (**HP**) was concentrated under reduced pressure to yield 20 g (2%) of hexane phase, while the MeOH phase (**MP**) was lyophilized to afford 15 g (yield: 1.5%). Part of **MP** (8 g) was fractionated over Sephadex LH-20 using MeOH as eluent, affording five fractions: **F1** (2 g), **F2** (0.119 g), **F3** (0.090 g), **F4** (0.353 g), and **F5** (0.090 g).

2.3. Chemical Analysis. All lyophilized crude **EtOH** extract, **MP** and **HP** phases, and fractions (**F1**–**F5**) were dissolved in MeOH (2 mg/mL) and analyzed using a HPLC 1260 (Agilent Technologies) chromatograph, equipped with diode array detector (DAD) and a Zorbax-C18 (250 × 4.6 mm, 3.5 μm, Agilent, USA) column at 40°C. Solvents used were 0.1% acetic acid (AcOH) and acetonitrile (CH_3CN), starting with 15% of CH_3CN (0–20 min), increasing to 100% (20–25 min), isocratic (5 min), and decreasing to 15% (30–32 min), and isocratic (3 min). Solvent flow rates were 1.5 mL/min (0–25 min), 1.0 mL/min (25-26 min), and 1.5 mL/min (26–35 min); injection volume was 3 μL, and detection was at 352 nm and 280 nm. Quercetin and kaempferol at concentrations from 0.6 to 360 ng/mL were used to prepare calibration curves following the same analysis conditions. Results are expressed in milligrams per gram of dry sample (mg/g).

MeOH phase (**MP**) was also analyzed using a Bruker Daltonics equipment Esquire 3000 Plus HPLC with a Zorbax-C18 (250 × 4.6 mm, 3.5 μm, Agilent, USA) column at 40°C, using the same conditions cited above. Solvent flow rates was .90 μL/min, voltage 4000 V, nebulizer 27 psi, drying gas at 320°C, and flow of 7 L/min. Constituents were identified by comparing the corresponding UV-Vis and ESI/MS-MS spectra with MS data from the literature.

A purified compound from **F5** was analyzed by ^{1}H NMR at 500 MHz, using a Bruker DRX-500 spectrometer. DMSO-d_6 (Aldrich) was used as solvent and the residual peak of the nondeuterated solvent as internal standard.

2.4. Antiproliferative Assay. Cancer cell lines used were kindly provided by the National Cancer Institute (NCI) at Frederick MA-USA and included NCI-H460 (nonsmall cell lung), MCF-7 (breast cancer), and U251 (glioma). Stock cell cultures were grown in medium containing RPMI 1640, supplemented with 5% of fetal bovine serum. Experimental cultures were supplemented also with penicilin : streptomicin (10 μg/mL : 10 UI/mL).

Cells (100 μL cells/well, inoculation density from 3–6 × 10^4 cell/mL) in 96-well plates were exposed to various sample concentrations (0.25 to 250 μg/mL, 100 μL/well) in DMSO/RPMI 1640/FBS 5% at 37°C, 5% of CO_2 in air for 48 h. Final DMSO concentration did not affect cell viability. Cells were then fixed with 50% trichloroacetic acid and cell proliferation was determined by spectrophotometric quantification of cellular protein content at 540 nm, using the sulforhodamine B assay. Doxorubicin (DOX; 0.025–25 μg/mL) was used as positive control. Three measurements were obtained at the beginning of incubation (time zero, T_0) and 48 h after incubation for compound-free (C) and tested (T) cells. Cell proliferation was determined according to the equation $100 \times [(T - T_0)/C - T_0]$, for $T_0 < T \leq C$, and $100 \times [(T - T_0)/T_0]$, for $T \leq T_0$ and a concentration-response curve for each cell line was plotted using software ORIGIN 7.5 (OriginLab Corporation) [21].

Table 1: Major constituents of the crude EtOH extract (**EE**), MeOH (**MP**) and hexane (**HP**) phases, and fractions (**F1–F5**) from of *Croton sphaerogynus* leaves, characterized by HPLC-DAD (352 nm) and HPLC-MS.

Constituent	Rt (min)	UV/visible (nm)	Mass spectrum		Suggestion
			$[m/z]^+$	$[m/z]^-$	
1	1.75	254, 264 (om), 348			Quercetin derivative
2	2.96	256, 264 (om), 296 (om), 354	757.8; 611.1; 465; 303	755.7	Quercetin triglycoside (2 rhamnose; 1 hexose)
3	3.16	260, 296, 356	741.8; 595.1; 433.1; 286.8		Kaempferol triglycoside (2 rhamnose; 1 hexose)
4	4.05	264, 292, 346	741.8; 595.1; 287		Kaempferol triglycoside (2 rhamnose; 1 hexose)
5	4.30	264, 294, 348	741.9; 595.2; 448.7; 287	739.6	Kaempferol triglycoside (2 rhamnose; 1 hexose)
6	4.99	256, 266 (om), 294 (om), 354	595, 303		Quercetin diglycoside (1 pentose; 1 hexose)
7	5.33	256, 266 (om), 294 (om), 354	661.1; 465	608.9	Rutin
8	6.04	264, 294, 348	595, 286.9	593	Kaempferol diglycoside (1 rhamnose; 1 glucose)
9	6.35	256, 264 (om), 296 (om), 354	479, 316.9		Isorhamnetin monoglycoside (1 hexose)
10	7.30	264, 294, 348	448.9; 286.9		Kaempferol monoglycoside (1 hexose)
11	9.23	264, 294, 346			Kaempferol derivative
12	10.10	256, 268 (om), 356			Quercetin derivative
13	10.72	264, 294, 346			Kaempferol derivative
14	10.97	256, 264 (om), 306 (om), 348	449.0; 302.9	447	Quercitrin
15	20.44	262, 294, 340			Kaempferol derivative
16	22.95	254, 270, 298, 370			Quercetin
17*	23.23	256, 266 (om), 298 (om), 356	317, 302	314.8	Quercetin 3-*O*-methyl ether
18	23.55	264, 292, 320, 366			Kaempferol
19	23.73	266, 294, 350			Kaempferol derivative
20	23.84	254, 268 (om), 294 (om), 356			Quercetin derivative

Rt: average retention time in minutes. *Compound confirmed by ^{1}H NMR.

2.5. Data Analysis. Using the concentration-response curve for each cell line, GI_{50} (concentration causing 50% growth inhibition) [22] was determined by means of nonlinear regression analysis, using software ORIGIN 7.5 (OriginLab Corporation). The average activity (mean of log GI_{50}) of the extracts tested was also determined using MS Excel software. Extracts were regarded as inactive (mean > 1.5), weakly (1.1 < mean < 1.5), moderately (0 < mean < 1.1), or potently (mean < 0) active on basis of the NCI criteria for the mean of log GI_{50} [23].

3. Results and Discussion

Retention times and UV and MS data analysis of the constituents from the crude EtOH extract (**EE**), MeOH (**MP**) and hexane (**HP**) partition phases, and fractions **F1–F5** are given in Table 1. Twenty substances were detected, mainly quercetin and kaempferol derivatives. **F1, F2,** and **F3** exhibited similar flavonol composition. **F4** contains three major compounds: quercitrin, quercetin 3-*O*-methyl ether, and a kaempferol derivative, while **F5** contains quercetin 3-*O*-methyl ether (Table 1, compound **17**).

Comparison of spectroscopic data with those from the literature [24] allowed the identification of compound **17** as 5,7,3′,4′-tetrahydroxy-3-methoxy-flavonol (quercetin-3-*O*-methyl ether) (Table 1).

Flavonoids found in *Croton* are mostly highly methoxylated aglycones, such as artemetin [3]. It has been reported that several *Croton* species produce acylated flavonoids, such as tiliroside (kaempferol-*p*-coumaroyl glucoside) [25–27]. Rutin (Table 1, compound **7**) was also detected in the MeOH extract from leaves of *C. lechleri* Mull. Arg. [28]; fresh latex of *C. celtidifolius* Baill. has flavonols, such as kaempferol, quercetin, and myricetin in its composition [29]. Savietto et al. [30] detected apigenin dihexoside and tiliroside (kaempferol-*p*-coumaroyl glucoside) as ubiquitous constituents of the MeOH leaf extract of *C. dichrous* Müll. Arg., *C. erythroxyloides* Baill., and *C. myrianthus* Mull. Arg.

C. sphaerogynus was previously described as a major producer of diterpenes. Using serial extraction with hexane,

Table 2: Antiproliferative activity (GI_{50}, μg/mL) of the leaf extract and fractions of *Croton sphaerogynus* on culture cell lines.

Material tested	Cell lines[a]			Mean log GI_{50}[c]
	U251	MCF-7	NCI-H460	
Doxorubicin[b]	<0.025	<0.025	<0.025	–1.60 **P**
EE	23.4	53.4	3.00	1.19 W
MP	8.10	20.0	0.25	0.54 **M**
HP	24.7	27.2	3.80	1.14 W
F1	16.7	20.3	1.20	1.19 W
F2	41.8	61.1	12.3	1.50 W
F3	58.7	47.0	12.4	1.51 I
F4	15.0	8.10	11.8	1.05 **M**
F5	31.6	17.9	21.8	1.36 W

[a]U251: glioma; MCF-7: breast cancer; NCI-H460: nonsmall cell lung.
[b]Positive control. NCI's criteria (Fouche et al., 2008 [23]): I: mean log GI_{50} > 1.5 = inactive; W: weak activity: mean log GI_{50} > 1.1–1.5; M: moderate activity: mean log GI_{50} > 0–1.1; P: potent activity: mean log GI_{50} < 0.
[c]log GI_{50}.
Crude EtOH extract (**EE**); MeOH (**MP**) and hexane (**HP**) phases, and fractions (**F1**, **F2**, **F3**, **F4**, and **F5**).

CH_2Cl_2, and MeOH, Motta et al. [20] identified a great diversity of diterpenes, especially in the CH_2Cl_2 extract. In the present study, maceration with EtOH at room temperature yielded an extract with a diterpene profile similar to that described by Motta et al. [20]. The lyophilized crude ethanol extract was resuspended in MeOH and partitioned with hexane. Partition did not eliminate the diterpenes from the polar fraction **MP**. Column chromatography using Sephadex and MeOH gave five fractions (**F1**–**F5**), the first of which (**F1**) contained diterpenes and flavonoids, while the further fractions (**F2**–**F5**) contained flavonoids exclusively.

Crude EtOH extract(**EE**), hexane phase (**HP**), **F1**, and **F2** showed weak antiproliferative activity (Table 2). Methanol phase (**MP**) and **F4** showed moderate activity, mainly against cell lines NCI-H460 (nonsmall cell lung) (mean log GI_{50} 0.54 and 1.05, resp.). On the other hand, **F3** was inactive, while **F5**, containing virtually only quercetin-3-*O*-methyl ether (Table 1, compound **17**), also showed weak antiproliferative activity (Table 2).

According to Motta et al. [20] the antiproliferative activity of *C. sphaerogynus* extract was a result of the massive presence of abietane and/or podocarpane diterpenes in nonpolar extracts. The present study tested two different sets of samples: extract and phases composed by different proportions of diterpenes and flavonoids (**EE**, **HP**, **MP**,and fraction **F1**) and fractions composed exclusively by flavonoids (**F2**–**F5**). Table 3 compares data obtained by Motta et al. [20] and the diterpene mixture obtained in the present work. According to Motta et al. [20] the CH_2Cl_2 extract showed higher activity (mean log GI_{50} 0.86), compared with hexane and MeOH extracts (mean log GI_{50} 1.26 and 1.49, resp.). Regarding the diterpene profile, the latter extract was the most similar to **MP** and **HP** phases, although some qualitative and quantitative differences are evident. No crotonin derivative was detected in the present study, which may explain the moderate antiproliferative activity of the CH_2CL_2 extract (mean 0.86 log GI_{50}) reported by Motta et al. [20] and the weak antiproliferative activity exerted by **HP**. The CH_2Cl_2 extract from *C. macrobothrys*, which contains a crotonin derivative, showed moderate antiproliferative activity (mean log GI_{50} 0.89) [11]. Grynberg et al. [31] tested *trans*-dehydrocrotonin and *trans*-crotonin isolated from *C. cajucara* Benth. on the survival of mice bearing Sarcoma 180 and Ehrlich carcinoma and observed a significant antitumor activity when mice were treated with *trans*-dehydrocrotonin.

MP phase was the most active sample, showing moderate antiproliferative activity. The relative proportion of diterpenes and flavonoids (Table 4) might be important to enhance the antiproliferative activity. Either extracts with high contents of diterpenes or fractions with high contents of flavonoids presented weak or no antiproliferative activity. **F2**, **F3**, and **F4** (fractions lacking diterpenes) were shown to be inactive. **F1**, though still containing diterpenes, showed flavonols in smaller amount than **MP**; **F5**, composed virtually by quercetin-3-*O*-methyl ether, also showed weak antiproliferative activity. The hexane phase (**HP**) contained no detectable flavonoids. These results suggest that *Croton* species lacking crotonin derivatives might have moderate antiproliferative activity if they have a combination of other diterpenes and flavonols.

Extracts from *Croton* species are frequently reported as exerting antiproliferative activity. The essential oil from the stem bark of *C. lechleri* showed mutagen-protective efficacy [32] and crude extracts from stems of *C. cajucara* [19], containing clerodane diterpenes, exert antitumor activity against the K562 leukemic cell line. The CH_2Cl_2 extract of *C. macrobothrys* leaves, also containing clerodane diterpenes, exhibited moderate antiproliferative activity against several cell lines, in particular NCI-H460 (nonsmall cell lung) and K562 (leukemia) [11].

On the other hand, flavonoids such as apigenin dihexoside and tiliroside (kaempferol-*p*-coumaroyl glucoside) detected in leaf extract of *C. dichrous, C. myrianthus*, and *C. erythroxyloides* showed weak or no growth cell inhibition. However, extracts or fractions with substantial amounts of these compounds showed weak activity [30]. However, MeOH extract from *C. erythroxyloides* obtained under reflux

Table 3: Main constituents of leaf extract and fractions from *Croton sphaerogynus* leaves and respective GC/EIMS data. **EE**: crude EtOH extract; **MP**: methanol phase; **HP**: hexane phase; **F1**: fraction 1. RT: retention time (min); MM: molecular mass; N.I.: not identified.

	RT (min)	MM	Characterization*	Relative amount (%)					
				Dch*	Met*	EE	MP	HP	F1
1	14.8	272	Abieta-8, 11-diene	2.2	2.3	—	—	3.8	—
2	15.2	278	NI			—	0.9	1.6	—
3	16.2	306	NI			—	—	1.3	—
4	16.4	286	Abieta-8,11-dien-3-one	20.2	20.1	36.0	22.3	27.6	23.8
5	16.7	286	Abieta-8,11,13-trien-3-ol	6.2	13.1	5.4	6.5	7.7	7.1
6	16.9	288	Abieta-8,11-dien-3-ol	3.8	16.7	4.6	8.0	3.3	8.9
7	17.2	286	Podocarp-7-en,13-methyl-13-vinyl-3-one	12.9	4.7	11.2	17.9	18.5	17.9
8	17.5	286	NI			2.1	2.5	0.9	2.7
9	17.7	288	NI			0.9	3.8	1.5	4.6
10	18.0	284	NI			3.6	1.7	1.6	1.4
11	18.1	286	NI			—	1.3	1.8	1.6
12	18.2	286	NI			6.7	4.0	3.3	3.4
13	18.6	286	Abieta-8,11,13-trien-12-ol	11.9	18.5	10.3	13.9	21.8	13.5
14	19.2	288	Podocarp-7-en-3-ol, 13-methyl-13-vinyl	4.5		1.6	6.2	4.0	6.0
15	19.3	302	13-hydroxy-abieta-8,11-dien-7-one	4.8		4.2	2.1	—	1.9
16	20.3	300	11-hydroxy-abieta-8,11,13-trien-7-one	3.4		2.2	0.9	—	1.2
17	20.5	302	NI			—	1.2	—	1.3
18	20.6	300	Abieta-6,8,11,13-tetraen-3,12-diol	0.7		10.2	4.8	0.7	4.2
19	21.1	286	NI			—	1.2	—	0.4
20	21.2	302	Abieta-8,11,13-trien-6,14-diol	0.8		0.9	0.9	—	—
21	—	316	Crotonin derivative*	5.2		—	—	—	—
NI				23.4	24.6	8.8	9.7	7.1	7.8

*Main constituents of leaf extract of *Croton sphaerogynus* and respective GC/EIMS data and characterization according to Motta et al. [20]. Dch, CH_2Cl_2; Met, MeOH.

Table 4: Relative amount of major flavonoids in crude EtOH extract (**EE**), MeOH phase (**MP**), and fractions (**F1–F5**) of *C. sphaerogynus*, detected by HPLC-DAD (352 nm).

Constituent*	EE	MP	F1	F2	F3	F4	F5
1	nd	0.10^{Q}	—	0.47^{Q}	—	—	—
2	0.20^{Q}	1.17^{Q}	0.94^{Q}	—	—	—	—
3	nd	—	—	2.23^{K}	3.00^{K}	—	—
4	0.57^{K}	2.45^{K}	2.01^{K}	—	—	—	—
5	1.03^{K}	3.73^{K}	3.04^{K}	—	—	—	—
6	0.09^{Q}	0.35^{Q}	—	4.65^{Q}	5.18^{Q}	—	—
7	0.37^{Q}	1.63^{Q}	0.89^{Q}	19.35^{Q}	8.39^{Q}	—	—
8	0.10^{K}	0.51^{K}	0.50^{K}	—	—	—	—
9	0.09^{Q}	0.48^{Q}	—	0.91^{Q}	6.51^{Q}	8.42^{Q}	—
10	0.18^{K}	0.67^{K}	0.48^{K}	5.5^{K}	1.84^{K}	—	—
11	0.99^{K}	3.04^{K}	2.42^{K}	19.71^{K}	4.42^{K}	—	—
12	nd	—	—	7.47^{Q}	8.39^{Q}	—	—
13	nd	—	—	4.15^{K}	—	—	—
14	0.51^{Q}	3.13^{Q}	—	3.65^{Q}	34.51^{Q}	47.06^{Q}	—
15	nd	—	—	2.54^{K}	7.89^{K}	—	—
16	nd	—	—	2.47^{Q}	3.68^{Q}	nd	—
17	0.59^{Q}	3.26^{Q}	0.13^{Q}	3.06^{Q}	2.16^{Q}	70.96^{Q}	58.31^{Q}
18	nd	—	—	2.94^{K}	1.70^{K}	—	—
19	0.48^{K}	0.97^{K}	—	—	2.13^{K}	29.68^{K}	—
20	nd	—	—	—	2.23^{Q}	nd	—

*Identification suggestions in Table 1.

^{Q}Values expressed as milligram per gram of quercetin equivalent (mg/g QE).

^{K}Values expressed as milligram per gram of kaempferol equivalent (mg/g KE).

nd: trace amounts.

showed moderate antiproliferative activity (mean of log GI_{50} 1.00) [30].

Angst et al. [33] observed that the flavonol quercetin inhibits the growth of pancreatic cancer cell lines by inducing apoptosis. The association of gemcitabine (a standard chemotherapeutic drug administered to patients with pancreatic cancer) and quercetin had no additional effect when compared with quercetin administered alone. The authors also observed a significant apoptotic effect and reduced tumor cell proliferation in *in vivo* assay using quercetin.

Besides synergism, the chemical structure of the flavonoids seems to be directly related to their antiproliferative activity. Burmistrova et al. [34] showed that synthetic flavonols with a hydroxyl group at the C3 position are 7-fold more potent than flavonols with a methoxyl group at the same position. This result suggests that a C3 methoxyl group at C3 is a reducing factor of cytotoxicity. In the present study, quercetin-3-*O*-methyl ether alone showed weak antiproliferative activity (mean of log GI_{50} 1.36). However, according to Seito et al. [35] flavonoids with methoxyl groups at positions other than C3 seem to have inhibitory effect on cell growth.

4. Conclusion

The antiproliferative activity of *Croton sphaerogynus* seems to be related to the presence of diterpenes and flavonoids. MeOH phase (**MP**) presented the highest antiproliferative activity among all samples tested and is showed to be composed by diterpenes and a high amount of flavonoids, in comparison with the crude EtOH extract (**EE**) and **F1**. Fractions containing no diterpenes showed weak antiproliferative activity. Samples containing small proportions of flavonoids also showed weak antiproliferative activity. The relative proportions of representatives of these two metabolite classes (flavonoids and diterpenes) in *C. sphaerogynus* extracts seem to be crucial to determine their antiproliferative activity.

Conflict of Interests

The authors declare that there is no conflict of interests regarding the publication of this paper.

Acknowledgments

The authors thank Fundação de Amparo à Pesquisa do Estado de São Paulo (FAPESP) for financial support (FAPESP 2012/10079-0) and Frederick Cancer Research & Development Center of the National Cancer Institute (Frederick, MA, USA) for the kind provision of cell lines. Antonio Salatino, Cláudia M. Furlan, Deborah Y. A. C. Santos, João E. de Carvalho, João Henrique G. Lago, Marcelo J. Pena Ferreira, and Maria L. F. Salatino are fellow researchers of Conselho Nacional de Desenvolvimento Científico e Tecnológico (CNPq). Kátia Pereira Santos thanks the Coordenação de Aperfeiçoamento de Pessoal de Nível Superior (CAPES) for a Master's research grant.

References

[1] B. W. van Ee, R. Riina, and P. E. Berry, "A revised infrageneric classification and molecular phylogeny of new world *Croton* (Euphorbiaceae)," *Taxon*, vol. 60, no. 3, pp. 791–823, 2011.

[2] I. Cordeiro, R. Secco, D. S. Carneiro-Torres et al., "*Croton* in Lista de Espécies da Flora do Brasil," Jardim Botânico do Rio de Janeiro, 2014, http://floradobrasil.jbrj.gov.br/jabot/listaBrasil/FichaPublicaTaxonUC/FichaPublicaTaxonUC.do?id=FB17497.

[3] A. Salatino, M. L. F. Salatino, and G. Negri, "Traditional uses, chemistry and pharmacology of *Croton* species (Euphorbiaceae)," *Journal of the Brazilian Chemical Society*, vol. 18, no. 1, pp. 11–33, 2007.

[4] P. R. H. Moreno, M. E. L. Lima, M. B. R. Caruzo, D. S. C. Torres, I. Cordeiro, and M. C. M. Young, "Chemical composition and antimicrobial activity of the essential oil from *Croton heterocalyx* Baill. (Euphorbiaceaes) leaves," *Journal of Essential Oil Research*, vol. 21, no. 2, pp. 190–192, 2009.

[5] F. F. Perazzo, J. C. T. Carvalho, M. Rodrigues, E. K. L. Morais, and M. A. M. Maciel, "Comparative anti-inflammatory and antinociceptive effects of terpenoids and an aqueous extract obtained from *Croton cajucara* Benth," *Brazilian Journal of Pharmacognosy*, vol. 17, no. 4, pp. 521–528, 2007.

[6] World Health Organization, *World Cancer Report*, International Agency for Research on Cancer, Lyon, France, 2009.

[7] Instituto Nacional de Câncer, *Estimativa 2014: incidência de câncer no Brasil*, INCA, 2014, http://www.inca.gov.br/estimativa/2014/estimativa-24042014.pdf.

[8] G. M. Cragg and D. J. Newman, "Nature: a vital source of leads for anticancer drug development," *Phytochemistry Reviews*, vol. 8, no. 2, pp. 313–331, 2009.

[9] R. Gupta, B. Gabrielsen, and S. M. Ferguson, "Nature's medicines: traditional knowledge and intellectual property management. Case studies from the National Institutes of Health (NIH), USA," *Current Drug Discovery Technologies*, vol. 2, no. 4, pp. 203–219, 2005.

[10] C. A. N. Catalán, C. S. de Heluani, C. Kotowicz, T. E. Gedris, and W. Herz, "A linear sesterterpene, two squalene derivatives and two peptide derivatives from *Croton hieronymi*," *Phytochemistry*, vol. 64, no. 2, pp. 625–629, 2003.

[11] L. B. Motta, C. M. Furlan, D. Y. A. C. Santos et al., "Constituents and antiproliferative activity of extracts from leaves of *Croton macrobothrys*," *Brazilian Journal of Pharmacognosy*, vol. 21, no. 6, pp. 972–977, 2011.

[12] S. Block, C. Stévigny, M.-C. de Pauw-Gillet et al., "ent-trachyloban-3beta-ol, a new cytotoxic diterpene from *Croton zambesicus*," *Planta Medica*, vol. 68, no. 7, pp. 647–649, 2002.

[13] P. T. Thuong, N. M. Khoi, S. Ohta et al., "ent-kaurane diterpenoids from *Croton tonkinensis* induce apoptosis in colorectal cancer cells through the phosphorylation of JNK mediated by reactive oxygen species and dual-specificity JNK kinase MKK4," *Anti-Cancer Agents in Medicinal Chemistry*, vol. 14, no. 7, pp. 1051–1061, 2014.

[14] P. K. S. Uchôa, J. N. da Silva Jr., E. R. Silveira et al., "Trachylobane and kaurane diterpenes from *Croton floribundus* spreng," *Quimica Nova*, vol. 36, no. 6, pp. 778–782, 2013.

[15] S. Block, C. Baccelli, B. Tinant et al., "Diterpenes from the leaves of *Croton zambesicus*," *Phytochemistry*, vol. 65, no. 8, pp. 1165–1171, 2004.

[16] V. C. Fernandes, S. I. V. Pereira, J. Coppede et al., "The epimer of kaurenoic acid from *Croton antisyphiliticus* is cytotoxic toward

B-16 and HeLa tumor cells through apoptosis induction," *Genetics and Molecular Research*, vol. 12, no. 2, pp. 1005–1011, 2013.

[17] B. C. Cavalcanti, D. P. Bezerra, H. I. F. Magalhães et al., "Kauren-19-oic acid induces DNA damage followed by apoptosis in human leukemia cells," *Journal of Applied Toxicology*, vol. 29, no. 7, pp. 560–568, 2009.

[18] E. Mongelli, A. B. Pomilio, J. B. Sánchez, F. M. Guerra, and G. M. Massanet, "ent-Kaur-16-en-19-oic acid, a KB cells cytotoxic diterpenoid from *Elaeoselinum foetidum*," *Phytotherapy Research*, vol. 16, no. 4, pp. 387–388, 2002.

[19] M. A. M. Maciel, J. R. Martins, A. C. Pinto, C. R. Kaiser, A. Esteves-Souza, and A. Echevarria, "Natural and semi-synthetic clerodanes of *Croton cajucara* and their cytotoxic effects against ehrlich carcinoma and human K562 leukemia cells," *Journal of the Brazilian Chemical Society*, vol. 18, no. 2, pp. 391–396, 2007.

[20] L. B. Motta, C. M. Furlan, D. Y. A. C. Santos et al., "Antiproliferative activity and constituents of leaf extracts of *Croton sphaerogynus* Baill. (Euphorbiaceae)," *Industrial Crops and Products*, vol. 50, pp. 661–665, 2013.

[21] A. Monks, D. Scudiero, P. Skehan et al., "Feasibility of a high-flux anticancer drug screen using a diverse panel of cultured human tumor cell lines," *Journal of the National Cancer Institute*, vol. 83, no. 11, pp. 757–766, 1991.

[22] R. H. Shoemaker, "The NCI60 human tumour cell line anticancer drug screen," *Nature Reviews Cancer*, vol. 6, no. 10, pp. 813–823, 2006.

[23] G. Fouche, G. M. Cragg, P. Pillay, N. Kolesnikova, V. J. Maharaj, and J. Senabe, "In vitro anticancer screening of South African plants," *Journal of Ethnopharmacology*, vol. 119, no. 3, pp. 455–461, 2008.

[24] L. Krenn, A. Miron, E. Pemp, U. Petr, and B. Kopp, "Flavonoids from *Achillea nobilis* L.," *Verlag der Zeitschrift für Naturforschung: Section C*, vol. 58, no. 1-2, pp. 11–16, 2003.

[25] L. M. M. Matos, *Química de espécies nativas de Croton L. (Euphorbiaceae) [M.S. dissertation]*, Instituto de Biociências, Universidade de São Paulo, 2011.

[26] N. R. Athayde, *Perfil químico e atividades biológicas de Croton echinocarpus Baill. e Croton vulnerarius Müll. Arg. [Dissertação de Mestrado]*, Instituto de Biociências, Universidade de São Paulo, 2013.

[27] C. M. Furlan, K. P. Santos, M. D. Sedano et al., "Flavonoids and antioxidant potential of nine Argentinian species of *Croton* (Euphorbiaceae)," *Brazilian Journal of Botany*. In press.

[28] A. J. Alonso-Castro, E. Ortiz-Sánchez, F. Domínguez et al., "Antitumor effect of *Croton lechleri* Mull. Arg. (Euphorbiaceae)," *Journal of Ethnopharmacology*, vol. 140, no. 2, pp. 438–442, 2012.

[29] F. Biscaro, E. B. Parisotto, V. C. Zanette et al., "Anticancer activity of flavonol and flavan-3-ol rich extracts from *Croton celtidifolius* latex," *Pharmaceutical Biology*, vol. 51, no. 6, pp. 737–743, 2013.

[30] J. P. Savietto, C. M. Furlan, L. B. Motta et al., "Antiproliferative activity of methanol extracts of four species of *Croton* on different human cell lines," *Revista Brasileira de Farmacognosia*, vol. 23, no. 4, pp. 662–667, 2013.

[31] N. F. Grynberg, A. Echevarria, J. E. Lima, S. S. R. Pamplona, A. C. Pinto, and M. A. M. Maciel, "Anti-tumour activity of two 19-nor-clerodane diterpenes, trans- dehydrocrotonin and trans-crotonin, from *Croton cajucara*," *Planta Medica*, vol. 65, no. 8, pp. 687–689, 1999.

[32] D. Rossi, A. Guerrini, G. Paganetto et al., "*Croton lechleri* Müll. Arg. (Euphorbiaceae) stem bark essential oil as possible mutagen-protective food ingredient against heterocyclic amines from cooked food," *Food Chemistry*, vol. 139, no. 1–4, pp. 439–447, 2013.

[33] E. Angst, J. L. Park, A. Moro et al., "The flavonoid quercetin inhibits pancreatic cancer growth in vitro and *in vivo*," *Pancreas*, vol. 42, no. 2, pp. 223–229, 2013.

[34] O. Burmistrova, M. T. Marrero, S. Estévez et al., "Synthesis and effects on cell viability of flavonols and 3-methyl ether derivatives on human leukemia cells," *European Journal of Medicinal Chemistry*, vol. 84, pp. 30–41, 2014.

[35] L. N. Seito, A. L. T. G. Ruiz, D. Vendramini-Costa et al., "Antiproliferative activity of three methoxylated flavonoids isolated from *Zeyheria montana* mart. (Bignoniaceae) leaves," *Phytotherapy Research*, vol. 25, no. 10, pp. 1447–1450, 2011.

Hindawi Publishing Corporation
BioMed Research International
Volume 2015, Article ID 968981, 11 pages
http://dx.doi.org/10.1155/2015/968981

Research Article

Curcumin and Its Analogue Induce Apoptosis in Leukemia Cells and Have Additive Effects with Bortezomib in Cellular and Xenograft Models

L. I. Nagy,[1] L. Z. Fehér,[1] G. J. Szebeni,[1] M. Gyuris,[1] P. Sipos,[2] R. Alföldi,[1] B. Ózsvári,[1] L. Hackler Jr.,[1] A. Balázs,[1] P. Batár,[3] I. Kanizsai,[1] and L. G. Puskás[1,4]

[1] *AVIDIN Ltd., Alsókikötő Sor 11, Szeged, Hungary*
[2] *Department of Pharmaceutical Technology, University of Szeged, Eötvös u 6, Szeged 6720, Hungary*
[3] *Department of Hematology, Institute of Internal Medicine, University of Debrecen, Nagyerdei Körút 98, Debrecen 4032, Hungary*
[4] *Institute of Genetics, Biological Research Center of the Hungarian Academy of Sciences, Temesvári Körút 62, Szeged 6726, Hungary*

Correspondence should be addressed to L. G. Puskás; laszlo@avidinbiotech.com

Received 26 February 2015; Accepted 4 March 2015

Academic Editor: Walter Jaeger

Combination therapy of bortezomib with other chemotherapeutics is an emerging treatment strategy. Since both curcumin and bortezomib inhibit NF-κB, we tested the effects of their combination on leukemia cells. To improve potency, a novel Mannich-type curcumin derivative, C-150, was synthesized. Curcumin and its analogue showed potent antiproliferative and apoptotic effects on the human leukemia cell line, HL60, with different potency but similar additive properties with bortezomib. Additive antiproliferative effects were correlated well with LPS-induced NF-κB inhibition results. Gene expression data on cell cycle and apoptosis related genes, obtained by high-throughput QPCR, showed that curcumin and its analogue act through similar signaling pathways. In correlation with in vitro results similar additive effect could be obsereved in SCID mice inoculated systemically with HL60 cells. C-150 in a liposomal formulation given intravenously in combination with bortezomib was more efficient than either of the drugs alone. As our novel curcumin analogue exerted anticancer effects in leukemic cells at submicromolar concentration in vitro and at 3 mg/kg dose in vivo, which was potentiated by bortezomib, it holds a great promise as a future therapeutic agent in the treatment of leukemia alone or in combination.

1. Introduction

Curcumin, also known as diferuloyl methane, a natural component of the rhizome of *Curcuma longa* has emerged as one of the most powerful chemopreventive and anticancer agents. It has been reported to exert anti-inflammatory, antiangiogenic, and antiproliferative activity in various types of cancer [1–3]. It has also been shown that curcumin elevates intracellular ROS and induces loss of mitochondrial membrane potential and apoptosis in leukemia cells [4, 5]. In concert with these observations, the potent antileukemic action of curcumin and some of its derivatives have been reviewed recently [6]. This natural compound not only can be used as chemotherapeutics but also was suggested for chemoprevention [6].

A variety of molecular mechanisms have been proposed to mediate anticancer effects of curcumin, but its ability to inhibit the growth of various types of cancer cells at various stages of cancer progression is probably due to its potential to act on multiple targets [7–9]. Among others, it acts as a scavenger of free radicals [10], inhibits NF-κB activation [11], and modulates histone deacetylase (HDAC) and histone acetyltransferase (HAT) enzyme activities [12, 13] and DNA methyltransferase 1 [10]. The main underlying action mechanisms of curcumin are probably based on the modulation of multiple important cellular signaling pathways including NF-κB, TRAIL, PI3K/Akt, JAK/STAT, Notch-1, and JNK [5, 14].

Several preclinical and clinical studies suggest that curcumin may represent a novel strategy to treat cancer patients

alone or in combination with already existing therapeutic regimens [2, 15]. However, the in vivo application of curcumin has been limited for its low potency and unsatisfactory bioavailability [16], which necessitates the application of new formulation solutions and the synthesis of novel curcumin analogues with improved pharmacological properties, while retaining a similar safety profile.

Different synthetic concepts have been therefore developed to expand the molecular diversity, from the side-chain and diketone transformations to alkyl and alkenyl functionalizations on C-4 in the central position or with different substituents at the 4 positions of the phenyl group of curcumin [17–20]. Here, we report the application of a novel Mannich-type curcumin derivative, C-150, possessing metahydroxyphenyl side-chains and 3-phenyl-3-acrylamido branched central motif. The new analogue is one of the most potent members of the synthesized analogues [21].

Previous reports demonstrated that bortezomib (Velcade, formerly known as PS-341), a potent and selective proteasome inhibitor approved by the FDA for the treatment of patients with multiple myeloma, is able to block chemotherapy-induced NF-κB activation and augment the apoptotic response to chemotherapeutic agents [22].

NF-κB signaling plays a critical role in cancer development and progression; constitutive activation of NF-κB pathway has been reported in different types of cancer, including multiple myeloma and acute myeloid leukemias [23, 24]. After stimulation and activation of the canonical NF-κB pathway in noncancer cells, IκB is phosphorylated by IKK then degradated by the 26S proteasome allowing the nuclear transport of NF-κB. Since IκB is a substrate of the proteasome, the initial rationale for use of bortezomib in multiple myeloma was inhibition of NF-κB activity and inhibition of cell proliferation and survival [25, 26].

Beside the canonical pathway, several studies show a critical role for the noncanonical NF-κB pathway in cancer pathogenesis as well. Hideshima et al. found that bortezomib could inhibit the noncanonical pathway via inhibition of conversion of p100 to p52 and its nuclear translocation in multiple myeloma cells [27].

It has been shown that bortezomib possesses in vitro and in vivo activity against a variety of malignancies, including acute and chronic lymphocytic leukemia, prostate cancer, pancreatic cancer, and colon cancer [22]. Combination therapy of bortezomib with other chemotherapeutical agents is an emerging treatment strategy not only in myeloma but also in leukemia [28]. Since both curcumin and bortezomib inhibit NF-κB, we hypothesized their additive anticancer effects on leukemia cells.

Several studies reported enhanced cytotoxicity of bortezomib in multiple myeloma cells when combined with curcumin or its analogues both in vitro and in vivo [28–31]. In multiple myeloma cells, the combined treatment inactivated NF-κB while it activated JNK signaling [31], but no information has been available on leukemia cells.

In this report, we studied curcumin and a novel Mannich-type curcumin analogue C-150 alone and in combination with bortezomib. Effects of cotreatment were studied on cytotoxicity, NF-κB inhibition, gene expression, and in an in vivo mouse model.

2. Materials and Methods

2.1. Cell Culturing. Human leukemia cells (HL60) were obtained from ATCC, USA. Cells were cultured at 37°C under 5% CO_2 and 100% humidity in LeviTubes designed for use in the bench top bioreactor-incubator hybrid BioLevitator (Hamilton, Hungary). During cultivation, cells were proliferated in suspension with rotation without the use of microcarriers. Rotation period was 2 seconds with 1 second pause at 65 rpm. LeviTubes were filled with 40 mL RPMI cell culture medium containing 10% fetal bovine serum, 1x GlutaMAX, and penicillin-streptomycin antibiotics (Life Technologies, Hungary). Culture medium was changed after 48 hours by removing half of the volume of the culture medium and replacing it with fresh medium.

2.2. Cell Viability Measurements. Viability of HL60 human leukemia cells was determined by the colorimetric MTS assay (CellTiter 96 AQueous Assay, Promega, Madison, WI) and by the CellTiter-Glo luminescent cell viability assay (Promega, Madison, WI). The cells were seeded into 96-well plates at 7000 cells/well density and cultured overnight before treatment. Effects of curcumin (5, 10, 25, and 50 μM), C-150 (50, 100, and 500 nM and 1 μM), bortezomib (0.78, 3.125, 12.5, and 50 nM), and their combinations were recorded 48 hours after treatment. MTS reagent (3-(4,5-dimethylthiazol-2-yl)-5-(3-carboxymethoxy-phenyl)-2-(4-sulfophenyl)-2H-tetrazo-lium) or CellTiter-Glo reagent was applied to drug treated and control (0.2% DMSO) cells according to the manufacturer's protocol. Absorbance (at 490 nm) and luminescence were recorded on a multimode microplate reader (Victor, Perkin Elmer).

Viability was calculated with relation to untreated control cells from three parallel measurements for all conditions. For statistical significance, two-tailed Student's t-test was used.

2.3. Measurements of NF-κB Inhibition. Mouse B16 melanoma cell line was obtained from ATCC, USA. Cells were cultured in RPMI medium (Life Technologies, Hungary) supplemented with 10% FCS (Life Technologies, Hungary). NF-κB reporter cell lines were created by transfection with the pNF-κB-Luc/neo reporter construct with the Lipofectamine 2000 reagent (Invitrogen) and stable cell lines were selected by G418 (Sigma) treatment.

B16/NF-κB-Luc cells (6×10^4 cells/well) were grown on luminoplates (Corning Life Sciences, Kentucky, USA) overnight under standard cell culturing conditions. Before treatment with curcumin (5, 10, 25, and 50 μM), C-150 (50, 100, and 500 nM and 1 μM), bortezomib (0.78, 3.125, 12.5, and 50 nM) and their combinations, the NF-κB-Luc reporter gene was induced by adding LPS (500 ng/mL) into the cell culture media (500 ng/mL). After 6 hours of incubation with curcumin, C-150, bortezomib, or their combinations, the medium was removed; cells were washed and lysed for 10 min at room temperature in cell culture lysis reagent (20 μL/well;

Promega). Substrate was added (20 μL/well; Promega), and luciferase activity was measured in a microplate reader (Victor, Perkin Elmer). NF-κB inhibition was calculated with relation to untreated control cells from three parallel measurements for all conditions.

2.4. FACS Analysis. HL60 cells (10^5) were plated in 24-well tissue culture plates (Corning Life Sciences). Cells were treated with curcumin (25 μM), C-150 (300 and 600 nM), bortezomib (20 nM), and their combinations in triplicates. After 48 hours, cells were collected and resuspended in annexin V binding buffer (0.01 M HEPES, 0.14 M NaCl, and 2.5 mM $CaCl_2$). Annexin V-Alexa 488 (Life Technologies, 2.5 : 100) and propidium iodide (PI) (Sigma-Aldrich, 10 μg/mL) were added to the cells and placed for 15 min in dark at room temperature. After washing, the cells were analyzed on the FACSCalibur cytofluorimeter (Becton Dickinson). Percentage of FL1 (annexin V-Alexa 488) positive and FL3 (propidium iodide) negative early apoptotic cells and FL1 (annexin V-Alexa 488) positive and FL3 (propidium iodide) positive late apoptotic cells was determined. For statistical significance, two-tailed Student's t-test was used.

2.5. Gene Expression Analysis by High-Throughput QPCR. HL60 leukemia cells (10^6) were plated on 10 cm^2 tissue culture plates (Corning Life Sciences). Cells were treated with curcumin, C-150, bortezomib, and their combinations. 48 h after treatment, cells were collected and centrifuged (3000 rpm, 5 min) and total RNA was purified from treated and control (0.2% DMSO) cells using AccuPrep Viral RNA Extraction kit (Bioneer Corp., Korea) with a modified protocol as described earlier [32]. Briefly, cells were lysed with RA1 lysis buffer (Macherey-Nagel, Düren, Germany) and applied to the Viral RNA Extraction binding tube and then washed and eluted with the protocol recommended by the manufacturer. The quantity of total RNA was measured by NanoDrop 1000 spectrophotometer. 6 μg total RNA was converted into cDNA with the High-Capacity cDNA Archive Kit (Applied Biosystems, Foster City, CA) in a total volume of 60 μL.

Identical reaction volumes were prepared by the Agilent Bravo Liquid handling Platform (Agilent Technologies) in a 16 × 96-well design according to Agilent and Roche's recommendations. Each 2 μL reaction mixture contained 6 ng cDNA, 10 pmole gene specific primers, and 1 μL 2x LightCycler1536 Probes Master (Roche). The following amplification protocol was used: 95°C for 1 minute (activation), 60 cycles of 95°C for 10 seconds, and 60°C for 10 seconds, followed by 40°C for 10 second final cooling. Amplification was performed on the LightCycler 1536 System (Roche Applied Science) using the real-time ready human cell cycle regulation panel and the real-time ready human apoptosis panel (Roche Applied Science). Each panel consists of 84 cell cycles and apoptosis related assays along with seven human reference genes (ACTB, β2M, GAPDH, HPRT1, RPL13A, 18S, and YWHAZ).

Data was collected and processed using the LightCycler 1536 SW 1.0 software. Curves were analyzed by using dynamic tube and slope correction methods. Relative expression of the analyzed genes was normalized to the mean value of the reference genes.

2.6. Liposome Formulation of C-150. Liquid phase C-150 containing liposomes was produced by dissolving lipid powder of CHOL/PC/DSPE-mPEG (62/28/0.6 mol%) and C-150 (9.2 mol%) in ethanol. The solution was transferred to a rotary evaporator and dried overnight in vacuum. The lipid film was hydrated and redispersed in PBS solution to a final C-150 concentration of 0.5 mM for 25 min over the phase transition temperature of the organic components. The dispersion was subjected to size extrusion (0.45 μm pore size) and finally filtered through sterile filters (0.22 μm pore size). After preparation, droplet size and polydispersity index of the liposomes were determined. The droplet size, SSA, and PDI of liposomes were measured by laser diffractometry ($n = 5$) by the wet method. The d0.1, d0.5 as median and d0.9 droplet size values, SSA, and PDI values were 75±19 nm, 114±20 nm, 178 ± 24 nm, 54.5 m^2/g, and 0.901 ± 0.20, respectively.

2.7. In Vivo Effects of C-150 and Bortezomib in a Xenograft Model. 8-week-old male NOD CB17-Prkdc^{scid}/NcrCrl mice (Charles River, Innovo Kft., Hungary) were used. The animals were kept in individual ventilated cages to avoid any infection. All mice were fed a commercial sterile diet and water ad libitum and were housed in an animal facility under a 12 h light/dark cycle at constant temperature and humidity.

For the induction of rodent model of human leukemia 10^6 HL60, human leukemia cells were injected in 100 μL volume intravenously. 3 days after cancer cell inoculation mice were randomized and treated 5 times a week for 2 weeks.

Four different groups, each containing 8 mice, were studied: PBS control, bortezomib (0.15 mg/kg), C-150 (3 mg/kg), and C-150 (3 mg/kg) + bortezomib (0.15 mg/kg). All animals were treated moribund and were euthanized at the observation of the first sign of torment. The study was performed according to the Institutional and National Animal Experimentation and Ethics Guidelines in possession of an ethical clearance (XXIX./3610/2012).

2.8. Statistical Analysis. All data presented are means ± standard deviation (SD) as indicated in the text. The statistical comparisons were performed by two-tailed Student's t-test using Microsoft Excel. In all statistical comparisons, a probability (P) value of less than 0.05 was considered significant.

3. Results and Discussion

3.1. In Vitro Effect of Curcumin and Its Analogue Alone and in Combination with Bortezomib. We have utilised two common viability assays to assess the cytotoxic effects of curcumin and the novel analogue C-150 on HL60 cells. Combinations of curcumin or C-150 with bortezomib were also investigated. The colorimetric MTS assay and the luminescence based CellTiter-Glo (CTG) assay yielded comparable results; however, additive effects could be registered at different concentrations (Tables 1 and 2). We found that the CellTiter-Glo assay resulted in additive effects at lower

Table 1: Cell viability measurements (MTS) of curcumin (C), C-150, and bortezomib (BTZ) alone and combined. Curcumin and its analogue C-150 and bortezomib significantly decreased the cell viability of HL-60 human leukemia cells in a dose-dependent manner. C-150 exhibited dose-dependent effect on HL60 cells in submicromolar concentrations and was effective at 27 times lower concentration than curcumin. Both curcumin and its analogue exhibited additive effects with bortezomib (bold data with significant values) (P_1: bortezomib versus combination; P_2: curcumin or C-150 versus combination; two-tailed Student's t-test).

	—	BTZ (50 nM)	BTZ (12.5 nM)	BTZ (3.125 nM)	BTZ (0.78 nM)
—		0.35	0.45	1.26	1.34
C (50 μM)	0.34	0.33	0.35	0.39	0.37
C (25 μM)	0.26	0.23	0.31	0.28	0.27
C (10 μM)	0.48	**0.28 ($P_1 < 0.05, P_2 < 0.01$)**	**0.31 ($P_1 < 0.05, P_2 < 0.01$)**	0.42	0.60
C (5 μM)	1.10	0.33	0.43	1.21	1.26
C-150 (1 μM)	0.25	0.21	**0.19 ($P_1 < 0.01, P_2 < 0.05$)**	0.23	0.25
C-150 (0.5 μM)	0.40	**0.26 ($P_1, P_2 < 0.01$)**	0.27	**0.27 ($P_1 < 0.01, P_2 < 0.05$)**	0.33
C-150 (0.1 μM)	0.94	0.25	0.41	0.83	1.02
C-150 (0.05 μM)	1.16	0.32	0.39	1.13	1.22

Table 2: Cell viability measurements of curcumin (C), C-150, and bortezomib (BTZ) alone and in combination with CellTiter-Glo assay. Curcumin and its analogue C-150 significantly potentiated the effect of bortezomib (P_1: bortezomib versus combination; P_2: curcumin or C-150 versus combination; two-tailed Student's t-test).

	—	BTZ (50 nM)	BTZ (12.5 nM)	BTZ (3.125 nM)	BTZ (0.78 nM)
—		0.11	0.16	0.91	0.94
C (50 μM)	0.12	0.11	0.12	0.12	0.11
C (25 μM)	0.17	0.15	0.13	**0.13 ($P_1 < 0.01, P_2 < 0.05$)**	**0.13 ($P_1 < 0.01, P_2 < 0.05$)**
C (10 μM)	0.99	0.11	0.15	0.52 **($P_1, P_2 < 0.01$)**	0.87
C (5 μM)	1.08	0.11	0.17	0.79	1.05
C-150 (1 μM)	0.09	0.10	**0.10 ($P_1 < 0.01, P_2 < 0.05$)**	0.08	0.08
C-150 (0.5 μM)	0.16	0.10	0.10	0.12	0.16
C-150 (0.1 μM)	0.99	**0.08 ($P_1 < 0.05, P_2 < 0.01$)**	0.12 **($P_1 < 0.05, P_2 < 0.01$)**	**0.58 ($P_1, P_2 < 0.01$)**	0.90
C-150 (0.05 μM)	0.93	0.10	0.15	**0.69 ($P_1 < 0.01, P_2 < 0.05$)**	1.02

concentrations both in case of curcumin and C-150, which can be explained by the difference in sensitivity of the two assays. While MTS assay measures the activity of NAD(P)H-dependent cellular oxidoreductase enzymes of the mitochondria, the CellTiter-Glo assay detects cellular ATP content.

We found that curcumin had a dose-dependent cytotoxic effect on HL60 cells (MTS IC_{50} = 8.21 μM CTG: IC_{50} = 16.77 μM). C-150 also exhibited a dose-dependent effect on HL60 cells but with 27–60-fold higher potency than curcumin (MTS IC_{50} = 0.30 μM, CTG IC_{50} = 0.27 μM). In the combination experiments, bortezomib was used at nanomolar concentrations and the determined IC_{50} value of bortezomib alone was 6.56 and 6.90 nM in the MTS and the CTG assays, respectively.

At the highest applied concentrations, both curcumin and bortezomib alone produced robust cell death, which could not be further enhanced by the combined treatment. At the lowest applied concentration, both curcumin and bortezomib showed no cytotoxic effect neither alone nor in combination. Interestingly, only the CTG assay detected appreciable and statistically significant additive effects. Viability dramatically decreased after combination of 10 μM curcumin and 3.125 nM bortezomib, by 47 and 39% compared to curcumin or bortezomib alone. Similarly, combination of 5 μM curcumin and 3.125 nM bortezomib also decreased viability compared to either of the compounds alone (see Table 2).

Combination of C-150 and bortezomib also showed additive effects. Both methods detected a statistically significant

Table 3: In vitro effect of curcumin and C-150 on NF-κB signaling. Curcumin and its analogue C-150 alone or in coadministration with bortezomib decreased the activation of NF-κB pathway in a dose-dependent manner. Modest significant additive effect was recorded after coadministration of C-150 with bortezomib (P_1: bortezomib versus combination; P_2: curcumin or C-150 versus combination; two-tailed Student's t-test).

	—	BTZ (50 nM)	BTZ (12.5 nM)	BTZ (3.125 nM)	BTZ (0.78 nM)
—		0.36	0.44	0.54	0.94
C (50 μM)	0.19	0.20	0.22	0.28	0.28
C (25 μM)	0.20	0.24	0.31	0.44	0.34
C (10 μM)	0.43	0.32	0.25	0.47	0.54
C (5 μM)	1.05	0.54	0.61	0.64	0.94
C-150 (1 μM)	0.58	0.37	0.41	**0.44** ($\mathbf{P_1 < 0.01, P_2 < 0.05}$)	0.65
C-150 (0.5 μM)	0.82	0.36	0.50	0.56	0.72
C-150 (0.1 μM)	1.17	**0.32** ($\mathbf{P_1 < 0.05, P_2 < 0.01}$)	0.54	0.58	**0.79** ($\mathbf{P_1 < 0.05, P_2 < 0.01}$)
C-150 (0.05 μM)	0.99	0.38	0.54	**0.49** ($\mathbf{P_1, P_2 < 0.01}$)	0.95

decrease in viability following the combination of 0.1 μM of C-150 and 3.125 nM of bortezomib. Again, more dramatic changes were detected by the CTG assay than MTS.

In conclusion, cytotoxic effects of curcumin and its analogue were detected by two cell viability measurements. Furthermore, we showed that both curcumin and C-150 additively potentiated the effect of bortezomib.

3.2. In Vitro Effects on the NF-κB Pathway. In the same concentration ranges as in the viability tests, we determined the effect of curcumin, C-150, and bortezomib on NF-κB induction inhibition. All three compounds decreased the activation of NF-κB markedly in a dose-dependent manner. IC_{50} values were 9.6 μM for curcumin, 0.8 μM for C-150, and 2.0 nM for bortezomib. Significant additive effects could not be recorded for curcumin and bortezomib while, in case of C-150, a modest additive effect was found in some concentration combinations (Table 3).

Several studies show a critical role for the NF-κB pathway in multiple myeloma and leukemia pathogenesis as well [23, 24]. Hideshima et al. found that bortezomib triggers the canonical pathway of NF-κB and downregulates IκBα in primary cells from patients with MM. However, they also found that bortezomib could inhibit the noncanonical pathway via inhibition of conversion of p100 to p52 and its nuclear translocation in MM.1S cells [27]. It was also shown that the main underlying mechanisms of action of curcumin were probably based on the modulation of multiple important cellular signaling pathways including NF-κB [5, 14]. Here, we demonstrated that both types of anticancer agents inhibited NF-κB induction and curcumin and C-150, in concordance with their additive cytotoxic potential confirmed by our in vitro studies, which potentiated the effects of bortezomib.

3.3. Apoptosis Detection. Using FACS analysis and annexin V and PI staining, the percentage of cells in early or late apoptosis was determined.

Two doses of curcumin (15 and 25 μM) and C-150 (0.3 and 0.6 μM) were applied. Bortezomib was applied at 20 nM concentration. Both curcumin and C-150 at their higher concentration induced 100% and 70% programmed cell death, respectively. No additive effect could be observed when bortezomib was coadministered (Table 4).

At the lower curcumin concentration (15 μM), we could detect a statistically significant additive effect between curcumin and bortezomib (Figure 1(a)). C-150 at 0.3 μM (50 times lower concentration) possessed a similar apoptotic effect compared to curcumin at 15 μM (Figure 1(b)). Coadministration of bortezomib also showed a significant additive effect (Figure 1(b)) with 0.3 μM C-150.

From these results, we can conclude that the novel curcumin analogue induced a similar level of apoptosis at 50-fold lower concentration than curcumin, while retaining the ability to potentiate the effect of bortezomib. In addition, we found that both curcumin and C-150 induced apoptosis and not necrosis, since the only propidium iodide positive population did not change (data not shown).

3.4. Analysis of Apoptosis and Cell Cycle Related Gene Expression Affected by Combination Treatments. We have analysed the effects of curcumin on the expression of apoptosis and cell cycle related genes using high-throughput QPCR. Figure 2 depicts the hierarchical cluster analysis of the obtained gene expression patterns. Previous studies highlighted that treatment with curcumin and bortezomib activated JNK signaling in multiple myeloma cells [33]. In agreement with that, we observed increased expression of JUN (jun protooncogene), a target of JNK (MAPK8, mitogen-activated protein kinase 8), following both curcumin and bortezomib treatment, and this overexpression was enhanced by their combined use. A negatively regulated target of JNK signaling BCL2 (B-cell CLL/lymphoma 2) was also affected; it was downregulated by curcumin and bortezomib and by their combination. Here, a significant additive effect was also observed. (b), (c), (d),

Table 4: Summary of FACS analysis. Percentage of cells in early and late stages of apoptosis and total apoptotic cells as determined by annexin V and PI staining. The curcumin analogue C-150 induced a similar rate of apoptosis at 50-fold lower concentration than curcumin. Furthermore, it retained the ability to potentiate the effect of bortezomib.

	Early apoptotic cells Annexin V+/PI−		Late apoptotic cells Annexin V+/PI+		Total apoptotic cells	
	%	+/−	%	+/−	%	+/−
Control	4.5	0.5	3.4	0.6	7.9	1.1
BTZ 20 nM	21.4	0.4	16.5	4.2	37.9	4.6
C 15 μM	18.6	0.8	21.9	4.2	40.5	5.0
C 15 μM + BTZ 20 nM	21.3	1.3	29.1	1.6	50.4	2.9
C 25 μM	45.6	5.0	54.1	4.9	99.6	9.9
C 25 μM + BTZ 20 nM	53.3	8.0	46.5	7.9	99.7	15.9
C-150 0.3 μM	23.8	4.1	7.0	2.7	30.8	6.9
C-150 0.3 μM + BTZ 20 nM	25.4	0.1	21.4	4.4	46.9	4.5
C-150 0.6 μM	24.5	1.0	45.9	3.9	70.4	4.9
C-150 0.6 μM + BTZ 20 nM	24.2	2.0	45.7	3.2	69.8	5.3

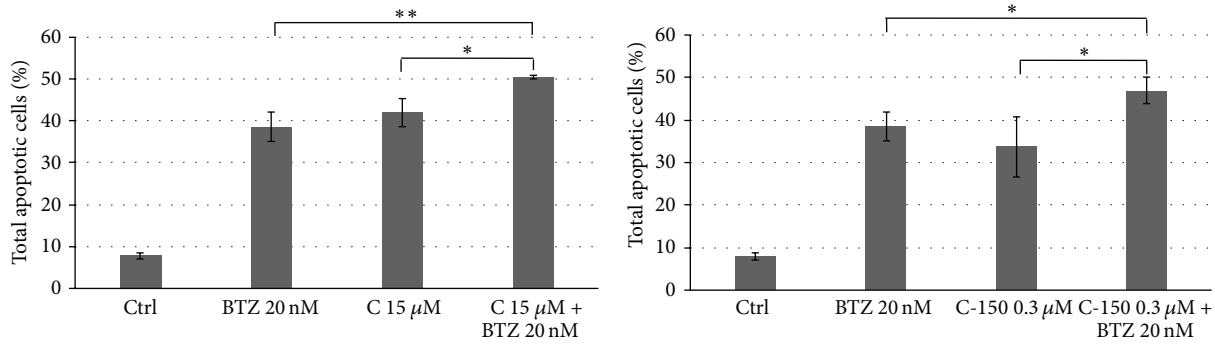

Figure 1: Effect of curcumin (C) or C-150 treatments alone or in combination with bortezomib (BTZ) on cell viability. C-150 (0.3 μM) could potentiate the cytotoxic effect of 20 nM bortezomib at 50-fold lower concentration than curcumin (15 μM). Data represent total apoptotic cells ($^{*}P \leq 0.05$; $^{**}P \leq 0.01$, two-tailed Student's t-test).

(e), (f), and (g) panels of Figure 2 depict representative genes of the identified clusters. Panel (b) contains genes that were activated by both curcumin and bortezomib with additive effects following the combined treatment. Panels (c) and (d) contain genes that were markedly downregulated: by all treatments (Panel (c)) or by only the combined treatment (Panel (d)). Panels (e), (f), and (g) plot those genes that were upregulated following combined treatment, suggesting a role in the observed additive effects between curcumin and bortezomib.

We can conclude that both apoptosis and cell cycle related genes were differentially expressed by curcumin and by its combination with bortezomib.

We have also investigated the effects of the novel analogue C-150 alone and in combination on genes related to apoptosis and cell cycle. Figure 3 summarizes the results of hierarchical cluster analysis and highlights representative genes of the identified gene expression patterns.

In conclusion, C-150 possessed dose-dependent effects on certain apoptosis and cell cycle related genes which could be enhanced by coadministration with bortezomib. In comparison with cotreatment of bortezomib and curcumin or C-150, similar gene expression changes were detected, which suggests a similar mechanism of action.

3.5. Common Genes Influenced by Both Curcumin and C-150. When gene expression values from curcumin and C-150 treated cells were plotted against each other and their correlation was investigated, we concluded that genes most affected by treatment behaved in a similar fashion suggesting that the related compounds act with similar mechanism of action (Figure 4). Several cyclins were unaffected by treatment but two previously described genes CCND1 (cyclin D1) and CCND2 (cyclin D2) [34] were both downregulated by curcumin and C-150. BIRC3 (BIRC3 baculoviral IAP repeat containing 3) and CASP4 (caspase 4, apoptosis-related cysteine peptidase) expression was also activated by both compounds agreeing with previous reports [35, 36].

While fewer genes responded to C-150 treatment alone compared to curcumin alone (with at least 2-fold induction

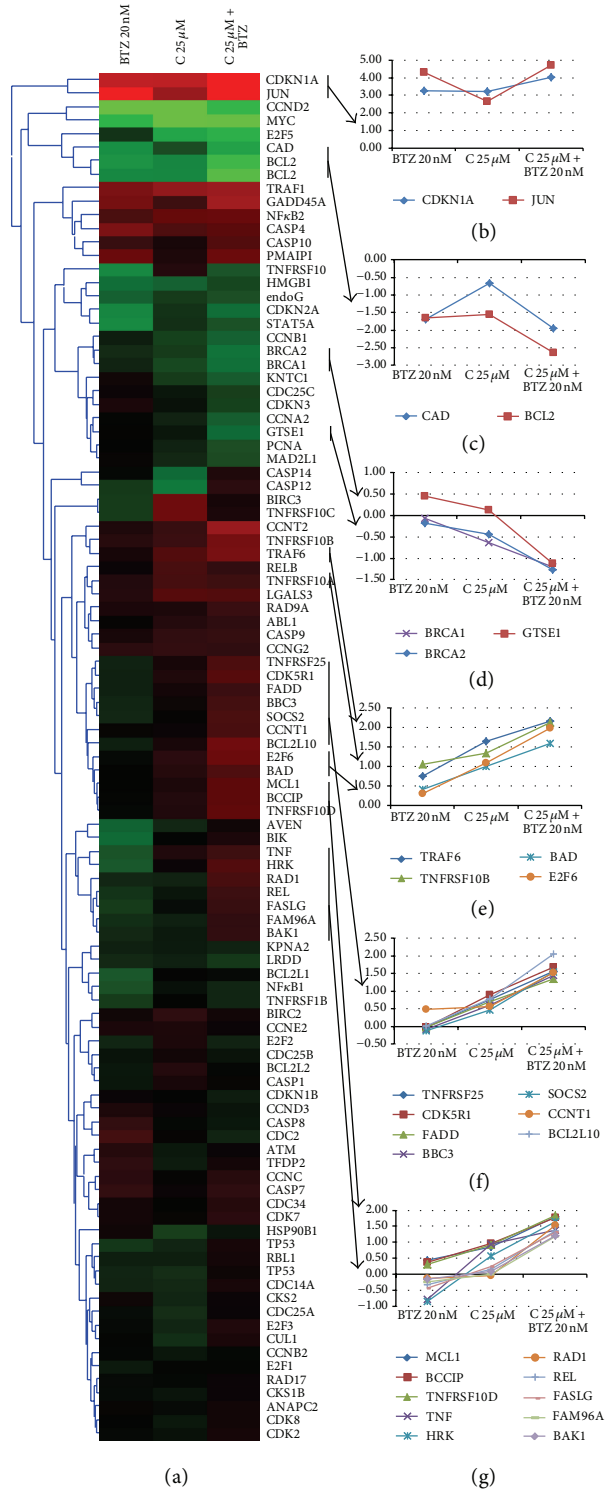

FIGURE 2: Gene expression analysis of curcumin (C) and bortezomib (BTZ) treatment. Curcumin influenced the expression of a wide range of cell cycle and apoptosis related genes.

or repression), combined treatment of C-150 and bortezomib affected the same genes with a similar profile as curcumin and bortezomib together (Figure 4(b)). Similar to viability measurements with MTS or CTG and FACS analysis, C-150 induced comparable results to curcumin at more than 40 times less concentration (25 μM versus 0.6 μM).

3.6. Genes Influenced Differentially by Curcumin and C-150. It seems that, among the tested members of the tumor necrosis factor receptor superfamily TNFRSF10A, B and C were differentially affected by curcumin and C-150. All three genes were upregulated by curcumin, while C-150 did not alter their expression. GADD45A (growth arrest

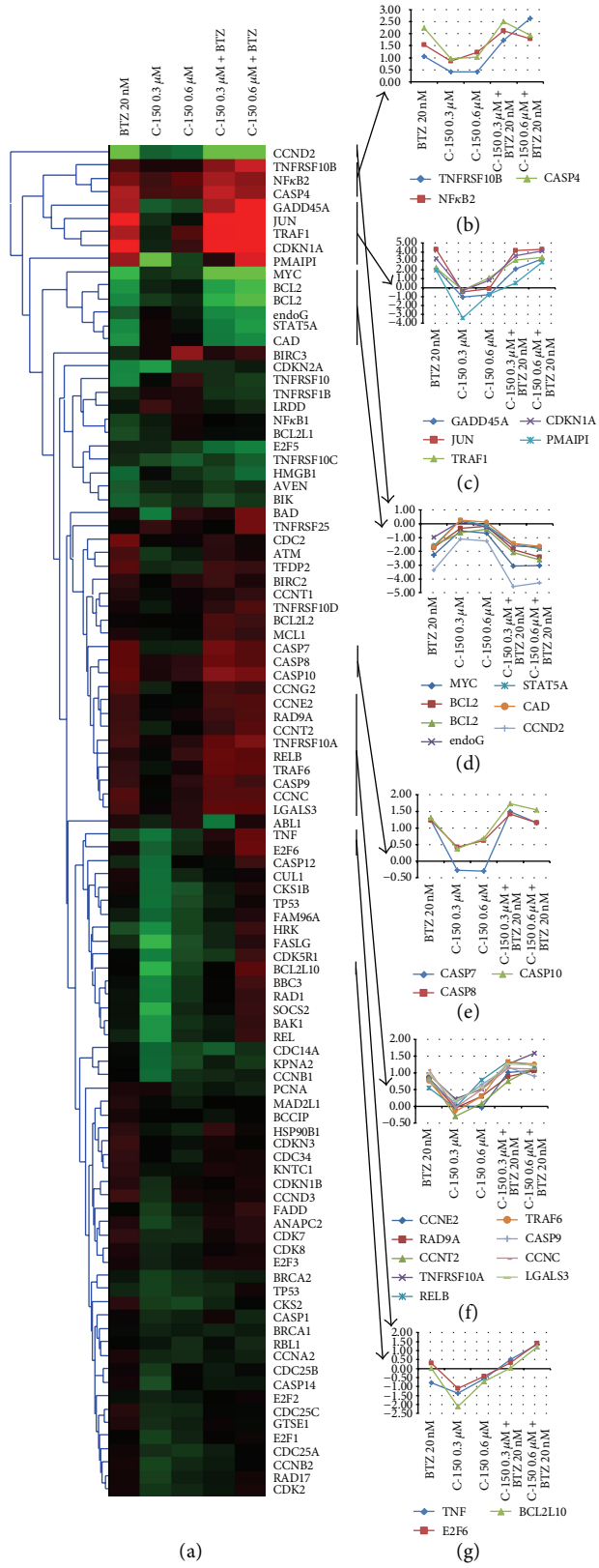

FIGURE 3: Gene expression analysis of curcumin analogue C-150 and bortezomib treatment. C-150 influenced the expression of a wide range of cell cycle and apoptosis related genes at 40–80-fold lower concentration compared to curcumin.

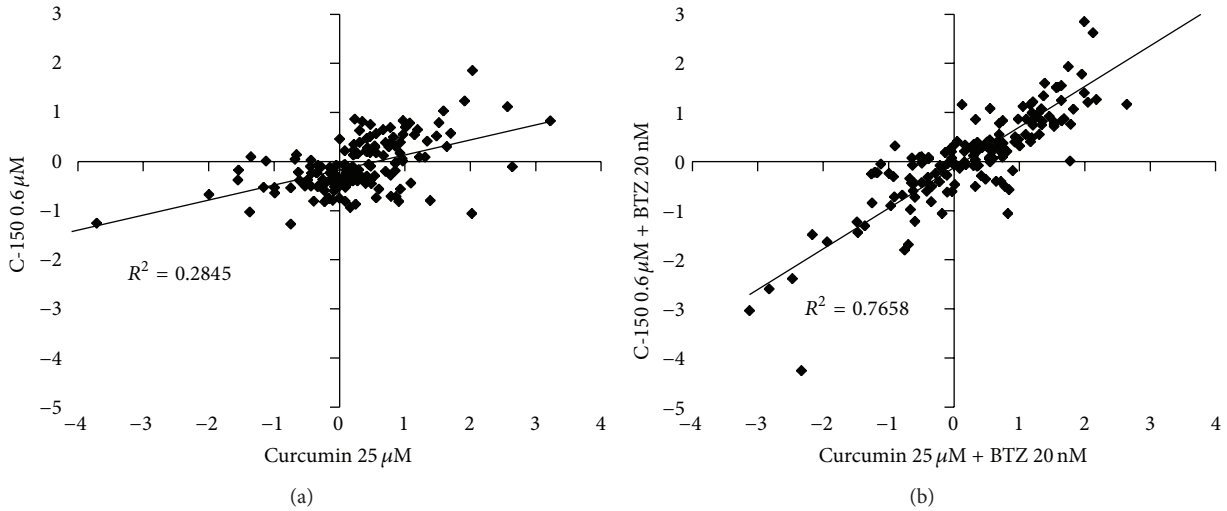

Figure 4: Correlation of gene expression changes following curcumin and C-150 treatment (a). Correlation of gene expression values of the combined treatments of curcumin + bortezomib and C-150 (0.6 μM) + bortezomib (b). The natural compound curcumin and its synthetic analogue C-150 affected nearly the same genes in a similar fashion, but curcumin analogue exerted its effect at 40-fold lower concentration.

and DNA-damage-inducible, alpha) was also differentially affected by curcumin and its analog. This stress response gene also mediates the activation of the JNK pathway [37], which also showed difference in the expression of JUN that was upregulated by curcumin and was not affected by C-150. These differences may rise from differences of the two compounds in target affinity or more likely effectiveness of the applied concentrations. Further studies are needed to validate these findings.

3.7. In Vivo Effects of Liposome-Formulated C-150 and Bortezomib Alone and in Combination. The effective therapy of acute myelocytic leukemia still remains problematic. Single treatment of leukemia and similar hematological cancer types has shown modest improvement. Despite chemotherapy, nearly half of the patients with myelocytic leukemias will fall prey to the disease because of the maturation of multiresistant subclones of leukemia cells [38, 39]. Numerous studies aimed to find effective compounds that are coadministered with chemotherapeutic agents which can increase efficacy of the treatment and lower its side effects. Several studies concluded that the sensitivity of some cancer cells can be increased by inhibiting several intracellular pathways in parallel which finally result in apoptosis. From this evidence, it can make sense to use the conventional chemotherapeutic agents in combination with other compounds that can sensitize the target cells.

We found that curcumin and its synthetic analogue C-150 can improve the effect of bortezomib in vitro. From the evidence published by Bai and Zhang and from our findings, curcumin and its analogue C-150 can modulate and inactivate the NF-κB pathway which is necessary to cell survival and activates the JNK pathway an activator of apoptosis [33]. In order to prove our hypothesis that C-150 could increase the effect of bortezomib against promyelocytic leukemia in vivo also, a study using a rodent model system was performed in SCID mice. In our in vivo study, 8 mice were used in 4 groups.

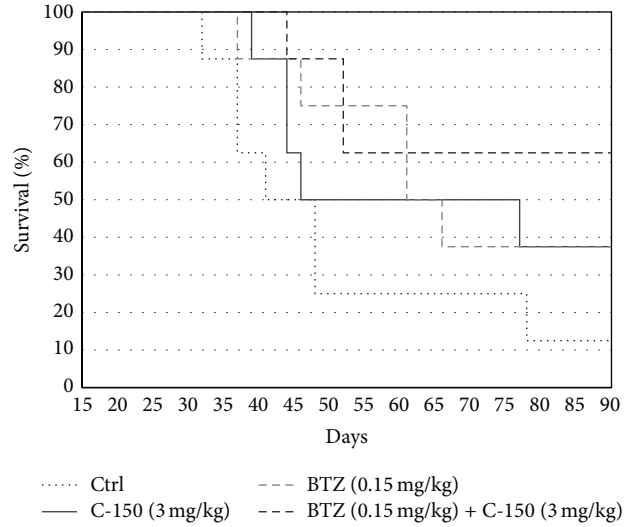

Figure 5: Survival of HL-60 xenograft mice treated with C-150 (3 mg/kg), bortezomib (0.15 mg/kg), or their combination. The curcumin analogue C-150 and bortezomib alone exhibited antitumor activity in HL-60 xenograft SCID mice, whereas combined treatment (bortezomib + C-150) developed a greater antitumor activity compared to single treatments.

We found that 1/8 mice survived in the control group, while both bortezomib and C-150 treatment alone was effective; 3/8 survived after 90 days in both groups. When C-150 and bortezomib were administered in combination, 5/8 mice survived. In addition, we found that this survival ratio did not change until 120 days, when the experiment was terminated (Figure 5).

Consistent with the results obtained in vitro, bortezomib or liposome formulated C-150 alone exhibited antitumor activity in HL-60 xenograft SCID mice, whereas combined bortezomib and C-150 treatment resulted in greater antitumor activity than single treatments. These results suggest that the combined use of bortezomib and C-150 could be developed into an effective option in the treatment of AML.

4. Conclusion

The multitarget action of curcumin and its analog, C-150, showed additive cytotoxic effects with bortezomib. Curcumin and its analogue induced expression changes in apoptotic and cell cycle related genes as determined by high-throughput QPCR. Most of the affected genes showed similar changes suggesting that the related compounds act through similar signaling pathways. Differences in tumor necrosis factor receptor superfamily and GADD45a gene activity profiles induced by curcumin and C-150 could be explained by differences in their target affinity or more likely, effectiveness of the applied concentrations. The enhanced proliferation inhibition capability of curcumin and C-150 analogue with bortezomib was confirmed by in vitro as well as in vivo studies. Pronounced positive effects of the liposomal formulated curcumin analogue on survival of HL60 xenograft mice would render this molecule a potent clinical candidate against leukemia alone or in combination with other antineoplastic agents.

Conflict of Interests

The authors declare that there is no conflict of interests regarding the publication of this paper.

Acknowledgment

This work was supported by the following Grant: GOP-1.1.1-11-2011-0003.

References

[1] P. Fresco, F. Borges, M. P. M. Marques, and C. Diniz, "The anticancer properties of dietary polyphenols and its relation with apoptosis," *Current Pharmaceutical Design*, vol. 16, no. 1, pp. 114–134, 2010.

[2] B. B. Aggarwal, A. Kumar, and A. C. Bharti, "Anticancer potential of curcumin: preclinical and clinical studies," *Anticancer Research*, vol. 23, no. 1, pp. 363–398, 2003.

[3] J. L. Arbiser, N. Klauber, R. Rohan et al., "Curcumin is an in vivo inhibitor of angiogenesis," *Molecular Medicine*, vol. 4, no. 6, pp. 376–383, 1998.

[4] P. K. Gopal, M. Paul, and S. Paul, "Curcumin induces caspase mediated apoptosis in JURKAT cells by disrupting the redox balance," *Asian Pacific Journal of Cancer Prevention*, vol. 15, no. 1, pp. 93–100, 2014.

[5] Y. Guo, Q. Shan, Y. Gong et al., "Curcumin induces apoptosis via simultaneously targeting AKT/mTOR and RAF/MEK/ERK survival signaling pathways in human leukemia THP-1 cells," *Die Pharmazie*, vol. 69, no. 3, pp. 229–233, 2014.

[6] M. Kelkel, C. Jacob, M. Dicato, and M. Diederich, "Potential of the dietary antioxidants resveratrol and curcumin in prevention and treatment of hematologic malignancies," *Molecules*, vol. 15, no. 10, pp. 7035–7074, 2010.

[7] B. B. Aggarwal and B. Sung, "Pharmacological basis for the role of curcumin in chronic diseases: an age-old spice with modern targets," *Trends in Pharmacological Sciences*, vol. 30, no. 2, pp. 85–94, 2009.

[8] A. B. Kunnumakkara, P. Anand, and B. B. Aggarwal, "Curcumin inhibits proliferation, invasion, angiogenesis and metastasis of different cancers through interaction with multiple cell signaling proteins," *Cancer Letters*, vol. 269, no. 2, pp. 199–225, 2008.

[9] J. Yu, Y. Peng, L.-C. Wu et al., "Curcumin down-regulates DNA methyltransferase 1 and plays an anti-leukemic role in acute myeloid leukemia," *PLoS ONE*, vol. 8, no. 2, Article ID e55934, 2013.

[10] V. P. Menon and A. R. Sudheer, "Antioxidant and anti-inflammatory properties of curcumin," *Advances in Experimental Medicine and Biology*, vol. 595, pp. 105–125, 2007.

[11] S. Singh and A. Khar, "Biological effects of curcumin and its role in cancer chemoprevention and therapy," *Anti-Cancer Agents in Medicinal Chemistry*, vol. 6, no. 3, pp. 259–270, 2006.

[12] K. Balasubramanyam, R. A. Varier, M. Altaf et al., "Curcumin, a novel p300/CREB-binding protein-specific inhibitor of acetyltransferase, represses the acetylation of histone/nonhistone proteins and histone acetyltransferase-dependent chromatin transcription," *The Journal of Biological Chemistry*, vol. 279, no. 49, pp. 51163–51171, 2004.

[13] X.-G. Li, Y. Chen, Q. Wu, and H.-L. Liu, "Effects of curcumin on the acetylation of histone H3, P53 and the proliferation of NB4 cells," *Zhonghua Xue Ye Xue Za Zhi*, vol. 26, no. 9, pp. 551–553, 2005.

[14] J. Chen, F. L. Wang, and W. D. Chen, "Modulation of apoptosis-related cell signalling pathways by curcumin as a strategy to inhibit tumor progression," *Molecular Biology Reports*, vol. 41, no. 7, pp. 4583–4594, 2014.

[15] H. Hatcher, R. Planalp, J. Cho, F. M. Torti, and S. V. Torti, "Curcumin: from ancient medicine to current clinical trials," *Cellular and Molecular Life Sciences*, vol. 65, no. 11, pp. 1631–1652, 2008.

[16] P. Anand, A. B. Kunnumakkara, R. A. Newman, and B. B. Aggarwal, "Bioavailability of curcumin: problems and promises," *Molecular Pharmaceutics*, vol. 4, no. 6, pp. 807–818, 2007.

[17] L. X. Wu, Y. Wu, R. J. Chen et al., "Curcumin derivative C817 inhibits proliferation of imatinib-resistant chronic myeloid leukemia cells with wild-type or mutant Bcr-Abl in vitro," *Acta Pharmacologica Sinica*, vol. 35, no. 3, pp. 401–409, 2014.

[18] D. K. Agrawal and P. K. Mishra, "Curcumin and its analogues: potential anticancer agents," *Medicinal Research Reviews*, vol. 30, no. 5, pp. 818–860, 2010.

[19] L. Lin, Q. Shi, A. K. Nyarko et al., "Antitumor agents. 250. Design and synthesis of new curcumin analogues as potential anti-prostate cancer agents," *Journal of Medicinal Chemistry*, vol. 49, no. 13, pp. 3963–3972, 2006.

[20] Q. Zhang, Y. Zhong, L.-N. Yan, X. Sun, T. Gong, and Z.-R. Zhang, "Synthesis and preliminary evaluation of curcumin analogues as cytotoxic agents," *Bioorganic & Medicinal Chemistry Letters*, vol. 21, no. 3, pp. 1010–1014, 2011.

[21] M. Gyuris, L. G. Puskas, I. Kanizsai, B. Ozsvari, L. Hackler Jr., and L. I. Nagy, "Subtituted curcumin derivates, process for

their preparation, and pharmaceutical compositions containing them," HU 20110000532 2011092, 2013.

[22] N. Mitsiades, C. S. Mitsiades, P. G. Richardson et al., "The proteasome inhibitor PS-341 potentiates sensitivity of multiple myeloma cells to conventional chemotherapeutic agents: therapeutic applications," *Blood*, vol. 101, no. 6, pp. 2377–2380, 2003.

[23] M. Karin, "Nuclear factor-κB in cancer development and progression," *Nature*, vol. 441, no. 7092, pp. 431–436, 2006.

[24] J. J. Wright, "Combination therapy of bortezomib with novel targeted agents: an emerging treatment strategy," *Clinical Cancer Research*, vol. 16, no. 16, pp. 4094–4104, 2010.

[25] J. Adams and M. Kauffman, "Development of the proteasome inhibitor Velcade (Bortezomib)," *Cancer Investigation*, vol. 22, no. 2, pp. 304–311, 2004.

[26] C. Fabre, N. Mimura, K. Bobb et al., "Dual inhibition of canonical and noncanonical NF-κB pathways demonstrates significant antitumor activities in multiple myeloma," *Clinical Cancer Research*, vol. 18, no. 17, pp. 4669–4681, 2012.

[27] T. Hideshima, H. Ikeda, D. Chauhan et al., "Bortezomib induces canonical nuclear factor-κB activation in multiple myeloma cells," *Blood*, vol. 114, no. 5, pp. 1046–1052, 2009.

[28] J. Park, V. Ayyappan, E.-K. Bae et al., "Curcumin in combination with bortezomib synergistically induced apoptosis in human multiple myeloma U266 cells," *Molecular Oncology*, vol. 2, no. 4, pp. 317–326, 2008.

[29] X.-Y. Zhang, Q.-X. Bai, G.-S. Huang, H. Zhao, J.-J. Chen, and L.-J. Yang, "Effect of curcumin in combination with bortezomib on proliferation and apoptosis of human multiple myeloma cell line H929 and its mechanism," *Zhongguo Shi Yan Xue Ye Xue Za Zhi*, vol. 19, no. 3, pp. 684–688, 2011.

[30] B. Sung, A. B. Kunnumakkara, G. Sethi et al., "Curcumin circumvents chemoresistance in vitro and potentiates the effect of thalidomide and bortezomib against human multiple myeloma in nude mice model," *Molecular Cancer Therapeutics*, vol. 8, pp. 959–970, 2009.

[31] T. Mujtaba, J. Kanwar, S. B. Wan, T. H. Chan, and Q. P. Dou, "Sensitizing human multiple myeloma cells to the proteasome inhibitor bortezomib by novel curcumin analogs," *International Journal of Molecular Medicine*, vol. 29, no. 1, pp. 102–106, 2012.

[32] A. Palotas, L. G. Puskas, K. Kitajka et al., "The effect of citalopram on gene expression profile of Alzheimer lymphocytes," *Neurochemical Research*, vol. 29, no. 8, pp. 1563–1570, 2004.

[33] Q.-X. Bai and X.-Y. Zhang, "Curcumin enhances cytotoxic effects of bortezomib in human multiple myeloma H929 cells: potential roles of NF-κB/JNK," *International Journal of Molecular Sciences*, vol. 13, no. 4, pp. 4831–4838, 2012.

[34] F. Tzifi, C. Economopoulou, D. Gourgiotis, A. Ardavanis, S. Papageorgiou, and A. Scorilas, "The role of BCL2 family of apoptosis regulator proteins in acute and chronic leukemias," *Advances in Hematology*, vol. 2012, Article ID 524308, 15 pages, 2012.

[35] C. Ramachandran, S. Rodriguez, R. Ramachandran et al., "Expression profiles of apoptotic genes induced by curcumin in human breast cancer and mammary epithelial cell lines," *Anticancer Research*, vol. 25, no. 5, pp. 3293–3302, 2005.

[36] H.-O. Pae, S.-O. Jeong, G.-S. Jeong et al., "Curcumin induces pro-apoptotic endoplasmic reticulum stress in human leukemia HL-60 cells," *Biochemical and Biophysical Research Communications*, vol. 353, no. 4, pp. 1040–1045, 2007.

[37] M. Gao, W. Dong, M. Hu et al., "GADD45α mediates arsenite-induced cell apoptotic effect in human hepatoma cells via JNKs/AP-1-dependent pathway," *Journal of Cellular Biochemistry*, vol. 109, no. 6, pp. 1264–1273, 2010.

[38] M. M. Gottesman and I. Pastan, "Biochemistry of multidrug resistance mediated by the multidrug transporter," *Annual Review of Biochemistry*, vol. 62, pp. 385–427, 1993.

[39] H. Sato, H. Preisler, R. Day et al., "MDR_1 transcript levels as an indication of resistant disease in acute myelogenous leukaemia," *British Journal of Haematology*, vol. 75, no. 3, pp. 340–345, 1990.

Hindawi Publishing Corporation
BioMed Research International
Volume 2015, Article ID 618021, 13 pages
http://dx.doi.org/10.1155/2015/618021

Research Article

Organotypic Culture of Breast Tumor Explants as a Multicellular System for the Screening of Natural Compounds with Antineoplastic Potential

Irma Edith Carranza-Torres,[1,2] Nancy Elena Guzmán-Delgado,[3] Consuelo Coronado-Martínez,[1] José Inocente Bañuelos-García,[4] Ezequiel Viveros-Valdez,[2] Javier Morán-Martínez,[5] and Pilar Carranza-Rosales[1]

[1]*Centro de Investigación Biomédica del Noreste, Instituto Mexicano del Seguro Social, 64720 Monterrey, NL, Mexico*
[2]*Facultad de Ciencias Biológicas, Universidad Autónoma de Nuevo León, 64460 San Nicolás de los Garza, NL, Mexico*
[3]*Unidad Médica de Alta Especialidad No. 34, Instituto Mexicano del Seguro Social, 64730 Monterrey, NL, Mexico*
[4]*Unidad Médica de Alta Especialidad No. 23, Instituto Mexicano del Seguro Social, 64010 Monterrey, NL, Mexico*
[5]*Facultad de Medicina, Universidad Autónoma de Coahuila, 66451 Torreón, COAH, Mexico*

Correspondence should be addressed to Pilar Carranza-Rosales; pilarcarranza@cibinmty.net

Received 4 November 2014; Revised 23 February 2015; Accepted 2 March 2015

Academic Editor: Zeki Topcu

Breast cancer is the leading cause of death in women worldwide. The search for novel compounds with antitumor activity, with less adverse effects and higher efficacy, and the development of methods to evaluate their toxicity is an area of intense research. In this study we implemented the preparation and culture of breast tumor explants, which were obtained from precision-cut breast tumor slices. In order to validate the model we are proposing to screen antineoplastic effect of natural compounds, we selected caffeic acid, ursolic acid, and rosmarinic acid. Using the Krumdieck tissue slicer, precision-cut tissue slices were prepared from breast cancer samples; from these slices, 4 mm explants were obtained and incubated with the selected compounds. Viability was assessed by Alamar Blue assay, LDH release, and histopathological criteria. Results showed that the viability of the explants cultured in the presence of paclitaxel (positive control) decreased significantly ($P < 0.05$); however, tumor samples responded differently to each compound. When the explants were coincubated with paclitaxel and compounds, a synergic effect was observed. This study shows that *ex vivo* culture of breast cancer explants offers a suitable alternative model for evaluating natural or synthetic compounds with antitumor properties within the complex microenvironment of the tumor.

1. Introduction

Cancer is the leading cause of mortality worldwide, with 8.2 million deaths and 14.1 million new cases recorded during 2012 alone. According to the World Health Organization, the number of deaths will continue to rise across the globe, with the alarming prediction of 19.3 million new cases by 2025. Breast cancer is the most frequent cancer found in women; it possesses the most elevated morbidity and mortality. In 2012, approximately 1.7 million women were diagnosed with breast cancer in the world, and 522,000 died as a direct result of this disease [1].

Conventional cancer therapies include surgery, radiation, and chemotherapy. Although the latter is widely used, in most cases it produces undesirable side effects. Chemoresistance and/or recurrence of cancer after chemotherapy are frequent events seen with treatment of this disease [2]. Thus, different research groups are now focused on finding novel drugs or anticancer compounds [3, 4] while others are developing methodologies for the evaluation of these drugs [5–7].

One of the current approaches for investigating novel antineoplastic or chemopreventive compounds is based on natural products research. This is because some of these compounds inhibit cell proliferation and promote apoptosis

Table 1: Bioactive compounds in commonly used herbs and spices.

Caffeic acid	Rosmarinic acid	Ursolic acid
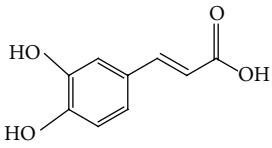	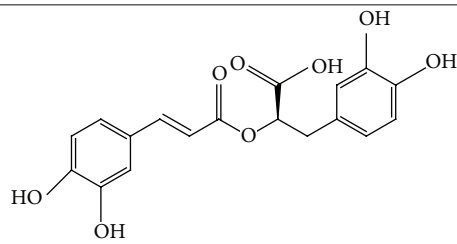	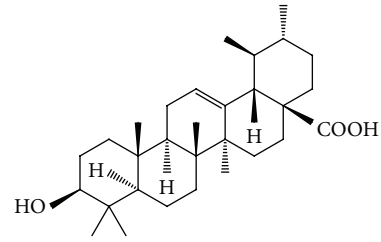
Coffee, parsley	Rosemary	Basil
Cardamom, rosemary	Marjoram	Marjoram
Cumin, sage	Oregano	Sage
Fennel, tarragon	Basil	Thyme
Nutmeg, thyme	Sage	
Oregano	Thyme	

in various types of tumor cells including breast cancer cells. Furthermore, it is well known that approximately 60% of the drugs administered in cancer treatment were isolated from natural products [8–10].

For the purpose of this study, we selected three naturally occurring compounds which possess antitumor and chemopreventive activities, namely, caffeic acid (CA), ursolic acid (UA), and rosmarinic acid (RA). These bioactive compounds are present in fruits, vegetables, medicinal plants, and culinary species. Table 1 shows their chemical structures and some examples of culinary herbs and spices where they are abundantly found [11–13]. CA is known to inhibit DNA methylation in human breast cancer cells and it has been suggested that it may reduce the risk of acquiring breast cancer [14]; however, epidemiological studies have been inconsistent and no established association between coffee intake and breast cancer development has been discovered [15]. We have previously reported that CA obtained from *Hedeoma drummondii* extracts possesses antiproliferative effect against MCF-7 and HeLa cells [16]. UA is known to inhibit proliferation of MCF-7 cells [17, 18], induce apoptosis, and inhibit oxygen consumption in various tumor cell lines [19, 20]. It suppresses the migration and invasion of MDA-MB-231 cells [21] and exerts antitumor effects on multidrug-resistant cancer cells [22]. RA has antioxidant, antitumor, antimutagenic, and chemopreventive activities [12, 23–25]. The effect of RA on cell proliferation and apoptosis induction has been determined in MCF-7, MDA-MB-361, MDA-MB-453, and HeLa cells [26, 27]; RA induces apoptosis and inhibits metastasis of MDA-MB-231BO cells. Hence, RA is also considered a good candidate for new therapeutic approaches in the treatment of breast cancer [28].

On the other hand, the antitumor activity and mechanisms involved in the inhibition of carcinogenesis by novel compounds with antineoplastic potential must be evaluated and validated using models that extrapolate their effects in humans. The results obtained from cells cultured *in vitro* and from experiments conducted on animals do not reflect what happens in humans, especially with regard to the full physiology, metabolism, pharmacokinetics, and other factors of high complexity. Therefore, it is important to use experimental models for easy and proper observation of the effects of bioactive compounds in tumor samples where tumor microenvironment is preserved. Conde et al. suggest that to study behavior of tumors it is necessary to maintain or reconstitute a similar environment of the tumor *in situ* [29]. From the experimental point of view, a way to preserve tissue architecture with little or no manipulation is through the organotypic culture of intact and fresh tumor tissues. Tissue slices, one of the methods recently used, is an intermediate system between *in vivo* and *in vitro* models, which offers a new perspective to the results obtained with cell lines.

Tissue slices contain virtually all the cells from the tissue under study. They retain histological and three-dimensional structure (3D), with inter- and extracellular interactions, cell matrix components, and, most interestingly, metabolic capacity. Hence, cultured tissue slices are considered a suitable tool for the study of multicellular processes [30].

Precision-cut tissue slices have mainly been used to study metabolism and toxicity of xenobiotics [31, 32], biotransformation of drugs, gene expression studies, and morphological analysis, among other studies [33, 34]. Our group has recently described their application as an infection model for the parasitic protozoa *Entamoeba histolytica* [35, 36]. Other than normal tissue slices, tumor slices are 3D cultures in which it is possible to evaluate *ex vivo* therapeutic efficacy of oncolytic vectors [37–41] and drugs such as meloxicam and Taxol [42–44] or study the interactions between stromal components and epithelial cells with the extracellular environment, as well as the response to cytokines and drugs [45]. The taxoid paclitaxel (abbreviated TX in this work), known by its original brand name, Taxol, represents the most important first-line antineoplastic drug for treatment of various types of cancer, including breast cancer, ovarian cancer, non-small cell lung cancer, and AIDS related Kaposi's sarcoma, among others. TX was purified and identified as the active constituent from the bark of the Pacific yew, *Taxus brevifolia*, in 1971 [46, 47]. Its mechanism of action relies on the promotion of microtubule

Table 2: Clinical and histopathological data of the subjects.

Patient	Age	Clinical stage	Histologic type	Tumor size	Estrogen receptor (ER)	Progesterone receptor (PR)	Her2 status	Molecular classification
A	50 yr	T2N1M0 (grading: IIB)	Ductal infiltrating	3 cm	(−)	(−)	(+)	Her2+
B	59 yr	T3N0M0 (grading: IIB)	Ductal infiltrating	5 cm	(+)	(+)	(+)	Luminal B
C	41 yr	T2N1M0 (grading: IIB)	Ductal infiltrating	4 cm	(+)	(+)	(−)	Luminal A

assembly and inhibition of microtubule disassembly; cells exposed to paclitaxel cannot form a mitotic spindle; this interferes with cell division and induces cell death [48].

Using *ex vivo* organotypic cultures of breast cancer explants treated with CA, UA, RA, and TX, we found that this model is an alternative system for studying anticancer activity or synergistic potential assessing natural products. Cultured explants retain their typical morphology and viability for at least 3 days. With this method, a sufficient number of slices and explants can be obtained from minimal amounts of tissue, enabling the study of several compounds within a single tumor specimen.

2. Materials and Methods

2.1. Chemicals. Caffeic acid, ursolic acid, rosmarinic acid, paclitaxel, and insulin-transferrin-selenium were purchased from Sigma-Aldrich (St. Louis, MO, USA). DMEM/F12 medium, fetal bovine serum, gentamicin, penicillin-streptomycin, and Alamar Blue were obtained from Invitrogen (Grand Island, NY, USA). The antibody against Ki 67 was obtained from Santa Cruz Biotechnology (Santa Cruz, CA, USA). The reagents for general use were purchased from Sigma-Aldrich (St. Louis, MO, USA).

2.2. Tumor Samples. Infiltrating ductal adenocarcinoma specimens were collected from 11 patients during surgery at the Hospital of Gynecology and Obstetrics (UMAE # 23) from the Mexican Institute of Social Security (IMSS). The pathologist dissected the specimen immediately after surgery to confirm its tumorous nature and to avoid contamination. Informed consent was obtained from all patients. Tissues were collected in cold serum-free DMEM/F12 medium (Invitrogen, Grand Island, NY, USA) and transported at 4°C to the organotypic culture laboratory for immediate processing. Approval was obtained from the Institutional Review Board (Mexican Institute of Social Security) before initiation of studies on human tissue. The clinical and histopathological data of these patients are described in Table 2.

2.3. Preparation of Slices and Explants from Breast Tumor. From representative tumor samples, cylindrical tissue cores of 10 mm diameter were obtained; from these, tissue slices of 250–300 μm thickness were prepared using the Krumdieck tissue slicer (Alabama Research & Development, Munford, AL, USA), with constant flow of Krebs Henseleit bicarbonate buffer (KB) at 4°C which was gassed with carbogen. The slices were collected in KB buffer at 4°C. To optimize the tumor sample and homogenize the size of tissues, small tumor explants, 4 mm in diameter and 250–300 μm in thickness, were prepared using a biopsy punch from the first-obtained slices. Tumor explants were placed in six-well microplates containing DMEM/F12 culture medium supplemented with 10% fetal bovine serum, 5 μg/mL bovine insulin, 100 μg/mL gentamicin, insulin-transferrin-selenium, and 25 mM glucose (DMEM/F12 supplemented medium). Plates were preincubated for 1 h at 37°C, 5% CO_2/95% air, and agitation at 25 rpm. The interval between resection of the tumor and the incubation of the explants was no more than 2 h. The entire process was performed under aseptic conditions.

2.4. Viability of Tumor Explants. In order to confirm that the tumor samples were still viable during the entire experiments, the viability of the tumor explants was determined at different times before testing the antineoplastic effect of CA, UA, and RA. To test this, explants with 4 mm diameter/250–300 μm thickness were placed in 24-well microplates containing 1 mL of DMEM/F12 supplemented medium and incubated for 4 days at 37°C, 5% CO_2/95% air, and constant agitation of 25 rpm. Viability was determined every 24 h in a group of four explants. Protocols for metabolic viability (AB), cytotoxicity (LDH release), cellular proliferation (Ki 67 expression), and morphological integrity (histopathological analysis) are described in the corresponding section. The culture medium was changed every 24 h through 96 h, and each time viability, proliferation, and morphology were assessed.

2.5. Treatment of Tumor Explants with TX and Bioactive Compounds. After 1 h of preincubation, the tumor explants were transferred to 24-well microplates containing 1 mL of DMEM/F12 supplemented medium. Afterwards, the following compounds were added: 20 μg/mL TX (positive control), 11–33 μg/mL CA, 20–60 μg/mL for RA and UA, and combinations of these compounds with TX. These concentrations were selected on the basis of IC_{50} values reported in cell lines [16, 20, 49]. Control group (100% viability) consisted of untreated explants, which were incubated only with culture medium. Afterwards, the microplate with the explants and their corresponding treatments were incubated for 48 h at 37°C, 5% CO_2/95% air, and constant agitation at 25 rpm.

2.6. Alamar Blue Viability Assay. The effect of treatment with CA, UA, and RA on the viability of the tumor explants was assessed by the Alamar Blue assay. Alamar Blue (AB) is a blue nonfluorescent dye reduced to a pink-colored, highly fluorescent resorufin by metabolically active cells. It is known that viable cells reduce the microenvironment to a pink color, while dead or inactive cells do not change

the original blue color of resazurin, the active ingredient of AB. After 48 h of incubation with compounds, as well as with cell culture medium and TX (controls), the explants were incubated for additional 4 h with 10% Alamar Blue in 500 μL DMEM/F12 supplemented medium at 37°C in the conditions described earlier. Afterwards, 100 μL was collected from each sample and transferred to a 96-well microplate. Fluorescence values were read using a multinode microplate reader (Synergy BioTek HT) at 530 nm excitation/590 nm emission wavelengths. The percentage of viability relative to control was calculated using the free software AbD Serotec fluorometric calculator for AB assays (http://www.abdserotec.com/colorimetric-calculator-fluorometric-alamarblue.html).

2.7. Lactate Dehydrogenase Assessment. Another way to assess the viability of the explants treated with the compounds and that of the untreated controls was by assessment of the leakage of the enzyme lactate dehydrogenase (LDH) into the supernatant of the culture medium [50]. The assay is based on the release of the cytosolic enzyme LDH into the media by cells with damaged plasma membranes [51]. The cytotoxicity induced by CA, UA, and RA on the tumor explants can be quantitatively determined by measuring the activity of this enzyme. The total amount of released enzyme was determined using an Architect C400 clinical chemical analyzer (Abbott).

2.8. Histopathological Analysis. After each experimental time point, the explants were fixed in 10% neutral formalin and then embedded in paraffin using the conventional histological technique. Tissue sections of 4 μm were prepared on a microtome and mounted on glass slides. Afterwards, the slides were deparaffinized and stained with hematoxylin and eosin (H&E). Then permanent sections were prepared with coverslips and synthetic resin. The stained preparations were observed by a pathologist using a Zeiss Axiostar Plus Brightfield microscope. Morphological parameters analyzed in treated and control explants included necrosis, viable/damaged tumor cells, and inflammation. Representative photographs of all treatments were obtained with a 5.0 MP Moticam camera.

2.9. Immunohistochemistry for Ki 67 Expression. Analysis of Ki 67 expression was performed on paraffin sections using the Dako LSAB System-HRP methodology to assess the rate of cell proliferation from treated and untreated tumor explants. The procedure was performed according to the recommendations of the manufacturer. The expression of this marker is nuclear, and the proliferation index was defined as follows: low: expression in ≤10% of cells; intermediate: expression in 10–20% of cells; and high: expression in ≥20% of cells [52].

2.10. Statistical Analysis. Statistical analysis was performed with SPSS version 22.0 software. Quantitative data were expressed as mean and standard deviation. Differences in continuous variables with normal distribution were analyzed with Student's t-test or the Mann-Whitney U test for nonnormal distributions.

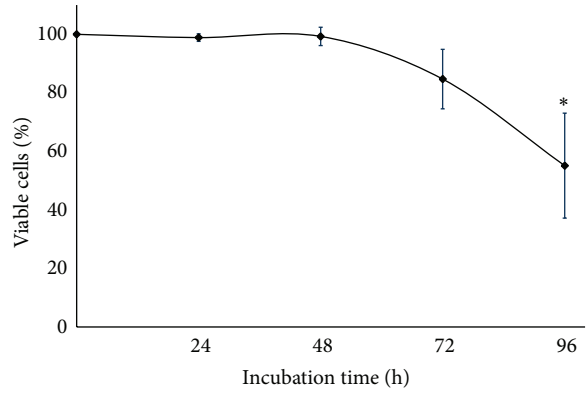

Figure 1: Viability of cultures breast cancer explants. To determine the optimal time for performing the experiments with bioactive compounds, explants were cultivated in DMEM/F12 supplemented medium for 24, 48, 72, and 96 h. The viability was assessed by the Alamar Blue assay. Values reflect means ± SD. Asterisks (∗) indicate significant statistical differences ($P < 0.05$).

3. Results

3.1. Characteristics of Patient Samples Used for the Preparation and Culture of Breast Cancer Tissue Explants. Eleven samples of human breast cancer with histopathological diagnosis of infiltrating ductal adenocarcinoma with nonspecific pattern were collected fresh from the operating room. Three samples were used to standardize and optimize the preparation of precision-cut breast tumor slices, and, from these, explants of a defined size and thickness (4 mm in diameter and 250–300 μm thick) were obtained for *ex vivo* culture under controlled conditions. Three more samples were used to standardize the concentrations to test each of the bioactive compounds and TX. Three other samples were included in three independent assays to assess the effect of CA, UA, RA, and TX on the viability of tumor tissue explants. The last two samples were discarded due to abundant necrosis, as well as elevated adipose and fibrous tissues, which prevented proper processing.

3.2. Viability of Tumor Explants

3.2.1. Metabolic Activity: Alamar Blue Assay. Tumor explants cultured for 24 and 48 h remained viable throughout the incubation period, with mean viability of 99% compared to basal value (100%). At 72 h, a slight decrease was observed in viability (84.7% ± 10.2), whereas, at 96 h, the percentage decreased to 55.1% ± 17.9 ($P < 0.05$). These results showed the metabolism of explants of breast tumors, and hence, their viability remained intact during at least the first 48 h of culture. With these results, we decided that 48 h was the optimal time to perform cytotoxicity assays with the bioactive compounds (Figure 1).

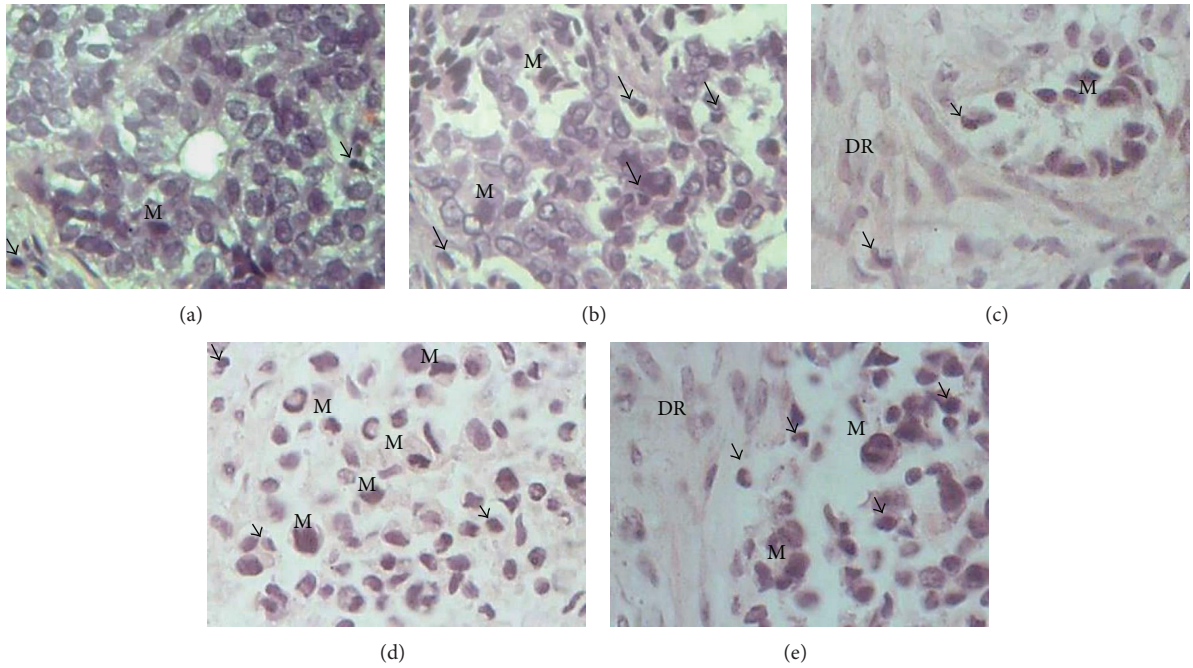

Figure 2: Morphological integrity of tumor tissue explants cultured *ex vivo*. Histopathological findings of tumor tissue at zero time (basal) and cultivated during different times in DMEM/F12 supplemented medium show that neoplastic tissue remains viable. It is possible to observe cells in active mitosis (M), desmoplastic reaction (DR) adjacent to the tumor cells, and presence of inflammatory cells (arrow). Desmoplasia or desmoplastic reaction is usually only associated with malignant neoplasms, which can evoke a fibrosis response by invading healthy tissue. All these characteristics are typical of tumor tissue. (a) 0 h, (b) 24 h, (c) 48 h, (d) 72 h, and (e) 96 h in culture, respectively. H&E staining (40x).

3.2.2. Morphological Integrity: Histopathological Analysis. After 96 h in culture, it was found that the typical histology of the tumor tissue was preserved in breast tumor explants. As shown in Figure 2, in the explants cultured for 24, 48, 72, and 96 h, neoplastic cells retained their characteristic morphology and mitotic activity. It was possible to identify microcalcifications, fibrous connective tissue, desmoplastic stromal reaction, inflammatory cells, and adipose tissue; furthermore, mitotic cells were observed at all-time points. These results (as shown in Figure 3) confirm that breast cancer explants remained viable and actively proliferating for up to 96 h.

3.2.3. Proliferative Activity: Immunohistochemical Expression of Ki 67. Compared to normal breast and tumor tissues (negative and positive controls, resp.), the proliferation index of the cultivated explants was greater than 50% during all the incubation times (24–72 h). This result corresponds to a high proliferation index according to the criteria defined in Materials and Methods and suggests that the tissue remains viable and actively proliferating during *ex vivo* culture conditions (Figure 3).

3.2.4. Effects of Bioactive Compounds and TX on Breast Tumor Explants. In order to ascertain that the breast tumor explants responded to the *ex vivo* treatment with CA, UA, and RA, we decided to first evaluate the metabolic activity of these explants after 48 h of incubation with varying doses of TX (5, 10, 15, and 20 μg/mL). As expected, a dose-response curve of cytotoxicity, directly proportional to the concentration of TX, was observed. Since 20 μg/mL of TX reduced tumor viability to less than 50% ($P < 0.05$), we selected this concentration for assays in which TX was a reference for antineoplastic activity (Figure 4). In the case of the effect of the bioactive compounds on the viability of breast tumor explants, the initial concentrations tested for CA, UA, and RA were 11–33, 20–60, and 20–60 μg/mL, respectively. These concentrations were not cytotoxic since the explants remained viable and also conserved their intact histological structure (data not shown). Because of this, it was necessary to increase the experimental concentrations of CA and UA to 100 μg/mL and of RA to 120 μg/mL.

When the histological structure of uncultured tumor explants was compared with explants cultivated for 48 h without any treatment, poorly differentiated neoplastic with nonspecific pattern neoplastic cells, which retained their viability, were observed. However, when the explants were cultured in the presence of only TX and with combinations of TX plus bioactive compounds, scattered necrotic areas as well as a remarkable reduction (more than 40%) in the population of neoplastic cells were also observed (Figure 5). These results suggest a potential antineoplastic effect of the bioactive compounds, reinforced when they are combined with TX. Additionally, by analyzing the metabolic activity of the explants incubated with these new concentrations, it was observed, as expected, that individual samples from each patient responded differently to the tested compounds. CA was the most effective in patient A, reducing tumor viability to 67.2%, while the combination of TX + CA decreased

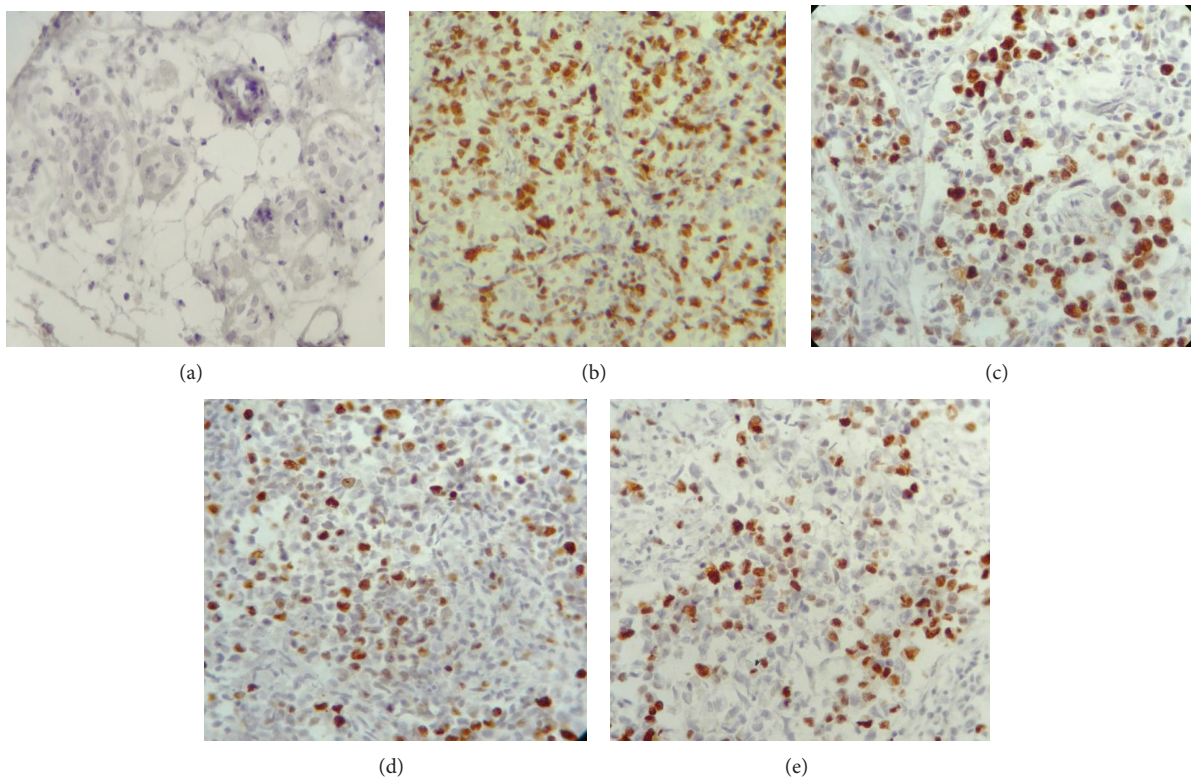

Figure 3: Nuclear expression of the cell proliferation marker Ki 67 in cultures of breast cancer explants. Representative images showing that over 40% of the neoplastic cells express Ki 67 at all-time points. The proliferation index is considered "high" when >20% of the cells are positive for this marker. (a) Normal breast tissue (negative control); (b) breast tumor (positive control); (c), (d), and (e) breast tumor explants cultured for 24, 48, and 72 h, respectively. Immunohistochemical staining (10x).

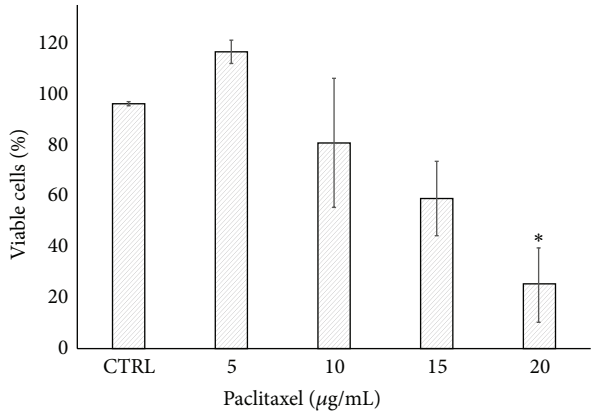

Figure 4: Effect of paclitaxel on the viability of tumor explants. Breast tumor explants were cultured during 48 h in the presence of different concentrations of paclitaxel. The viability was assessed at the indicated times using the Alamar Blue assay. Values reflect means ± SD. Asterisks (∗) indicate significant statistical differences ($P < 0.05$).

viability to 17.1%. Likewise, CA was the most active compound against the tumor of patient B, in which viability was reduced by 32.5; also, combination with TX had an important effect on viability, with a reduction of 20.2%. In contrast, none of the compounds had a cytotoxic effect against the patient C sample; however, a marked reduction in viability was observed when individual compounds combined with TX were tested. Interestingly, all of the compounds exerted a synergistic effect, enhancing the tissue toxicity of TX in all three tumor samples (Figure 6).

The cytotoxicity of TX alone and combinations with bioactive compounds was assessed via the release of the cytosolic enzyme LDH into the supernatants from the culture media in which tumor explants were cultivated. As shown by the data, the combination of TX + CA induced 1.42- and 1.80-fold increase of LDH release in the tumor explants from patients A and B, respectively, compared to untreated control. For patient C, the combination of TX with RA induced a 2.34-fold increase (Figure 7). These values were statistically significant ($P < 0.05$).

4. Discussion

The aim of this study was to demonstrate the use of *ex vivo* organotypic culture of human breast tumor explants as an alternative model system for evaluating natural compounds with antineoplastic potential. The most important characteristic of these explants is that they are obtained from precision-cut breast tissue slices which possess a defined size and thickness.

This is an interesting model which allows the study of different aspects of cancer. It has all the advantages of normal

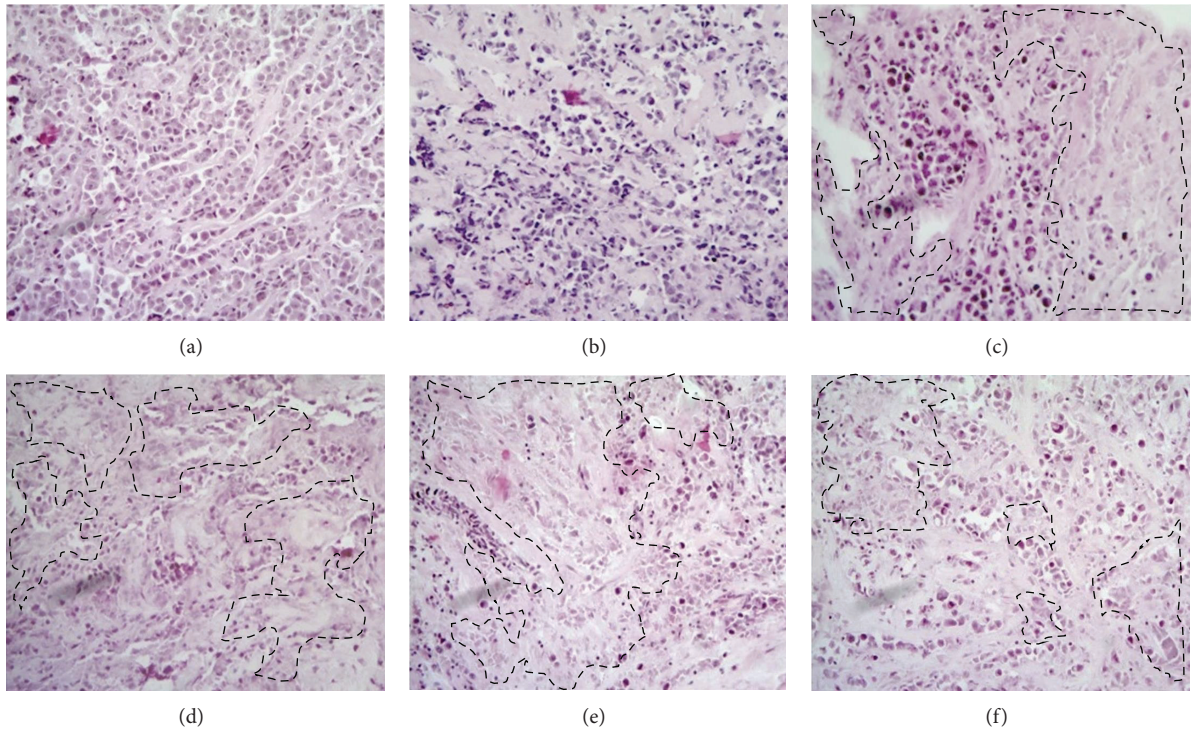

Figure 5: Effect of the bioactive compounds and their combination with paclitaxel on cultures of breast cancer explants. Explants from control at zero h (a) and control without any treatment cultured for 48 h (b) show poorly differentiated invasive neoplasm and no evidence of tumor necrosis areas. In contrast, in explants incubated with TX (c) and their combinations with CA (d), RA (e), and UA (f), an evident pathological response was observed, which is mainly reflected as a notable diminution of the neoplastic cells (40–80%) which can be appreciated as extensive areas of necrosis induced by treatments (dotted lines) H&E staining (10x).

tissues slices and also contributes to the significant decrease in the number of animals used in experimentation [30, 35]. Also, it enables the optimization of the amount of available tissue and favors the realization of a large number of assays that capture many aspects of tumor heterogeneity and complexity [53]. One of the difficulties we faced during the preparation of breast tumor slices was the viscosity or the very soft consistency of some tumors; thus, based on this fact, 2 of the 11 samples were discarded. This disadvantage correlated with those reported by other investigators [54, 55].

To be certain that this system is reliable and adequate to assess the effect of these bioactive compounds, the most critical step was to maintain the viability of the explants during *ex vivo* culture conditions and during subsequent treatment with these compounds. To monitor viability, we used the AB assay because it is a simple and affordable method that allows assessing cell viability by adding AB reagent directly to the culture medium. The active compound of AB is resazurin, which is reduced to resorufin through mitochondrial metabolism in living cells. Moreover the AB assay does not require additional steps as do other viability tests, in which it is necessary to lyse or damage cell membranes in order to release the reduced metabolite [56, 57]. This assay gives reliable measurements of the number of metabolically active cells and is one of the most commonly used methods for assessing cell proliferation. Other advantages include its homogeneous nature, the stability of generated signal, high sensitivity, compatibility with absorbance or fluorescence instruments and different biological models, and also safety for the user and the environment [58, 59]. The results from histopathological and AB analysis demonstrate that both metabolic activity and morphological integrity were conserved for at least 72 h (Figures 1 and 2).

On the other hand, immunohistochemical analysis of Ki 67 showed that cellular proliferation remained stable over the experimental period. Ki 67 is a proliferation marker strongly associated with cells undergoing mitosis in the cellular cycle [60]. Proliferation index in cancer cells from cultivated explants was >40% in all-time points, which is considered "high" according to accepted criteria (Figure 3) [52] and is similar to the reports from other authors, who conducted tests of selective toxicity in breast cancer tissue and were able to maintain viability and proliferation for 24 h [61] and 96 h [44, 62] or up to 7 days [55].

In order to validate the usefulness of the model, we incubated the breast tumor explants with different concentrations of TX, a well-known antineoplastic drug. As was expected, a dose-response curve was observed (Figure 4). With results from three different tumor samples, we used 20 μg/mL as a positive control in the following studies. Afterwards, three independent experiments were carried out to test the effect of CA, UA, and RA, which are naturally occurring products whose anticancer and chemopreventive properties have been reported previously [10, 12, 14, 21, 22, 63, 64].

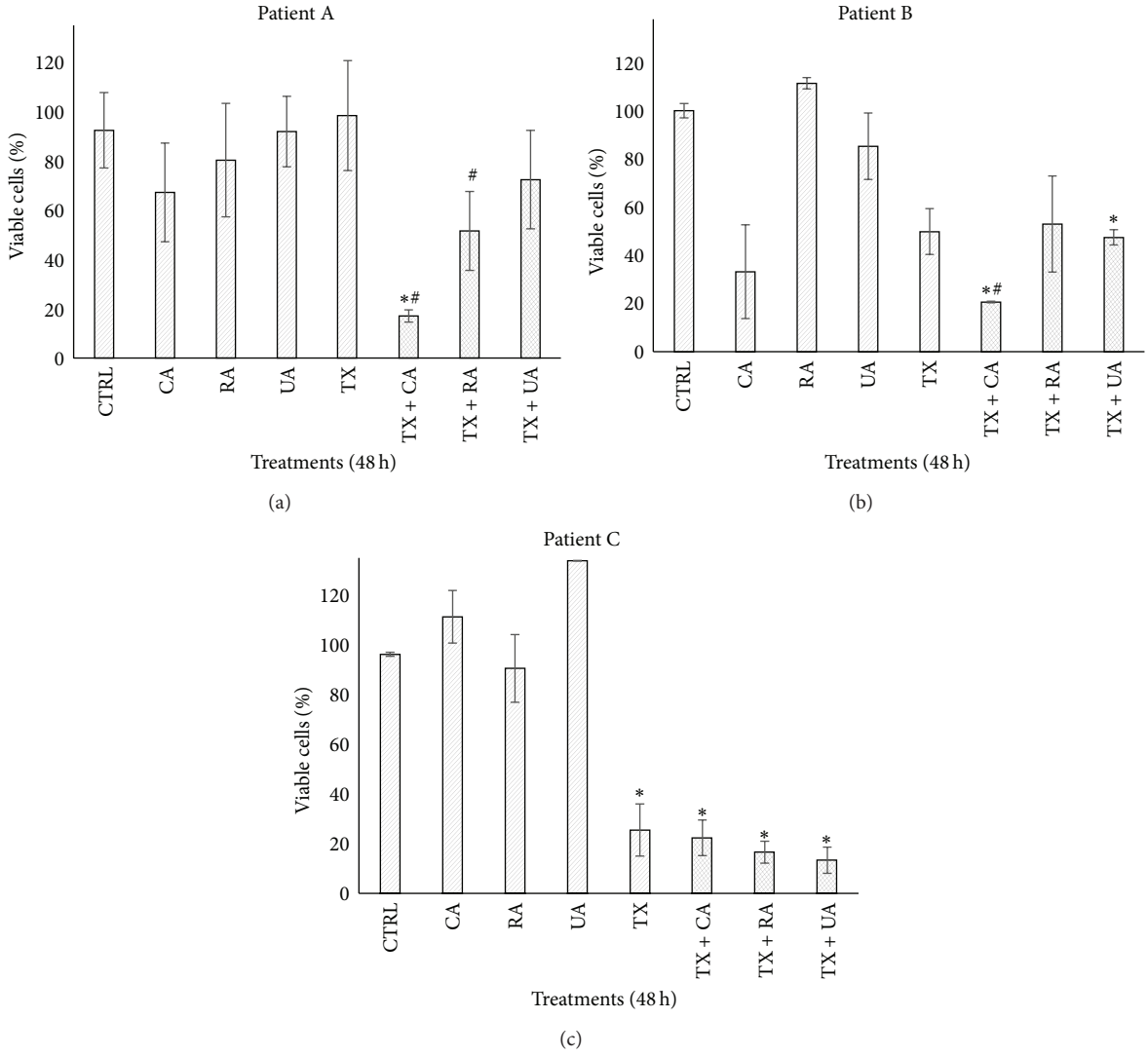

Figure 6: Effect of different treatments on the viability of breast cancer explants. Tumor explants were incubated with the bioactive compounds for 48 h and then cell viability was determined using the Alamar Blue assay. Control explants did not receive any treatment. Concentrations of compounds were 100 μg/mL CA and UA, 120 μg/mL RA, and 20 μg/mL TX. The same concentrations were used in the combinations. Results were compared to the untreated control. Values reflect means ± SD. Asterisks (∗) indicate significant statistical differences ($P < 0.05$) compared to control. Pound key (#) indicates significant statistical differences ($P < 0.05$) compared to paclitaxel.

The concentrations used first were selected on the basis of IC_{50} values reported in cell lines [16, 20, 49]; however, we did not observe a cytotoxic effect on the tumor tissue explants. This can be attributed to the differences between *in vitro* cell cultures and tissue explants, because in tissue explants there is more than one cell lineage interacting with each other and with extracellular matrix components. It is well known that the extracellular matrix and the tumor microenvironment protect neoplastic cells from cytotoxic agents [65]. When we increased the concentrations of the bioactive compounds to 100 μg/mL for CA and UA and 120 μg/mL for RA, we found that CA had the greatest effect, decreasing in tumor viability (Figure 6). The concentration used for CA, as well as the results observed, was similar to those described by Chang et al., who reported that CA induced apoptosis and decreased viability in gastric cancer cells [66].

With regard to the synergistic effect between the bioactive compounds and TX, there are several reports using cell lines which combine antineoplastic agents with extracts from phenolic compounds, such as UA and RA, which enhance treatments effectiveness. These results suggest a great potential for the use of natural compounds, when added to TX or another antineoplastic agent, in order to reduce the dosage, and the side effects associated with chemotherapy, without sacrificing therapeutic results [67–70].

In addition to the aforementioned, performing such studies in organotypic *ex vivo* models, such as the one used in this work, which more closely resemble an *in vivo*

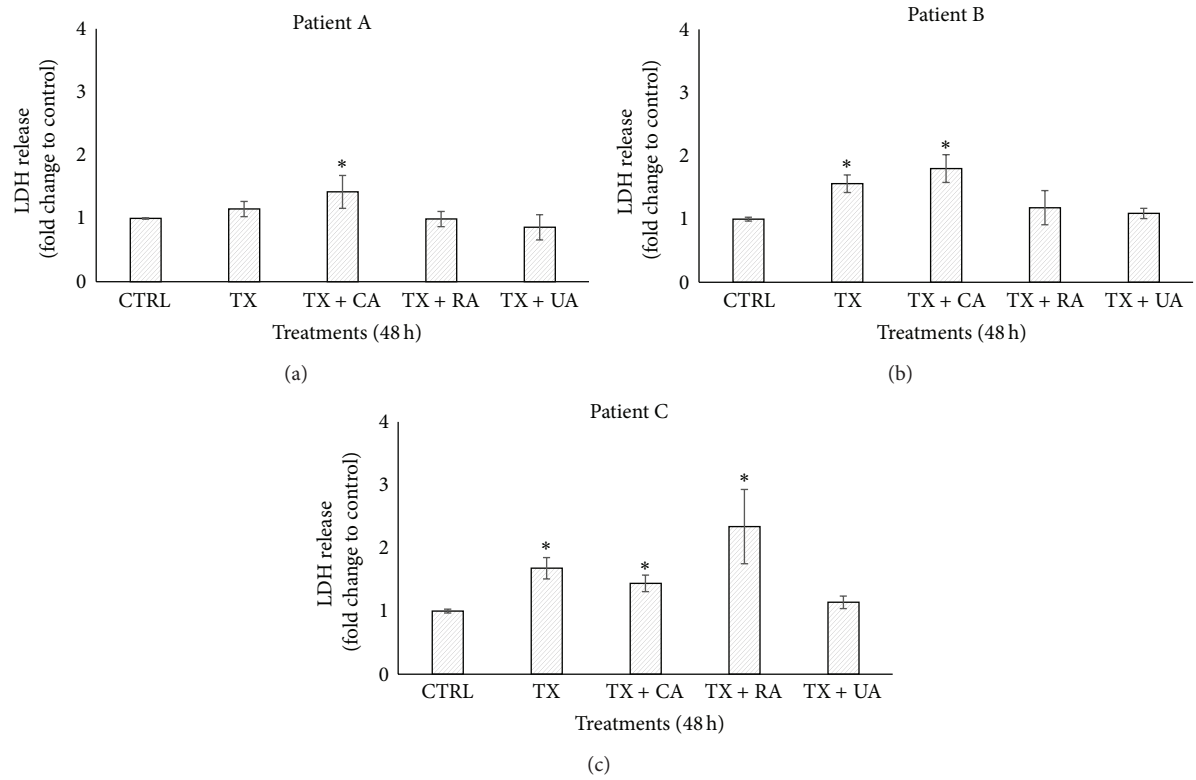

Figure 7: Effect of the combinations of paclitaxel with bioactive compounds on LDH release. Four tumor explants per treatment were incubated with combinations of TX and compounds for 48 h and then LDH activity was quantified by measuring the units of enzyme released into the supernatants from the culture medium. Control explants received no treatment. Concentrations in the combinations were 20 μg/mL + 100 μg/mL (TX + CA and TX + UA) and 20 μg/mL + 120 μg/mL (TX + RA). Results of LDH release are expressed as fold of change relative to control. Values represent means ± SD. Asterisks (∗) indicate significant statistical differences ($P < 0.05$).

scenario, might be more useful for extrapolating results in humans. An important factor to be considered is the administration time of the bioactive compound to the tissue, which can be done before, during, or after incubation with the antineoplastic agent. In our case, we coincubated tumor explants in the presence of compounds plus TX based on the experimental points we previously defined; however, new assays can be designed by pretreating or posttreating tissues with different compounds and antineoplastic agents. When combinations of CA, UA, or RA plus TX were studied, CA acted synergistically with this antineoplastic drug since viability was lower than with TX alone (Figure 6). This result is different from those reported by Lin et al., who found that CA at 100–150 μM induced a slight increase in the proliferation of A549 and H1299 lung cancer cells and that pretreatment of cells with CA protects these cells from growth inhibition when they are incubated with TX [71]. This discrepancy in the results can be attributed to the difference in biological models (cell lines *versus* tumor explants), the pretreatment used, and also the fact that the CA concentrations were different. Furthermore, RA induced more pronounced membrane damage when coadministered with TX in the sample from patient C (Figure 7). Although the synergism between CA and TX was the strongest, a synergistic response in reducing tumor viability for all compounds compared to compounds alone was observed (Figure 6).

The relationship between viability and cytotoxicity data is discrete since, although it is possible to observe that at lower percentage of viability LDH release increases, the values of LDH are relatively low considering that viability decreased at an average of 18% in the synergies between TX + CA in patients A and B and TX + RA in patient C; therefore one would expect LDH levels to be more elevated. One possible explanation for this fact is that inactivation of the enzyme could have occurred in the culture medium, as has been reported by Lash and Zalups, Kendig and Tarloff, Hohnholt et al., and Tulpule et al. [72–75]. Another possibility is that some natural compounds that have antioxidant effects protect cells and prevent the release of LDH. For example, da Silva Morrone et al. found that extracts of *Passiflora manicata* leaves protect from damage induced by reactive oxygen species, and the release of LDH was significantly reduced in precision-cut rat liver slices [76]. On the other hand, Liu et al. found that lipopolysaccharides obtained from *Lycium barbarum* inhibited the elevation of liver enzymes, among them, LDH in slices of liver exposed to carbon tetrachloride [77]. We believe that these last two reports may better explain our findings because these authors also

used tissue slices, while, in the reports mentioned above, cell cultures were used. On the other hand, as was described in the introduction, the bioactive compounds we used have antioxidant properties. These findings suggest that inactivation or inhibition of LDH may be more common than previously thought, and investigators should be aware of this at the moment of selecting LDH release as an endpoint for evaluating cytotoxicity.

Taken together, variability in the obtained results is possibly due to the fact that each patient's tumor behaves differently to anticancer drugs, which in turn is due in part to the extensive intratumoral heterogeneity present in each individual tumor [43, 78]. With regard to the last statement, since the 1950s, differential responses to the same drugs in patients with the same histological type of cancer have been reported, including adverse side effects [79]. These differences have been studied in the following years and today it is an accepted fact that individual response to drugs (resistance or sensitivity) depends, among other factors, on the mechanisms of disease (pharmacodynamics), the handling of the drug by patients (pharmacokinetics), the intratumoral heterogeneity, and complex signaling pathways, many of which are still unknown [78, 80, 81]. All these variations are reflected in the intratumoral heterogeneity because of factors that cause genomic instability [29, 78]. Intratumoral heterogeneity and the tumor microenvironment are conserved in the *ex vivo* model we are proposing, and it is possibly one of the reasons why the response to bioactive compounds is different in samples from patients, even when they had breast cancer at the same clinical stage, the same histological type, but different molecular classification.

5. Conclusions

In conclusion, our results show that organotypic cultures of breast cancer explants offer an alternative model for the *ex vivo* evaluation of novel compounds with potential anticancer properties, assessing the synergic effect with known anticancer compounds. This model opens perspectives to study biological effects of conventional and innovative treatment strategies in breast cancer research and to analyze different mechanisms of carcinogenesis in other human tumors.

Conflict of Interests

The authors declare that they have no conflict of interests.

Acknowledgments

This work was partially supported by a grant from the Fondo de Investigación en Salud (CIS/IMSS) FIS/IMSS/PROT/G1145. Irma Edith Carranza-Torres received a Fellowship for Ph.D. studies from CONACYT (no. 338954).

References

[1] J. Ferlay, I. Soerjomataram, M. Ervik et al., *GLOBOCAN 2012 v1.0, Cancer Incidence and Mortality Worldwide in 2012: IARC Cancer Base No.11*, International Agency for Research on Cancer, Lyon, France, 2013, http://globocan.iarc.fr.

[2] L. Vera-Ramirez, P. Sanchez-Rovira, C. L. Ramirez-Tortosa, J. L. Quiles, M. Ramirez-Tortosa, and J. A. Lorente, "Transcriptional shift identifies a set of genes driving breast cancer chemoresistance," *PLoS ONE*, vol. 8, no. 1, Article ID e53983, 2013.

[3] C. Morrissey, B. Gallis, J. W. Solazzi et al., "Effect of artemisinin derivatives on apoptosis and cell cycle in prostate cancer cells," *Anti-Cancer Drugs*, vol. 21, no. 4, pp. 423–432, 2010.

[4] G.-J. Du, Q. Dai, S. Williams, C.-Z. Wang, and C.-S. Yuan, "Synthesis of protopanaxadiol derivatives and evaluation of their anticancer activities," *Anti-Cancer Drugs*, vol. 22, no. 1, pp. 35–45, 2011.

[5] H. J. Kang, S. H. Lee, J. E. Price, and L. S. Kim, "Curcumin suppresses the paclitaxel-induced nuclear factor-kappaB in breast cancer cells and potentiates the growth inhibitory effect of paclitaxel in a breast cancer nude mice model," *The Breast Journal*, vol. 15, no. 3, pp. 223–229, 2009.

[6] Y. Wang, L. Rouggly, M. You, and R. Lubet, "Animal models of lung cancer: characterization and use for chemoprevention research," *Progress in Molecular Biology and Translational Science*, vol. 105, pp. 211–226, 2012.

[7] X.-W. Yang, X.-L. Wang, L.-Q. Cao et al., "Green tea polyphenol epigallocatechin-3-gallate enhances 5-fluorouracil-induced cell growth inhibition of hepatocellular carcinoma cells," *Hepatology Research*, vol. 42, no. 5, pp. 494–501, 2012.

[8] A. J. Alonso-Castro, M. L. Villarreal, L. A. Salazar-Olivo, M. Gomez-Sanchez, F. Dominguez, and A. Garcia-Carranca, "Mexican medicinal plants used for cancer treatment: pharmacological, phytochemical and ethnobotanical studies," *Journal of Ethnopharmacology*, vol. 133, no. 3, pp. 945–972, 2011.

[9] K.-K. Bai, F.-L. Chen, Z. Yu, Y.-Q. Zheng, Y.-N. Li, and Y.-H. Guo, "Synthesis of [3β-acetoxy-urs-12-en-28-oyl]-1-monoglyceride and investigation on its anti tumor effects against BGC-823," *Bioorganic and Medicinal Chemistry*, vol. 19, no. 13, pp. 4043–4050, 2011.

[10] I. Berdowska, B. Zieliński, I. Fecka, J. Kulbacka, J. Saczko, and A. Gamian, "Cytotoxic impact of phenolics from Lamiaceae species on human breast cancer cells," *Food Chemistry*, vol. 141, no. 2, pp. 1313–1321, 2013.

[11] C. M. Kaefer and J. A. Milner, "The role of herbs and spices in cancer prevention," *The Journal of Nutritional Biochemistry*, vol. 19, no. 6, pp. 347–361, 2008.

[12] A. Link, F. Balaguer, and A. Goel, "Cancer chemoprevention by dietary polyphenols: promising role for epigenetics," *Biochemical Pharmacology*, vol. 80, no. 12, pp. 1771–1792, 2010.

[13] H. Wang, T. O. Khor, L. Shu et al., "Plants vs. cancer: a review on natural phytochemicals in preventing and treating cancers and their druggability," *Anti-Cancer Agents in Medicinal Chemistry*, vol. 12, no. 10, pp. 1281–1305, 2012.

[14] W. J. Lee and B. T. Zhu, "Inhibition of DNA methylation by caffeic acid and chlorogenic acid, two common catechol-containing coffee polyphenols," *Carcinogenesis*, vol. 27, no. 2, pp. 269–277, 2006.

[15] G. L. Gierach, N. D. Freedman, A. Andaya et al., "Coffee intake and breast cancer risk in the NIH-AARP diet and health study cohort," *International Journal of Cancer*, vol. 131, no. 2, pp. 452–460, 2012.

[16] E. Viveros-Valdez, C. Rivas-Morales, A. Oranday-Cárdenas, J. Castro-Garza, and P. Carranza-Rosales, "Antiproliferative effect from the Mexican poleo (*Hedeoma drummondii*)," *Journal of Medicinal Food*, vol. 13, no. 3, pp. 740–742, 2010.

[17] D. Es-Saady, A. Simon, C. Jayat-Vignoles, A. J. Chulia, and C. Delage, "MCF-7 cell cycle arrested at G1 through ursolic acid, and increased reduction of tetrazolium salts," *Anticancer Research*, vol. 16, no. 1, pp. 481–486, 1996.

[18] C. Martín-Cordero, M. Reyes, M. J. Ayuso, and M. V. Toro, "Cytotoxic triterpenoids from *Erica andevalensis*," *Zeitschrift fur Naturforschung Section C: Journal of Biosciences*, vol. 56, no. 1-2, pp. 45–48, 2001.

[19] I. Lee, J. Lee, Y. H. Lee, and J. Leonard, "Ursolic acid-induced changes in tumor growth, O_2 consumption, and tumor interstitial fluid pressure," *Anticancer Research*, vol. 21, no. 4, pp. 2827–2833, 2001.

[20] E. Kassi, T. G. Sourlingas, M. Spiliotaki et al., "Ursolic acid triggers apoptosis and Bcl-2 downregulation in MCF-7 breast cancer cells," *Cancer Investigation*, vol. 27, no. 7, pp. 723–733, 2009.

[21] C.-T. Yeh, C.-H. Wu, and G.-C. Yen, "Ursolic acid, a naturally occurring triterpenoid, suppresses migration and invasion of human breast cancer cells by modulating c-Jun *N*-terminal kinase, Akt and mammalian target of rapamycin signaling," *Molecular Nutrition & Food Researc*, vol. 54, no. 9, pp. 1285–1295, 2010.

[22] J.-Z. Shan, Y.-Y. Xuan, S.-Q. Ruan, and M. Sun, "Proliferation-inhibiting and apoptosis-inducing effects of ursolic acid and oleanolic acid on multi-drug resistance cancer cells *in vitro*," *Chinese Journal of Integrative Medicine*, vol. 17, no. 8, pp. 607–611, 2011.

[23] M. A. Furtado, L. C. F. de Almeida, R. A. Furtado, W. R. Cunha, and D. C. Tavares, "Antimutagenicity of rosmarinic acid in Swiss mice evaluated by the micronucleus assay," *Mutation Research—Genetic Toxicology and Environmental Mutagenesis*, vol. 657, no. 2, pp. 150–154, 2008.

[24] M. Shekarchi, H. Hajimehdipoor, S. Saeidnia, A. R. Gohari, and M. P. Hamedani, "Comparative study of rosmarinic acid content in some plants of Labiatae family," *Pharmacognosy Magazine*, vol. 8, no. 29, pp. 37–41, 2012.

[25] K. Venkatachalam, S. Gunasekaran, V. A. S. Jesudoss, and N. Namasivayam, "The effect of rosmarinic acid on 1,2-dimethylhydrazine induced colon carcinogenesis," *Experimental and Toxicologic Pathology*, vol. 65, no. 4, pp. 409–418, 2013.

[26] J. Paluszczak, V. Krajka-Kuźniak, and W. Baer-Dubowska, "The effect of dietary polyphenols on the epigenetic regulation of gene expression in MCF7 breast cancer cells," *Toxicology Letters*, vol. 192, no. 2, pp. 119–125, 2010.

[27] T. P. Stanojković, A. Konić-Ristić, Z. D. Juranić et al., "Cytotoxic and cell cycle effects induced by two herbal extracts on human cervix carcinoma and human breast cancer cell lines.," *Journal of medicinal food*, vol. 13, no. 2, pp. 291–297, 2010.

[28] Y. Xu, Z. Jiang, G. Ji, and J. Liu, "Inhibition of bone metastasis from breast carcinoma by rosmarinic acid," *Planta Medica*, vol. 76, no. 10, pp. 956–962, 2010.

[29] S. J. Conde, R. D. A. M. Luvizotto, M. T. De Síbio, and C. R. Nogueira, "Human breast tumor slices as an alternative approach to cell lines to individualize research for each patient," *European Journal of Cancer Prevention*, vol. 21, no. 4, pp. 333–335, 2012.

[30] I. A. M. de Graaf, P. Olinga, M. H. de Jager et al., "Preparation and incubation of precision-cut liver and intestinal slices for application in drug metabolism and toxicity studies," *Nature Protocols*, vol. 5, no. 9, pp. 1540–1551, 2010.

[31] M. Possidente, S. Dragoni, G. Franco et al., "Rat intestinal precision-cut slices as an *in vitro* model to study xenobiotic interaction with transporters," *European Journal of Pharmaceutics and Biopharmaceutics*, vol. 79, no. 2, pp. 343–348, 2011.

[32] P. Olinga and D. Schuppan, "Precision-cut liver slices: a tool to model the liver *ex vivo*," *Journal of Hepatology*, vol. 58, no. 6, pp. 1252–1253, 2013.

[33] R. De Kanter, A. Tuin, E. van de Kerkhof et al., "A new technique for preparing precision-cut slices from small intestine and colon for drug biotransformation studies," *Journal of Pharmacological and Toxicological Methods*, vol. 51, no. 1, pp. 65–72, 2005.

[34] H.-U. Kasper, V. Dries, U. Drebber, M. A. Kern, H. P. Dienes, and P. Schirmacher, "Precision cut tissue slices of the liver as morphological tool for investigation of apoptosis," *In Vivo*, vol. 19, no. 2, pp. 423–432, 2005.

[35] P. Carranza-Rosales, M. G. Santiago-Mauricio, N. E. Guzmán-Delgado et al., "Precision-cut hamster liver slices as an *ex vivo* model to study amoebic liver abscess," *Experimental Parasitology*, vol. 126, no. 2, pp. 117–125, 2010.

[36] P. Carranza-Rosales, M. G. Santiago-Mauricio, N. E. Guzmán-Delgado et al., "Induction of virulence factors, apoptosis, and cytokines in precision-cut hamster liver slices infected with *Entamoeba histolytica*," *Experimental Parasitology*, vol. 132, no. 4, pp. 424–433, 2012.

[37] T. O. Kirby, A. Rivera, D. Rein et al., "A novel *ex vivo* model system for evaluation of conditionally replicative adenoviruses therapeutic efficacy and toxicity," *Clinical Cancer Research*, vol. 10, no. 24, pp. 8697–8703, 2004.

[38] M. A. Stoff-Khalili, A. A. Rivera, L. P. Le et al., "Employment of liver tissue slice analysis to assay hepatotoxicity linked to replicative and nonreplicative adenoviral agents," *Cancer Gene Therapy*, vol. 13, no. 6, pp. 606–618, 2006.

[39] M. G. Rots, M. G. L. Elferink, W. M. Gommans et al., "An ex vivo human model system to evaluate specificity of replicating and non-replicating gene therapy agents," *The Journal of Gene Medicine*, vol. 8, no. 1, pp. 35–41, 2006.

[40] M. Zimmermann, S. Armeanu, I. Smirnow et al., "Human presicion-cut liver tumor slices as a tumor patient-individual predictives test system for oncolytic measles vaccine viruses," *International Journal of Oncology*, vol. 34, no. 5, pp. 1247–1256, 2009.

[41] M. A. van Geer, K. F. D. Kuhlmann, C. T. Bakker, F. J. W. ten Kate, R. P. J. O. Elferink, and P. J. Bosma, "*Ex-vivo* evaluation of gene therapy vectors in human pancreatic (cancer) tissue slices," *World Journal of Gastroenterology*, vol. 15, no. 11, pp. 1359–1366, 2009.

[42] M. A. Kern, A. M. Haugg, E. Eiteneuer et al., "*Ex vivo* analysis of antineoplastic agents in precision-cut tissue slices of human origin: effects of cyclooxygenase-2 inhibition in hepatocellular carcinoma," *Liver International*, vol. 26, no. 5, pp. 604–612, 2006.

[43] P. Mestres, A. Morguet, W. Schmidt, A. Kob, and E. Thedinga, "A new method to assess drug sensitivity on breast tumor acute slices preparation," *Annals of the New York Academy of Sciences*, vol. 1091, pp. 460–469, 2006.

[44] H. van der Kuip, T. E. Mürdter, M. Sonnenberg et al., "Short term culture of breast cancer tissues to study the activity of the anticancer drug taxol in an intact tumor environment," *BMC Cancer*, vol. 6, article 86, 2006.

[45] N. Parajuli and W. Doppler, "Precision-cut slice cultures of tumors from MMTV-neu mice for the study of the *ex vivo* response to cytokines and cytotoxic drugs," *In Vitro Cellular & Developmental Biology—Animal*, vol. 45, no. 8, pp. 442–450, 2009.

[46] R. Pazdur, A. P. Kudelka, J. J. Kavanagh, P. R. Cohen, and M. N. Raber, "The taxoids: paclitaxel (Taxol) and docetaxel (Taxotere)," *Cancer Treatment Reviews*, vol. 19, no. 4, pp. 351–386, 1993.

[47] D. Lister-Sharp, M. S. McDonagh, K. S. Khan, and J. Kleijnen, "A rapid and systematic review of the effectiveness and cost-effectiveness of the taxanes used in the treatment of advanced breast and ovarian cancer," *Health Technology Assessment*, vol. 4, no. 17, pp. 1–113, 2000.

[48] K. D. Miller and G. W. Sledge Jr., "Taxanes in the treatment of breast cancer: a prodigy comes of age," *Cancer Investigation*, vol. 17, no. 2, pp. 121–136, 1999.

[49] C. C. Neto, A. J. Vaisberg, B.-N. Zhou, D. G. I. Kingston, and G. B. Hammond, "Cytotoxic triterpene acids from the peruvian medicinal plant *Polylepis racemosa*," *Planta Medica*, vol. 66, no. 5, pp. 483–484, 2000.

[50] E. Evdokimova, H. Taper, and P. B. Calderon, "Effects of bacterial endotoxin (lipopolysaccharides) on survival and metabolism of cultured precision-cut rat liver slices," *Toxicology in Vitro*, vol. 16, no. 1, pp. 47–54, 2002.

[51] S. Gurunathan, J. W. Han, V. Eppakayala, M. Jeyaraj, and J.-H. Kim, "Cytotoxicity of biologically synthesized silver nanoparticles in MDA-MB-231 human breast cancer cells," *BioMed Research International*, vol. 2013, Article ID 535796, 10 pages, 2013.

[52] S. M. Veronese, M. Gambacorta, O. Gottardi, F. Scanzi, M. Ferrari, and P. Lampertico, "Proliferation index as a prognostic marker in breast cancer," *Cancer*, vol. 71, no. 12, pp. 3926–3931, 1993.

[53] J. A. Hickman, R. Graeser, R. de Hoogt et al., "Three-dimensional models of cancer for pharmacology and cancer cell biology: capturing tumor complexity *in vitro*/*ex vivo*," *Biotechnology Journal*, vol. 9, no. 9, pp. 1115–1128, 2014.

[54] J.-S. Diallo, D. Roy, H. Abdelbary, N. de Silva, and J. C. Bell, "*Ex vivo* infection of live tissue with oncolytic viruses," *Journal of Visualized Experiments*, no. 52, Article ID e2854, 2011.

[55] D. L. Holliday, M. A. Moss, S. Pollock et al., "The practicalities of using tissue slices as preclinical organotypic breast cancer models," *Journal of Clinical Pathology*, vol. 66, no. 3, pp. 253–255, 2013.

[56] F. Pirnia, S. Frese, B. Gloor et al., "*Ex vivo* assessment of chemotherapy-induced apoptosis and associated molecular changes in patient tumor samples," *Anticancer Research*, vol. 26, no. 3, pp. 1765–1772, 2006.

[57] L. Horev-Azaria, G. Baldi, D. Beno et al., "Predictive Toxicology of cobalt ferrite nanoparticles: comparative *in-vitro* study of different cellular models using methods of *knowledge discovery from data*," *Particle and Fibre Toxicology*, vol. 10, no. 1, article 32, 2013.

[58] C. N. Ramirez, C. Antczak, and H. Djaballah, "Cell viability assessment: toward content-rich platforms," *Expert Opinion on Drug Discovery*, vol. 5, no. 3, pp. 223–233, 2010.

[59] S. N. Rampersad, "Multiple applications of alamar blue as an indicator of metabolic function and cellular health in cell viability bioassays," *Sensors*, vol. 12, no. 9, pp. 12347–12360, 2012.

[60] R. Yerushalmi, R. Woods, P. M. Ravdin, M. M. Hayes, and K. A. Gelmon, "Ki67 in breast cancer: prognostic and predictive potential," *The Lancet Oncology*, vol. 11, no. 2, pp. 174–183, 2010.

[61] C. Milani, J. Welsh, M. L. H. Katayama et al., "Human breast tumor slices: a model for identification of vitamin D regulated genes in the tumor microenvironment," *The Journal of Steroid Biochemistry and Molecular Biology*, vol. 121, no. 1-2, pp. 151–155, 2010.

[62] M. Sonnenberg, H. van der Kuip, S. Haubeiß et al., "Highly variable response to cytotoxic chemotherapy in carcinoma-associated fibroblasts (CAFs) from lung and breast," *BMC Cancer*, vol. 8, article 364, 2008.

[63] M. Kampa, V.-I. Alexaki, G. Notas et al., "Antiproliferative and apoptotic effects of selective phenolic acids on T47D human breast cancer cells: potential mechanisms of action," *Breast Cancer Research*, vol. 6, no. 2, pp. R63–R74, 2004.

[64] A. Bishayee, S. Ahmed, N. Brankov, and M. Perloff, "Triterpenoids as potential agents for the chemoprevention and therapy of breast cancer," *Frontiers in Bioscience*, vol. 16, no. 3, pp. 980–996, 2011.

[65] P. J. Morin, "Drug resistance and the microenvironment: nature and nurture," *Drug Resistance Updates*, vol. 6, no. 4, pp. 169–172, 2003.

[66] H.-T. Chang, I.-L. Chen, C.-T. Chou et al., "Effect of caffeic acid on Ca^{2+} homeostasis and apoptosis in SCM1 human gastric cancer cells," *Archives of Toxicology*, vol. 87, no. 12, pp. 2141–2150, 2013.

[67] T. Luo, J. Wang, Y. Yin et al., "(-)-Epigallocatechin gallate sensitizes breast cancer cells to paclitaxel in a murine model of breast carcinoma," *Breast Cancer Research*, vol. 12, no. 1, article R8, 2010.

[68] Y. Li, D. Xing, Q. Chen, and W. R. Chen, "Enhancement of chemotherapeutic agent-induced apoptosis by inhibition of NF-kappaB using ursolic acid," *International Journal of Cancer*, vol. 127, no. 2, pp. 462–473, 2010.

[69] G.-Q. Chen, Z.-W. Yao, W.-P. Zheng, L. Chen, H. Duan, and Y. Shen, "Combined antitumor effect of ursolic acid and 5-fluorouracil on human esophageal carcinoma cell Eca-109 *in vitro*," *Chinese Journal of Cancer Research*, vol. 22, no. 1, pp. 62–67, 2010.

[70] M. González-Vallinas, S. Molina, G. Vicente et al., "Antitumor effect of 5-fluorouracil is enhanced by rosemary extract in both drug sensitive and resistant colon cancer cells," *Pharmacological Research*, vol. 72, pp. 61–68, 2013.

[71] C.-L. Lin, R.-F. Chen, J. Y.-F. Chen et al., "Protective effect of caffeic acid on paclitaxel induced anti-proliferation and apoptosis of lung cancer cells involves NF-κb pathway," *International Journal of Molecular Sciences*, vol. 13, no. 5, pp. 6236–6245, 2012.

[72] L. H. Lash and R. K. Zalups, "Mercuric chloride-induced cytotoxicity and compensatory hypertrophy in rat kidney proximal tubular cells," *Journal of Pharmacology and Experimental Therapeutics*, vol. 261, no. 2, pp. 819–829, 1992.

[73] D. M. Kendig and J. B. Tarloff, "Inactivation of lactate dehydrogenase by several chemicals: implications for *in vitro* toxicology studies," *Toxicology in Vitro*, vol. 21, no. 1, pp. 125–132, 2007.

[74] M. C. Hohnholt, E. M. Blumrich, and R. Dringen, "Multiassay analysis of the toxic potential of hydrogen peroxide on cultured neurons," *Journal of Neuroscience Research*, 2014.

[75] K. Tulpule, M. C. Hohnholt, J. Hirrlinger, and R. Dringen, "Primary cultures of astrocytes and neurons as model systems to study the metabolism and metabolite export from brain cells," in *Brain Energy Metabolism*, J. Hirrlinger and W. S. Waagepetersen, Eds., vol. 90, pp. 45–72, Springer, New York, NY, USA, 2014.

[76] M. da Silva Morrone, A. M. de Assis, R. F. da Rocha et al., "*Passiflora manicata* (Juss.) aqueous leaf extract protects against reactive oxygen species and protein glycation in vitro and ex

vivo models," *Food and Chemical Toxicology*, vol. 60, pp. 45–51, 2013.

[77] Y. Liu, L. Cao, J. Du et al., "Protective effects of *Lycium barbarum* polysaccharides against carbon tetrachloride-induced hepatotoxicity in precision-cut liver slices in vitro and in vivo in common carp (*Cyprinus carpio* L.)," *Comparative Biochemistry and Physiology Part C: Toxicology and Pharmacology*, vol. 169, pp. 65–72, 2015.

[78] M. Gerlinger, A. J. Rowan, S. Horswell et al., "Intratumor heterogeneity and branched evolution revealed by multiregion sequencing," *The New England Journal of Medicine*, vol. 366, no. 10, pp. 883–892, 2012.

[79] M. Eichelbaum, N. Spannbrucker, and H. J. Dengler, "Proceedings: N-oxidation of sparteine in man and its interindividual differences," *Naunyn-Schmiedeberg's Archives of Pharmacology*, vol. 287, supplement R94, 1975.

[80] W.-Q. Ge, J.-X. Pu, and S.-Y. Zheng, "Clinical application of the adenosine triphosphate-based response assay in intravesical chemotherapy for superficial bladder cancer," *Asian Pacific Journal of Cancer Prevention*, vol. 13, no. 2, pp. 689–692, 2012.

[81] C. Marquette and L. Nabell, "Chemotherapy-resistant metastatic breast cancer," *Current Treatment Options in Oncology*, vol. 13, no. 2, pp. 263–275, 2012.

Hindawi Publishing Corporation
BioMed Research International
Volume 2015, Article ID 561589, 11 pages
http://dx.doi.org/10.1155/2015/561589

Research Article

Antioxidant and Proapoptotic Activities of *Sclerocarya birrea* [(A. Rich.) Hochst.] Methanolic Root Extract on the Hepatocellular Carcinoma Cell Line HepG2

Maria Francesca Armentano,[1] Faustino Bisaccia,[1] Rocchina Miglionico,[1] Daniela Russo,[1] Nicoletta Nolfi,[1] Monica Carmosino,[1] Paula B. Andrade,[2] Patrícia Valentão,[2] Moussoukhoye Sissokho Diop,[3] and Luigi Milella[1]

[1]*Department of Science, Basilicata University, Viale dell'Ateneo Lucano 10, 85100 Potenza, Italy*
[2]*REQUIMTE/LAQV, Laboratório de Farmacognosia, Departamento de Química, Faculdade de Farmácia, Universidade do Porto, Rua de Jorge Viterbo Ferreira No. 228, 4050-313 Porto, Portugal*
[3]*Faculte des Sciences et Techniques, Universite Cheikh Anta Diop de Dakar, BP 5005, Dakar-Fann, Senegal*

Correspondence should be addressed to Luigi Milella; luigi.milella@unibas.it

Received 25 December 2014; Revised 9 March 2015; Accepted 14 March 2015

Academic Editor: Chin-Chung Wu

The main goal of this study was to characterize the *in vitro* antioxidant activity and the apoptotic potential of *S. birrea* methanolic root extract (MRE). Among four tested extracts, obtained with different solvents, MRE showed the highest content of polyphenols, flavonoids, and tannins together with antioxidant activities tested with superoxide, nitric oxide, ABTS, and beta-carotene bleaching assays. Moreover, the cytotoxic effect of MRE was evaluated on the hepatocarcinoma cell line HepG2. In these cells, MRE treatment induced apoptosis and generated reactive oxygen species (ROS) in dose-dependent manner. The cytotoxic effect promoted by MRE was prevented by pretreatment of HepG2 cells with N-acetyl-L-cysteine (NAC), suggesting that oxidative stress was pivotal in MRE-mediated cell death. Moreover, we showed that the MRE treatment induced the mitochondrial membrane depolarization and the cytochrome *c* release from mitochondria into the cytosol. It suggests that the apoptosis occurred in a mitochondrial-dependent pathway. Interestingly, MRE showed a sensibly lower cytotoxicity, associated with a low increase of ROS, in normal human dermal fibroblasts compared to HepG2 cells. It is suggested that the methanolic root extract of *S. Birrea* is able to selectively increase intracellular ROS levels in cancer cells, promoting cell death.

1. Introduction

Natural products have found many applications in the fields of medicine, pharmacy, and biology. A considerable number (approximately 60%) of currently used antitumor agents are molecules identified and isolated from plants or their synthetic or semisynthetic derivatives [1, 2]. Some natural compounds are able to trigger the apoptosis signalling system in cancer cells disturbing their proliferation [3, 4], though their molecular mechanisms of action are not always well understood.

It is well established that carcinogenesis is closely associated with elevated levels of intracellular free radicals (ROS/RNS) to drive proliferation and other events required for tumor progression. This event establishes a state of increased basal oxidative stress, making cells vulnerable to chemotherapeutic agents, including plant-derived polyphenols, that further increase ROS generation or that weaken cell antioxidant defenses [5].

Sclerocarya birrea (A. Rich.) Hochst., known as marula, is a savannah tree belonging to the Anacardiaceae family [6]. The marula tree has been the subject of numerous chemical, biological, and environmental investigations since 1906 [7]. It has been identified as one of five fruit tree species that should be integrated in the domestication process because it is an important food and medicinal source for rural areas

[8, 9]. Different parts of the plant are traditionally used: the fruits are eaten or processed to make beer or jam; the kernels are eaten or used for oil extraction; the leaves are used as forage for livestock; the stem-bark, root, and leaf extracts of *S. birrea* are used against human ailments [6]. Hamza et al. (2006) have reported that methanolic extracts from *S. birrea* roots inhibited the growth of *Candida* spp. and *Cryptococcus neoformans* [9]. It was also demonstrated that methanol and water root extracts act as potent antioxidants [10, 11]. Moreover, water and acetone extracts of *S. birrea* stem bark showed anticancer and proapoptotic activities [12].

The aim of this study was to examine the efficacy of *S. birrea* methanolic root extract (MRE) as an antioxidant, using *in vitro* assays. Additionally, its cytotoxic activity on the human hepatocarcinoma cell line HepG2 was evaluated here for the first time.

Obtained results show that MRE presents a strong antioxidant activity *in vitro* and a prooxidant activity in cells. Moreover, this extract shows higher ROS-mediated cytotoxic effect in HepG2 cells compared to normal human fibroblasts, suggesting its possible use for selectively killing malignant cells [5].

2. Materials and Methods

2.1. Plant Materials. Roots of *Sclerocarya birrea* (Anacardiaceae family) were collected in Senegal in September 2010. Roots were cleaned to remove foreign particles, cut into small pieces, and dried at room temperature. Plant material was successively extracted with 5 volumes (v/w) of *n*-hexane, chloroform, chloroform : methanol 9 : 1, and methanol by a sequential maceration, as described previously [11], obtaining 4 extracts with increasing polarity: *n*-hexane (HRE), $CHCl_3$ (CRE), $CHCl_3$: MeOH (9 : 1) (CMRE), and MeOH (MRE) root extracts. Extracts were dried and stored at 4°C until the use.

2.2. Chemicals. Folin Ciocalteu's reagent, sodium carbonate (Na_2CO_3), aluminium chloride ($AlCl_3$), sodium nitrate ($NaNO_3$), sodium hydroxide (NaOH), bovine serum albumin (BSA), sodium dodecyl sulphate (SDS), triethanolamine, iron(III) chloride ($FeCl_3$), ABTS [2,2′-azinobis(3-ethylbenzothiazoline-6-sulfonic acid)], potassium persulfate, β-carotene, linoleic acid, Tween 20, ascorbic acid, sodium nitroprusside (SNP), sulfanilamide, naphthylethylenediamine, nicotinamide adenine dinucleotide (NADH), phenazine methosulphate (PMS), nitroblue tetrazolium (NBT), potassium phosphate monobasic (KH_2PO_4), gallic acid, quercetin, tannic acid, 6-hydroxy-2,5,7,8-tetramethylchromane-2-carboxylic acid (trolox), butylated hydroxytoluene (BHT), Dulbecco's Modified Eagle Medium (DMEM), dimethyl sulfoxide (DMSO), Calcein-AM, 2′,7′-dichlorodihydrofluorescein diacetate (DCFH-DA), Hoechst 33258 solution, and N-acetyl-L-cysteine (NAC) were purchased from Sigma-Aldrich (Milan, Italy). Solvents as acetic acid (CH_3COOH), hydrochloric acid (HCl), chloroform ($CHCl_3$), and phosphoric acid (H_3PO_4) were purchased from Carlo Erba Reagents (Milan, Italy).

Trypsin-EDTA solution, FBS, glutamine, penicillin-streptomycin, and PBS were purchased from Euroclone (Milan, Italy). TMRM (Life Technologies) was a kind gift from Dr. M. Lasorsa (IBBE, CNR, Bari).

2.3. Total Phenolic Content. The total phenolic content (TPC) was determined for each extract, by Folin-Ciocalteu assay, as previously reported with slight modification [13]. Briefly, 75 μL of diluted extract and 425 μL of distilled water were added to 500 μL Folin-Ciocalteu reagent and 500 μL of Na_2CO_3 (10% w/v). The mixture was mixed and incubated for 1 h in the dark at room temperature. After incubation, the absorbance was measured at 723 nm. Gallic acid was used as standard to plot the regression curve. TPC was than expressed as mg gallic acid equivalent (GAE)/g of dried extract.

For all spectrophotometric measurements, a CARY 1E UV-VIS spectrophotometer (Varian, Leini, Italy) was used.

2.4. Total Flavonoid Content. An aliquot (150 μL) of each extract was added to 45 μL of 5% $NaNO_3$ into microcentrifuge tube. In the fifth and in the sixth minute, respectively, 90 μL of 10% $AlCl_3$ and 300 μL of 1 M NaOH solution were added. The final volume of the mixture was then brought to 1.5 mL by adding distilled water. The absorbance was measured against blank reagent at 510 nm after 10 minutes of incubation at room temperature [14]. Quercetin was used as standard to plot the regression curve. The total flavonoid content (TFC) was expressed as mg of quercetin equivalent/g of dried extract (mg QE/g of extract).

2.5. Total Tannin Content. To 250 μL of each extract, 500 μL of bovine serum albumin solution in 0.2 M acetic buffer, pH 5.0 with 0.17 M NaCl was added and mixed carefully [15]. After 15 min, samples were centrifuged at 5000 g for 15 min. The supernatant was removed, and the pellet was dissolved in 1 mL of aqueous solution containing 1% SDS and 4% triethanolamine. Then 250 μL of 0.01 M $FeCl_3$ in 0.01 M HCl was added. After 30 min, the absorbance was recorded at 510 nm. Total tannin content (TTC) was expressed as mg of tannic acid equivalent/g of dried extract (mg TAE/g of extract), in this case tannic acid was used to construct a regression curve.

2.6. ABTS Assay. The free radical scavenging capacity of each plant extract was also studied using the 2,2′-azinobis(3-ethylbenzothiazoline-6-sulfonic acid) diammonium salt ($ABTS^{\bullet}$) radical assay [16]. ABTS was dissolved in deionized water to a 7 mM concentration and its radical cation ($ABTS^{+\bullet}$) was produced by reacting ABTS solution with 2.45 mM potassium persulfate and allowing the mixture to stand in the dark at room temperature for 12–16 h before use. Each extract (75 μL) was added to 1425 μL of $ABTS^{+\bullet}$ solution and the absorbance was measured after 2 h of incubation in the dark. All solutions were fresh prepared for the analysis. Results are expressed as percentage of radical inhibition. Trolox was used as reference standard.

2.7. Beta-Carotene Bleaching Assay. The antioxidant activity was evaluated by the β-carotene-linoleic acid bleaching method (BCB) as previously described [17, 18]. The absorbance was measured at 470 nm. Results are expressed as percentage of antioxidant activity (% AA).

2.8. Nitric Oxide ($NO^{\bullet}$) Radical Scavenging Activity. The antiradical activity was determined spectrophotometrically, according to a previously described procedure [19]. EC50 was calculated from three independent assays, performed in triplicate. Results are expressed as percentage of radical inhibition. Ascorbic acid was used as positive control.

2.9. Superoxide Anion ($O_2^{\bullet-}$) Scavenging Activity. The effect of each extract on the superoxide radical-induced reduction of NBT was monitored at 560 nm. Superoxide radicals were generated by the NADH/PMS system, as previously reported [19]. For each extract, different concentrations were tested. Results are expressed as percentage of radical inhibition. Ascorbic acid was used as positive control.

2.10. Cell Culture and Drug Treatment. The human hepatocellular carcinoma cell line HepG2 was kindly gifted from Dr. V. Infantino (University of Basilicata-Italy). HepG2 cells were cultured in DMEM (supplemented with 10% fetal bovine serum, 2 mM glutamine, 100 U/mL penicillin, and 100 μg/mL streptomycin) and maintained at 37°C in a humidified atmosphere containing 5% CO_2.

Normal human dermal fibroblasts (adult, HDFa, Life Technologies) were cultured in DMEM (supplemented with 10% fetal bovine serum, 2 mM glutamine, 100 U/mL penicillin, 100 μg/mL streptomycin, and 1% nonessential amino acids) and maintained at 37°C in a humidified atmosphere containing 5% CO_2. Cultures were routinely passed at 70–80% of confluence and, for this study, cultures were not expanded for more than 4–8 passages.

The methanolic root extract was dissolved in DMSO at 50 mg/mL as a stock solution and diluted to the required concentrations with fresh medium immediately before use. The final DMSO concentration in the cultures was 0.4% (v/v), which did not affect cell growth when compared with the vehicle-free controls. DMSO treated cells were used as control in all the experiments.

2.11. Cytotoxicity Assay. The cytotoxicity of *S. birrea* methanolic root extract was tested against HepG2 and normal human dermal fibroblasts cell lines using Calcein-AM viability assay. Calcein-AM is a nonfluorescent, hydrophobic compound that easily permeates intact, live cells. Once inside the cells, the hydrolysis of Calcein-AM by endogenous esterases produces calcein, a hydrophilic, highly negatively charged fluorescent compound that is well-retained in the cytoplasm of live cells. The fluorescent signal generated from the assay is proportional to the number of living cells in the sample. In brief, HepG2 and fibroblasts cells were seeded at a density of 1×10^4/well in 96-well black-walled plates for 24 h and then treated with different concentrations of MRE (10, 50, 100, and 200 μg/mL) for 24 h and 48 h. Moreover, HepG2 cells were pretreated with 10 mM NAC, added 1 h before each treatment. After discarding the medium from wells, 100 μL of 1 μM Calcein-AM in PBS was added to each well, incubating at 37°C for 30 min. The fluorescence was measured by GLOMAX Multidetection System (Promega, Madison, WI, USA) using blue filter (Ex 490 nm, Em 510–570 nm).

2.12. Observation of Morphological Changes. HepG2 cells were cultured as above, seeded in 12-well plates at a density of 2×10^5 cells per well, and treated with extract at different concentrations (10, 50, 100, and 200 μg/mL) for 24 h, with or without 10 mM of N-acetyl-L-cysteine (NAC), added 1 h before each treatment. The cellular morphology was observed using inverted phase contrast microscopy (Nikon Eclipse TS100).

Apoptosis was determined by the assessment of nuclear morphology using Hoechst 33258 DNA staining. Briefly, cells were seeded at a density of 2×10^5/well in 12-well plates and were allowed to adhere overnight to glass coverslips. After treatment with root extract at different concentrations (10, 50, 100, and 200 μg/mL) for 24 h, cells were fixed with 4% paraformaldehyde for 20 min, washed with PBS, and stained with 10 μg/mL Hoechst 33258 at room temperature for 10 min in the dark. The cells were washed with PBS for morphologic observation by fluorescence microscopy (NIKON Eclipse 80i).

2.13. Measurement of Reactive Oxygen Species Generation. The intracellular level of ROS was determined using a cell-permeable fluorogenic probe, 2′,7′-dichlorofluorescein diacetate (DCFH-DA). This molecule is deacetylated by intracellular esterases and converted to nonfluorescent dichlorodihydrofluorescein (DCFH), which is oxidized rapidly to the highly fluorescent compound dichlorofluorescein (DCF) in the presence of ROS. HepG2 and fibroblasts cells were seeded into dark 96-well tissue culture plates at a density of 5×10^4 cells/well treated with methanolic root extract (10, 50, 100, and 200 μg/mL) for 3 h. Then, cells were stained with 10 μM DCFH-DA for 30 min at 37°C in the dark and washed three times with PBS. The fluorescence was measured by GLOMAX Multidetection System (Promega, Madison, WI, USA) using blue filter (Ex 490 nm, Em 510–570 nm). For HepG2 cells, the experiment was performed also with 10 mM NAC, added 1 h before each treatment.

2.14. Annexin V/7-AAD Staining Assay. The percentage of cells undergoing apoptosis and necrosis after treatment with different concentrations of methanolic root extract was quantified using FITC Annexin V-7-AAD kit (BD Pharmingen). HepG2 cells were seeded at a density of 2×10^5 cells/well in 12-well plates and treated with different concentrations of extract (50, 100, and 200 μg/mL) for 24 h. The cells were harvested and resuspended in binding buffer and finally 5 μL of Annexin V-FITC and 5 μL of 7-AAD were added. Each tube was incubated in the dark for 15 min at room temperature. The stained cells were analysed on a FACS Canto II flow cytometer.

2.15. Measurement of Mitochondrial Membrane Potential ($\Delta\Psi_m$). The level of $\Delta\Psi_m$ was monitored by flow cytometry (FACSCanto II) equipped with DIVA software (BD Biosciences, San Jose, CA) using the TMRM probe, a cell-permeant, cationic, red-orange fluorescent dye that is capable of selectively entering active mitochondria. Briefly, 2×10^5 cells/well in 12-well plates were treated with different concentrations of root extract (10, 50, 100, and 200 μg/mL) for 3 h. Cells were trypsinized, washed in ice-cold PBS, and incubated with 150 nM TMRM at 37°C for 20 minutes in darkness. Subsequently, cells were collected and diluted with PBS and then analysed by flow cytometry. Excitation wavelength was set at 488 nm and emission wavelength was collected at 575 nm.

2.16. Mitochondria Enrichment and Western Blotting. HepG2 cells were seeded into 100 mm dishes (1×10^7 cells/dish) and then treated with 109 μg/mL of root extract (IC_{50} value at 24 h) for different time periods (3 h, 6 h, and 24 h). Cells were harvested, resuspended in ice-cold isotonic buffer (0.25 M sucrose, 5 mM Tris-HCl, pH 7.5, and 1 mM EDTA), and homogenized using a glass Teflon homogenizer (35–40 times up and down). Unbroken cells and nuclei were sedimented by centrifugation at 600 ×g for 10 min. Supernatants were centrifuged at 10,000 ×g for 30 min, the supernatants (cytosolic fraction) were removed, and the mitochondrial pellets were resuspended in RIPA buffer (PBS pH 7.4, 1% NP-40, 0.5% sodium deoxycholate, and 0.1% sodium dodecyl sulfate) and supplemented with proteases and phosphatases inhibitor cocktail (Sigma). Protein concentration was measured using Bio-Rad Protein Assay (Bio-Rad, Hercules, CA, USA). Equal amounts of protein lysates were resolved on 4–17% SDS-PAGE and then blotted onto a nitrocellulose membrane (GE). The membrane was blocked with 5% nonfat dry milk in TBST buffer (100 mM Tris-HCl pH 7.5, 150 mM NaCl, and 0.05% Tween 20) for 1 h and then incubated overnight at 4°C with primary antibody against cytochrome *c* (1 : 2000, Abcam). After that, the membrane was washed three times with TBST buffer and incubated at room temperature for 1 h with anti-mouse horseradish-peroxidase-conjugated secondary antibody (1 : 3000, Sigma). Detection was performed using the enhanced chemiluminescence (ECL) kit (GE).

2.17. Statistical Analysis and Spectrophotometric Measurement. All the results are presented as mean ± SD of three independent experiments. In the viability assay, the percentage survival values were normalized by an arcsine square root transformation and then compared with analysis of variance (ANOVA) and Tukey's HSD test. In the measurement of reactive oxygen species and mitochondrial membrane potential, statistical significances were analysed by one-way analysis of variance (ANOVA) and Tukey's HSD test. Both analyses were performed using software R version 2.8.1 (R Development Core Team, 2008). Significant differences ($P < 0.05$) are denoted by different letters. In the assessment of apoptosis, we performed a chi-square test ($P < 0.05$ was considered significant). All statistical procedures related to antioxidant tests were computed using the statistical package Statistica for Windows (ver. 5.1., 1997) (Statsoft Inc., Tulsa, USA). To avoid the error due to extract absorbance, from each experimental measure, the absorbance of extract solubilized at the same concentration in the same solvent at the same wavelength was subtracted.

Table 1: Total phenolic (TPC), flavonoid (TFC), and tannin (TTC) content in *Sclerocarya birrea* extracts.

Extract	TPC*	TFC**	TTC***
HRE	46.99 ± 1.25	7.99 ± 0.87	166.45 ± 8.01
CRE	42.77 ± 2.44	16.67 ± 2.14	215.04 ± 12.25
CMRE	100.94 ± 5.74	24.33 ± 4.78	376.30 ± 18.51
MRE	861.94 ± 12.25	95.47 ± 8.27	1109.68 ± 21.59

Root extracts: HRE (*n*-hexane); CRE ($CHCl_3$); CMRE [$CHCl_3$: MeOH (9 : 1)]; MRE (MeOH).
*TPC was expressed as mg gallic acid equivalent/g of dried extract.
**TFC was expressed as mg of quercetin equivalent/g of dried extract.
***TTC was expressed as mg of tannic acid equivalent/g of dried extract.
Results were expressed as mean ($n = 3$) ± standard deviation; $P < 0.01$.

3. Results and Discussion

Numerous studies using cancer cell lines and animal models of carcinogenesis showed that among polyphenols, generally recognized as antioxidants, a wide range possesses anticancer and apoptosis-inducing properties [19–23]. In fact, it is well known that plant-derived antioxidant polyphenols possess dual prooxidative and antioxidative activities, depending on some factors such as their metal-reducing potential, chelating behavior, and pH ad solubility characteristics [24, 25].

Prominent is the goal to clarify the molecular mechanism whereby a plant-derived extract, rich in phenolic compounds, exerts an anticarcinogenic effect, through intrinsic and newly generated ROS, both of which are able to modulate chemical signaling pathways leading to apoptotic effects [26].

3.1. Total Phenols, Flavonoids, and Tannins Content of Extracts. *Sclerocarya birrea* is traditionally used for the treatment of various complaints and, as described above, several studies reported the relevant biological activities of different parts of this plant. A recent work underlined as *Sclerocarya birrea* extracts, with particular regard to the seed cake and root extracts, could be used as prophylactic antioxidant agents [9]. To select the most promising extract to be effective as antioxidant in *in vitro* assays, all root extracts were evaluated for their TPC, TFC, and TTC. Quantitative results demonstrated that crude methanol root extract (MRE) possesses the highest content of TPC, TFC, and TTC in comparison with other extracts (Table 1). MRE showed a content up to 20 times higher than HRE and sensibly higher than the others, with 861.94 ± 12.25 mg/g of total phenolics (GAE/g of extract), 95.47 ± 8.27 mg/g of total flavonoids (QE/g of extract) and 1109.68 ± 21.59 mg/g of total tannins (TAE/g of extract). Unlike previously reported [10], TPC measured in our study was sensibly higher. This is reasonably due to our extraction procedure: *n*-hexane, $CHCl_3$, $CHCl_3$: MeOH (9 : 1), and MeOH versus *n*-hexane

and 60% methanol described by Mariod et al. [10]. It is evident that our extraction procedure allowed the increase of phenolics in MRE.

3.2. Antioxidant Assays on Selected Extract. A preliminary screening of all extracts with antioxidant tests (data not shown) was performed and our results confirmed the effectiveness of MRE among others. In details, extract antioxidant activity, at different concentrations, was assayed by 4 different tests. It was previously underlined that at least two *in vitro* procedures should be carried out for the evaluation of extract antioxidant activities [27, 28]. In particular, MRE was evaluated firstly for its antiradical activity with the most popular ABTS method. ABTS decolorization assay is applicable for both hydrophilic and lipophilic antioxidants: the preformed radical monocation of $ABTS^{+\bullet}$ is generated by oxidation of ABTS with potassium persulfate and is reduced in the presence of such hydrogen-donating antioxidants. The EC50 calculated was 12.54 ± 0.47 μg/mL.

The antioxidant effect of the extract on the peroxidation of linoleic acid in the β-carotene/linoleic acid system was also investigated. The oxidation of linoleic acid generates Peroxyl free radicals, which will then oxidize the highly unsaturated β-carotene. The presence of antioxidants minimizes the oxidation of β-carotene. The ability of MRE to inhibit β-carotene bleaching was 60.29 ± 1.15% at 200 μg/mL (Figure 1) while the EC50 was found to be 151.02 ± 4.72 μg/mL.

Superoxide anion is a ROS normally produced inside the body. Controlled production of this radical is essential to maintain a healthy environment, but it is known to be very harmful to cellular components as a precursor of a more reactive oxygen species, for example, the hydroxyl radical [29]. The extract is found to be an efficient scavenger of superoxide radical generated in NADH/PMS system *in vitro* and its activity is comparable to that of ascorbic acid. The scavenging effect of the root extract was of 97.47 ± 2.52% at 200 μg/mL concentration (Figure 1) and in this case the EC50 was 21.21 ± 2.14 μg/mL.

MRE also caused a dose-dependent inhibition of nitric oxide (Figure 1): it is evident a nitric oxide scavenger activity (78.08 ± 3.24% at 200 μg/mL). It is well known that nitric oxide is involved in many physiological processes and it is also implicated in inflammation, cancer, and other pathological conditions [30, 31]. NO has both cytoprotective and cytotoxic role. Its cytotoxic activity is related to the production of peroxynitrite ions when it reacts with O_2^- ions. These compounds are responsible for altering the structural and functional behavior of many cellular components. In aqueous solution, at the physiological pH, SNP spontaneously generates nitric oxide that interacts with oxygen to produce nitrite, which can be determined by Griess reaction. EC50 calculated for NO assay was 32.18 ± 3.24 μg/mL. Radical scavenging tests showed that MRE has an interesting antioxidant and dose-dependent activity (Figure 1). Considering the EC50 values of all radical scavenging tests, we can assess that MRE has a noticeable effect on cationic and anionic radicals. The lower lipid peroxidation activity is probably due to the characteristics of this assay that resulted in being more suitable for more lipophilic compounds [18].

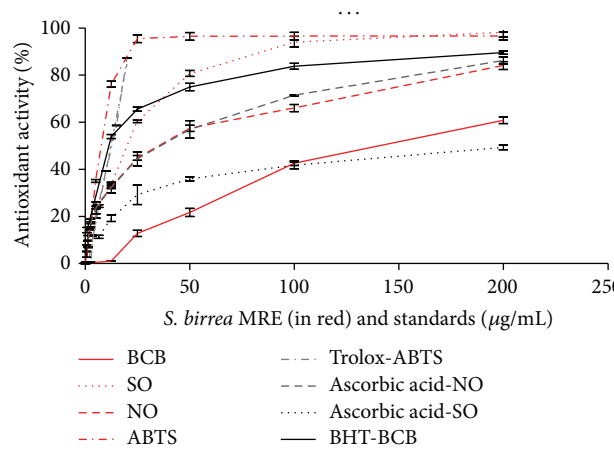

Figure 1: Antioxidant activity of *Sclerocarya birrea* methanolic root extract (MRE) compared with the reference standards. Antioxidant activity was measured by 4 different tests and in each one it is demonstrated to be dose-dependent. ABTS, nitric oxide (NO), superoxide anion (SO), and β-carotene bleaching (BCB) assays.

None of the antioxidant assays (NO, SO, or ABTS test) was previously reported for measuring the activity of *S. birrea* methanolic root extract. The phytochemical investigation, reported by Russo et al. [11], demonstrated that roots of *S. birrea* are principally constituted by galloylated tannins and this is congruent with our results. In fact, the presence of galloyl groups at the 3 position plays an important role in antioxidant and protective activity [32] and it justifies the high antioxidant activity of MRE.

These results agree with those available in literature in which a direct correlation between phenolic compound levels in the extracts and their *in vitro* antioxidant activities was found [10, 18, 33].

3.3. Cytotoxic Effect of Methanolic Root Extract on HepG2 Cells. The neoplastic evolution needs both a deregulation of cell proliferation and a suppression of apoptosis, so both cellular processes represent obvious targets for therapeutic intervention in all cancer therapies [34]. In this context, several studies have focused on the antiproliferative and cytotoxic properties of natural extracts, such as phenolics, carotenoids, and tocotrienols, demonstrating their significant potential as anticancer agents [35–37].

A previous study showed that the acetone extract of the stem bark of *S. birrea* inhibited the proliferation of different cancer cell lines (MCF-7, HT-29, HeLa) in a dose- and time-dependent manner [12]. In this study, we investigated the cytotoxicity of MRE of *S. birrea* on the hepatocarcinoma cell line HepG2 using Calcein-AM viability assay. As shown in Figure 2, the extract induced cell death in a dose- and time-dependent manner as compared with vehicle controls. The IC_{50} values at 24 h and 48 h were 109 μg/mL and 42 μg/mL, respectively. Cells pretreatment with 10 mM NAC, typically used as exogenously added antioxidant to lessen the potency

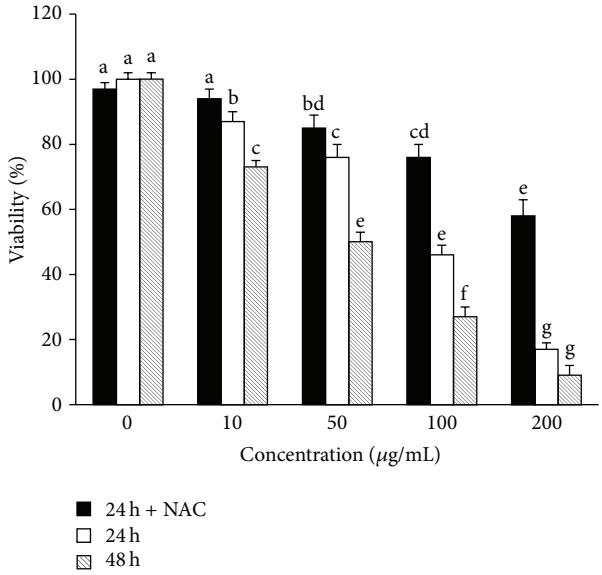

Figure 2: Cytotoxic effect of MRE of *S. birrea* on HepG2 cells. Cells were treated with methanolic extract at the concentration of 10, 50, 100, and 200 μg/mL for 24 h, in the presence or absence of 10 mM NAC, and for 48 h. MRE inhibited the growth of HepG2 cells in a dose- and time-dependent manner. Values are means ± SD of three replicates from three independent experiments. Significant differences ($P < 0.05$) are denoted by different letters.

of prooxidant polyphenols, markedly reduces MRE cytotoxic effect ($IC_{50} > 200$ μg/mL at 24 h).

Next, we evaluated the effect of MRE treatment on HepG2 cell morphology using a phase-contrast microscope. As shown in Figure 3, control cells (a) showed the normal cellular morphology, while the cells treated with different concentration of MRE for 24 h revealed remarkable morphological changes ((c), (e), (g), and (i)). Many cytoplasmic vacuoles were observed, which progressively increase in number and size, proportionally to MRE concentration. Moreover, at higher dose, the majority of cells became round-shaped and shrunken, showing blebbing or floating in the medium. Finally, cells pretreatment with 10 mM NAC considerably reduces MRE effects on HepG2 morphology ((d), (f), (h), and (j)). So, apparently, for these cells, MRE induces apoptotic-like morphology via oxidative stress.

3.4. Apoptosis Evaluation on HepG2 Cells. To better characterize the cytotoxic effect of *S. birrea* MRE, some assays were performed on HepG2 cells treated with different MRE concentrations (10, 50, 100, and 200 μg/mL) for 24 h. Firstly, the nuclear morphology was examined by staining with Hoechst 33258. As shown in Figure 4, nuclei were regular, round-shaped, and homogeneously stained in control cells (a), while the accumulation of fluorescent dye, due to morphological changes of cell apoptosis such as chromatin condensation (pycnosis), nuclear fragmentation (karyorrhexis), and cell shrinkage, was detected in treated cells in dose-dependent manner ((b)–(e)). These findings suggest that MRE treatment kills HepG2 cells via apoptotic mechanism.

Secondly, the onset of apoptosis was investigated by phosphoserine biomarker staining at the cell surface. HepG2 cells were incubated with different concentrations (50, 100, and 200 μg/mL) of MRE for 24 h and then stained with Annexin V-FITC/7-AAD to assess the apoptotic and necrotic cell populations. Our data show that the exposure to MRE increased the number of Annexin V-FITC-positive cells (Figure 5). In control cells, apoptotic population was 1.0 ± 0.1%; after treatment with root extract, the apoptotic rate was raised to 61.2±7.1%, 76.6±7.3%, and 92.0±3.2%, respectively, in a dose-dependent manner.

3.5. Methanolic Root Extract Induces ROS Production and Reduces Mitochondria Membrane Potential ($\Delta\Psi_m$). Mitochondrial damage is a significant and early event in cellular death [38]. Elevated intracellular ROS are sufficient to trigger cell death and it has been suggested that ROS are biochemical mediators of apoptosis, mainly via interactions with proteins of mitochondrial permeability transition complex (PTPC) [39–41]. To investigate the effect of MRE on the intracellular redox status, levels of ROS production were determined after 3 h of treatment by measuring the oxidation of nonfluorescent probe DCFH-DA to its fluorescent reduced form 2′,7′-dichlorofluorescein (DCF), in the presence or not of a ROS quencher (10 mM NAC).

As shown in Figure 6, MRE stimulated ROS formation in a concentration-dependent manner, as compared with control cells. Moreover, pretreatment with NAC markedly inhibited apoptosis, suggesting that MRE-induced cell death is strictly related to ROS production. These data are in agreement with the increased cell viability in the presence of NAC (Figure 2). So, we speculated that high levels of ROS lead to a severe cellular damage, which directly involves the mitochondria and leads to cell death by apoptosis [41], driving these already stressed cells beyond their limit [5].

In order to verify whether the production of MRE-induced ROS in HepG2 cells could fit with changes or loss in mitochondrial transmembrane potential ($\Delta\Psi_m$), the mitochondrial membrane polarization was investigated using a cationic fluorescent probe TMRM, easily incorporated into mitochondria of viable cells. As shown in Figure 7, cells exposed to different concentrations of the methanolic root extract for 3 h showed a consistent depolarization of mitochondrial membrane potential, with TMRM fluorescence decreasing from 100% of control to 64.4 ± 1.5%, 47.7 ± 5.2%, 42.4 ± 5.3%, and 37.1 ± 6.0% of HepG2 cells treated with 10, 50, 100, and 200 μg/mL, respectively.

The loss in mitochondrial membrane potential ($\Delta\psi_m$), an early event in apoptosis [42], represents a mitochondrial dysfunction which is one of several hallmarks of mitochondrial membrane permeabilization (MMP), together with the release of several soluble proteins (usually retained within mitochondria) in the intermembrane space (IMS), such as cytochrome *c*, Smac/DIABLO or Omi/HtrA2, with subsequent activation of effector caspases, and/or as AIF and Endo G, which are caspase-independent apoptogenic death effectors. MMP is a feature of cell death and is often considered as the "point of no return" in the cascade of events

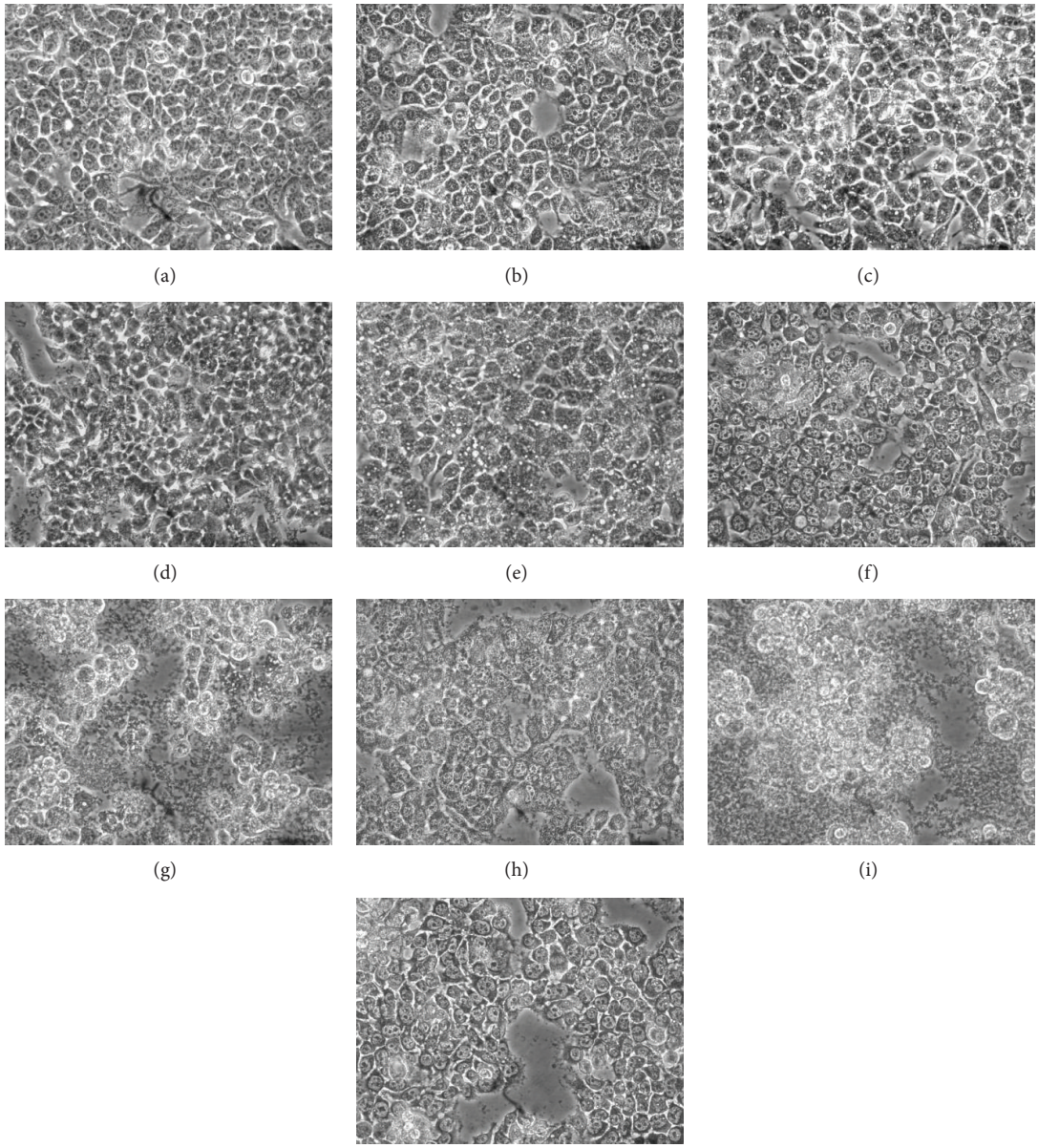

Figure 3: Effect of MRE exposure on HepG2 cell morphology. HepG2 cells were treated with different concentrations of root extract for 24 h and morphological changes were observed using phase-contrast microscopy. The control cells show the normal morphology. In contrast, cells treated with intermediate concentrations of MRE show abundant cytoplasmic vacuoles. At high dosage of treatment, cells became round and shrunken. The photographs were taken at a magnification ×40. Images are representative of three independent experiments ((a)-(b) control; (c)-(d) 10 μg/mL; (e)-(f) 50 μg/mL; (g)-(h) 100 μg/mL; (i)-(j) 200 μg/mL; (b), (d), (f), (h), and (j) +10 mM NAC).

leading to apoptosis [43]. So, we investigated the release of cyt *c* from IMS to the cytosol, a key step in the mitochondrial pathway of apoptosis [44]. As shown in Figure 8, western blotting analysis reveals that MRE treatment at IC_{50} concentration caused the cytochrome *c* release into the cytosol, which increases over time (up to 24 h), in comparison to the untreated cells. Taken together, all these data demonstrate that MRE-induced apoptosis may be tightly related to loss of mitochondrial function.

3.6. MRE Treatment on Human Dermal Fibroblasts. Normal dermal fibroblasts provide an ideal nonneoplastic cell system to study toxicology or basic cell biology, routinely used in *in vitro* assessments [45, 46]. So, cytotoxicity and intracellular ROS levels were determined on this normal cell line treated with MRE. As shown in Figure 9(a), fibroblasts were not much affected by MRE treatment (IC_{50} > 200 μg/mL in all cases), probably due to the low ROS production measured (Figure 9(b)). These data suggest that MRE treatment may be

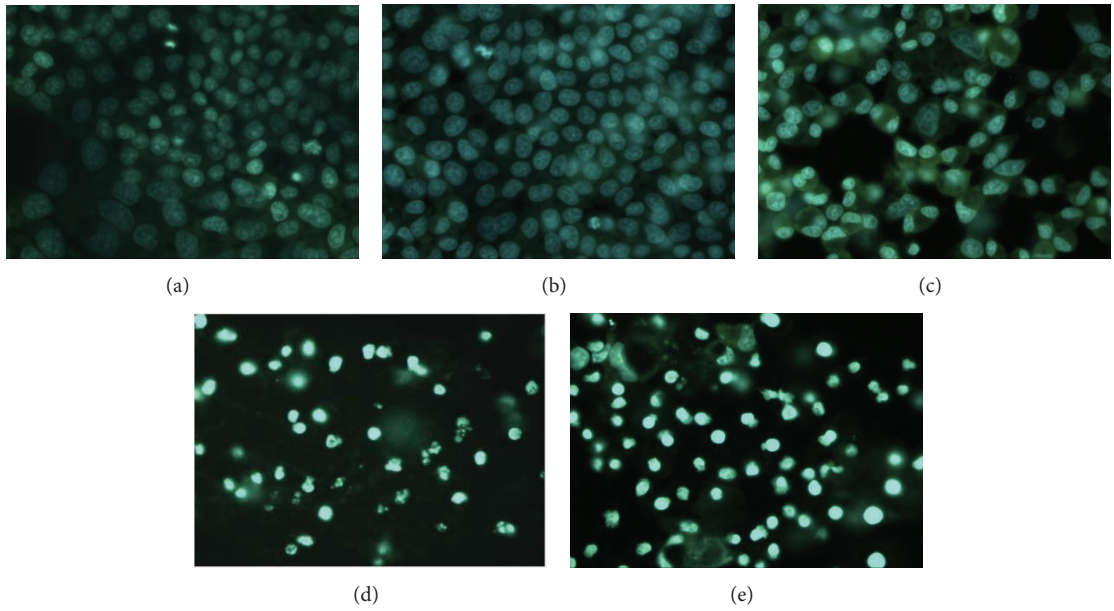

Figure 4: Effect of MRE treatment on the morphology of HepG2 cell nuclei. Cells were treated with vehicle (a) and methanolic root extract at 10 (b), 50 (c), 100 (d), and 200 μg/mL for 24 h; cells were then stained with Hoechst 33258 and observed under a fluorescent microscope. Marked morphological changes (chromatin condensation and nuclear fragmentation) of cell apoptosis were clearly found.

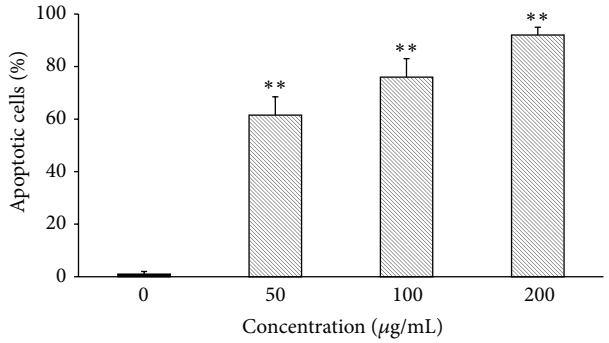

Figure 5: Flow cytometric analysis of apoptosis in MRE-treated HepG2 cells. HepG2 cells were incubated for 24 h with 50, 100, and 200 μg/mL of methanolic root extract and apoptosis was assessed by Annexin V/7-AAD double staining. Values are means ± SD of three replicates from three independent experiments. Significant differences between the control versus treated cells are indicated by $^{**}(P < 0.01)$.

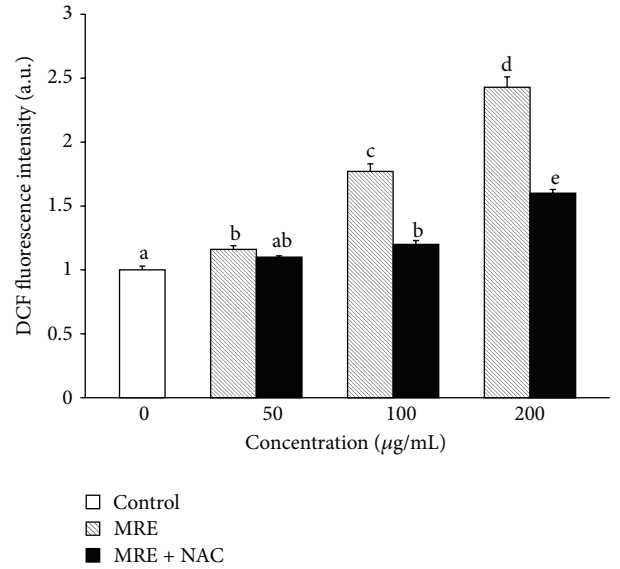

Figure 6: Effect of MRE on the ROS generation in HepG2 cells. Cells were incubated for 3 h with 50, 100, and 200 μg/mL of methanolic root extract, generating ROS in a dose-dependent manner. NAC suppressed MRE-induced ROS generation. Values are means ± SD of three replicates from three independent experiments. Significant differences ($P < 0.05$) are denoted by different letters.

selective towards cancers cells with minimal adverse effects on normal cells.

4. Conclusions

In this study, our findings indicated that *S. birrea* methanolic root extract exhibits higher levels of phenolics compared to the less polar extracts, showing an important *in vitro* antioxidant activity, with particular regard to its free radical scavenging activity. Moreover, the cytotoxic effect of MRE linked to increased amounts of ROS on HepG2 cells was evident. Even if this behavior could seem contradictory, several recent papers underlined that phenolic compounds could exert both antioxidant and prooxidant activities [22, 23, 47]. In our case it is reasonable that MRE prooxidant effect could exceed its antioxidant potential on HepG2 cells. Both the

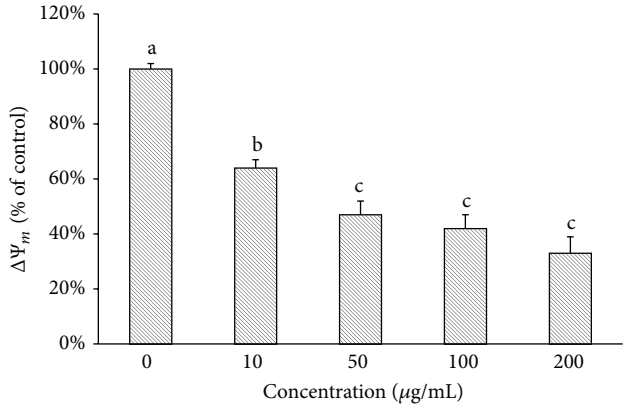

Figure 7: MRE-induced $\Delta\Psi_m$ depolarization in HepG2 cells. The integrity of mitochondrial membranes of the cells was investigated, after 3 h of treatment, measuring TMRM fluorescence intensity of methanolic root extract-treated cells. Change in $\Delta\Psi_m$ was determined by flow cytometry. Values are means ± SD of three replicates from three independent experiments. Significant differences ($P < 0.05$) are denoted by different letters.

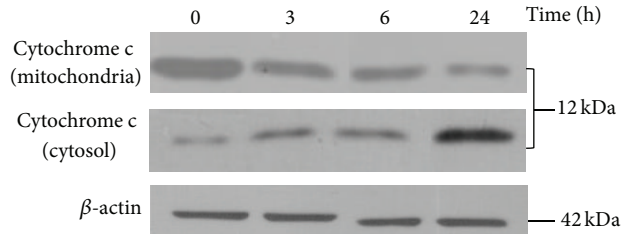

Figure 8: Effect of MRE treatment on cytochrome *c* in HepG2 cells. Cells were incubated for 3, 6, and 24 h with 109 μg/mL (IC_{50} value at 24 h) of methanolic root extract of *S. birrea*. The cell lysates were resolved by 17% SDS-PAGE and cyt *c* expression, in both mitocondrial and cytosolic fractions, was analysed by immunoblotting.

loss of membrane potential and the release of cytochrome *c*, which ultimately contribute to typical morphological manifestations of apoptosis, (e.g., chromatin condensation and nuclear fragmentation) suggest that cytotoxic effect has triggered ROS-induced apoptosis in HepG2 cells, more than in human normal cells. This evidence could be associated with a cell signalling by which extract can contribute to the coordination of cell functions. The presence of different classes of secondary metabolites detected in the extract provides a preliminary explanation of the experimental evidences, suggesting the need to investigate the effects of MRE individual constituents.

Although the mechanism by which MRE treatment induces these effects remains undefined and will be the subject of further study, our findings demonstrate that compounds present in MRE are selectively able to interfere with cellular mechanisms, which are specific of malignant cells and are also linked to ROS production. This evidence suggests the potential use of MRE in therapeutic application for cancer treatment.

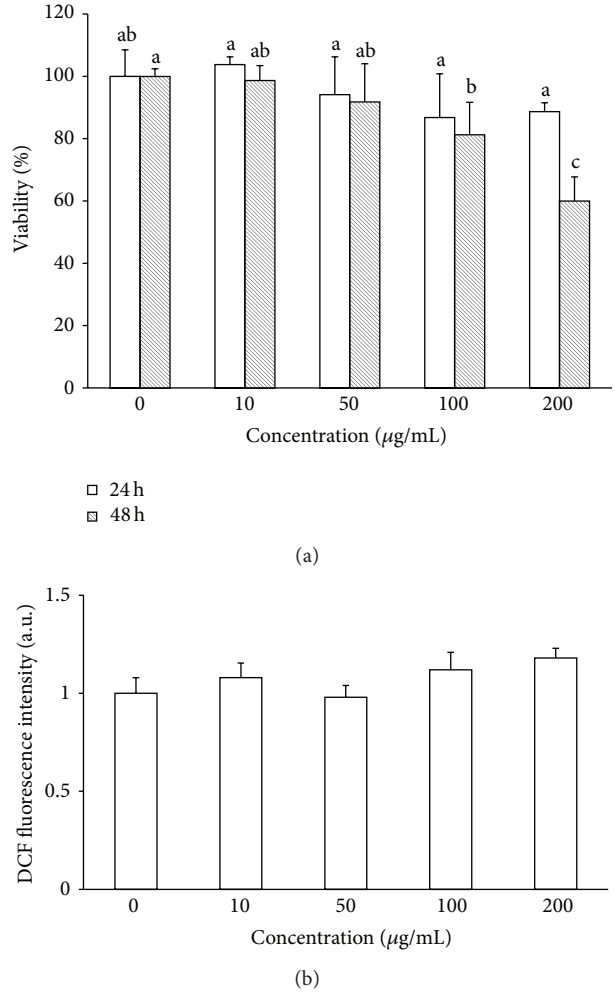

Figure 9: MRE treatment on human dermal fibroblasts. (a) Cells were treated with methanolic extract at the concentration of 10, 50, 100, and 200 μg/mL for 24 h and 48 h. MRE shows little cytotoxicity towards fibroblasts cells. Values are means ± SD of three replicates from three independent experiments. Significant differences ($P < 0.05$) are denoted by different letters. (b) Cells were incubated for 3 h with 50, 100, and 200 μg/mL of MRE, generating very low amount of ROS. Values are means ± SD of three replicates from three independent experiments. No significant differences were found ($P > 0.05$ in all cases).

Abbreviations

ABTS:	2,2′-Azinobis(3-ethylbenzothiazoline-6-sulfonic acid)
BCB:	β-Carotene bleaching assay
BHT:	Butylated hydroxytoluene
BSA:	Bovine serum albumin
CMRE:	Chloroform : methanol root extract
CRE:	Chloroform root extract
Calcein-AM:	Calcein acetoxymethyl ester
DCF:	Dichlorofluorescein
DCFH-DA:	2′,7′-Dichorodihydrofluorescein diacetate
$\Delta\Psi_m$:	Mitochondrial membrane potential
DMEM:	Dulbecco's Modified Eagle Medium

DMSO: Dimethyl sulfoxide
EDTA: Ethylenediaminetetraacetic acid
FBS: Fetal bovine serum
HRE: *n*-hexane root extract
MMP: Mitochondrial membrane permeabilization
MRE: Methanolic root extract
NAC: N-Acetyl-L-cysteine
NADH: Nicotinamide adenine dinucleotide
NBT: Nitroblue tetrazolium
PBS: Phosphate buffered saline
PMS: Phenazine methosulphate
RIPA buffer: Radioimmunoprecipitation buffer
RNS: Reactive nitrogen species
ROS: Reactive oxygen species
SDS-PAGE: Sodium dodecyl sulphate-polyacrylamide gel electrophoresis
SNP: Sodium nitroprusside
TBST: Trisbuffered saline-Tween 20
TFC: Total flavonoid content
TMRM: Tetramethylrhodamine methyl ester
TPC: Total phenolic content
TTC: Total tannin content.

Conflict of Interests

The authors declare that there is no conflict of interests regarding the publication of this paper.

Acknowledgments

Authors would like to thank Dr. Vincenzo Trotta (Basilicata University, Italy) for his support in statistical data analysis. Methods used in this study have been developed with the financial support of Programma Operativo FSE Basilicata 2007–2013 Cod. no. 4/AP/05/2013/REG, CUP G43G13000430009.

References

[1] M. Gordaliza, "Natural products as leads to anticancer drugs," *Clinical and Translational Oncology*, vol. 9, no. 12, pp. 767–776, 2007.

[2] W.-Y. Huang, Y.-Z. Cai, and Y. Zhang, "Natural phenolic compounds from medicinal herbs and dietary plants: potential use for cancer prevention," *Nutrition and Cancer*, vol. 62, no. 1, pp. 1–20, 2010.

[3] E. Safarzadeh, S. S. Shotorbani, and B. Baradaran, "Herbal medicine as inducers of apoptosis in cancer treatment," *Advanced Pharmaceutical Bulletin*, vol. 4, no. 5, supplement 1, pp. 421–427, 2014.

[4] Y. K. Yong, J. J. Tan, S. S. Teh et al., "*Clinacanthus nutans* extracts are antioxidant with antiproliferative effect on cultured human cancer cell lines," *Evidence-Based Complementary and Alternative Medicine*, vol. 2013, Article ID 462751, 8 pages, 2013.

[5] P. Schumacker, "Reactive oxygen species in cancer: a dance with the devil," *Cancer Cell*, vol. 27, no. 2, pp. 156–157, 2015.

[6] G. N. Gouwakinnou, A. M. Lykke, A. E. Assogbadjo, and B. Sinsin, "Local knowledge, pattern and diversity of use of *Sclerocarya birrea*," *Journal of Ethnobiology and Ethnomedicine*, vol. 7, article 8, 2011.

[7] R. Wynberg, J. Cribbins, R. Leakey et al., "Knowledge on *Sclerocarya birrea* subsp.*caffra* with emphasis on its importance as a non-timber forest product in South and southern Africa: a summary," *The Southern African Forestry Journal*, vol. 196, no. 1, pp. 67–77, 2002.

[8] B. A. Jama, A. M. Mohamed, J. Mulatya, and A. N. Njui, "Comparing the 'Big Five': a framework for the sustainable management of indigenous fruit trees in the drylands of East and Central Africa," *Ecological Indicators*, vol. 8, no. 2, pp. 170–179, 2008.

[9] O. J. M. Hamza, C. J. P. van den Bout-van den Beukel, M. I. N. Matee et al., "Antifungal activity of some Tanzanian plants used traditionally for the treatment of fungal infections," *Journal of Ethnopharmacology*, vol. 108, no. 1, pp. 124–132, 2006.

[10] A. A. Mariod, B. Matthäus, and I. H. Hussein, "Antioxidant properties of methanolic extracts from different parts of *Sclerocarya birrea*," *International Journal of Food Science and Technology*, vol. 43, no. 5, pp. 921–926, 2008.

[11] D. Russo, O. Kenny, T. J. Smyth et al., "Profiling of phytochemicals in tissues from *Sclerocarya birrea* by HPLC-MS and their link with antioxidant activity," *ISRN Chromatography*, vol. 2013, Article ID 283462, 11 pages, 2013.

[12] N. F. Tanih and R. N. Ndip, "The acetone extract of *Sclerocarya birrea* (Anacardiaceae) possesses antiproliferative and apoptotic potential against human breast cancer cell lines (MCF-7)," *The Scientific World Journal*, vol. 2013, Article ID 956206, 7 pages, 2013.

[13] L. Milella, M. Caruso, F. Galgano, F. Favati, M. C. Padula, and G. Martelli, "Role of the cultivar in choosing Clementine fruits with a high level of health-promoting compounds," *Journal of Agricultural and Food Chemistry*, vol. 59, no. 10, pp. 5293–5298, 2011.

[14] K. A. Lombard, E. Geoffriau, and E. Peffley, "Flavonoid quantification in onion by spectrophotometric and high performance liquid chromatography analysis," *HortScience*, vol. 37, no. 4, pp. 682–685, 2002.

[15] A. E. Hagerman and L. G. Butler, "Protein precipitation method for the quantitative determination of tannins," *Journal of Agricultural and Food Chemistry*, vol. 26, no. 4, pp. 809–812, 1978.

[16] P. Costa, S. Gonçalves, P. Valentão et al., "Metabolic profile and biological activities of *Lavandula pedunculata* subsp. *lusitanica* (Chaytor) Franco: Studies on the essential oil and polar extracts," *Food Chemistry*, vol. 141, no. 3, pp. 2501–2506, 2013.

[17] D. Russo, M. G. Bonomo, G. Salzano, G. Martelli, and L. Milella, "Nutraceutical properties of *Citrus clementina* juices," *Pharmacologyonline*, vol. 1, no. 1, pp. 84–93, 2012.

[18] L. Milella, A. Bader, N. De Tommasi, D. Russo, and A. Braca, "Antioxidant and free radical-scavenging activity of constituents from two Scorzonera species," *Food Chemistry*, vol. 160, pp. 298–304, 2014.

[19] F. Ferreres, A. Gil-Izquierdo, J. Vinholes, S. T. Silva, P. Valentão, and P. B. Andrade, "*Bauhinia forficata* Link authenticity using flavonoids profile: relation with their biological properties," *Food Chemistry*, vol. 134, no. 2, pp. 894–904, 2012.

[20] H. Y. Khan, H. Zubair, M. F. Ullah, A. Ahmad, and S. M. Hadi, "A prooxidant mechanism for the anticancer and chemopreventive properties of plant polyphenols," *Current Drug Targets*, vol. 13, no. 14, pp. 1738–1749, 2012.

[21] A. Russo, V. Cardile, L. Lombardo, L. Vanella, A. Vanella, and J. A. Garbarino, "Antioxidant activity and antiproliferative action

of methanolic extract of *Geum quellyon* Sweet roots in human tumor cell lines," *Journal of Ethnopharmacology*, vol. 100, no. 3, pp. 323–332, 2005.

[22] L. Choueiri, V. S. Chedea, A. Calokerinos, and P. Kefalas, "Antioxidant/pro-oxidant properties of model phenolic compounds. Part II: studies on mixtures of polyphenols at different molar ratios by chemiluminescence and LC-MS," *Food Chemistry*, vol. 133, no. 3, pp. 1039–1044, 2012.

[23] D. Procházková, I. Boušová, and N. Wilhelmová, "Antioxidant and prooxidant properties of flavonoids," *Fitoterapia*, vol. 82, no. 4, pp. 513–523, 2011.

[24] E. A. Decker, "Phenolics: prooxidants or antioxidants?" *Nutrition Reviews*, vol. 55, no. 11, part 1, pp. 396–398, 1997.

[25] L. R. Fukumoto and G. Mazza, "Assessing antioxidant and prooxidant activities of phenolic compounds," *Journal of Agricultural and Food Chemistry*, vol. 48, no. 8, pp. 3597–3604, 2000.

[26] H. Babich, A. G. Schuck, J. H. Weisburg, and H. L. Zuckerbraun, "Research strategies in the study of the pro-oxidant nature of polyphenol nutraceuticals," *Journal of Toxicology*, vol. 2011, Article ID 467305, 12 pages, 2011.

[27] M. N. Alam, N. J. Bristi, and M. Rafiquzzaman, "Review on *in vivo* and *in vitro* methods evaluation of antioxidant activity," *Saudi Pharmaceutical Journal*, vol. 21, no. 2, pp. 143–152, 2013.

[28] H. Wangensteen, A. B. Samuelsen, and K. E. Malterud, "Antioxidant activity in extracts from coriander," *Food Chemistry*, vol. 88, no. 2, pp. 293–297, 2004.

[29] B. Halliwell, "Reactive oxygen species in living systems: Source, biochemistry, and role in human disease," *The American Journal of Medicine*, vol. 91, no. 3, 1991.

[30] T. Kawasaki, T. Kitao, K. Nakagawa et al., "Nitric oxide-induced apoptosis in cultured rat astrocytes: protection by edaravone, a radical scavenger," *GLIA*, vol. 55, no. 13, pp. 1325–1333, 2007.

[31] F. A. Martín, D. Rojas-Díaz, M. L. Luis-García, J. L. González-Mora, and M. A. Castellano, "Simultaneous monitoring of nitric oxide, oxyhemoglobin and deoxyhemoglobin from small areas of the rat brain by in vivo visible spectroscopy and a least-square approach," *Journal of Neuroscience Methods*, vol. 140, no. 1-2, pp. 75–80, 2004.

[32] T. Nakagawa, T. Yokozawa, K. Terasawa, S. Shu, and L. R. Juneja, "Protective activity of green tea against free radical- and glucose-mediated protein damage," *Journal of Agricultural and Food Chemistry*, vol. 50, no. 8, pp. 2418–2422, 2002.

[33] J. Kumar, P. Dhar, A. B. Tayade et al., "Antioxidant capacities, phenolic profile and cytotoxic effects of saxicolous lichens from trans-Himalayan cold desert of Ladakh," *PLoS ONE*, vol. 9, no. 6, 2014.

[34] G. I. Evan and K. H. Vousden, "Proliferation, cell cycle and apoptosis in cancer," *Nature*, vol. 411, no. 6835, pp. 342–348, 2001.

[35] F. Jiang, W. Li, Y. Huang et al., "Antioxidant, antityrosinase and antitumor activity comparison: the potential utilization of fibrous root part of *Bletilla striata* (Thunb.) Reichb.f.," *PLoS ONE*, vol. 8, no. 2, Article ID e58004, 2013.

[36] C.-C. Yeh, J.-I. Yang, J.-C. Lee et al., "Anti-proliferative effect of methanolic extract of *Gracilaria tenuistipitata* on oral cancer cells involves apoptosis, DNA damage, and oxidative stress," *BMC Complementary and Alternative Medicine*, vol. 12, article 142, 2012.

[37] S. Wada, Y. Satomi, M. Murakoshi, N. Noguchi, T. Yoshikawa, and H. Nishino, "Tumor suppressive effects of tocotrienol in vivo and in vitro," *Cancer Letters*, vol. 229, no. 2, pp. 181–191, 2005.

[38] J. J. Lemasters, "Mechanisms of hepatic toxicity—V. Necrapoptosis and the mitochondrial permeability transition: shared pathways to necrosis and apoptosis," *American Journal of Physiology—Gastrointestinal and Liver Physiology*, vol. 276, no. 1, pp. G1–G6, 1999.

[39] T. M. Buttke and P. A. Sandstrom, "Oxidative stress as a mediator of apoptosis," *Immunology Today*, vol. 15, no. 1, pp. 7–10, 1994.

[40] J. G. Pastorino and J. B. Hoek, "Ethanol potentiates tumor necrosis factor-α cytotoxicity in hepatoma cells and primary rat hepatocytes by promoting induction of the mitochondrial permeability transition," *Hepatology*, vol. 31, no. 5, pp. 1141–1152, 2000.

[41] M. L. Circu and T. Y. Aw, "Reactive oxygen species, cellular redox systems, and apoptosis," *Free Radical Biology and Medicine*, vol. 48, no. 6, pp. 749–762, 2010.

[42] K. R. Roy, K. M. Arunasree, N. P. Reddy, B. Dheeraj, G. V. Reddy, and P. Reddanna, "Alteration of mitochondrial membrane potential by *Spirulina platensis* C-phycocyanin induces apoptosis in the doxorubicinresistant human hepatocellular-carcinoma cell line HepG2," *Biotechnology and Applied Biochemistry*, vol. 47, no. 3, pp. 159–167, 2007.

[43] G. Kroemer, L. Galluzzi, and C. Brenner, "Mitochondrial membrane permeabilization in cell death," *Physiological Reviews*, vol. 87, no. 1, pp. 99–163, 2007.

[44] M. D. Esposti, I. Hatzinisiriou, H. McLennan, and S. Ralph, "Bcl-2 and mitochondrial oxygen radicals. New approaches with reactive oxygen species-sensitive probes," *The Journal of Biological Chemistry*, vol. 274, no. 42, pp. 29831–29837, 1999.

[45] B. Feizzadeh, J. T. Afshari, H. Rakhshandeh, A. Rahimi, A. Brook, and H. Doosti, "Cytotoxic effect of saffron stigma aqueous extract on human transitional cell carcinoma and mouse fibroblast," *Urology Journal*, vol. 5, no. 3, pp. 161–167, 2008.

[46] M. Shokrzadeh, M. Azadbakht, N. Ahangar, A. Hashemi, and S. S. Saeedi Saravi, "Cytotoxicity of hydro-alcoholic extracts of *Cucurbita pepo* and *Solanum nigrum* on HepG2 and CT26 cancer cell lines," *Pharmacognosy Magazine*, vol. 6, no. 23, pp. 176–179, 2010.

[47] V. S. Chedea, C. Braicu, and C. Socaciu, "Antioxidant/prooxidant activity of a polyphenolic grape seed extract," *Food Chemistry*, vol. 121, no. 1, pp. 132–139, 2010.

Hindawi Publishing Corporation
BioMed Research International
Volume 2014, Article ID 890904, 7 pages
http://dx.doi.org/10.1155/2014/890904

Research Article

Antiproliferative Activity of Hamigerone and Radicinol Isolated from *Bipolaris papendorfii*

Periyasamy Giridharan, Shilpa A. Verekar, Akash R. Gohil, Prabhu Dutt Mishra, Amit Khanna, and Sunil Kumar Deshmukh

Piramal Enterprises Ltd., 1 Nirlon Complex, Off Western Express Highway, Near NSE Complex, Goregaon (East), Mumbai 400 063, India

Correspondence should be addressed to Sunil Kumar Deshmukh; sunil.deshmukh@piramal.com

Received 27 May 2014; Accepted 16 July 2014; Published 12 August 2014

Academic Editor: Zeki Topcu

Secondary metabolites from fungi organisms have extensive past and present use in the treatment of many diseases and serve as compounds of interest both in their natural form and as templates for synthetic modification. Through high throughput screening (HTS) and bioassay-guided isolation, we isolated two bioactive compounds hamigerone (1) and radicinol (2). These compounds were isolated from fungus *Bipolaris papendorfii*, isolated from the rice fields of Dera, Himachal Pradesh, India. The structures of the compounds were established on the basis of spectroscopic data, namely, NMR (^{1}H, ^{13}C, mass, and UV). Both compounds were found to be antiproliferative against different cancer cells. Furthermore we have also noted that both compounds showed increase in apoptosis by favorably modulating both tumor suppressor protein (p53) and antiapoptic protein (BCL-2), and in turn increase caspase-3 expression in cancer cells. This is the first report of these compounds from fungus *Bipolaris papendorfii* and their anticancer activity.

1. Introduction

Microfungi are a rich source of chemical diversity [1–3], and its metabolites are used by the pharmaceutical industry either in the native form or as derivatives [4–6]. As only a small part of the Mycota is known and most fungi produce several unknown metabolites, fungi are still one of the most promising sources for new lead compounds. Hence fungi are the objective in numerous high throughput screening (HTS) programs targeting new pharmaceutics and other bioactive components [7–10].

In our ongoing pharmacological screening program on biodiversity of fungi present in Indian landscape using high throughput screening (HTS), we have identified a notable antiproliferative activity against cancer cells in extracts/fractions of a fungus *Bipolaris papendorfii*, coded as PM0853873 isolated from the rice fields of Dera, Himachal Pradesh, India. Hamigerone was originally reported as the major secondary metabolite of *Hamigera avellanea* but no pharmacological activity was reported [11]; similarly radicinol was isolated from *Cochliobolus lunata* but no pharmacological activity was reported [12]. Apoptosis is essential in the homeostasis of normal tissues of the body. The two important genes involved in this process are the BCL-2 gene and p53 gene. BCL-2 is a gene of antiapoptosis and is crucial in preventing apoptosis whereas p53 gene is known as tumor suppressor gene. Cellular stresses, particularly DNA damage, are sensed by proteins such as ATM and DNA-PK, which phosphorylate and stabilize p53 which in turn cause apoptosis to the cancer cells [13]. The apoptotic pathway is related to induction of p53 and this pathway is held in check by the antiapoptotic gene BCL-2 [14]. The protooncogene BAX forms a heterodimer with BCL-2 and accelerates the process of apoptosis. We describe here the identification and bioactivity of the lead compounds hamigerone and radicinol from this culture. In this study, we also demonstrate for the first time the novel *in vitro* antiproliferative properties

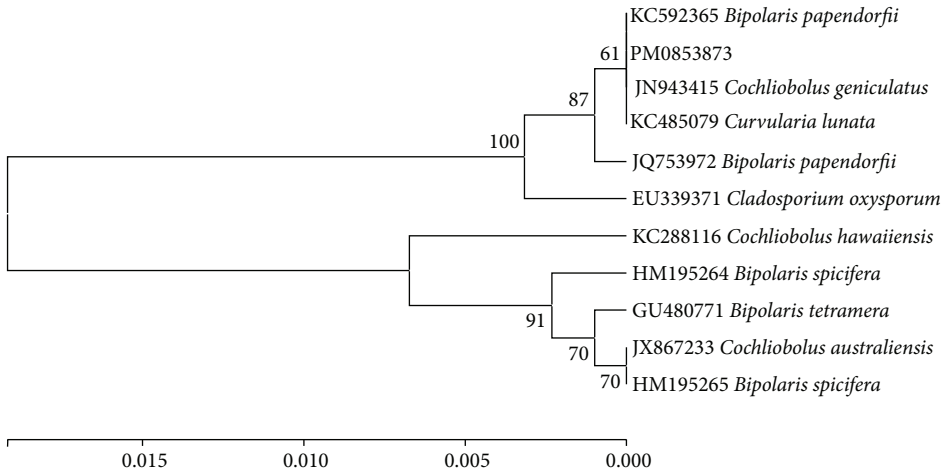

Figure 1: Phylogenetic analysis of the ITS region sequence obtained from sample PM0853873 in comparison with the nearest type strain sequences. The tree was constructed based on rRNA gene sequences (ITS region) using the Maximum Composite Likelihood Method.

of hamigerone and radicinol in cancer cells. Both the compounds are inducing apoptosis in Panc-1 cancer cells by favorably modulating p53, BCL-2, and caspase 3 expression.

2. Materials and Methods

2.1. General. HPLC was performed in Lichrosphere RP-18, 125 × 4 mm column using Shimadzu LC-2010 CHT Liquid Chromatography. Water preparative HPLC was used for final purification. Solvents used were of HPLC grade and normal column chromatography (CC) was performed with distilled commercial-grade solvents. Silica gel (SiO_2, 200–300 mesh) was used for CC and GF_{254}(30–40 mm). TLCs were procured from Merck. NMR spectra in $CDCl_3$ were recorded on Bruker 300 MHz spectrometer with TMS as the internal standard with chemical shift δ values in ppm and coupling constant J in Hz. ESI LC-MS was from Bruker Daltonics. Flash chromatography was performed on CombiFlash Sq 16X Teledyne Technologies Company ISCO attached with UV/VIS detector, (RediSep Flash Column silica 12 g, CHCl3/MeOH gradient system). Final purification was achieved by preparative HPLC using RP-18 column (10 × 25 mm, 10 μ) and acetonitrile/water as a solvent system.

2.2. Cell Culture Reagents. All the cell lines were obtained from ATTC, USA. McCoy's 5a medium, MEM, RPMI-1640, FBS, BSA, isopropanol, dimethylsulfoxide (DMSO), formaldehyde, 3-(4,5-dimethylthiazol-2-yl)-2,5-diphenyl tetrazolium bromide, Triton X-100, and PBS were obtained from Sigma, USA. Hoechst 3342 and Dylight 549 were obtained from Thermo Fisher Scientific, USA. All the antibodies, namely, BCL-2 (SC-738), p53 (SC-126), and cleaved caspase 3 (SC-22171), were procured from Santa Cruz Biotechnology, Inc., USA.

2.3. Isolation and Identification of Fungus. The strain PM0853873 was isolated from the soil samples collected from Dera rice field during October 2007. The culture was isolated using soil plate method [15] using potato carrot agar (Hi Media) supplemented with 50 mg/L of chloramphenicol and maintained on potato dextrose agar (Hi Media) supplemented with 50 mg/L of chloramphenicol for identification and fermentation. The strain was identified as *Bipolaris papendorfii* by partial sequence analysis of the internal transcribed spacer region (ITS) using ITS1 and ITS4 primers [16]. A nucleotide to nucleotide BLAST [17] query of the gene bank database (http://www.ncbi.nlm.nih.gov/BLAST) recovered KC592365 *Bipolaris papendorfii* (92%) as the closest match to the ITS rDNA of PM0853873 (100.0%). Evolutionary analyses (Figure 1) were performed using MEGA6 [18].

2.4. Large-Scale Production of the Fungus. A loop full of the well grown culture from slant maintained on potato dextrose agar (PDA) was transferred to a 500 mL conical flask with 100 mL liquid medium containing soluble starch 1.5 g; soya bean meal 1.5 g; yeast extract 0.2 g; corn steep liquor 0.1 g; glucose 0.5 g; $CaCO_3$ 0.2 g; NaCl 0.5 g; glycerol 1.0 g in demineralized water at pH 5.5. This was grown on rotary shaker at 220 rpm for 72 h at 28°C and was used as seed medium. Potato dextrose broth medium (Hi Media) was used for production. The pH of the medium was adjusted to 6.5 prior to sterilization. Twenty-five, 1000 mL flasks containing 200 mL of the above medium were inoculated with 1% of the seed culture and incubated on rotary shaker at 220 rpm for 72 h at 28°C.

2.5. Purification of Compounds. 5 L fermentation broth was filtered through Whatman number 1 filter paper to separate biomass. Methanol was added to the biomass, stirred for 40 min, and filtered. The filtrate was evaporated on rotary evaporator to remove methanol and aqueous residue was partitioned with ethyl acetate; the organic layer was concentrated on rotary evaporator to remove solvent, which yielded

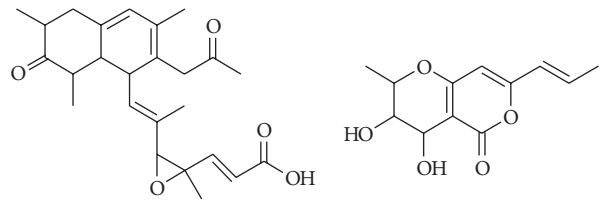

Compound **1** Compound **2**

Figure 2: Structures of hamigerone (**1**) and radicinol (**2**).

500 mg crude extract. The crude extract was subjected to flash chromatography 16X on ISCO Combiflash system using RediSep silica column (SiO_2, 200–300 mesh, 12 g; petroleum ether/ethyl acetate gradient). Semipure compounds **1** and **2** were obtained from the fractions eluted with 10% ethyl acetate in petroleum ether. Final purification of compound **1** and **2** was performed on preparative HPLC (Waters PrepLC 4000 system, RP-18 column 8 × 250 mm (Lichrosphere), 10 μ; 2–100% acetonitrile in 30 min gradient against water, 5 mL/min flow). The peak at RT 28.2 was collected and evaporated the solvent to get 8 mg pure compound **1**. In a similar preparative HPLC experiment semipure compound **2** appeared at 16 min to give 12 mg pure compound. The purity of the compounds were determined by Analytical HPLC.

2.6. Identification of the Substances. These compounds were characterized by spectroscopic data (UV, ^{1}H-NMR, ^{13}C-NMR, and LC-MS). Compounds **1** and **2** were identified as hamigerone and radicinol respectively. LC MS data indicated the molecular weight of compound **1** as 412 and compound **2** as 238.

3. Screening for Anticancer Activity

3.1. Cell Proliferation Assay. Cell growth was measured by 3-(4,5-dimethylthiazol-2-yl)-2,5-diphenyl tetrazolium bromide (MTT) method [19]. Cells were seeded at the appropriate concentrations to prevent confluence throughout the experiment. After 24 h of incubation, cells were treated with serial concentrations of the compounds. Control cells were treated with equal concentration of DMSO (never exceeding 0.1%). At 72 h after treatment, aliquots of 10 μL of MTT (5 mg/mL) were added to each well and incubated for 4 h at 37°C. The supernatant was removed and 100 μL of isopropanol was added. The color intensity of reduced MTT was measured using Tecan Sapphire multifluorescence microplate reader (Tecan, Germany, GmbH) at 595 nm. DMSO-treated cells were considered untreated control and assigned a value of 100%.

3.2. In Vitro Protein Expression (by High Content Screening). Panc-1 cells were seeded in 96-well plates at a density of 1×10^4 cells/well. 24 h after seeding, medium was replaced with fresh medium. Panc-1 cells were treated with 1.9 μM of hamigerone and 10.50 μM of radicinol for 12 h. At the end of every time point, to determine the protein expression, the cells were fixed with 3.7% formaldehyde in PBS for 10 minutes at room temperature, followed by permeabilization with 0.15% Triton X-100 for 10 minutes. After permeabilization, the cells were blocked with 5% BSA for 2 h. After blocking step specific primary antibody was added for 1 h. Following primary antibody incubation, the nucleus was stained with Hoechst 3342 (blue) and primary antibodies of different protein (BCL-2, p53, and caspase 3) were localized by secondary antibody labeled with Dylight 549 (red). Immunofluorescence of BCL-2, p53, and cleaved caspase 3 was determined by scanning the plates on Cellomics Array Scan VTI HCS Reader with 20X magnification (Thermo Fisher Scientific Inc., Waltham, MA).

All the data points were analyzed using the target activation and molecular translocation bioalgorithm of Cellomics and the quantitative data was expressed as percentage (%) activation in comparison to the DMSO control cells. 1000 cells were counted for each replicate well and the results were presented as an average ± SE. Bioapplication enables identification of the cell and cytoplasmic areas; the blue traces define the cell boundaries, while the orange traces cells rejected from the analysis. The scoring outputs used were total cellular/nuclear intensity and redistribution of fluorescence intensity from the nucleus to the cytoplasm (entropy intensity change) [20, 21].

3.3. Statistical Analysis. The data shown are the mean values of at least three replicate experiments and expressed as means ± SD. Differences between groups were analyzed using two sided t-test and ANOVA with $P < 0.05$ considered statistically significant. In cases in which averages were normalized to controls, the SDs of each nominator and denominator were taken into account in calculating the final SD. Statistical analyses were conducted using GraphPad Prism software 3.03 package (GraphPad Software, Inc., CA, USA).

4. Results and Discussion

4.1. Isolation and Structural Elucidation. The bioactivity guided purification of the crude extract obtained from the fermented whole broth yielded pure bioactive compounds **1** (hamigerone) and **2** (radicinol) (Figure 2). These compounds

Table 1: IC_{50} of hamigerone and radicinol in different cell lines.

Cell line	IC_{50} in μM (±SD)			
	Hamigerone	Radicinol	Gemcitabine	Flavopiridol
Panc-1 (pancreatic)	1.9 ± 0.92	10.50 ± 1.4	0.38 ± 0.04	0.62 ± 0.05
ACHN (renal)	4.3 ± 0.78	14.28 ± 1.8	0.78 ± 0.07	0.91 ± 0.11
Calu1 (lung)	2.91 ± 1.1	12.60 ± 0.87	0.98 ± 0.11	0.79 ± 0.19
H460 (non-small cell lung)	2.42 ± 0.63	21.6 ± 3.2	1.23 ± 0.23	0.82 ± 0.09
HCT116 (colon)	2.91 ± 0.87	25 ± 2.9	1.15 ± 0.21	0.73 ± 0.08
MCF10A (normal breast epithelium)	>30	>30	>10	>10

IC_{50} values of hamigerone and radicinol in different cancer cells at 48 h. The cells were exposed to different concentrations at end of 48 h; cytotoxicity was measured using live cell dehydrogenase assay.

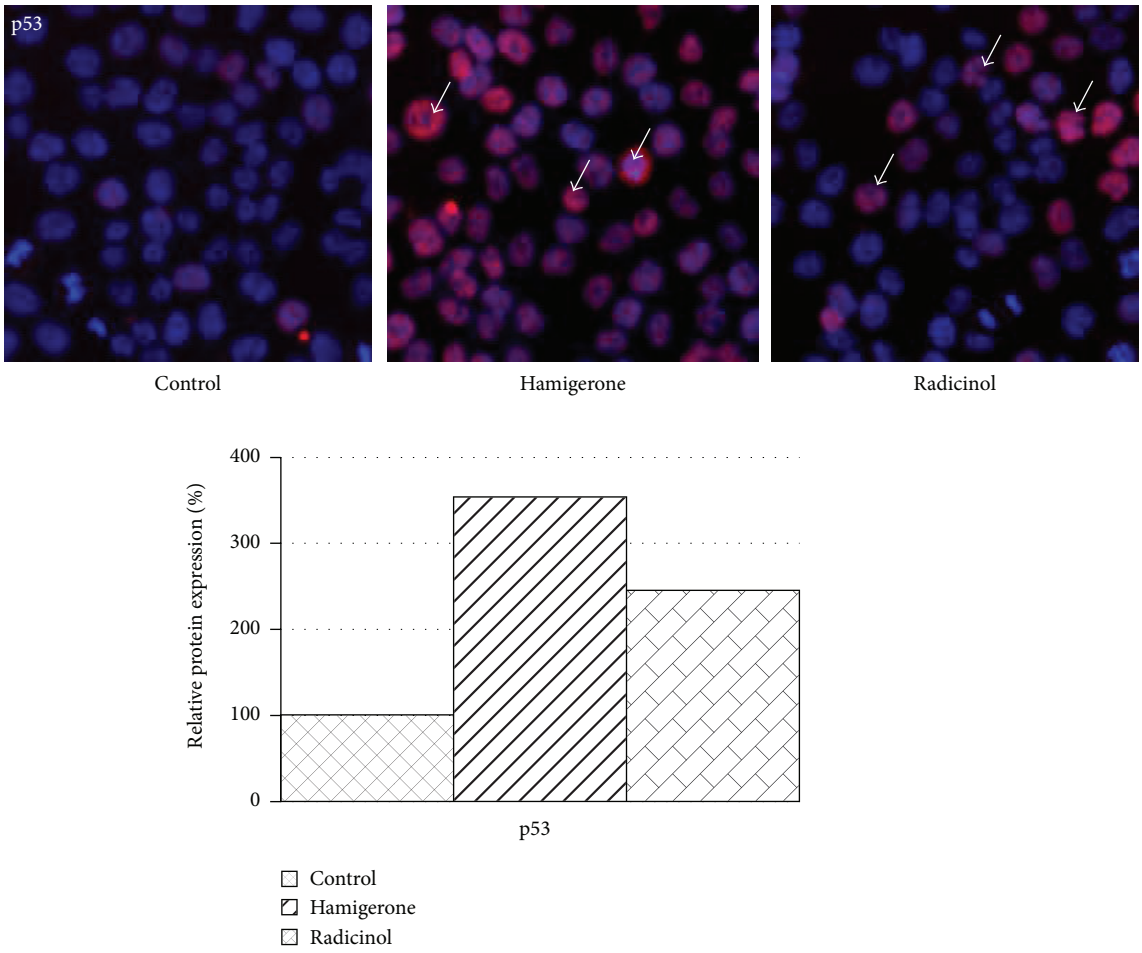

Figure 3: Elevation of p53 expression on treatment with hamigerone and radicinol in Panc-1 cells. The nucleus was stained with Hoechst 3342 (blue color), the expression of p53 protein levels was detected using Dylight 549 (red color), and the represented images are composite images of both channels. The quantitative data of p53 expression against untreated control cells is denoted as bar diagram. 1000 cells were counted for each replicate well and the results were presented as an average ± SE.

were characterized by spectroscopic data (UV, ^{1}H-NMR, ^{13}C-NMR, and LC-MS). All the values were in complete accord with that of the reported values [11, 12, 22].

Hamigerone was previously isolated from the fungus *Hamigera avellanea* and exhibits *in vitro* growth inhibitory activity against phytopathogenic fungi [11].

Radicinol, the phytotoxic compound, was produced on carrot disks by *Cochliobolus lunata* IFO 6288 [12]. It was also produced by *Bipolaris coicis*, *Alternaria radicina,* and *A. chrysanthemi* [22–24].

4.2. Antiproliferative Effect and In Vitro Protein Expression of Hamigerone and Radicinol. Hamigerone induced cytotoxicity in various cancer cell lines with an IC_{50} ranging from 1.9 μM to 4.3 μM. Similarly radicinol showed lesser

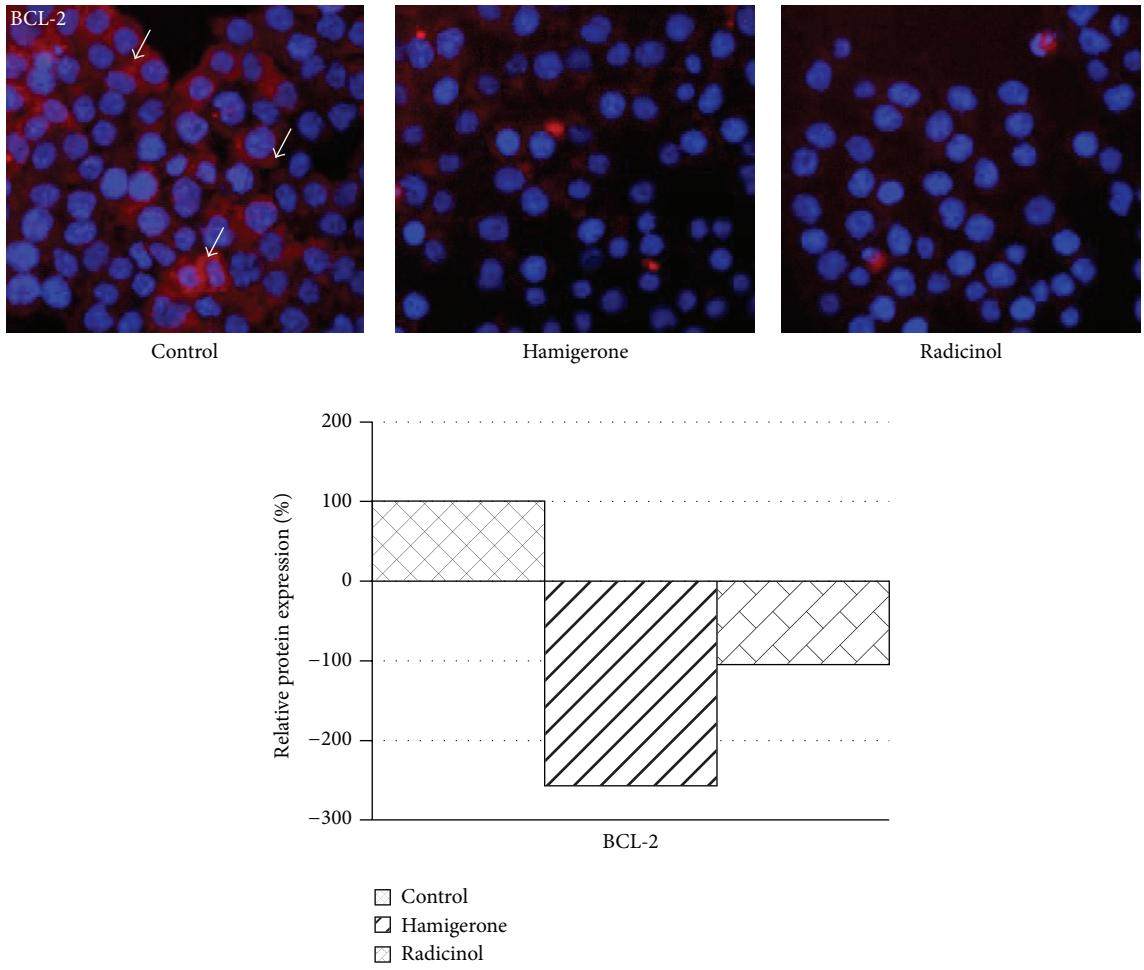

Figure 4: Decreased expression of BCL-2 levels on treatment with hamigerone and radicinol in Panc-1 cells. The nucleus was stained with Hoechst 3342 (blue color), the expression of BCL-2 protein levels was detected using Dylight 549 (red color), and the represented images are composite images of both channels. The quantitative data of BCL-2 expression against untreated control cells is represented as bar diagram. 1000 cells were counted for each replicate well and the results were presented as an average ± SE.

efficacy as a poor inducer of cytotoxicity towards the cancer cell lines with an IC_{50} in the range of 10.50 μM–25 μM (Table 1). Both the compounds were not toxic to normal breast epithelial cell line (MCF10A), as there was no growth inhibition up to a concentration of 30 μM. These findings suggest that these compounds are specific towards the abnormally proliferating cells [25] wherein hamigerone showed better toxicity to cancer cells as compared to radicinol. Based on the potent antiproliferation activity of both hamigerone and radicinol in Panc-1 cells, these compounds were further profiled for p53, BCL-2, and caspase 3 activity using high content screening tool Cellomics VTI Array Scan.

The p53 protein is known as a cellular gate-keeper. In general, in more than 70% of the tumors p53 status is either mutated or deleted. Activating p53 in cancer cells aids in driving the cancer cells into apoptosis. We have analyzed p53 protein expression in Panc-1 cells after 12 h of treatment with hamigerone and radicinol. The results showed 3.5-fold and 2.4- fold increased expression of p53 in Panc-1 cells (Figure 3), respectively. The quantitative expression level of this protein is represented as bar diagram.

It was also observed that hamigerone showed more significant induction of p53 (red color Ch2) when compared with radicinol. The significance of p53 in cell cycle arrest was also noted with *Selaginella tamariscina* extract in human ovarian cancer cell line A-2780 [26].

BCL-2 is an antiapoptotic protein. On treatment with hamigerone we noted 2.5-fold decreased expression of BCL-2 as compared with untreated control cells (Figure 4), while radicinol showed marginal reduction (1-fold). This data reveals that hamigerone was more potent than radicinol in reducing BCL-2 expression in Panc-1 cells. The bar diagram indicates the quantitative expression of BCL-2 protein levels. In another study resveratrol, a phytoalexin present in grapes and other food products, induces apoptosis in cancer cells by decreasing BCL-2 expression in HL-60 cells and gives rise to proteolytic cleavage of caspase substrate PARP [27] thereby causing apoptosis to the cancer cells.

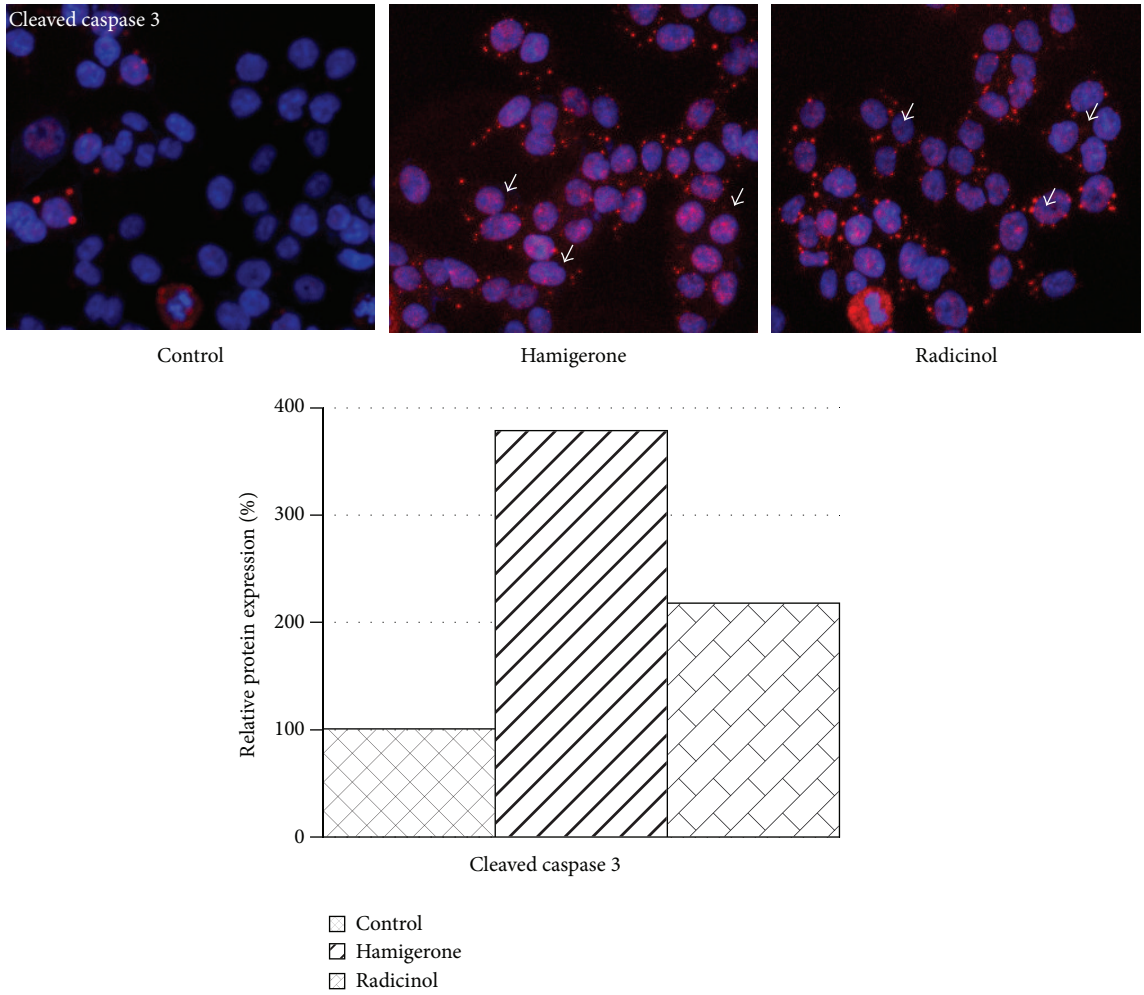

Figure 5: Induction of caspase 3 expression on treatment with hamigerone and radicinol in Panc-1 cells. The nucleus was stained with Hoechst 3342 (blue color), the expression of caspase 3 protein levels was detected using Dylight 549 (red color), and the represented images are composite images of both channels. The quantitative data of caspase 3 expression against control is showed as bar diagram. 1000 cells were counted for each replicate well and the results were presented as an average ± SE.

Furthermore we evaluated the cleaved caspase 3 activity in the cells treated with these compounds. In Panc-1 cells cleaved caspase 3 levels were higher (3.9-fold and 2.1-fold) in cells treated with hamigerone and radicinol as compared to untreated cells, respectively (Figure 5). These findings suggest the cytotoxicity effect of hamigerone and radicinol in cancer cells could be via induction of caspase 3 activation. The quantitative expression level of this protein against untreated controls is represented as bar diagram.

Of all the proteins involved in the activation and execution of apoptosis, the caspase 3 stands out as being crucial for this process [28].

In this study we have identified that hamigerone and radicinol interact with multiple cancer targets whose implication in cancer drug discovery is well described previously. Based on our findings, these molecules can become a potential start-up point for developing new scaffold which can modulate potential cancer targets.

Conflict of Interests

The authors declare that there is no conflict of interests regarding the publication of this paper.

Acknowledgment

We are thankful to the analytical discovery group at Piramal Enterprises Limited for recording spectral data.

References

[1] D. J. Newman and G. M. Cragg, "Natural products as sources of new drugs over the last 25 years," *Journal of Natural Products*, vol. 70, no. 3, pp. 461–477, 2007.

[2] J. C. Frisvad, U. Thrane, and O. Filtenborg, "Role and use of metabolites in fungal taxonomy," in *Chemical Fungal Taxonomy*, J. C. Frisvad, P. D. Bridge, and D. K. Arora, Eds., pp. 289–319, Marcel Dekker, New York, NY, USA, 1998.

[3] A. A. L. Gunatilaka, "Natural products from plant-associated microorganisms: distribution, structural diversity, bioactivity, and implications of their occurrence," *Journal of Natural Products*, vol. 69, no. 3, pp. 509–526, 2006.

[4] S. G. Bernier, D. D. Lazarus, E. Clark et al., "A methionine aminopeptidase-2 inhibitor, PPI-2458, for the treatment of rheumatoid arthritis," *Proceedings of the National Academy of Sciences of the United States of America*, vol. 101, no. 29, pp. 10768–10773, 2004.

[5] J. Wang, T. Wiltshire, Y. Wang et al., "ATM-dependent CHK2 activation induced by anticancer agent, irofulven," *The Journal of Biological Chemistry*, vol. 279, no. 38, pp. 39584–39592, 2004.

[6] Y. W. Chin, M. J. Balunas, H. B. Chai, and A. D. Kinghorn, "Drug discovery from natural sources," *AAPS Journal*, vol. 8, no. 2, pp. E239–E253, 2006.

[7] A. L. Harvey, "Natural products in drug discovery," *Drug Discovery Today*, vol. 13, no. 19-20, pp. 894–901, 2008.

[8] G. R. Eldridge, H. C. Vervoort, C. M. Lee et al., "High-throughput method for the production and analysis of large natural product libraries for drug discovery," *Analytical Chemistry*, vol. 74, no. 16, pp. 3963–3971, 2002.

[9] S. K. Deshmukh, P. D. Mishra, A. Kulkarni-Almeida et al., "Anti-inflammatory and anticancer activity of ergoflavin isolated from an endophytic fungus," *Chemistry and Biodiversity*, vol. 6, no. 5, pp. 784–789, 2009.

[10] P. Giridharan, S. A. Verekar, A. Khanna, P. D. Mishra, and S. K. Deshmukh, "Anticancer activity of sclerotiorin, isolated from an endophytic fungus *Cephalotheca faveolata* Yaguchi, Nishim. & Udagawa," *Indian Journal of Experimental Biology*, vol. 50, no. 7, pp. 464–468, 2012.

[11] J. Breinholt, A. Kjœr, C. E. Olsen, B. R. Rassing, and C. N. Rosendahl, "Hamigerone and dihydrohamigerone: two acetate-derived, antifungal metabolites from *Hamigera avellanea*," *Acta Chemica Scandinavica*, vol. 51, no. 12, pp. 1241–1244, 1997.

[12] N. Manabu and M. Shingo, "Radicinol, a new metabolite of *Cochliobolus lunata*, and absolute stereochemistry of radicinin," *Tetrahedron Letters*, vol. 18, no. 37, pp. 3271–3272, 1977.

[13] R. J. Bold, P. M. Termuhlen, and D. J. McConkey, "Apoptosis, cancer and cancer therapy," *Surgical Oncology*, vol. 6, no. 3, pp. 133–142, 1997.

[14] G. C. Shore and J. Viallet, "Modulating the bcl-2 family of apoptosis suppressors for potential therapeutic benefit in cancer," *The American Society of Hematology*, vol. 1, pp. 226–230, 2005.

[15] J. H. Warcup, "The soil-plate method for isolation of fungi from soil," *Nature*, vol. 166, no. 4211, pp. 117–118, 1950.

[16] T. J. White, T. Bruns, S. Lee, and J. Taylor, "Amplification and direct sequencing of fungal ribosomal RNA genes for phylogenetics," in *PCR Protocols: A Guide to Methods and Applications*, M. A. Innis, D. H. Gelfand, J. J. Sninsky, and T. J. White, Eds., pp. 315–322, Academic Press, San Diego, Calif, USA, 1990.

[17] S. F. Altschul, W. Gish, W. Miller, E. W. Myers, and D. J. Lipman, "Basic local alignment search tool," *Journal of Molecular Biology*, vol. 215, no. 3, pp. 403–410, 1990.

[18] K. Tamura, G. Stecher, D. Peterson, A. Filipski, and S. Kumar, "MEGA6: molecular evolutionary genetics analysis version 6.0," *Molecular Biology and Evolution*, vol. 30, pp. 2725–2729, 2013.

[19] T. Mosmann, "Rapid colorimetric assay for cellular growth and survival: application to proliferation and cytotoxicity assays," *Journal of Immunological Methods*, vol. 65, no. 1-2, pp. 55–63, 1983.

[20] J. Low, L. Stancato, J. Lee, and J. J. Sutherland, "Prioritizing hits from phenotypic high-content screens," *Current Opinion in Drug Discovery and Development*, vol. 11, no. 3, pp. 338–345, 2008.

[21] G. J. F. Ding, P. A. Fischer, R. C. Boltz et al., "Characterization and quantitation of NF-κB nuclear translocation induced by interleukin-1 and tumor necrosis factor-α," *The Journal of Biological Chemistry*, vol. 273, no. 44, pp. 28897–28905, 1998.

[22] H. Nakajima, T. Ishida, Y. Otsuka, T. Hamasaki, and M. Ichinoe, "Phytotoxins and related metabolites produced by *Bipolaris coicis*, the pathogen of job's tears," *Phytochemistry*, vol. 45, no. 1, pp. 41–45, 1997.

[23] M. Solfrizzo, C. Vitti, A. de Girolamo, A. Visconti, A. Logrieco, and F. P. Fanizzi, "Radicinols and radicinin phytotoxins produced by *Alternaria radicina* on carrots," *Journal of Agricultural and Food Chemistry*, vol. 52, no. 11, pp. 3655–3660, 2004.

[24] H. Sheridan and A. Canning, "Novel radicinol derivatives from long-term cultures of *Alternaria chrysanthemi*," *Journal of Natural Products*, vol. 62, no. 11, pp. 1568–1569, 1999.

[25] R. Yang, H. Hanwell, J. Zhang, R. Tsao, and K. A. Meckling, "Antiproliferative activity of pomiferin in normal (MCF-10A) and transformed (MCF-7) breast epithelial cells," *Journal of Agricultural and Food Chemistry*, vol. 59, no. 24, pp. 13328–13336, 2011.

[26] I. Lee, A. Nishikawa, F. Furukawa, K. Kasahara, and S. Kim, "Effects of *Selaginella tamariscina* on in vitro tumor cell growth, p53 expression, G1 arrest and in vivo gastric cell proliferation," *Cancer Letters*, vol. 144, no. 1, pp. 93–99, 1999.

[27] Y. J. Surh, Y. J. Hurh, J. Y. Kang, E. Lee, G. Kong, and S. J. Lee, "Resveratrol, an antioxidant present in red wine, induces apoptosis in human promyelocytic leukemia (HL-60) cells," *Cancer Letters*, vol. 140, no. 1, pp. 1–10, 1999.

[28] D. W. Nicholson and N. A. Thornberry, "Caspases: killer proteases," *Trends in Biochemical Sciences*, vol. 22, no. 8, pp. 299–306, 1997.